(1)

AFGL-TR-88-0003(I)

Source Characterization and Heavy Gas Dispersion Models for Reactive Chemicals. Volume 1.

Author(s): Raj, Phani K., Morris, John A.

Technology & Management Systems, Inc.
93 South Bedford Street
Suite 211
Burlington, MA 01803-5128

18 December 1987

Final Report, Volume I
Period Covered: 22 January 1986 - 21 December 1987

Approved for Public Release; Distribution Unlimited

AIR FORCE GEOPHYSICS LABORATORY
AIR FORCE SYSTEMS COMMAND
UNITED STATES AIR FORCE
HANSCOM AIR FORCE BASE, MASSACHUSETTS 01731-5000

DISCLAIMER NOTICE

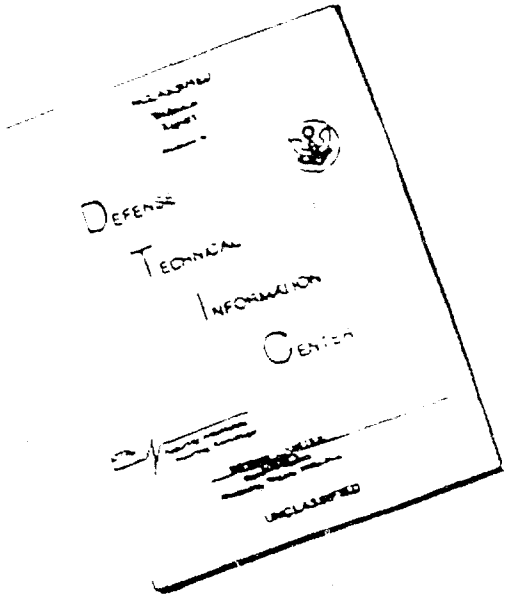

THIS DOCUMENT IS BEST QUALITY AVAILABLE. THE COPY FURNISHED TO DTIC CONTAINED A SIGNIFICANT NUMBER OF PAGES WHICH DO NOT REPRODUCE LEGIBLY.

"This technical report has been reviewed and is approved for publication"

Bruce Kunkel
BRUCE KUNKEL
Contract Manager

Donald D Grantham
DONALD GRANTHAM
Branch Chief

FOR THE COMMANDER

For Donald D Grantham Acting
ROBERT A. MC CLATCHEY
Division Director

This report has been reviewed by the ESD Public Affairs Office (PA) and is releasable to the National Technical Information Service (NTIS).

Qualified requestors may obtain additional copies from the Defense Technical Information Center. All others should apply to the National Technical Information Service.

If your address has changed, or if you wish to be removed from the mailing list, or if the addressee is no longer employed by your organization, please notify AFGL/DAA, Hanscom AFB, MA 01731. This will assist us in maintaining a current mailing list.

Do not return copies of this report unless contractual obligations or notices on a specific document requires that it be returned.

Unclassified
SECURITY CLASSIFICATION OF THIS PAGE

REPORT DOCUMENTATION PAGE

1a. REPORT SECURITY CLASSIFICATION Unclassified	1b. RESTRICTIVE MARKINGS
2a. SECURITY CLASSIFICATION AUTHORITY	3. DISTRIBUTION/AVAILABILITY OF REPORT Approved for Public Release; Distribution Unlimited
2b. DECLASSIFICATION/DOWNGRADING SCHEDULE	
4. PERFORMING ORGANIZATION REPORT NUMBER(S)	5. MONITORING ORGANIZATION REPORT NUMBER(S) AFGL-TR-88-0003(I)
6a. NAME OF PERFORMING ORGANIZATION Technology & Management Systems, Inc. 6b. OFFICE SYMBOL (If applicable)	7a. NAME OF MONITORING ORGANIZATION Air Force Geophysics Laboratory
6c. ADDRESS (City, State, and ZIP Code) 99 South Bedford Street, Suite 211 Burlington, MA 01803-5128	7b. ADDRESS (City, State, and ZIP Code) Hanscom AFB Massachusetts 01731
8a. NAME OF FUNDING/SPONSORING ORGANIZATION 8b. OFFICE SYMBOL (If applicable)	9. PROCUREMENT INSTRUMENT IDENTIFICATION NUMBER F19628-86-C-0036
8c. ADDRESS (City, State, and ZIP Code)	10. SOURCE OF FUNDING NUMBERS PROGRAM ELEMENT NO: 61102F; PROJECT NO: 2310; TASK NO: G7; WORK UNIT ACCESSION NO: BB
11. TITLE (Include Security Classification) Source Characterization and Heavy Gas Dispersion Models for Reactive Chemicals	
12. PERSONAL AUTHOR(S) Raj, Phani K.; Morris, John A.	
13a. TYPE OF REPORT Final Report,Vol.1	13b. TIME COVERED FROM 1/22/86 TO 12/21/87
14. DATE OF REPORT (Year, Month, Day) 18 December 1987	15. PAGE COUNT 258
16. SUPPLEMENTARY NOTATION Volume-2-AD-A192209	
17. COSATI CODES FIELD / GROUP / SUB-GROUP	18. SUBJECT TERMS (Continue on reverse if necessary and identify by block number) Heavy Gas, Dispersion, Mathematical Model, Reaction, Source Models, Concentration Contours . (mgm)

19. ABSTRACT (Continue on reverse if necessary and identify by block number)

U.S. Air Force and other agencies which handle, store and transport chemicals, fuels and oxidizers are interested in determining the potential area of hazard posed by the dispersion of vapors generated by accidental spills. This report describes the mathematical models developed to describe a variety of source types and the dispersion of vapor clouds/plumes in the atmosphere.

Sixteen different source types are modeled including pressurized liquid releases, flashing and aerosol formation, two phase jet releases, explosive releases and releases of high vapor pressure liquids, cryogenic liquids and gases. Dispersion model takes into account the differences in source characteristics, higher-than-air density of clouds (due to aerosol presence, temperature or molecular weight). Reactions of the chemicals, if any, ...th water vapor in the air are modeled and considered in the dispersion model. Transition from heavy gas dispersion to near neutral density dispersion is modeled without abrupt changes in size or discontinuity in concentrations.

SEE REVERSE SIDE.

20. DISTRIBUTION/AVAILABILITY OF ABSTRACT X ☒ UNCLASSIFIED/UNLIMITED ☐ SAME AS RPT ☐ DTIC USERS	21. ABSTRACT SECURITY CLASSIFICATION Unclassified
22a. NAME OF RESPONSIBLE INDIVIDUAL Bruce Kunkel	22b. TELEPHONE (Include Area Code) 617-377-2972 / 22c. OFFICE SYMBOL AFGL/LYA

DD FORM 1473, 84 MAR — 83 APR edition may be used until exhausted. All other editions are obsolete.

SECURITY CLASSIFICATION OF THIS PAGE

19. ABSTRACT (Continued)

Far field dispersion is modeled using modified area source (continuous plumes) or a volume source (instantaneous puff).

Six specific chemicals of interest to the USAF have been considered in detail and thermodynamic models for the reactions have been developed. The chemicals considered are (i) nitrogen tetroxide; (ii) chlorine; (iii) anhydrous ammonia; (iv) phosgene, (v) hydrogen sulphide; and (vi) sulphur dioxide.

The results of the model (such as concentration variation with distance, plume or cloud size, height, cross wind extent, arrival time, etc.) have been compared with available large field scale data for phosgene, chlorine, ammonia, nitrogen tetroxide, freon and liquefied natural gas. The agreement in all cases are very good. The model constants have been fine-tuned using the data from Thorney Island Series of Tests (involving the release of 2000 m^3 of freon of various densities and in different weather conditions).

The computer code developed is user friendly for data input and the results are presented graphically on a computer screen as contours of various concentrations of interest. Wind meander effects are also included. Typical program execution time on an IBM-AT or similar desktop computer is between 30 seconds to 90 seconds. This model is called ADAM (Air Force Dispersion Assessment Model).

ACKNOWLEDGMENTS

This study was undertaken by Technology & Management Systems, Inc. (TMS) under contract # F19628-86-C-0036 from the U.S. Air Force, Electronic Systems Divisions, PKR, Air Force Systems Command, Hanscom AFB, MA 01731-5260. The Contracting Officer's Technical Representative on this project was Mr. Bruce Kunkel. The project manager at TMS was Dr. Phani K. Raj. The project team at TMS consisted of Dr. Phani Raj and Mr. John Morris. Initial contributions to the project were also made by Dr. Mohan Venkataramana. Dr. Robert C. Reid, Professor (Emeritus) of Chemical Engineering, MIT, provided very valuable analyses of the reaction kinetics and thermodynamics.

The TMS team acknowledges with thanks the valuable technical input and guidance provided throughout the project by the Technical Project Monitor, Mr. Bruce Kunkel, of the USAF Geophysics Laboratory, Hanscom AFB. We also thank Capt. Larry Key, Tyndall AFB, for providing numerous reports on field tests, and other related information.

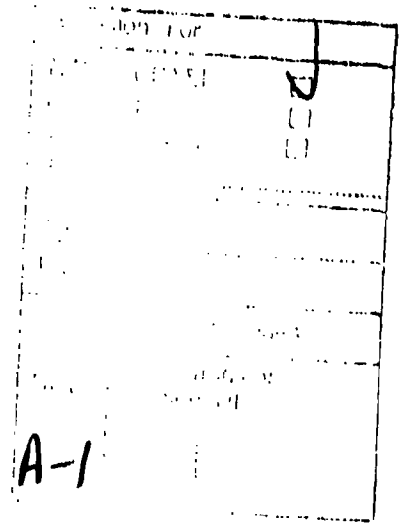

"THIS PAGE IS INTENTIONALLY LEFT BLANK."

TABLE OF CONTENTS

TABLE OF CONTENTS (Continued)

TABLE OF CONTENTS (Continued)

TABLE OF CONTENTS (Continued)

TABLE OF CONTENTS (Continued)

TABLE OF CONTENTS (Continued)

TABLE OF CONTENTS (Continued)

LIST OF TABLES

LIST OF TABLES (Continued)

LIST OF FIGURES

LIST OF FIGURES (Continued)

LIST OF FIGURES (Continued)

LIST OF FIGURES (Continued)

LIST OF FIGURES (Continued)

LIST OF FIGURES (Continued)

LIST OF FIGURES (Continued)

EXECUTIVE SUMMARY

Scientific models have been developed and described in this report for estimating the down wind extent and the cross wind area over which chemical vapor clouds remain hazardous. A number of chemicals with diverse properties are considered for modeling. Various accident caused release scenarios are postulated and modeled. The chemical reaction, if any, of the chemical released with ambient air or the water vapor are analyzed for three types of chemicals. The classification of the chemicals into three groups covers chemicals with a wide range of reactivity. The vapor cloud or plume formation, air entrainment and the dispersion of the cloud have been evaluated and modeled. The results from the models are compared with available field experimental data from five different field tests conducted with different chemicals.

It is found that the dispersion model developed in this project and described in this report predicts the cloud size, concentration data and the arrival times of the clouds with remarkable accuracy. The model uses a single set of parameter values to predict the behavior of clouds and plumes from a variety of chemicals and release conditions. These models are programmed to run on a microcomputer. The output from the dispersion models are presented graphically.

BACKGROUND

The U.S. Air Force (USAF) handles a number of chemicals including rocket propellants and oxidizers (such as nitrogen tetroxide). Therefore, the USAF is interested in assessing the potential hazards, especially the hazards due to the dispersion of chemical vapors released accidentally from stationary storage containers or road transports. In addition, the USAF is called upon to render technical and other assistance to the local communities should accidents involving hazardous materials and chemicals occur. The chemicals of particular interest to the USAF are the oxidizers such as the nitrogen tetroxide (N_2O_4), the chemical weapons related chemicals such as the Phosgene ($COCl_2$), and other common commercial chemicals such as ammonia (NH_3), chlorine (Cl_2), sulphur dioxide (SO_2), hydrogen sulphide (H_2S), etc.

The above chemicals have different physical and chemical properties. It has been recognized that the dispersion behavior of the vapor clouds of these chemicals will show considerable variety. For example, the vapor clouds formed may be more dense than the ambient air density due to the molecular weight of the chemical or due to the presence of liquid aerosols. The models currently used by the Air Weather Service of the USAF (namely, the Ocean Breeze and Dry Gulch Model) does not account for the variations in the chemical properties. Also, the current model does not take into account the effects of higher-than-air density of the vapor clouds.

It is a with a view to enhancing the knowledge of the cloud dispersion behavior of some of the chemicals and to develop a comprehensive and generic dispersion model applicable to a variety of situations, chemicals and weather conditions that this project was initiated by the Air Force Geophysical Laboratory at Hanscom Air Force Base.

OBJECTIVE & SCOPE OF THE PROJECT

The principal objective of the project was to develop mathematical models describing a variety of source conditions, and dispersion of vapor clouds (and plumes) of chemicals under different weather and release conditions. The second objective was to evaluate the effects of the various physical, chemical and thermodynamic phenomena on the dispersion of several selected chemicals.

The Scope of Work included the development of appropriate mathematical models and performance of a detailed study of the dispersion characteristics of the following six chemicals:

1.	Nitrogen tetroxide (N_2O_4) :	4.	Chlorine (Cl_2)
2.	Phosgene ($COCl_2$):	5.	Sulphur dioxide (SO_2)
3.	Anhydrous ammonia (NH_3) :	6.	Hydrogen sulphide (H_2S)

The above set of chemicals represent a good sample of the spectrum of chemicals with a variety in properties and different storage conditions.

The Scope of Work further included the,

- o analysis of the reaction between the released chemical and air/humidity in the atmosphere.
- o development of mathematical models for characterizing different types of sources and determining the source strengths.
- o development of dispersion models for predicting the hazard area, down wind distance and the depth of the vapor clouds generated by the release of the chemicals into the atmosphere.
- o comparison of the model results with available field test data.
- o compilation of a computer code for the models developed for execution on a microcomputer.

PROJECT ACCOMPLISHMENTS

Source Modeling

In this project we have developed mathematical models to describe the quantity and the rate of release of chemical from a variety of sources. The models are presented in such a way that the results are directly applicable to and useful for the subsequent calculations in the dispersion models.

The types of storage conditions considered include the ambient temperature pressurized liquid storage, gas storage and cryogenic liquid storage. We have developed criteria for classifying the releases into cryogenic or non cryogenic releases. These are based on the comparison of the temperature of the liquid that hits the ground with the ground temperature. The calculation of the liquid temperature outside the tank is accomplished by modeling the flashing process (for pressurized liquid releases). It is seen that for chlorine and ammonia a substantial fraction (15 to 25%) of the chemical released flashes directly into vapor. A part of the remaining liquid may be entrained into this vapor cloud as fine liquid droplets or aerosol. However, in this effort we have not been able to develop any analysis to determine the degree of aerosol entrainment into the initial vapor cloud formed.

The spread of a liquid pool on the ground and its evaporation have also been modeled. The low vapor pressure liquid pool evaporation model, originally proposed by Ille and Springer (1978), has been simplified and improved to provide better estimates of the evaporation rates. Comparison of our model predictions with available laboratory scale test data for the evaporation of nitrogen tetroxide pool indicates excellent agreement.

We have also developed a model to describe the entrainment ("uptake") of vapor produced by an evaporating liquid pool. This model provides the strength of a two dimensional "window" source of vapor and its physical dimensions at the down wind edge of the liquid pool. This source description is in conformity with the source characterization used in the continuous vapor dispersion model.

In the case of a pressurized release through a relatively small hole it is expected that the flow will be in the form of a two phase jet containing flashed vapor and liquid aerosols. Because of the high velocity of the jet, the down stream distance up to which the jet effects are dominant is large. We have developed a model to describe the characteristics of this jet (including the air entrainment and chemical reaction in the jet). The comparison of the results from this model with the field test data (from the Desert Tortoise series of ammonia release tests,

conducted by the Lawrence Livermore National Laboratory) indicates that the model predicts the jet length, area of the jet and the observed vapor concentration very closely.

In modeling different sources we have also taken into account the possibility of gas venting from pressurized gas storage containers. The models indicated in this report are basically compressible gas flow models and provide the values for such parameters as the mass flow rate, the density and temperature of the gas, the dimensions of the gas plume outside the tank and the velocity of the gas stream.

Overall, the source models described in this report cover a wide variety of chemical release situations and are useful in estimating the strength, dimensions and the initial conditions of the vapor clouds (or plumes) for dispersion calculations. Many of the source models have been verified with the available field test data and have been suitably modified to provide reasonably accurate predictions.

CHEMICAL REACTION MODELING

If a reactive chemical is released into the environment, there results a reaction between the released chemical and the entrained air. Models describing the final thermodynamic state resulting from the mixing of humid air and the chemical vapor cloud have been developed based on the assumption that the reaction rate (or the characteristic time for reaction) is much faster than the air mixing rate. That is, the reaction kinetics have been decoupled from the air entrainment and dispersion phenomena. These models take into account the energetics of the reaction, if any, and the heat exchange with the external surroundings (atmosphere, ground).

The models provide the final condition of the mixture for specified initial condition of the chemical, the humidity and temperature of the atmospheric air and the mass of air mixed. The initial chemical conditions are described by the vapor temperature, mass of liquid aerosols in the vapor cloud and the mass of the chemical. The final conditions of the mixture of air and the chemical vapor are described by the density, temperature and the mass fractions of various species in the gaseous and liquid phase, if any.

The analyses performed indicate that, in general, the chemicals can be grouped into three types depending on their reactivity with the ambient air. In the first type, termed "PASSIVE CHEMICALS", no reaction of water vapor with the chemical occurs. For a cloud containing liquid aerosols of this type of chemical, the cloud temperature decreases as the dilution with air increases until such time as all of the liquid aerosols have evaporated. During the initial phases of mixing with air when liquid aerosols are present in the cloud, the temperature of the

cloud can be substantially below the saturation temperature of the chemical at ambient pressure. However, the density decreases continuously as the mass of air in the mixture increases. Chlorine, phosgene, sulphur dioxide and hydrogen sulphide belong to this group.

The second chemical grouping is termed "WATER SOLUBLE CHEMICALS". The chemicals belonging to this group exhibit strong solubility in liquid water. The presence of liquid aerosols of either the chemical or of the condensed water will lead to the dissolution of the chemical vapor in the liquid phase. The heat of dissolution and the phase equilibrium properties of the chemical-water system will determine the distribution of the vapor and liquid phases in the vapor cloud. Ammonia is an example of this type of chemical.

The third type of chemical is termed "REACTIVE CHEMICAL". The mixing of this type of chemical with humid air results in reactions leading to the formation of new chemical species. Nitrogen tetroxide and silicon tetra fluoride are examples of this type of chemical. We have considered the reaction of nitrogen tetroxide-humid air reactions in detail. It is seen that the N_2O_4 dissociates into NO_2 and at any given time there is an equilibrium mixture of these two species. Depending on the partial pressure of the nitrogen oxides in the vapor cloud and the relative humidity of the air aqueous nitric acid may be formed in the mixture.

Our modeling effort in this project has included the considerations of all three of the above types of chemicals. These thermodynamic and reaction models have been coded into a computer program for use independently or as a part of the dispersion analysis. The results from these models indicate the following features of the air and chemical mixing process.

- The presence of liquid aerosols makes the density of the vapor cloud significantly higher than that of the air. Addition of air reduces the density of the mixture.

- Mixing of air with vapor clouds of type 1 chemicals consisting of liquid aerosols results in substantial decrease in the mixture cloud temperature. The temperature starts to increase when all aerosols have evaporated. This occurs within the range of dilution ratio of 1:1 to 1:10 (mass of chemical : mass of air) for a range of initial aerosol fractions of 20% to 50% by mass. The temperature of the vapor cloud subsequently approaches that of the ambient air with further dilution.

- In the case of type 2 chemicals (ammonia) the aqueous aerosols are present until the dilution is such that the cloud temperature goes above the wet bulb temperature of the air (consistent with the relative humidity). This means that in high humidity atmospheres a cloud will be visible

for a very long distance. The aerosols present at high dilutions will be essentially condensed water with very little chemical bound in the aqueous form.

- No generalization can be made of the behavior of the chemical of type 3 when mixed with air. The results depend very much on the reaction chemistry.

  In the case of nitrogen tetroxide, for example, the dissociation reaction of N_2O_4 to NO_2 is an endothermic reaction resulting in the cooling of the vapor cloud as soon as it is released from the tank. The resulting condensation of water from the atmosphere and the reaction of NO_2 with this condensed water will lead to the formation of aqueous nitric acid (HNO_3). The model indicates that above a (HNO_3) concentration of 50 ppm condensation of nitric acid results. This result is, to some extent, substantiated by the nitrogen tetroxide release tests conducted by Lawrence Livermore National Laboratory.

- The density of the chemical and air mixture is very insensitive to the relative humidity of the air. In calculating the density of the cloud, therefore, ignoring the effect of humidity is completely acceptable if the calculations are for describing the dispersion process. However, as indicated above, humidity has considerable effect on the reaction or dissolution (and therefore on the presence or absence of additional chemical species in the cloud as well as the distance up to which the cloud is visible).

DISPERSION MODELING

Dispersion models have been developed for the case of an instantaneously released vapor cloud as well for the continuously released plume of vapor. The initial conditions (such as the mass of vapor released or the mass rate of vapor release, the amount of aerosol in the vapor, the mass of air mixed, the thermodynamic condition and the size of the cloud) are determined from the source models and the application of the thermodynamic models described earlier. The models for both the cloud dispersion and the plume dispersion assume that the dispersing vapor+aerosol+air system is heavier than air. Dispersion is modeled in two distinct regimes, namely (i) the "heavy gas" or high cloud density dominated regime, and (ii) atmospheric turbulence controlled dispersion regime.

The dispersion models developed predict the concentration distributions, both vertically and horizontally at any point down wind of the source, the dosage at any point over which the cloud passes, the thermodynamic condition (temperature, density and species fractions in the vapor and liquid phases, if any) of

the cloud at any position, the cloud translation velocity, the cloud size, etc. Similar parameters are calculated for the plume release.

In the case of "puff" or "cloud" dispersion in the heavy gas regime we assume the cloud to be cylindrical ("box") and calculate the down wind motion of this cylindrical cloud due to wind induced drag. The cloud is diluted due to the entrainment of air over the top and sides of the cylinder. The air entrainment rates are expressed as functions of the gravity induced radial expansion velocity as well as the atmospheric turbulent velocities modified by the cloud stratification. In addition, the expansion of the edges due to atmospheric turbulent diffusion is super imposed on the box dispersion by the use of a modified volume source Gaussian dispersion phenomenon. The result of this "hybrid" model is that there results a central core region in the cylindrical cloud within which the concentration distribution is essentially uniform and the outer regions of the cloud in which the concentration falls off. This is a truer representation of the real phenomenon compared to that in the box model in which all property values within the box are uniform and outside of which there is no vapor concentration.

In the heavy gas dispersion regime the thermodynamic condition of the cloud is calculated at every position of the cloud noting the amount of air entrained up to that position and the total amount of heat exchanged between the cloud and the surroundings. The heavy gas type of dispersion is terminated when the local Richardson number is of the order of unity. However, the volume source Gaussian dispersion is continued beyond the transition region. This ensures that the property value changes with distance are smooth and continuous. In addition, the concentration and other distribution profiles smoothly change from the initial "top hat" profiles to the Gaussian profiles at the far field.

The same type of approach is used for modeling the plume (continuous release) dispersion. The profiles are assumed "top hat" in the lateral and vertical directions close to the source but change gradually to Gaussian profiles at the far field. The same type of "hybrid" model with heavy gas effects and the edge diffusion effects (modeled with an area source Gaussian model) is used to describe the dispersion of vapor in the plume. In the case of the plume dispersion it is assumed that the conditions at the source are steady (i.e., the rate of release of vapor is constant).

The results from the models developed in this report have been compared with data from several field dispersion tests involving the release of chemical vapors. The tests with which our model results have been compared include, (i) the Thorney Island series of tests in which 2000 m^3 of Freon was released instantaneously, (ii) the Desert Tortoise tests in which anhydrous ammonia was released continuously, (iii) the Eagle series of nitrogen

tetroxide release tests at the Nevada test site, (iv) Lyme Bay test of continuous chlorine release over the ocean, (v) tests involving the explosive release of phosgene. Principally, in all these tests data on the concentration variation with down wind distance has been compared with the model predictions. In some cases, the cloud area (or cross sectional area for plumes), height, cloud translation velocity have been compared with model results.

The model we have developed predicts the test results for different chemicals and release conditions with a remarkable degree of accuracy. The downwind concentration variations and the cloud sizes are predicted extremely well for almost all chemicals for which test data are available. The "box" models available in the literature do a poor job of matching the data over the whole range of tests. This is because of the inherent problem of matching the conditions in a box (within which all properties are uniform) to a continuously varying Gaussian profiles in the far field region.

Our hybrid model is a substantial improvement over the models available in the literature in that no artificial "virtual sources" are used. Also, our model does not have the problem of "mass loss" which most literature models have at the transition region.

In the dispersion model we have developed, there are a number of parameters with constant values in several equations describing the cloud or plume lateral expansion rate, air entrainment rate, wind-cloud momentum exchange rate, ground friction coefficient, etc. It is seen that the model predicts the data from the diverse tests (both in scope and chemical) with remarkable accuracy with only one unique set of parameters. The values of the different parameters were determined by calibrating the model results with a selected set of Thorney Island Test Series data. The parameter values that resulted in the best fit for these data, and which are the values we used in the model, are indicated in Table 1.

In our modeling effort we have also considered the description of the atmospheric stability according to a continuous scale. That is, the stability of the atmosphere can vary from extremely stable to an extremely unstable condition over a continuous scale. The exact stability condition is determined from a number of observational parameters including the solar angle, the wind speed, the cloud cover, time of day, etc. In addition, in the dispersion models the atmospheric dispersion parameter values are modified according to the roughness of the terrain and the concentration averaging period.

TABLE 1:

VALUES OF MODEL PARAMETERS FOR BEST FIT PREDICTIONS AND DATA FROM SEVERAL FIELD TESTS

Physical Phenomenon	Parameter	Value
Heavy Gas Dispersion	Gravity velocity factor (k)	1.07
	Top Entrainment Coefficient (α)	0.7
	Side Entrainment Coefficient (β_1)	0.08
	Side Entrainment Coefficient (β_2)	0.30
Wind-to-Cloud Drag Factor	Drag coefficient (C_D)	0.5
	Wind momentum transfer efficiency factor (f)	0.55
Transition Regime	Transition Richardson # ($Ri_{t,r}$)	1
	Fractional Density Deviation (Δ')	10^{-3}

MICROCOMPUTER PROGRAMS

The entire set of models developed under this project have been translated into FORTRAN computer code. These set of programs are executable on an advanced microcomputer with execution times of the order of 5 minutes for each run. The output from the programs are presented both in graphical form on the screen and in the form of tables.

CONCLUSIONS

In this project, we have developed a heavy gas chemical dispersion model which is comprehensive, accurate and is applicable to a variety of chemicals and release situations. We have,

- tested the model against all available field test data. The model predicts the observed data from many different field tests and chemicals very accurately.
- studied the sensitivity of the model to various parameters in the model and have determined a set of values which provide the best estimate for vapor cloud dispersion behavior.
- modeled a variety of release situations to determine the strength and size of vapor sources.
- analyzed the reaction chemistry of various chemicals with air/humidity and have developed a method of considering these effects in the dispersion process. Also, we have identified the important effects.
- Coded the entire set of models into microcomputer executable programs.

The dispersion model developed is simple in concept but yet predicts downwind vapor concentrations with good accuracy. The model is better than any "box" type models currently available in the literature.

RECOMMENDATIONS

The dispersion model developed does not consider the details of the local topography. This may present a serious limitation if the model is used for predicting heavy cloud behavior in a hilly or valley region.

It is therefore recommended that the heavy gas dispersion model developed in this project be modified to take into account the details of local topography and predict not only the cloud or plume concentrations but also where the cloud or plume will be at any given time.

CHAPTER 1

INTRODUCTION

1.1 BACKGROUND

The U.S. Air Force (USAF) handles, stores and transports rocket fuels (liquids), oxidizers and other chemicals. These chemicals include nitrogen textroxide (N_2O_4), phosgene, chlorine, ammonia, etc. The quantity of chemicals handled, transported and stored varies depending on the use. For example, liquid rocket fuels and oxidizers are handled in large quantities, whereas other chemicals are not used in large quantities by the USAF.

A number of these chemicals are inflammable and/or toxic. Therefore, they pose potential health and safety problems to people exposed to excessive vapor concentrations downwind of an accidental release of the chemical. When spills occur on or near an Air Force base, the Air Weather Service of the USAF is tasked to provide predictions of the toxic corridor. The determination of the hazard area requires knowledge of the toxic (or inflammable) properties of the chemical, the reaction (if any) the chemical undergoes in the atmosphere, the type of source and its strength, the meteorological data, and the dispersion characteristics of the vapor in the environment. All of these variables are interconnected and affect the final hazard area.

At present, the Air Weather Service of the USAF uses the Ocean Breeze and Dry Gulch Diffusion program (Kahler, 1980) to predict the potential hazard areas. This model is based on an empirical equation derived more than 20 years ago from a series of diffusion experiments conducted by AFGL at Cape Canaveral, FL, Vandenberg AFB, CA and in Kansas. In general, this model is not applicable to chemicals whose vapors are heavier than air or which undergo chemical reactions in the atmosphere. Also, this model is not applicable to vapors containing liquid aerosols which undergo evaporation during dispersion. The error resulting in the use of Ocean Breeze and Dry Gulch model to predict the dispersion of the vapors of chemicals indicated earlier is substantial.

Considerable theoretical and experimental research investigations have been carried out, worldwide, to understand the dispersion physics of heavier-than-air gases. A few investigations have also been undertaken to understand the reactive chemical dispersion behavior. However, most of the models are very complex or are not easily available for use by the USAF. Also, very little attention has been directed in the investigations on modeling the source characteristics following an accidental release. The Air Force Geophysical Laboratories (AFGL) is therefore interested in developing a comprehensive model capability so that any reasonable spill (involving the chemicals indicated earlier) can be described mathematically and the

potential hazard area calculated to a higher degree of accuracy than is presently possible using the AWS model. It is the desire of the AFGL that these models be the state-of-the-art, yet simplified to the extent possible. It is desirable to develop the models so that they run on a microcomputer. These models can then be installed in the USAF's microcomputers at a number of bases.

Therefore, with a view toward enhancing the prediction capabilities of the dispersion models for use by the Air Force and to expand the applicability of the computerized prediction system that the Air Force Geophysics Laboratory at Hanscom AFB initiated this research effort. The principal goal of the project is to analyze various chemical release scenarios, develop appropriate models and computerize the models so as to be executable on a microcomputer. Technology & Management Systems, Inc. (TMS) was awarded the contract to perform the various tasks in this project.

1.2 BRIEF SURVEY OF STATE-OF-THE-ART IN SOURCE AND DISPERSION MODELING OF CHEMICAL RELEASES

Over the past 10 years, there has been considerable research on the dispersion of heavy gases. A number of conferences have taken place dealing specifically with heavy gas dispersion modeling and data from field tests. However, a substantial part of research has been devoted to non-reacting gas dispersion, especially dispersion of cold natural gas vapors. For details of the models, test results and other information the following review papers and publications can be referred to: Raj (1982), Raj (1985), Webber (1983), and the Symposium on Heavy Gas Dispersion Trials at Thorney Island (JHM, 1985; HSE, 1986). The significant findings from the heavy gas dispersion research are as follows: (i) The turbulent entrainment rate into a heavy gas is significantly affected (reduced) by the density stratification in the gas cloud or plume; (ii) the downwind distance for a given level of concentration is considerably smaller than that predicted by point source Gaussian models; however, the total area of hazard may be more than Gaussian predictions because of lateral spread; iii) heavy gas releases may also pose an upwind hazard. This, however, depends on the wind speed and initial relative density and mode of release of vapor.

While significant efforts have been expended in understanding the physics of heavy gas cloud dispersions (especially non-reacting gases) not enough tests or modeling work has been done on either characterizing the sources or understanding the physics of dispersion of gases containing liquid aerosols and/or reaction with ambient air. Kunkel (1983) has recently published work comparing evaporative source strength models for toxic chemical spills. This work has compared the few available models on characterizing non-pressurized liquid spills and evaporation on the ground. Raj (1980) has modeled the release of pressurized

liquid in the form of a jet. The spill on land and evaporation of cryogenic chemicals has been modeled by Raj (1981).

Models for calculating propellant spill source strength have been developed by Haas, et al (1981). These models also assume that liquid is spilled onto ground and the evaporation is due to vapor pressure of the chemical. Pressurized release and jet source in which liquid aerosol gets entrained with the vapor are not modeled.

Very few experiments have been conducted with the chemicals of interest to the USAF. Cryogenic ammonia spill tests (50 liters) on water have been conducted under U.S. Coast Guard sponsorship. These tests indicated that over 50% liquid dissolves in water. Pressurized ammonia release tests on land have been carried out by Lawrence Livermore Labs (LLNL) (Koopman, et al.,1984). These tests showed the heavy gas dispersion characteristics of the aerosol laden cloud. Quantitative data have recently become available (Ermak, et al., 1987) and have been compared to model results. LLNL has also conducted nitrogen tetroxide release tests for the USAF (see Koopman, et al., 1984). The tests indicated that there was hydrolysis of N_2O_4 to nitric acid, even in the very dry desert atmosphere conditions. Data are available (Ermak, et al., 1987) and have been compared with model results.

In the area of theoretical modeling of reactive chemical dispersion, only two or three investigations are available. Kaiser and Walker (1978) have developed a model to predict ammonia dispersion. This model includes the effect of aerosols and ground heat transfers. A more detailed model of ammonia dispersion with reaction kinetics included have been developed by Raj (1980). More recently, Kansa, et al., (1983) have modified the liquified natural gas dispersion model (numerical model) to take into account the reaction chemistry and presence of aerosols.

Recently declassified data have been released by the U.S. Army on phosgene field tests conducted several decades ago (Raj, 1983). These tests clearly indicated the heavy gas type of behavior of phosgene vapor and liquid aerosol clouds. Data from tests conducted on the sea with chlorine releases have been reported recently (Wheatley, et al., 1987). The chlorine was released from a ship sailing crosswind. The test results indicate the heavy gas nature of the chlorine plume formed over the ocean. Dense gas behaviors of Hydrogen Fluoride vapors have also been reported by Blewitt et al (1987). In the series of tests reported by Blewitt et all, both aerosol formation and polymerization (and hence increased molecular weight of the plume) were observed. Some of the heavy gas dispersion models discussed in the literature use numerical techniques to solve the turbulent diffusion equations. Several of these (such as FEM3, ZEPHYR, SIGMET, etc.) can be run only on large computers. Improved semi-numerical models such as HEGADAS and DEGADIS take considerable computation time (of the order of several hours of CPU) to calculate dispersion footprint on a microcomputer.

Finally, most models are useful only for one type of release condition; seldom do these models come integrated with different source characterization models. Several reviews of dense gas dispersion models are given in the proceedings of a recent conference on Vapor Cloud Models (AIChE, 1987).

This report describes the results from a research and development effort conducted by TMS on behalf of USAF/AFGL. The report describes the various models developed and the application of the models to the conditions of releases from different tests with various chemicals. Also described are the features of the computer model.

1.3 OBJECTIVES

The objectives of this project were to:

- perform necessary research to evaluate the effects of various physical, chemical and thermodynamic phenomena on heavy gas dispersion of several selected chemicals.
- develop toxic chemical dispersion models which include the above phenomena and which will also take into account the characteristics of different types of sources.

1.4 SCOPE OF WORK PERFORMED

In order to achieve the above objectives, the following tasks were performed:

- development of a database of properties relevant to dispersion of the following six chemicals: nitrogen tetroxide, phosgene, chlorine, ammonia, sulfur dioxide, and hydrogen sulfide.
- modeling and characterization of various source types including single source, confined and unconfined source, instantaneous and continuous, liquid and/or gas release, etc.
- development of dispersion models for predicting the hazard area resulting from the release of a heavier-than-air toxic chemical vapor. The models include consideration of parameters such as the cloud density, atmospheric humidity, chemical reactions, thermodynamic effects, heat exchange with ground and liquid aerosol effects.
- Coding of the models into a computer program and debugging the code.
- Comparing model results with data available from field tests.

- Performing model analysis to evaluate the importance of various physical, chemical, and thermodynamic phenomena (or parameter values) on the dispersion and hazard area.

- Generating this technical report containing all data collected, analyses performed, mathematical models developed, and results of investigations.

1.5 REPORT ORGANIZATION

This report is divided into logical parts. An overall project summary is given in the executive summary. This chapter gives a brief outline of the project background. The next four chapters (2-5) contain descriptions of the scientific models developed. The description of sources, the model details, and the results obtained by using the source models are discussed in Chapter 2. The thermodynamic behavior of the chemicals as they are released and dispersed is discussed in Chapter 3. The models used to describe the atmospheric conditions are covered in Chapter 4. The dispersion analysis models are discussed in Chapter 5. Chapter 6 has details of the comparisons of test data and model results. Finally, the overall project conclusions are in Chapter 7. The Appendices have detailed descriptions of the property database (Appendix A), dispersion modeling (Appendix B), and computer code organization (Appendix C). The computer program user's manual is presented in Volume II, so as to not overload the reader of this model development and evaluation volume.

CHAPTER 2

SOURCE MODELING

In this chapter, we discuss the storage and release conditions relevant to the six chemicals of interest to this study. The types and nature of releases possible are then discussed. Mathematical models for the different processes and phenomena that occur during the release of the chemicals are formulated and developed.

2.1 INTRODUCTION

The chemicals of interest to this study, chlorine, ammonia, nitrogen tetroxide, phosgene, sulfur dioxide and hydrogen sulfide, are stored and transported in various forms (pressurized or under atmospheric pressure, liquid or gas). The type and nature of chemical release from such a container depends on the severity of the accident involved. In the case of a tank rupture, for example, the entire content of the tank may be released into the atmosphere; on the other hand, if the release is due to a relatively small puncture in the tank wall or due to a pipeline rupture the chemical may be released into the atmosphere over an extended period of time. The former type of release in which the tank's contents are released in a relatively short time can be classified as an "instantaneous" release, and the latter, a "continuous" release.

Figure 2.1.1 illustrates the typical release scenarios considered in source modeling. Three types of chemical storage are considered, namely, (i) stationary liquid storage tank (pressurized or unpressurized) which is diked, (ii) undiked, stationary liquid storage tank (pressurized or un pressurized) and (iii) pressurized tank on a road transport. Several chemical release scenarios can be postulated depending on the type and extent of damage to the storage tanks. We discuss below a few of the important situations.

If a hole or a crack results on the wall of a pressurized tank vapor or liquid is released into the atmosphere depending on the location of the puncture relative to the liquid level; liquid is released if the hole is below the liquid level and gas is released when the hole is above the liquid line.

2.1.1 Liquid Releases

In general, if the liquid is stored under pressure it is at ambient temperature. When this liquid is released it "flashes" immediately. That is, a fraction of the released liquid evaporates, using its sensible heat, so as to adjust thermodynamically to the lower ambient pressure. This flashing phenomenon results in the formation of atmospheric pressure saturated vapor and saturated liquid. A part of the saturated liquid may be in the form of fine droplets ("aerosols") and may get entrained into the vapor cloud formed by the saturated vapor. The vapor cloud together with the entrained liquid aerosols

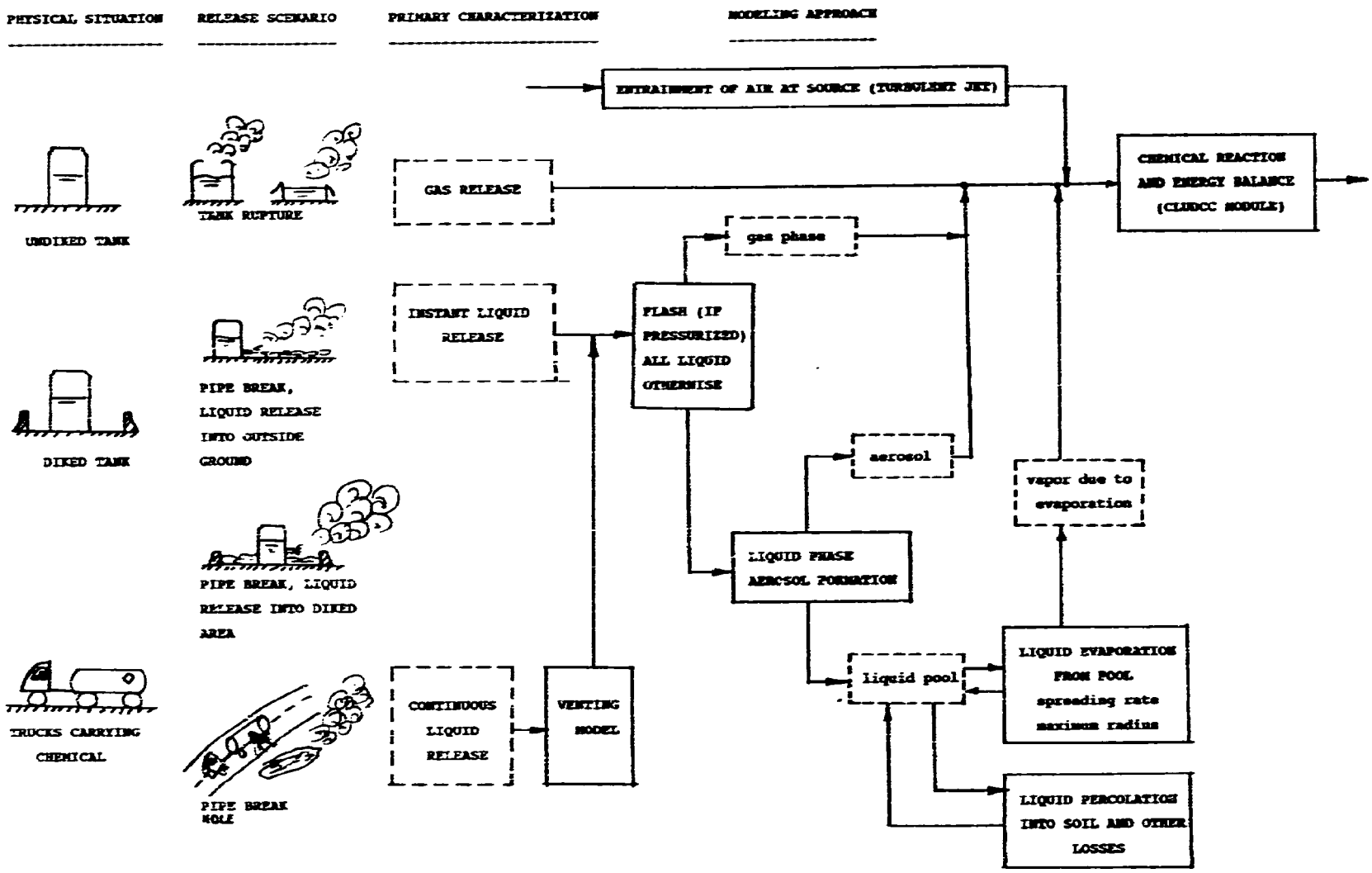

Figure 2.1.1: SOURCE MODELING OVERVIEW: RELEASE SCENARIOS, SOURCE CHARACTERIZATION AND MODELING APPROACH. SOLID BOXES INDICATE PHYSICAL MODELS. BROKEN BOXES DESCRIBE STATE OF THE SYSTEM.

and may get entrained into the vapor cloud formed by the saturated vapor. The vapor cloud together with the entrained liquid aerosols will disperse in the atmosphere. The remainder of the saturated liquid may spread on the ground, percolate into the ground and evaporate due to heat transfer from the ground and the atmosphere. The spread of the liquid on the ground may be impeded and a pool formed if a dike surrounds the storage tank. The vapor emanating from the evaporation of the pool of liquid on the ground will also form a gas cloud or plume depending on the duration of evaporation. These phenomena are schematically depicted in Figure 2.1.1. Also shown in this figure are the various "phenomena paths" depending on the storage, release and environmental conditions.

In this Chapter, the rates of release of the liquid from various storage conditions are calculated and discussed in section 2.3.1. Liquid flash is modeled in section 2.4. The spread and evaporation of liquid on the ground is discussed in section 2.5. If a large volume of pressurized liquid is released through a relatively small hole over a long duration of time a two phase jet of vapor and liquid jet results. The modeling of the characteristics of this jet is discussed in section 2.6.

2.1.2 Gas Releases:

Figure 2.1.1. shows schematically two situations in which only vapor will be released from the storage tank into the atmosphere. Vapor releases can occur due to (i) the pressure safety valve (on pressurized tanks) releases excess vapor build up within the tank caused by heat leak or other phenomena, (ii) the top of the tank is damaged exposing the liquid pool to the atmosphere. This occurs when the damage to the tank wall occurs above the liquid line. In the case of atmospheric pressure storage tanks, the liquid pool evaporates relatively slowly due to the heat transfer from the wind. In the case of pressurized tanks the rate of evaporation of the liquid will depend on the size of the hole in the tank wall. If the damage is large then the entire mass of the liquid participates in a flash process and massive amount of vapor is produced in a relatively short time. If the hole on the vapor space is small then the rate of production of vapor is slow but will occur over a long duration of time. In this case relatively pure vapor (free of liquid) will be released.

Gas release calculations for the case of relatively small holes and constant tank pressure are indicated in section 2.3.2.

The term "source modeling" used in this report signifies the (a) calculation of chemical release rates, (b) determination of the thermodynamic state of the chemical (temperature, phase, concentration of the different chemical species, etc) just after release, (c) evaluation of the physical dimensions of the vapor cloud or the plume at the source, flow rates of vapor and initially entrained air and the chemical concentration in the initial cloud or plume. These models are discussed below.

One other important phenomenon that occurs after the release of the chemical, especially during the release of a pressurized liquid, is the rapid entrainment of air very close to the source. The volume of air entrained will depend on the dynamics of release and the flash process. Thermodynamic equilibrium may be attained quickly by the mixture of chemical vapor, aerosols, if any, and the entrained air. This state defines the initial conditions for the subsequent dispersion calculations.

2.1.3 Literature Citations on Source Modeling

The source models available in the literature range from simple nomograms, to those based on empirical relations for specific chemicals and release scenarios to models that solve the heat balance equations for the pool temperature including solar radiation, heat transfer from the ground etc. Some of these are (i) Illinois EPA model to provide rapid and easy estimates for evacuation zones in the case of an accident, (ii) USAF AWS model to estimate propellant source strength, (iii) USAF ESL model which includes a simple empirical formula primarily for use with highly toxic liquid propellant releases, (iv) Whitacre and Myriski Army model which relates the evaporation rate to wind speed, (v) Ille and Springer model which takes into account detailed heat transfer modes into a liquid pool, and (vi) Shell Spills model. A recent review and evaluation of these models are available in reports by Kunkel (1983) and TRC Inc. (1986).

2.2 STORAGE/RELEASE CONDITIONS OF THE SIX CHEMICALS UNDER STUDY

The analysis of source modeling requires the knowledge of typical storage conditions adopted for the chemicals. Table 2.2.1 summarizes these conditions for the six chemicals, namely chlorine (CLX), ammonia (AMA), nitrogen tetroxide (NOX), phosgene (PHG), sulfur dioxide (SFD) and hydrogen sulfide (HDS). For each of these cases, storage conditions are characterized by the pressure and temperature at storage, as well as the physical state. It can be seen from Table 2.2.1 that the chemicals CLX, AMA, SFD and HDS are usually stored as pressurized liquids at ambient temperature. For phosgene and N_2O_4, the physical state at storage is clearly dependent on the storage temperature and pressure.

2.2.1 Classification of Storage Conditions

For the purposes of source modeling, it is important to distinguish between the various modes of storage, such as: (a) pressurized or non-pressurized, (b) liquid or gaseous storage and, (c) cryogenic or non-cryogenic. At present, no specific criteria exists for the classification of the liquid into cryogenic or non-cryogenic type release. It is therefore necessary to develop a consistent set of criteria that will allow us to classify the storage/release conditions. The characterization of storage/release conditions can be

Table 2.2.1: Typical Storage Conditions of Selected Chemicals

Chemical	Normal Boiling Temperature (K)	Sat. Pressure (atm) at 273 K (0 C)	298 K (25 C)	Typical Storage/Transportation Conditions
CHLORINE	239.1	3.62	7.65	Pressurized, in both liquid and gas phases (at 25 C, 7.6 atm)
AMMONIA	239.8	4.17	9.66	a. Pressurized Hortonspheres b. aqua ammonia in low pressure storage c. refrigerated liquid at P = 1 atm In Road & Rail Transport, it is carried as a pressurized liquid.
NITROGEN TETROXIDE	294.0	0.34	1.18	liquid & gas at atmospheric pressure
PHOSGENE	281.4	0.73	1.85	liquid & gas at atmospheric pressure
SULFUR DIOXIDE	263.2	1.52	3.85	Pressurized, in both liquid and gas phases (at 25 C, 3.8 atm) refrigerated liquid
HYDROGEN SULFIDE	212.8	10.0	13.4	Pressurized, in both liquid and gas phases (at 25 C, 13.4 atm) refrigerated liquid

conveniently described by a representation on a saturated vapor pressure - temperature diagram.

Figure 2.2.1 illustrates a typical saturated vapor pressure-temperature diagram, showing the location of the liquid-vapor boundary (line AB). Specification of the tank storage temperature (T_T) and tank storage pressure (P_T) allows us to represent the storage state on this plot. Four storage conditions are possible (represented in the figure by 1, 2, 3, and 4). Conditions 1 and 2 indicate the situation where the storage pressure is above the ambient pressure ("pressurized storage"). Conditions 3 and 4 represent ambient pressure storage at different temperatures (liquid or gaseous storage condition depending on the storage temperature relative to the saturation temperature at ambient pressure).

2.2.2 Classification of Releases

Cryogenic & Non Cryogenic Releases

In the case of liquid release we classify the release into cryogenic or non-cryogenic release depending on the temperature of the liquid when it hits the ground. The following criteria are used in this classification depending on the ground temperature (T_G).

If,

$T_{REL} < T_G$ release is CRYOGENIC

$T_{REL} >= T_G$ release is NON-CRYOGENIC

where the release temperature (T_{REL}) is calculated from the initial storage conditions and the flash calculation, if necessary.

If liquid is stored subcooled - such as storage of water at ambient temperature and pressure - then the release temperature will be equal to the storage temperature; on the other hand, if the liquid were saturated to begin with, on release the temperature will be the saturated temperature corresponding to the atmospheric pressure for the chemical. Thus, we can define the release temperature T_{REL} to be:

$$T_{REL} = \begin{cases} T_T & \text{if } T_T < T_{SAT} \text{ (at 1 atm pressure)} \\ T_{SAT} \text{ (@ 1 atm)} & \text{if } T_T > T_{SAT} \text{ (at 1 atm pressure)} \end{cases}$$

If the ground temperature, T_G is higher than T_{REL}, i.e., if a cryogenic spill occurs, the liquid evaporation is enhanced by the heating from the ground. On the other hand if $T_G < T_{REL}$, the liquid evaporation is dependent on the heat loss to the ground and the ambient.

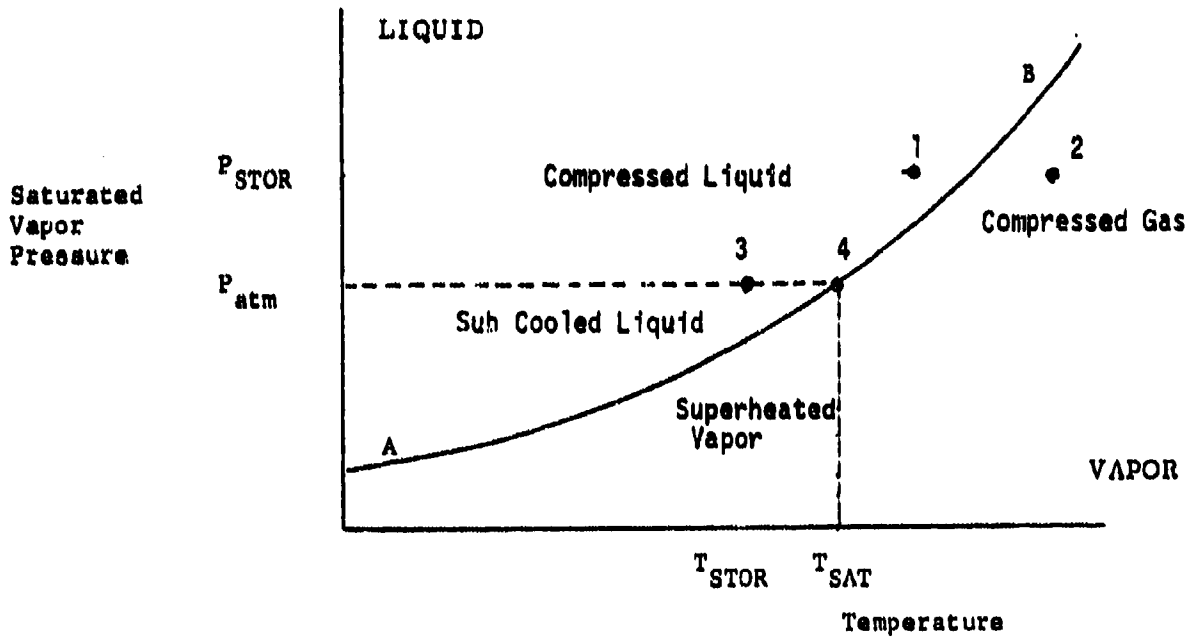

Figure 3.2.1 (b)

Figure 2.2.1: Determination of Storage Conditions of Chemicals: Liquid vs Gas, and Pressurized vs Non-Pressurized Cases.

Figure 2.2.2 shows the actual saturated vapor pressure - temperature diagrams for all the chemicals under study. The normal boiling points of the six chemicals are: nitrogen tetroxide (294.0 K), ammonia (239.8 K), chlorine (239.1 K), phosgene (281.4 K), sulfur dioxide (263.2 K) and hydrogen sulfide (212.8 K).

Confined & Unconfined Spills

Around many liquid storage tanks dikes are provided (alternately sumps are provided) to collect and contain any spilled liquid. A liquid spill tends to spread on the ground until the dike wall is reached at which time accumulation of liquid results. In our models a spill is termed "un confined" if the liquid pool spreads without any restriction. Similarly, when the spread is restricted due to the presence of a dike the spill is termed "confined". The spreading pool of a cryogenic liquid may evaporate due to the heat transfer from the ground during its un confined spread. However, under the condition of a confined spill the liquid may spread initially but will form a pool quickly. The rate of evaporation in the latter case will decrease with time because of cooling of the ground underneath the pool.

Instantaneous & Continuous Spills

The classification of a release into instantaneous or continuous depends very much on the purpose for which the definition is applied. For example, if the time duration of release of liquid from a storage container is short compared to the time over which the liquid in the pool evaporates then the release can be considered as "instantaneous". However, the same liquid pool may be evaporating over a time which is much larger than the time of dispersion of the vapors to reach a specified level of concentration down wind. In the latter case, the same release is considered to be "continuous". Therefore, spill classification into instantaneous or continuous involves the determination of two or more time scales. The calculation of dispersion time scale is difficult because the dispersion characteristics depend on the type of release. There does not exist in the literature any simple criterion by which a release can be easily classified as being either continuous or instantaneous.

Fortunately, the lack of knowledge of the classification of a release is not very detrimental in determining the extent or the area of hazard. In the dispersion models discussed in Chapter 5 we analyze both the instantaneous releases of vapor and continuous releases of vapor. We suggest, for those release situations in which the classification is nebulous, that the hazard distances be calculated using both the instantaneous release model and the continuous release model (over the duration of the spill) and using the larger hazard area or extent.

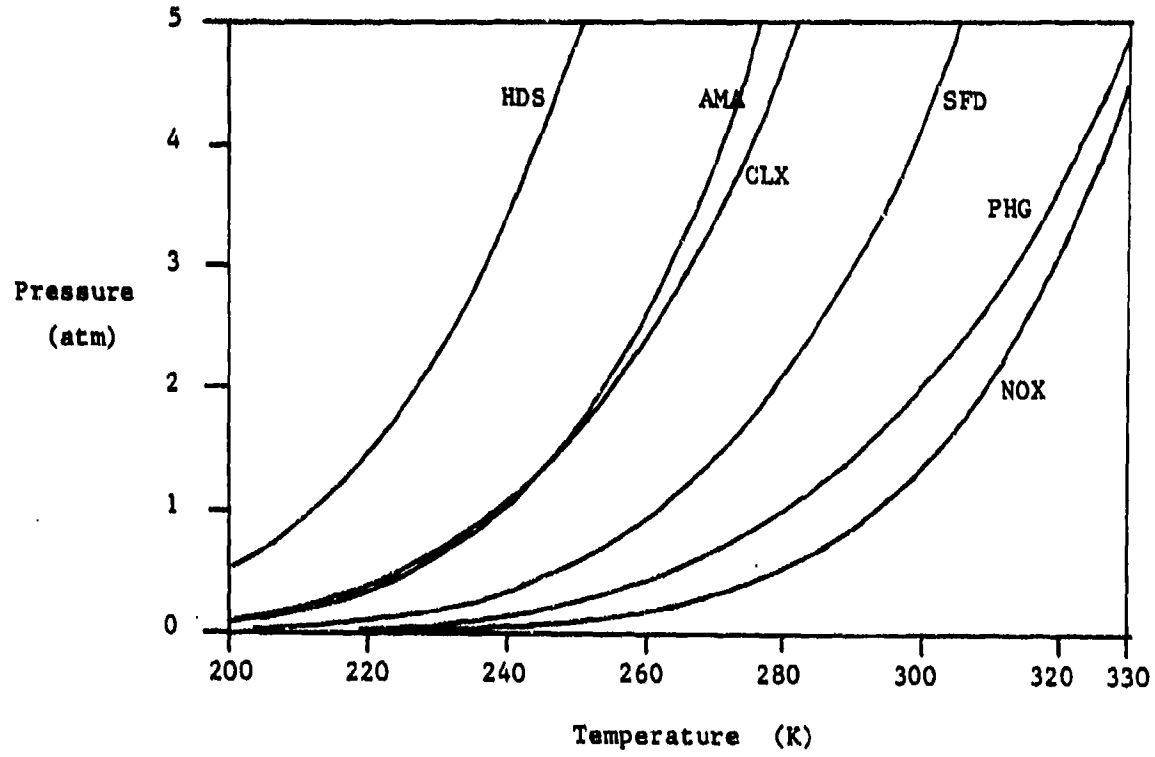

Figure 2.2.2: Saturated Vapor Pressure - Temperature Diagrams of Chemicals Under Study.

HDS	Hydrogen Sulfide
PHG	Phosgene
AMA	Ammonia
CLX	Chlorine
SFD	Sulfur dioxide
NOX	Nitrogen Tetroxide

Representation of Storage & Release Condition

In our analysis and computer codes the various modes of the storage/release conditions are identified by the following parameters. Each parameter has a zero or one value depending on the situation. The parameter and the conditions they represent are indicated below:

Parameter	Condition Represented
I_{CRYO}	Release is cryogenic or non cryogenic (applies to liquid releases only)
I_{PRES}	Chemical storage under pressure or otherwise
I_{LIQ}	Phase of the chemical under storage; liquid or gas
I_{DIKE}	Presence or absence of a dike surrounding the tank (indicates confined or unconfined spill)
I_{CONT}	Spill classified into continuous or instantaneous

Depending on the values of the above parameters, the actual release of the chemical can be classified into one of 20 categories. These categories are enumerated in Table 2.2.2. From physical considerations, the cryogenic gas releases are eliminated since the released gas is presumed not to receive appreciable heat transfer from the ground during its release from the container. In addition, the presence of the diked area also does not affect the gas release characteristics.

Typical description of accident situations are usually nebulous, such as, "a tank truck containing N_2O_4 spilled onto ground". While this information may be adequate to provide a sense of the problem on hand, it is not sufficient to obtain quantitative information either about the storage conditions or the parameters that define the release type.

It is evident from the above discussion that the overall source model will consist of various models that describe each of the above phenomena. The models are, (a) venting rate model, describing the rate of release of liquid or gas through a hole; (b) flash model, describing the fraction of the pressurized liquid released that is transformed into vapor by the flashing process; (c) cryogenic liquid spread model, describing the spreading and simultaneous evaporation of the cryogenic liquid; (d) model for the spread and evaporation of a low vapor pressure liquid pool on the ground, (e) an uptake model, which describes the entrainment into the wind stream of the vapor emanating from a pool of liquid, and (f) a model for estimating the characteristics and the entrainment of air into a two phase jet formed due to a pressurized liquid release from a hole.

Table 2.2.2: Types of Sources and Source Parameter Values

	RELEASE CATAGORY				CONSERVATIVE ESTIMATE FOR HAZARD CALCULATIONS	Source Parameters				
						I_{cryo}	I_{pres}	I_{liq}	I_{dike}	I_{cont}
1	noncryogenic	nonpressurized	liquid	undiked instant	evaporation from pool (t=0, R=Ro, h=ho)	0	0	1	0	0
2	noncryogenic	nonpressurized	liquid	undiked cont	negligible source typically	0	0	1	0	1
3	noncryogenic	nonpressurized	liquid	diked instant	evaporation from pool (from t=0 to prescribed t) with R = Rdike	0	0	1	1	0
4	noncryogenic	nonpressurized	liquid	diked cont	evaporation from pool with R = Rdike	0	0	1	1	1
5	noncryogenic	pressurized	liquid	undiked instant	all initially flashed vapor	0	1	1	0	0
6	noncryogenic	pressurized	liquid	undiked cont	all initially vented and flashed vapor	0	1	1	0	1
7	noncryogenic	pressurized	liquid	diked instant	all initially flashed vapor	0	1	1	1	0
8	noncryogenic	pressurized	liquid	diked cont	all initially vented and flashed vapor	0	1	1	1	1
9	cryogenic	nonpressurized	liquid	undiked instant	all material released	1	0	1	0	0
10	cryogenic	nonpressurized	liquid	undiked cont	all vented liquid released	1	0	1	0	1
11	cryogenic	nonpressurized	liquid	diked instant	all material released	1	0	1	1	0
12	cryogenic	nonpressurized	liquid	diked cont	all vented liquid released	1	0	1	1	1
13	cryogenic	pressurized	liquid	undiked instant	all material released	1	1	1	0	0
14	cryogenic	pressurized	liquid	undiked cont	all vented liquid released	1	1	1	0	1
15	cryogenic	pressurized	liquid	diked instant	all material released	1	1	1	1	0
16	cryogenic	pressurized	liquid	diked cont	all vented liquid released	1	1	1	1	1
17	noncryogenic	nonpressurized	gas	undiked instant	all the gas in the tank	0	0	0	0	0
18	noncryogenic	nonpressurized	gas	undiked cont	all the gas vented from the tank	0	0	0	0	1
19	noncryogenic	pressurized	gas	undiked instant	all the gas in the tank	0	1	0	0	0
20	noncryogenic	pressurized	gas	undiked cont	all the gas vented from the tank	0	1	0	0	1

We have not modeled the process of formation of the aerosols from the released liquid. This is a complex phenomenon and depends very much on the properties of the chemical, conditions of release, the geometry of the hole, angle of the jet issuing from the hole (and whether the jet impacts the ground or not), etc. The specification of the fraction of liquid that is converted into aerosol is left as a user input parameter. The rate of percolation of liquid from a pool on the ground into the substrate is dependent on the characteristics of the ground at the accident site. We have not included the percolation loss of the chemical in our source models. This omission is deliberate and is with a view to give conservative estimates of the mass of vapor injected into the atmosphere.

Since the primary purpose of the source characterization in this project is to estimate the dispersion hazard distances and areas, we use the models such that conservative estimate of the source strength results. Table 2.2.2 also provides a list of such conservative estimates for various source release conditions.

In the following sections, the physical models developed are described in detail. In each case, the equations developed have been coded into a FORTRAN computer program and constitute a module in the source library.

2.3 VENTING RATE MODELS

Venting rate model involves the release of the chemical through a hole. The driving force for such a flow is the liquid head in the tank and/or the (liquid or gas) pressure inside the tank. The friction at the exit and the finite size of the hole restricts the chemical flow rate through the hole. In this section, we derive the venting rate equations for both liquid and gas releases.

2.3.1 Liquid Release

Consider the situation where the liquid is stored in the tank under pressure P_T. Let the depth of the liquid be h_L. The liquid is released to the atmosphere (at P_a) through a hole of area A_H, at a location h_H from the tank bottom, with velocity U. The area of the tank A_T, is assumed to be much greater than the area of the hole, and thus, the exit flow through the hole does not significantly alter h_L or P_T. In addition, we define D_H as the equivalent hole diameter and D_T as the tank diameter. Application of Bernoulli's equation leads to:

$$P_T + \rho_l \; g \; (h_L - h_H) = P_a + \rho_l \; \frac{U^2}{2} \qquad (2.3.1)$$

where ρ_l is the liquid density. In general, the pressure has very little effect on liquid density.

Rearrangement of the above equation results in:

$$U = \sqrt{\left(\frac{2}{\rho_\ell}\right) * \left[(P_T - P_a) + \rho_\ell \; g \; (h_L - h_H) \right]} \qquad (2.3.2)$$

The mass flow rate is then given by:

$$\dot{m} = C_D \quad \rho_\ell \quad U \quad A_H \qquad (2.3.3)$$

where the constant C_D is the coefficient of discharge, a factor that depends on the nature of the hole, the hole size, the flow rate (and the Reynolds number) through the hole, and the compressibility. For liquids, which are incompressible, above equation holds rather well. The coefficients of discharge have been measured under various conditions, typically in conjunction with flow measurements through orifice meters. C_D for square-edged circular orifices with pressure taps as close as possible to the orifice plate, as a function of the Reynolds number and with the ratio (hole size/pipe diameter of orifice meters) as a parameter are available from literature (Figure 5-18, Perry and Chilton, 1973).

In the case of a liquid release through an irregular hole on the tank wall, the pipe diameter is ill-defined, and the flow streamlines upstream of the hole are not well established. Under these conditions, the value of coefficient of discharge C_D is expected to differ from that given in the literature. No actual data are reported in the literature for the cases of interest to this study. Considering the limiting diameter ratio as 0.2 (the smallest in the literature data), the coefficient of discharge ranges from 0.25 to about 0.7, depending on the Reynolds number. For large holes or large pressure heads (Re > 100), C_D is typically 0.65.

With this information, and using the equations derived above, we can calculate the venting rate of the liquid from the tank as a function of time. If the pressure above the tank is held constant (due to liquid evaporation or open to the atmosphere, for example), then the above equation can be integrated.

With

h = depth of liquid in the tank

we write the equation for the variation of liquid depth at any time as follows:

$$\rho_\ell \quad A_T \quad \frac{dh}{dt} = - \dot{m} = - C_D \quad \rho_\ell \quad U(h) \quad A_H \qquad (2.3.4)$$

where the velocity U(h) is now a function of the liquid depth h and is calculated by replacing h_L by h in equation 2.3.2. To integrate equation 2.3.4 we define the following parameters.

$$U = \sqrt{[\, A + B\, h \,]} \qquad (2.3.6)$$

$$A = (2/\rho_\ell)\ [(P_T - P_a) - \rho_\ell\ g\ h_H] \qquad (2.3.7)$$

$$B = 2\ g$$

Integration of equation 2.3.4 leads to

$$\dot{m}_o - \dot{m} = [C_D^2\ g\ \rho_\ell\ A_H^2/A_T]\ t = C\ t \qquad (2.3.8)$$

That is, the mass release rate decreases linearly with time. At time, t = 0, the spill rate is given by

$$\dot{m}_o = C_D\ \rho_\ell\ A_H\ U_o \qquad (2.3.9)$$

where U_o is the initial release velocity obtained from equation 2.3.2. The overall duration of the release, t_{spill} is calculated by noting the time for the liquid depth to be equal to the hole height (i.e., h = h_H). This spill duration is given by

$$t_{spill} = [\dot{m}_o/C] = [U_o/(C_D\ g)]\ (A_T/A_H) \qquad (2.3.10)$$

2.3.2 Gas Release

The energy equation indicated in equation 2.3.1 is not valid for compressible gas flows. In general, gas flow through a nozzle and an orifice is analyzed assuming the flow to be compressible and the gas expansion adiabatic, i.e., there is no heat exchange between the gas flowing out of the tank and the ambient (Liepman and Roshko, 1967).

If, in addition, the gas is assumed to be a perfect gas it can be shown that the following relationships hold good for the adiabatically expanding gas.

$$(P/P_T) = (\rho/\rho_T)^k = (T/T_T)^{\frac{k}{(k-1)}} \qquad (2.3.11)$$

where the P, ρ, and T respectively refer to the pressure, density and temperature of the gas in the flowing stream. The subscript T represent the conditions in the tank. The parameter "k" represents the ratio of the vapor specific heat at constant pressure to that of the specific heat at constant volume.

It can be shown by the application of the energy equation and the perfect gas law that the velocity of the gas at any position in the flowing stream is given by

$$U = \sqrt{2\ \frac{k}{(k-1)}\ \left(\frac{P_T}{\rho_T}\right)\ \left(1 - r^{\frac{(k-1)}{k}}\right)} \qquad (2.3.12)$$

where

$$r = (P_a / P_T) = \frac{\text{atmospheric pressure}}{\text{tank pressure}} \qquad (2.3.13)$$

For a given atmospheric pressure P_a as the tank pressure P_T is increased it is seen from equation 2.3.12 that the velocity at the section where the pressure is atmospheric also increases. For increasing tank pressures the exit velocity increases until the velocity at the minimum section ("throat") is equal to the local sonic velocity. Under this condition the flow is said to be "CHOKED" or "CRITICAL". If the tank pressure is further increased the flow is still choked at the throat and has a value consistent with the tank condition; however, the pressure at the throat is no longer equal to the atmospheric pressure, but is higher. The gas further expands from this throat pressure to the atmospheric pressure. In this 'expansion' region the velocity of the gas is further increased.

We discuss below the two conditions of flow of the gas through the orifice, namely, (i) the subsonic flow in which the velocity of gas every where within the flow system is less than the local sound velocity and (ii) the choked flow in which the flow rate is the maximum consistent with the tank conditions.

The critical pressure ratio (r_c) at which the flow is choked is given by,

$$r_c = \left(\frac{P_a}{P_T}\right)_{crit} = \left[\frac{2}{(k+1)}\right]^{\frac{k}{(k-1)}} \qquad (2.3.14)$$

Subsonic Gas Flow ($r > r_c$)

When the pressure ratio given by equation 2.3.13 is larger than the critical pressure ratio (equation 2.3.14) the flow is said to be subsonic. Under these conditions the exit conditions are the same as the conditions at the orifice section (which represents the minimum area of flow).

Velocity at exit is calculated using equation 2.3.12. The pressure at exit is the ambient pressure. The density and temperature at exit are given by equation 2.3.11. The area of the flow at exit is the same as the area of the orifice.

The mass flow rate ($\dot{m}$) is given by the following equation.

$$\dot{m} = A_H \quad \rho_H \quad U_H \, Y \qquad (2.3.15)$$

where the subscript H represents the conditions at the hole and Y is the expansion factor given by the following expressions (Perry and Chilton; 1973, p 5-11) for nozzles and orifices in which the hole size is small compared to the tank diameter.

$$Y = \left[r^{(2/k)} \frac{k}{(k-1)} \frac{1 - r^{(k-1)/k}}{1 - r} \right]^{1/2} \qquad (2.3.16)$$

The values expected of Y for various values of (1-r)/k for orifices, nozzles and venturies are given in the literature (Figure 5-14, Perry and Chilton, 1973). For large pressure difference (r = 0), Y is typically about 1, and decreases significantly for smaller pressure differences between P_T and P_s.

In the case of an orifice plate, the expansion factor Y for the subsonic flow of gas through the hole is given by

$$Y = 1 - 0.41\,[(1-r)/k] \qquad (2.3.17)$$

While the nozzle allows for the streamlines to properly converge at the exit, the orifice does not provide such a mechanism. A typical hole in a tank cannot be characterized by either type alone. Thus, the expansion factor for the actual case can be expected to fall in the range of values predicted by equations, 2.3.16 and 2.3.17, respectively, for the nozzle and for the orifice.

Sonic (Choked) Gas Flow ($r < r_c$)

The flow is choked and the velocity at the throat is equal to the local sonic speed if the ratio of the atmospheric pressure to that of the tank pressure is less than the critical value given in equation 2.3.14. Under these conditions, the overall flow characteristics differ from those described above. Such a situation will prevail, typically for small holes and high tank pressures.

The conditions at the throat can be described by the following equations.

$$T_{Th} = \frac{2}{(K+1)} T_T \qquad (2.3.18)$$

$$P_{Th} = r_c P_T \qquad (2.3.19)$$

$$U_{Th} = a = \sqrt{k R T_{Th}} \qquad (2.3.20)$$

$$\rho_{Th} = r_c^{(1/k)} \rho_T \qquad (2.3.21)$$

The choked mass flow (or the critical mass flow) is given by the expression,

$$\dot{m}_c = \rho_{Th} A_H U_{Th} Y \qquad (2.3.22)$$

In the above equations "a" represents the sonic velocity, subscript "Th" indicates the throat condition and all other parameters have the same meaning as before. If we assume that in the sonic flow situation the "throat" is represented by the orifice then the conditions at the exit (which are needed for the gas dispersion analyses) are determined from the throat conditions and the fact that the gas has to further expand to the atmospheric pressure.

Defining,

$$r = P_a/P_T$$

we can show that the following expressions represent the exit conditions for the gas (exit condition in this context is to be regarded as condition prevailing a few diameters down stream from the orifice).

$$\dot{m}_e = \dot{m}_c \qquad (2.3.23)$$

$$U_e = U_{Th} + [(P_{Th} - P_a)\, A_H]/\, \dot{m}_c \qquad (2.3.24)$$

$$T_e = r^{((k-1)/k)}\, T_T \qquad (2.3.25)$$

$$\rho_e = r^{(1/k)}\, \rho_T \qquad (2.3.26)$$

$$A_e = \frac{\dot{m}_c}{U_e\, \rho_e} \qquad (2.3.27)$$

where the subscript "e" represents the exit condition of the gas. The parameters given in equations 2.3.23 through 2.3.27 are used for assessing the down wind dispersion of the gas stream.

Tank Pressure Variation With Time

In the case of a liquid release through a small hole, we had assumed that the flow does not change the upstream pressure head significantly. The same cannot be said of the gas release situation. Gas vented from a pressurized gas storage reduces the tank pressure. Assuming the gas in the tank to behave as ideal gas, we write the mass balance equation as follows:

$$\frac{dM_T}{dt} = - \dot{m}(t) \qquad (2.3.28)$$

In the above equation, the mass of vapor in the tank (M_T) can be expressed in terms of tank pressure and temperature (ideal gas equation). Mass flow rate on the RHS of the above equation can be

expressed in terms of tank pressure and tank gas temperature (Equations 2.3.15 and 2.3.22).

To solve for the tank pressure as a function of time, the tank wall condition has to be specified; i.e., whether the tank wall is insulated ("adiabatic") or the tank gas temperature is maintained constant ("isothermal") is to be specified. The tank pressure "blow down" under these two conditions is analyzed below. Analytical solution can be obtained for the case when the flow rate out of the tank is critical. We first define the following common parameters.

$$t_{ch} = M_T / \dot{m}_o = \text{characteristic blow down time} \qquad (2.3.29)$$

$$P = P/P_T = \text{ratio of tank pressure to initial pressure} \qquad (2.3.30)$$

$$\tau = t/t_{ch} = \text{dimensionless time} \qquad (2.3.31)$$

Isothermal Tank and Critical Mass Flow

This condition implies

$$T = T_T = \text{constant with time}$$

Hence, the mass balance Equation 2.3.28 can be written using the perfect gas law as:

$$\frac{d}{dt}\left(\frac{P\,V}{R\,T}\right) = -\dot{m}_c(P,T) \qquad (2.3.32)$$

where $\dot{m}_c$ is the critical flow given in equation 2.3.22. Using the Equations 2.3.29, through 2.3.31, we write the above equation in the non-dimensional form as

$$\frac{dp'}{d\tau} = -p' \; ; \quad p' = 1 \text{ at } \tau = 0 \qquad (2.3.33)$$

The solution is

$$p' = P/P_T = e^{(-\tau)} \qquad (2.3.34)$$

This equation will be valid until the tank pressure drops to such a value that the mass flow rate is no longer critical.

Adiabatic Expansion of Tank Gas & Critical Flow

The relationship between the pressure and temperature for adiabatic expansion of the gas

$$T \; p^{(1-k)/k} = \text{constant} \qquad (2.3.35)$$

Substituting Equation 2.3.35 in Equation 2.3.32, using Equation 2.3.22 and the definitions in Equation 2.3.29 through 2.3.31, we get

$$\frac{d\,(p')^{1/k}}{d\,\tau} = (p')^{(k+1)/(2k)} \quad \text{with} \quad p' = 1 \text{ at } \tau = 0 \qquad (2.3.36)$$

The solution to the above equation is (for K > 1)

$$p' = \frac{1}{\left[1 + \frac{(k-1)}{2}\,\tau\right]^{(2k/(k-1))}} \qquad (2.3.37)$$

Application of Gas Flow Models to a Specific Case

The above equations are used to calculate the venting rates for the release of a pressurized chlorine gas from a tank. The following conditions are assumed.

Tank Volume	=	V_T	= 0.13	m^3
Initial Tank Pressure	=	P_T	= 1 to 3	atm
Tank Temperature (assumed held constant)	=	T_T	= 300	K
Diameter of hole thru which the gas escapes	=	D_H	= 0.035	m

The results from the above models are indicated in Figure 2.3.1 and Figure 2.3.2. The mass flow rate and the density of the vapor at exit are indicated in Figure 2.3.1 as function of the tank pressure. It is seen that as the tank pressure increases from the atmospheric value the exit mass rate and the exit gas density increase continuously. Choking condition results when the tank pressure is 1.84 atmospheres. For tank pressures above this the mass flow rate varies linearly with the tank pressure as should be the case for a choked flow (see equation 2.3.22).

In our calculations the exit condition is represented by that section down stream of the orifice at which the pressure is equal to the atmospheric pressure. For sub-sonic flow this condition occurs at the orifice section. For the critical flow the atmospheric pressure in the gas stream occurs a few hole diameters down stream of the orifice.

If the gas temperature in the tank is maintained a constant, the temperature at the throat remains a constant when the flow is choked.

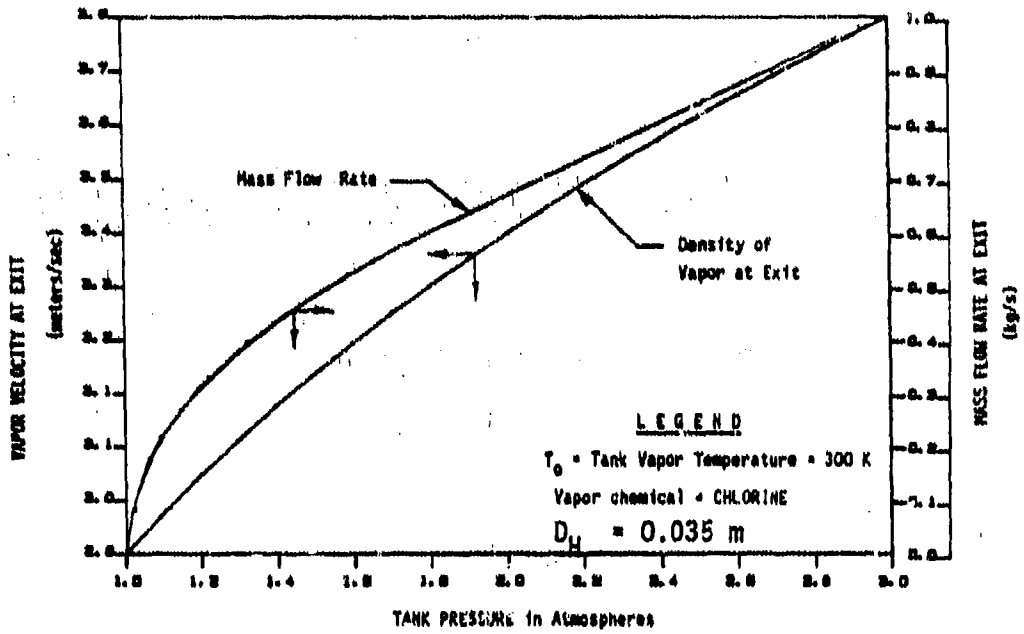

Figure 2.3.1: Results from Gas Flow Model: Variation of Mass Flow Rate and Density of Gas at Exit Section

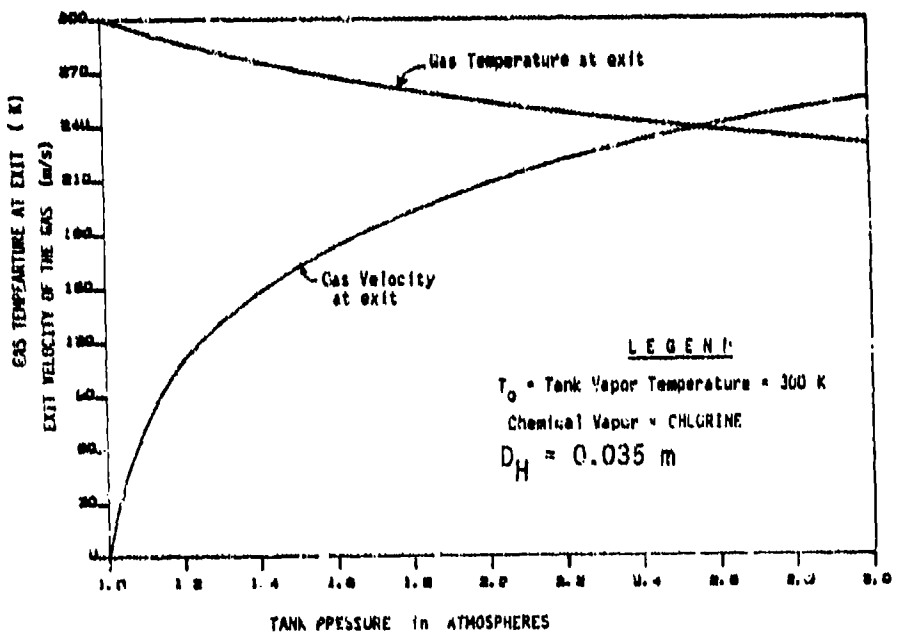

Figure 2.3.2: Results from Gas Flow Model: Variation of Exit Gas Temperature and Velocity

This is because the pressure ratio attains the critical value (and hence remains constant) and because of our assumption of perfect gas behavior. Figure 2.3.2 shows the gas exit velocity and the exit temperature as functions of tank pressure. It is seen that the temperature drops continuously and the gas velocity increases continuously as the tank pressure increases. It is to be noted that when the flow is choked, the velocity at the throat is sonic corresponding to the condition at the throat; however, the gas is further accelerated from the throat to the "exit" section.

At 3 atmospheres tank pressure and 300 K temperature the total mass of gas in the tank is 1.12 kg. It is also seen from Figure 2.3.1 that the mass release rate initially for the above condition is 1 kg/s. At this rate of mass flow the characteristic tank emptying time is about 1.12 s. From equation 2.3.34 it can be shown that the critical flow lasts for about 0.55 seconds and within this time about 40% of the mass within the tank is vented.

2.4 LIQUID FLASH MODEL

When a pressurized liquid stored at ambient temperature is released into the atmosphere it "flashes"; i.e., a part of the liquid released evaporates, spontaneously, to vapor. The vapor and the unflashed liquid at atmospheric pressure will be at the saturation temperature corresponding to the atmospheric pressure. This temperature is lower than the storage temperature. In this section we discuss the equations to calculate the mass fraction of the released liquid that flashes to vapor upon release.

Consider the release of 1 kg of liquid stored at a pressure of P_T and temperature T_T. It is assumed that the storage pressure is the saturation pressure corresponding to the storage temperature. Assuming the flashing to be an adiabatic process, we write the following energy balance equation on the unit mass of liquid chemical released.

$$h_\ell^{sat}(P_T) = f_v \; h_v^{sat}(P_a) + f_\ell \; h_\ell^{sat}(P_a) \qquad (2.4.1)$$

$$f_v + f_\ell = 1 \qquad (2.4.2)$$

where,

f_v = mass fraction of the chemical released which is in the form of saturated vapor, at atmospheric pressure.

f_ℓ = Mass fraction of the chemical released which is in the form of liquid at saturation temperature, at atmospheric pressure.

P_a = Atmospheric pressure

It can be shown from equations 2.4.1 and 2.4.2 that the fraction mass of vapor produced is,

$$f_v = \frac{[\, h_\ell^{sat}(P_T) - h_\ell^{sat}(P_a) \,]}{\lambda(P_a)} \qquad (2.4.3)$$

In the above equation λ represents the heat of vaporization of the liquid at ambient pressure conditions.

2.5 LIQUID POOL SPREAD & EVAPORATION MODELS

2.5.1 Description of Physical Process

A liquid spilled onto the ground spreads. The spreading will continue unless the pool is contained by a dike wall or channeled into a sump, or the liquid has spread to such an extent that its thickness is of the same order of magnitude as the ground roughness elements. Depending on the properties of the liquid and the ambient conditions (ground temperature vis-a-vis the liquid temperature, wind, ambient temperature, etc.), the pool may evaporate rapidly or slowly.

In this section, we discuss the spreading evaporation of liquid pools on the ground. In Section 2.5.2, the evaporation of a high vapor pressure liquid pool is discussed. These models are generally applicable to non-cryogenic liquid releases. In Section 2.5.3, the models and equations applicable to cryogenic liquid spills are described. Where appropriate, both evaporation and spreading are considered together.

The principal purpose of the models described below is to evaluate the total mass rate of generation of vapor which then subsequently disperses in the atmosphere. Vapors generated by an evaporating pool are moved to the downwind edge of the pool by the prevailing wind. A wind uptake model describing this process is discussed in Section 2.5.4.

2.5.2 Non-cryogenic Liquid Evaporation Model

2.5.2.1 The Evaporation Model

Consider the evaporation from a pool of liquid depicted, schematically, in Figure 2.5.1. The liquid pool is subject to heat transfer from a number of sources such as the wind (convective heat input), the ground, solar and ambient radiation, etc. If the net heat input into the pool is positive, evaporation occurs. We write the following energy balance equation for the liquid pool system under a quasi-steady state condition (i.e., neglecting the changes in the internal energy of the liquid).

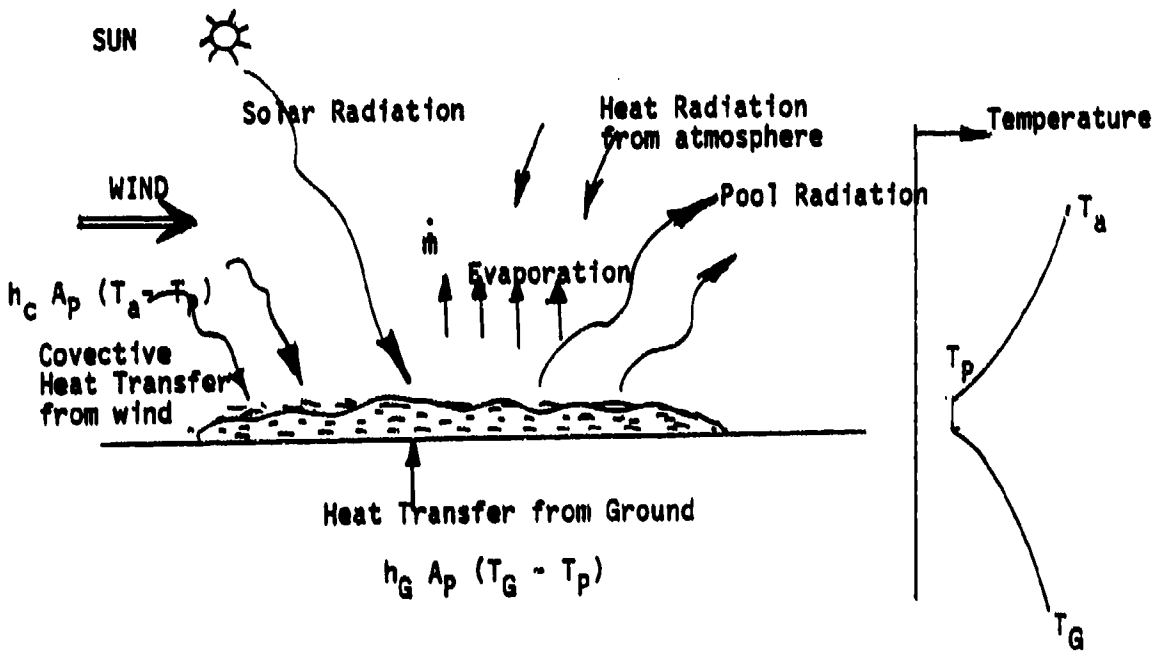

Figure 2.5.1: Schematic Representation of the Heat Transfer to a Liquid Pool on the Ground

$$\dot{m} = (A_p/\lambda)\ [\dot{q}''_A + \dot{q}''_s + \dot{q}''_G + \dot{q}''_c - \dot{q}''_E] \qquad (2.5.1)$$

where,

$\dot{m}$ = mass rate of evaporation

A_p = pool area

$\dot{q}''_G$ = heat flux from the ground

$\dot{q}''_s$ = heat flux into the pool due to solar radiation

$\dot{q}''_A$ = heat flux from diffuse atmospheric radiation

$\dot{q}''_c$ = convective heat flux from the wind

$\dot{q}''_E$ = radiative loss of heat (per unit area) from the pool.

Most of the heat flux terms are dependent on the liquid pool temperature (T_p). The value of T_p is determined by the equilibrium conditions (i.e., satisfaction of Equation 2.5.1) and has to be determined by a trial and error scheme. The liquid temperature is, however, expected to be between the normal boiling point and the normal freezing point of the chemical. Described below are the expressions for the various terms in the heat balance Equation 2.5.1.

Ground Heat Flux ($\dot{q}''_G$)

Assuming that initially the ground is at a uniform temperature (T_G) and is warmer than the liquid temperature, we write the following equation to estimate the heat flux from the ground (see Raj, 1981):

$$\dot{q}''_G = \frac{K_G\ (T_G - T_P)}{[\sqrt{\pi\ \alpha_G\ t} + K_G/h_{C,L}]} \qquad (2.5.2)$$

where,

α_G = thermal diffusivity of the ground

$h_{C,L}$ = natural convective heat transfer coefficient within the liquid layer

t = time from the instant the liquid contacts the ground

In writing the above equation, it has been assumed that

a) one dimensional heat transfer theory is applicable;

b) the liquid pool bulk temperature T_p does not change substantially.

Ille and Springer (1978) go to great lengths to estimate the heat transfer coefficient $h_{c,L}$ within the liquid layer. However, for non-cryogenic liquid spills, it is found that the contribution from ground to the overall heat input is relatively small compared to that from the wind. Also, in most cases of interest to this study, the liquid layer is expected to be relatively thin and, therefore, the natural convective effects within the liquid layer (for transferring heat from the ground surface to the liquid film) are negligible. In short, for most practical purposes, the heat transfer resistance due to the natural convection circulation within the liquid film can be neglected (i.e, $h_{c,L} \rightarrow \infty$) such an assumption reduces the complexity of the model substantially without compromising the accuracy of prediction of the evaporation value. This is a significant difference between our model and the model due to Ille and Springer (1978).

2.5.2.2 Net Radiation Exchange Between the Atmosphere and the Pool

The heat flux exchange between the atmosphere (at T_A) and the pool (at T_p) consists of two terms: $\dot{q}''_A$, heat flux radiated from atmosphere to the pool, and $\dot{q}''_E$, the heat flux emitted from the pool to the atmosphere. Assuming that the atmosphere forms a hemispherical canopy over the pool enclosure, the view factor between the pool and the atmosphere can be found to be unity. Under these conditions,

$$\dot{q}''_A = \dot{q}''_{atm \rightarrow pool} = \epsilon_A \sigma T_A^4 \qquad (2.5.3a)$$

$$\dot{q}''_E = \dot{q}''_{pool \rightarrow atm} = \epsilon_p \sigma T_p^4 \qquad (2.5.3b)$$

where,

ϵ_A - emissivity of the atmosphere (assumed to be 0.75)

ϵ_p - emissivity of the liquid pool (assumed to be 0.95)

σ - Stefan-Boltzman constant = 5.6697E-8 W/m^2k^4

It should be noted that the values assumed for the emissivities are tentative, and no rigorous basis exists for their estimation. For fully transparent media, one could assume the value of the emissivities to be close to zero, and for radiately "black" media, these values approach unity. It can be shown that the overall contribution of these two terms, namely the net radiation flux for heat exchange between the atmosphere and the pool

$$\dot{q}''_{Rad} = \dot{q}''_A - \dot{q}''_E = \sigma (\epsilon_A T_A^4 - \epsilon_p T_p^4) \qquad (2.5.4)$$

is much smaller than the other terms in the energy balance equation, and thus, the overall results are insensitive to the values selected for ϵ_A and ϵ_p.

Convective Heat Transfer into the Pool by the Prevailing Wind ($\dot{q}''_c$)

The wind, blowing at speed U_{wind}, over the liquid pool sets up a forced convection boundary layer. Heat is transferred across this boundary layer by convection. The wind heat transfer coefficient, h_{wind}, is normalized using the Nusselt number $Nu = (h_{wind}\ l_p/K_v)$ where l_p is the length of the pool along the wind direction and K_v is the vapor thermal conductivity. For computational purposes, l_p is taken to be the diameter of the circular liquid pool of area, A_p. Thus,

$$l_p = 2\ [A_p/\pi\ ]^{1/2} \qquad (2.5.5)$$

From heat transfer correlations, Nu can be expressed as

Nusselt Number: $Nu = 0.037\ (Re^{0.8} - 15500)\ Pr^{1/3}$ (2.5.6a)

Reynolds Number: $Re = (U_{wind}\ \ l_p)/\ \nu$ (2.5.6b)

Prandtl Number: $Pr = (\nu/\alpha)$ (2.5.6c)

where, ν and α are, respectively, the kinematic viscosity and the thermal diffusivity of the vapor emanating from the liquid pool. Strictly speaking, one should use the vapor-air mixture properties (as Ille and Springer do); our computations, however, indicate that the error incurred in using the pure vapor properties is not significant, and it considerably simplifies the overall computational scheme.

The net heat flux for transfer from the ambient air to the pool is then given by

$$\dot{q}''_c = h_{wind}\ [T_A - T_p\ ] \qquad (2.5.7)$$

where T_A is the ambient temperature.

Evaporative Loss from the Pool

The vapor is transferred to the ambient by mass transfer through the boundary layer. From mass transfer correlations, the rate of evaporation is governed by the relation

$$\dot{m} = h_m\ A_p\ (c_o - c_\infty) \qquad (2.5.8)$$

where h_m is the mass transfer coefficient, c_o and c_∞ are the concentrations of the chemical (vapor) at the surface $[c_o = (M_w\ P^{sat})/(R\ T_p)]$ and at locations very far from the pool. Using the transport analogies between heat transfer and mass transfer, one can express the mass transfer coefficient as

$$h_m = [\nu/l_p]\ \ 0.037\ \ Sc^{-2/3}\ (Re^{0.8} - 15500) \qquad (2.5.9)$$

where Sc is the Schmidt number ($Sc = \nu/D$), D is the molecular diffusion coefficient of the vapor in air, ν is the kinematic

viscosity of the vapor, l_p is the length of the pool, and Sc is the Schmidt number. Thus, the rate of evaporation from the pool is given by

$$\dot{m} = (\nu/l_p)\ 0.037\ Sc^{-2/3}\ (Re^{0.8} - 15500)\ *\ [A_p]\ *\ [(M_w\ P_{SAT})/(R\ T_p)] \qquad (2.5.10)$$

Solar Insolation to Liquid Pool

The heat influx into the pool due to solar insolation is dependent on parameters such as the location of the spill, the time of day, cloud conditions, etc. Algorithms are available with which one can evaluate the total energy incident on the surface by solar radiation, and these are detailed in Chapter 4 of this report. For the purpose of our calculations of solar heat flux, $\dot{q}''_s$, we adopt the algorithms outlined in Chapter 4.

2.5.2.1 Non-Cryogenic Liquid Pool Spread

In general, the rate of mass loss from a non-cryogenic liquid pool is low (compared to that in a cryogenic liquid) and therefore, for all practical purposes, the pool spread can be modeled assuming a mass conserved system. The spread of an instantaneously released liquid mass on a substrate has been modeled by Fay (1969) and Raj (1981). It is seen that the liquid spreads radially in three distinct regimes; namely, (i) gravity-inertia regime in which the gravitational acceleration on the liquid mass is counter balanced by the inertia, (ii) gravity-viscous regime in which the gravitational spreading force is opposed by the friction at the liquid-substrate interface and, finally (iii) when the liquid film is very thin, the surface tension forces become important.

For the purposes of downwind vapor dispersion hazard calculations arising from the spill of a low vapor pressure, non-cryogenic liquid, it is conservative to assume that the time to spread to the final area is relatively short compared to the total time to evaporate all of the liquid. With this assumption, we use the following criteria to determine the final liquid spread area for the case of an instantaneously released liquid.

Final Spread Area = [Dike area if the pool is diked
OR
The area of the pool when the mean film thickness is equal to the ground roughness element depth.]

In the case of a continuous release of a non-cryogenic liquid, we assume that the liquid film thickness is always equal to the mean ground roughness height. Therefore, the pool area is dependent on time.

2.5.2.4 Example for a Non-Cryogenic Spill Evaporation

Consider the spill of N_2O_4 liquid at its saturation temperature of 294K. Other conditions assumed are as follows:

Ambient Temperature	=	295 K (22°C)
Ground Temperature	=	295 K
Wind Speed	=	2 m/s to 12 m/s
Pool Area (assumed)	=	100 m^2

Using the model presented above, the mass rate of evaporation (m) is calculated for various times after spill. These results for different wind speeds are shown in Figure 2.5.2(a). The pool temperature variation with time is shown in Figure 2.5.2(b). The kinks in the graph occur where temperature iterations have been halted because the pool temperature is within one degree Kelvin of the freezing point.

It is seen that at a wind speed of 2 m/s the evaporation rate decreases from about 0.25 kg/s (9 kg/hr m^2) at 1 minute to about 0.125 kg/s (4.5 kg/hr m^2) at 30 minutes. Throughout this time, the pool temperature drops constantly from 277 K to 263 K. In fact, it can be seen clearly from Figure 2.5.2(a) that the evaporation rate is falling off as the inverse square root of time consistent with Equation 2.5.2.

At higher wind speeds, the pool evaporation rate is higher for all times and the pool temperature drops more quickly than the 2.0 m/s wind speed case. For example, at a wind speed of 6 m/s, the evaporation rate is about 0.45 kg/s (16.2 kg/hr m^2) at 1 minute and it drops to about 0.27 kg/s (9.7 kg/hr m^2) at 30 minutes. The pool temperature also drops from 272 K to 262 K.

These results indicate that, at effect of heat and mass transfer by the wind on the pool evaporation rate is significant. Direct solar radiation may be important depending on the time of the year, location of the spill and time of day.

2.5.2.5 Non-Cryogenic Spill Into a Diked Area

The model presented in the previous section (simplified Ille and Springer Model) is applicable to cases wherein the heat transfer exists from and to ground. If the heat transfer with the ground is

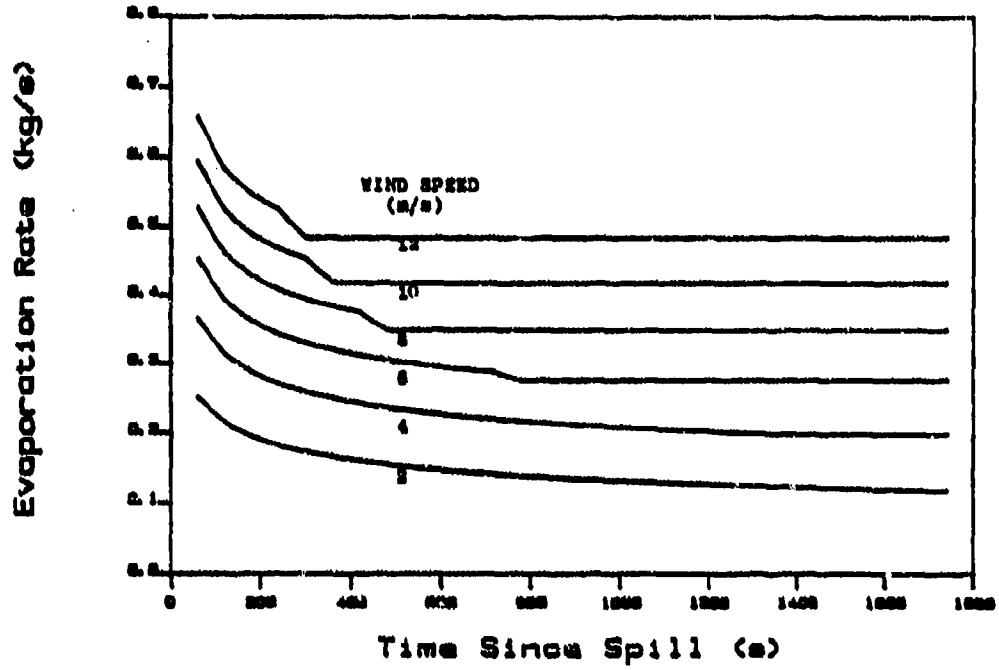

Figure 2.5.2 (a): Evaportion Rate vs Time for various Wind speeds

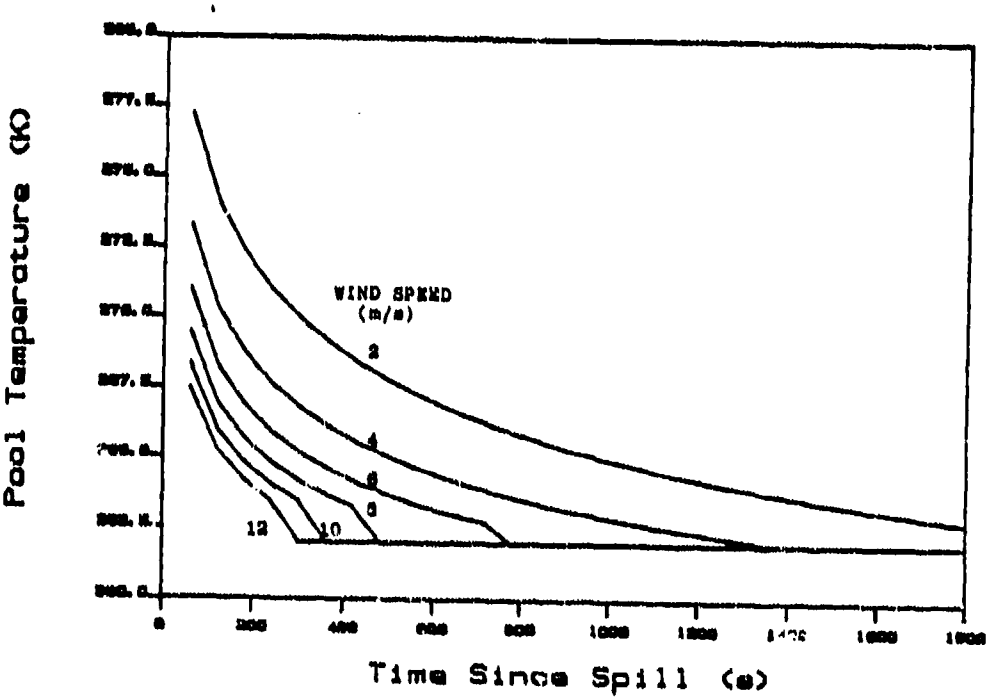

Figure 2.5.2 (b): Pool Liquid Temperature vs Time for different Wind Speeds

Figure 2.5.2: Changes in Evaporation Rate and Pool Temperature with Time for different Wind Speeds for N_2O_4 Liquid Pools

negligible (insulated ground), or if the liquid released is at ground temperature, then the resulting equations can be simplified. The results presented in this case pertain to non cryogenic case, wherein the heat transfer from the ground is negligible.

The pool is of radius R_p and height h. The dike size determines the pool radius. It is assumed that, as the evaporation proceeds, the radius of the pool is constant, and the height of the pool gradually decreases from h_o until the liquid in the pool disappears.

The material loss due to evaporation $\dot{m}$ can be related to the wind speed, U_{wind}, and the pool radius R_p. The relationship is

$$\dot{m} = h_m \left[(P^{sat} M_w)/(R T_p)\right] \pi R_p^2 \qquad (2.5.11)$$

where h_m is the mass transfer coefficient, given by

$$h_m = [\nu/2 R_p] \, 0.037 \, Sc^{-2/3} \, (Re^{0.8} - 15500) \qquad (2.5.12)$$

$$Re = (2 U_{wind} R_p/\nu) \qquad (2.5.13)$$

It should be noted that the above relation is valid for large Reynolds numbers and where the heat and mass transfer boundary layers are well developed, and may not be applicable for small spills.

Evaporation of nitrogen tetroxide (N_2O_4) was modeled using the above simplified equations and the results were compared with available test data. TRC (1986) report the results from a laboratory experiment to determine N_2O_4 evaporation. The test conditions and the measured evaporation rate are indicated in Table 2.5.1.

Table 2.5.2 compares the results obtained with the above model with those indicated in the TRC review report of the evaluation of various spill models. It can be observed that the results computed from the above equations are in excellent agreement with the observed results. Thus, we can conclude that, in Edgewood # 6 test, the dominant effect is due to the convective boundary layer set up by the wind, and other forms of heat transfer do not play a significant role.

2.5.3 Cryogenic Liquid Spill Spread & Evaporation Models

As explained in Section 2.2, a liquid spill is considered to be a cryogenic spill if the temperature of the liquid is substantially lower than that of the ambient ground temperature. In such a spill, the heat transfer rate from the ground is substantially higher than that of transfer rate from any other process (wind, solar, etc.). A finite volume of a cryogenic liquid spill into an unconfined area will result in spread and evaporation very rapidly before the ground cools off sufficiently to reduce the evaporation rate. However, in the case of a diked spill, the evaporation is high in the beginning but falls off rapidly as the liquid pool cools the ground.

TABLE 2.5.1

LABORATORY TEST RESULTS AND MODEL RESULTS FOR THE EVAPORATION OF N_2O_4 POOL

Test Conditions

Test:	Edgewood #6 reported by TRC (1986)
Substrate:	Stainless Steel tray 1.22 m x 1.22 m (square)
Volume Spilled:	0.03 m^3 (45.35 kg)
Initial Depth of Pool:	0.02 m
Initial Liquid Temperature:	268.4 K
Wind Speed:	5 .8 m/s
Air Temperature:	291.0 K
Measured Evaporation Rate:	18.6 kg/hr

Model Results (Equation 2.5.11)

Saturation Pressure of N_2O_4 at 268.4 K	=	26967.3 N/m^2	
Liquid Density	=	1511.9 kg/m^3	
Vapor Density	=	1.11 kg/m^3	
Schmidt Number	=	5	
Calculated Value of Reynolds #	=	Re =	2.03 x 10^6
Mass Transfer Coefficient	=	h_m =	11.1 m/hr
Calculated Evaporation Rate * (at 1000 s after spill)	=	m_{ev} =	18.11 kg/hr

---

* Note in our model because the heat transfer from the ground varies with time, a particular time at which evaporation has to be evaluated, has to be given. At times of the order of 1000 s, the ground heat transfer contribution is small and steady state evaporation results for the above case.

Table 2.5.2

COMPARISON OF RESULTS FROM VARIOUS POOL EVAPORATION MODELS IN THE LITERATURE (TRC, INC., 1986)

Model	Computed Evaporation Rate (kg/hr)
Illinois EPA	64
AWS Model	103
Army Model	172
USAF ESL Model	59
Ille & Springer	49
Shell SPILLS	59
Predictions from equations (2.5.11)	18.11
Experimental Value	18.6

The evaporation and spreading of a cryogenic liquid released into a diked area has been analyzed by Reid and Raj (1974). The spread and evaporation of a cryogenic liquid on land under a variety of conditions has been modeled by Raj (1981). In these analyses, the thermal boundary layer under a spreading liquid pool has been described, the heat transfer rate to the liquid pool is calculated and the coupling between the spreading (described by hydrodynamic equations) and the evaporative mass loss has been considered. Expressions have been obtained to calculate the spread radius and evaporation rate as a function of time for both instantaneous and continuous releases. Also given are the maximum radius and time to reach maximum radius.

Table 2.5.3 shows the results obtained. The Table defines the parameters and provides equations for calculating the non-dimensional radius of pool, the volume of liquid remaining and the rate of evaporation from the pool for any specified instant of time. Details of the models are not indicated here since they are described in detail in the referred technical publication.

2.5.4 Wind Uptake Model

The vapors emanating from a liquid pool are swept by the wind and carried downwind. Hence, at the downwind edge of the pool the mass flow rate of vapors will be given by a time weighted integral of evaporation rates from the various sections of the pool. For small radius pools and in cases where wind speed is high, the downwind vapor mass flow rate is equal to the total evaporation rate. In cases where these conditions are not true, the "transit" time of vapor from the location of generation to the downwind of edge of pool should be taken into consideration. A model is indicated below to calculate the vapor source strength at the downwind edge of the pool.

In this analysis, it is assumed that:

a. The pool is circular,
b. The gas released by liquid evaporation is immediately "picked up' by the wind,
c. wind speed is constant,
d. vapor moves downwind at wind speed,
e. evaporation rate varies with time, but is the same at all physical locations in the pool.

Consider an elemental area of circular pool formed (Figure 2.5.3) by a chord at upwind location x from the downwind edge of the pool and of width dx. Let $\dot{m}''(t)$ = evaporation flux at any time.

Table 2.5.3: Summary of Model Results for the Case of Cryogenic Liquid Spill On Water & Land

Spill environment	Spill characterization and details	Scaling parameters: length (L)	Scaling parameters: time (t_{ch})	Characteristic parameter
Land spill	Continuous spill at volumetric rate $\dot{V}_L$	$L = \left[\frac{2}{\pi^{3/2}} \frac{\lambda \rho_L \dot{V}_L}{\sqrt{(K\rho C)_G}\Delta T}\right]^{1/2} t_{ch}^{1/2}$	t_{ch} can be chosen arbitrarily	—
	Continuous spill for finite duration V_L, volume spilled over period t_s $\dot{V}_L = V_L/t_s$	$L = \left[\frac{2}{\pi^{3/2}} \frac{\lambda \rho_L \dot{V}_L}{\sqrt{(K\rho C)_G}\Delta T}\right]^{1/2} t_s^{1/2}$	$t_{ch} = t_s$	$A = \left[\frac{\pi L^4}{V_L c^3 g t_s^3}\right]^{1/2}$
	Instantaneous spill of volume V_L	$L = V_L^{1/3}$	$t_{ch} = \sqrt{\frac{L}{g}}$	$B = \left[\frac{\sqrt{\pi}}{2} \frac{\sqrt{(K\rho C)_G}\Delta T}{\lambda \rho_L \sqrt{t_{ch} g L}}\right]$
Water spill	Continuous spill at volumetric rate $\dot{V}_L$	$L = R_{max} = \left[\frac{\dot{V}_L}{\pi \dot{y}}\right]^{1/3}$	$t_{ch} = \frac{L}{[c^2 g L \dot{y}]^{1/3}}$	—
	Instantaneous spill of volume V_L	$L = V_L^{1/3}$	$t_{ch} = \sqrt{\frac{L}{g}}$	$D = \frac{\dot{y}}{\sqrt{gL}}$
Land spill	$t = \tau^{1/2}$	—	—	In the land spill, the heat transfer rate varies with inverse square root of time
	Approximate solutions given in eqns (18) and (19) exact solution has to be obtained numerically	See Fig. 1		$t = \frac{R}{L}$ $\tau = \frac{t}{t_{ch}}$ $\kappa = \frac{V}{V_L}$ $1 < c < \sqrt{2}$
	$t = [1.3\tau + 1.415\tau^{1/2}]^{1/2}$ $\kappa = 1 - [0.867 B \tau^{3/2} + 0.472 B^2 \tau^3]$	$t_e = \frac{0.897}{B^{1/3}}$	$\tau_e = \frac{0.4617}{B^{1/3}}$	
Water spill	$\tau = 1.7938 t^2 / 2(\frac{1}{2}, \frac{3}{2})$ $\kappa = (\frac{1}{c})^{1/2} t^{3/2} \left[1 - \frac{t^2}{2}\right]^{3/2}$	$t_e = 1$	$\tau_e = 0.897$	For spill on water, the heat flux is assumed to be a constant $g' = g\left(1 - \frac{\rho_L}{\rho_w}\right)$
	$t = [1.3\tau + 0.442\tau^2 D]^{1/2}$ $\kappa = 1 - 2.04 D\tau^2 - 0.3473 D^2 \tau^4$	$t_e = \frac{1}{D^{1/4}}$	$\tau_e = \frac{0.6743}{D^{1/2}}$	$I_\kappa(y,z)$ is the incomplete beta function

Source: Raj (1981)

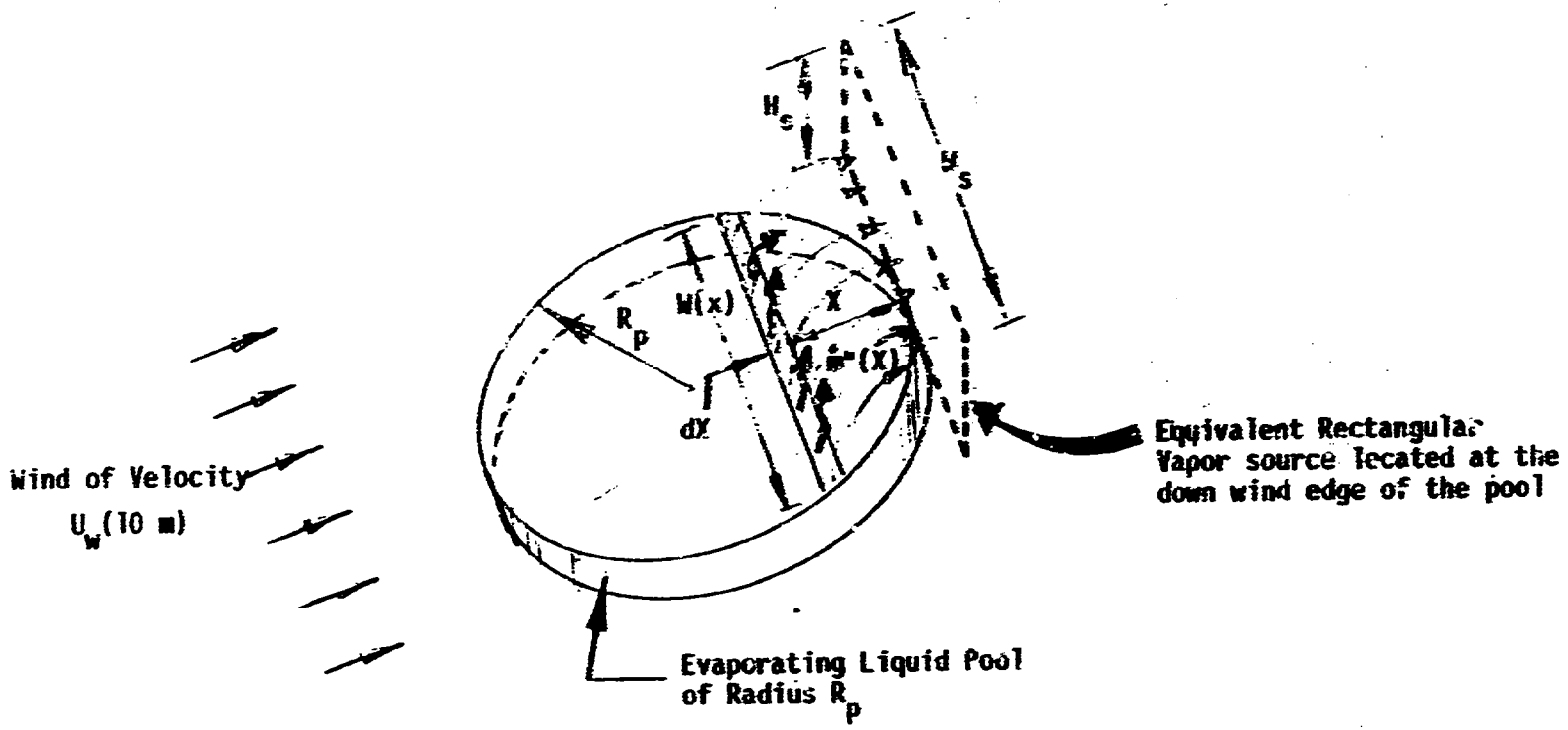

FIGURE 2.5.3: Schematic Representation of the Uptake of the Vapor Generated by an Evaporating Pool and the Down Wind Edge Vapor Source.

The total mass of vapor liberated in unit time by this elemental area is

$$\dot{M}_x(t) = W\,dx\;\dot{m}''(t) = 2R_p \sin\theta\;dx\;\dot{m}''(t) \qquad (2.5.14)$$

A mass of vapor generated at time $t-(x/U_{wind})$ arrives at the downwind edge at time t. Hence, the total mass flow rate at the downwind edge at any time t after the spill and beginning of the evaporation is

$$\dot{M}(t) = \int_{x=0}^{x \text{ or } D} W(x)\,dx\;\dot{m}''[t-(x/U_{wind})] \qquad (2.5.15)$$

Noting that,

$$W^2 = 4x(2R_p - x) \qquad (2.5.16)$$

$$\dot{M}(t) = 2\int_{x=0}^{x = U_{wind}\,t \text{ or } D \text{ (whichever is less)}} [x(2R_p-x)]^{1/2}\;\dot{m}''[t-(x/U_{wind})]\,dx \qquad (2.5.17)$$

or, in non dimensional coordinates,

$$\dot{M}(t) = 2D^2\int_{\eta=0}^{\eta = \tau \text{ or } 1 \text{ (whichever is less)}} \dot{m}''[t_{tr}(\tau-\eta)]\,[1-\eta]^{1/2}\,[\eta]^{1/2}\,d\eta \qquad (2.5.18)$$

where;

$$t_{tr} = \text{transit time} = (2R_p/U_{wind}),$$
$$\eta = \text{non dimensional length} = (x/2R_p) \qquad (2.5.19)$$
and $$\tau = \text{non dimensional time} = (t/t_{tr})$$

If the transit time t_{tr} is small compared to the evaporation and dispersion time scales, then, the uptake model does not significantly alter the calculated results. On the other hand, if this time is large compared to the other time scales, then one should include the wind uptake model to correct the expected source strength values.

For calculating the vapor dispersion hazard from a continuous vapor source, we assume a rectangular vapor source (see Chapter 5). In order to be compatible with this description of the vapor source, we define the vapor source width W_s to be equal to the pool diameter.

Estimation of the height of the source downwind is very difficult and there are no models available in the literature. If the vapors generated are heavier than air, then we calculate the vertical extent or the depth of the source by the following formula:

$$H_s = H_c + 2\ \sigma_z(2\ R_p) \qquad (2.5.20)$$

where,

H_c = The vertical extent or the depth of source in the case of pure vapor flow

$$H_c = \frac{\dot{M}(t)}{\rho_v\ W_s\ U_w\ (H_c)} \qquad (2.5.21)$$

$\sigma_z(2R_p)$ = Vertical diffusion coefficient for distance $2R_p$ assuming a stable atmosphere if the gases are dense and a neutral atmosphere if the gases are lighter than air (see Chapter 4).

and $\bar{U}_w(H_c)$ = Mean wind speed over a height H_c.

Hence, the vapor volumetric or molar concentration at the downwind edge source is

$$C_1 = \frac{H_c}{H_c + 2\ \sigma_z} \qquad (2.5.22)$$

The above equations completely define the vapor source for the dispersion model both in geometry and strength.

The mass flow rate of air ($\dot{M}_{a,1}$) at the source is given by,

$$\dot{M}_{a,1} = \rho_a\ U_w\ W_s\ (2\ \sigma_z) \qquad (2.5.23)$$

2.6 TURBULENT JET MODEL

2.6.1 Description of the Physical phenomena

Consider a pressurized, supersaturated liquid being released from a pipe. At the pipe exit, as the pressure drops to the atmospheric value, the liquid flashes adiabatically into vapor and saturated liquid at ambient pressure. The flash phenomenon was discussed in section 2.4.

Following the flash process saturated liquid and saturated vapor are formed. A part of the liquid formed may rain out on to the ground while the remainder is entrained into the vapor plume as fine droplets of aerosol. A rapid expansion of the flow area (from the pipe flow area) results due to the significant reduction in the density of the vapor-aerosol combination in the plume.

Jet Phase of the Plume

The plume velocity at the pipe exit is generally likely to be higher than that of the prevailing wind. The plume density will also, in general, be higher than that of air. Depending on the orientation of the pipe axis relative to the wind direction, there will be an initial "direction adjustment" phase during which the jet direction is turned around by the wind into its direction. Also, the plume being heavier than air will disperse in contact with the ground. It will also experience the friction from the ground.

For the model formulation purposes, we assume that the pipe axis is in the direction of the wind, i.e., the jet flows down wind at release. In such a case, as the vapor/aerosol material in the jet moves down wind it entrains air from the surroundings. It experiences turbulent shear drag at the wind-plume interface due to the difference in velocities between air and the plume. Similarly, the plume is subjected to ground friction. Because of the higher than air density, the plume may also expand laterally. During this phase the air entrainment rate is determined only by the plume velocity (axial). The effect of friction, air entrainment and the interfacial drag is to slow down the plume velocity. Ultimately, the axial velocity in the plume will be very close to that of the wind.

Post Jet Phase Dispersion

This phase occurs when the plume velocity is close to that of the wind. In such an event, the entrainment due to jet effects are small and entrainment will be influenced by the gravitational flow velocity and the atmospheric turbulence. Of course, when the plume is dilute (i.e., when the mean plume density is very close to that of the ambient air) the dilution of the plume occurs due to atmospheric turbulence only.

The above physical phenomena are modeled and described mathematically in the following sections.

2.6.2 Mathematical Models

The models below correspond to the descriptions above. The initial characteristics of the liquid leaving the pipe/tank, and of the flash that occurs are discussed in the first two sections below. The jet phase (where the velocity of the plume is greater than that of the wind) models follow in Section 2.6.1.3.

2.6.2.1 Initial Characteristics of the Jet

In formulating the model to calculate the characteristics of the jet very close to the pipe exit section, we make the following ASSUMPTIONS:

a. The flow in the pipe is all liquid (and does not have a two phase flow)

b. Flashing occurs immediately after the liquid exits the pipe.

c. The process of flashing is instantaneous.

d. The flow rate is steady.

e. The liquid is incompressible.

The flow out of a pipe is modeled as if just upstream of the pipe exit section the full tank pressure P_1 exits and that at the break there is an orifice. In this view of the flow through the break, we can further assume that there is no flashing of liquid on the down stream side (of the pipe exit section) for a very short length and then the flashing occurs. That is, for a short length there is a superheated liquid (see Figure 2.6.1 below).

The velocity at section BB (U_B) in Figure 2.6.1 can be determined from the following equation:

$$U_B = C_v \sqrt{2 \frac{(P_1 - P_a)}{\rho_\ell(P_1)} g (H_L - H_p)} \qquad (2.6.1)$$

where C_v is the velocity drag coefficient, P_1 is the pipeline pressure, P_a is atmospheric pressure, $\rho_\ell(P_1)$ is the density of the liquid at pressure P_1, g is gravity, H_L is the height of the liquid in the tank connected to the pipe, and H_p is the height of the pipe. Also, the mass and momentum continuity between sections BB and CC gives the following result:

$$U_{CJ} = U_B \qquad (2.6.2)$$

where U_{CJ} is the jet velocity at section CC.

The ratio of the area at BB to that of the orifice AA (See Figure 2.6.1) was taken to be 0.6 ($=C_c$), due to the expected vena contract effects of the orifice. This result yields an expressions for the area BB (A_B), and the velocity of the fluid at AA (U_A):

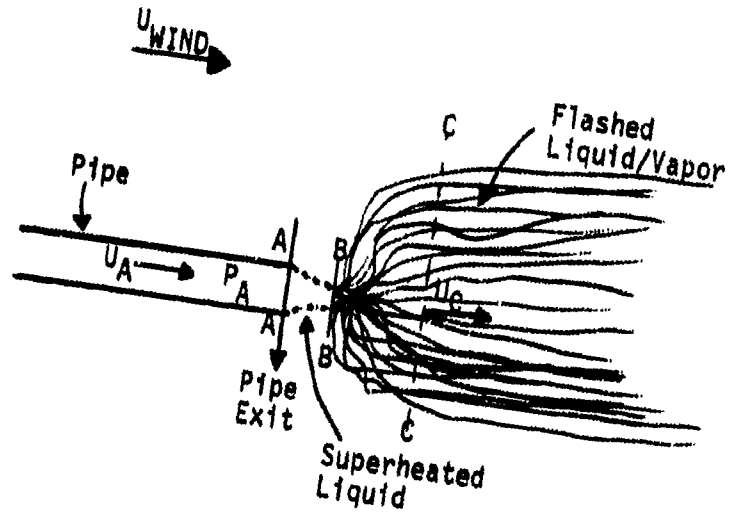

Figure 2.6.1 Schematic Illustration of the Flashing Process at the Pipe Exit and Desription of Plume Initial Characteristics.

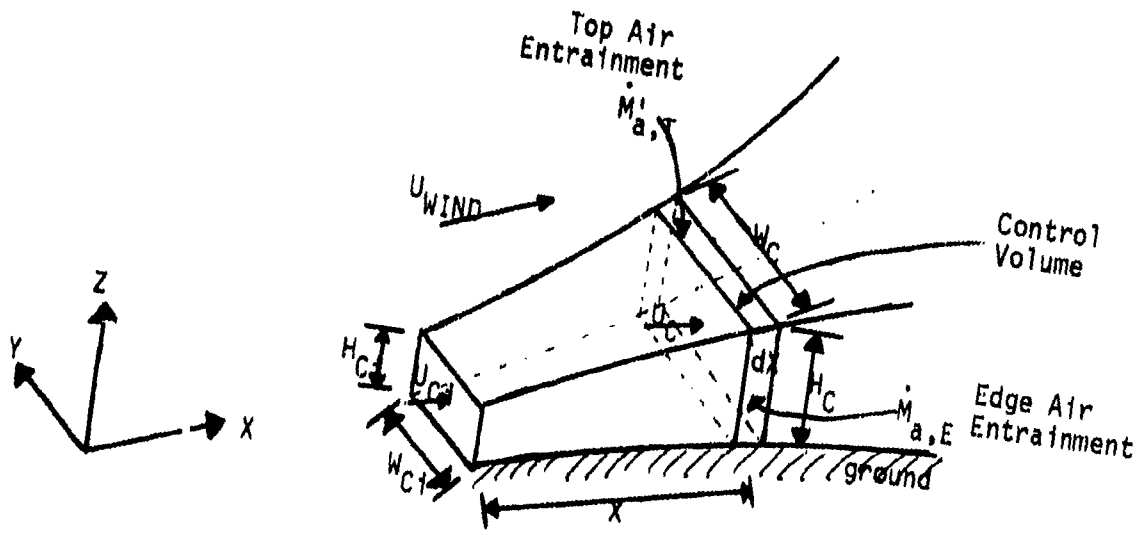

Figure 2.6.2 Schematic Representation of the Jet Dilution Model

$$A_B = C_C * A_A \tag{2.6.3}$$

$$U_A = \frac{\dot{M}_B}{A_A \rho_\ell} = \frac{\rho_\ell A_A C_C U_B}{\rho_\ell A_A} = C_C U_B \tag{2.6.4}$$

where A_A is the area of the orifice, $\dot{M}_B$ is the mass flow rate at section BB and ρ_ℓ is the liquid density at section AA.

2.6.2.2 Initial Flashing in the Jet

The superheated liquid jet flashes once it is released. The fraction of the liquid that flashes to vapor (f_v) is found using the flash models described in Section 2.4 The other initial parameters needed for the jet model are the mass flow rate of the jet ($\dot{M}_C$), the density of the jet ($\rho_{C,I}$), the fraction of the mass that is liquid aerosols ($f_{\ell,C,I}$), and the temperature of the jet ($T_{C,I}$). These are found using the following equations:

$$\dot{M}_C = \dot{M}_B * (f_v + \phi * f_\ell) \tag{2.6.5}$$

$$f_{\ell,C,I} = \frac{\phi * f_\ell}{(f_v + \phi * f_\ell)} \tag{2.6.6}$$

$$T_{C,I} = T_{sat}(P_a) \tag{2.6.7}$$

and

$$C_I = \frac{\rho_v^{sat}(P_a) * [\, 1 + \phi\ (f_\ell / f_v)\ ]}{1 + \phi * (f_\ell / f_v) * (\rho_v^{sat} / \rho_\ell^{sat})} \tag{2.6.8}$$

where f_ℓ is the fraction of the liquid that does not flash ($1-f_v$), ϕ is the fraction of the non-flashed liquid that is entrained by the vapor as liquid aerosols, $T_{sat}(P_a)$ is the temperature of the saturated vapor/liquid at atmospheric pressure, ρ_v is the density of the saturated vapor, and ρ_ℓ is the density of the liquid, at atmospheric pressure.

2.6.2.3 Jet Formation and Air Entrainment

The jet phase of the dispersion is the period from just after the flash, where the chemical plume has a velocity greater than that of the surrounding air, until the velocity of the plume slows to match that of the surroundings. The principal features of the model are indicated in Figures 2.6.1 and 2.6.2. The assumptions made in formulating the model follow.

Assumptions

It is assumed that:

a. The jet cross section is rectangular.

b. One face of the jet is in contact with the ground.

c. All properties within the jet (velocity, density, temperature, etc.) are uniform at any given sections. That is, a "top hat" distribution profile is assumed.

d. The normal jet entrainment law is used for air entrainment in both the horizontal (top) face of the plume, as well as the side faces of the

f. The pressure gradient in the plume axis direction is negligible.

g. Steady state flow is assumed

h. The wind velocity varies with height above ground. This variation depends on the stability of the atmosphere.

i. Gravity slumping of the cloud in the horizontal direction is taken into consideration.

Models

The models are developed considering the situation shown in Figure 2.6.2. A section of the plume (of width dX) at a distance X from the jet release point is examined. The mass and momentum equations are written for the control volume as shown in the figure. We write the following equations with respect to an inertial coordinate system (stationary with respect to the ground).

Mass Continuity

The equation for mass continuity between the sections at X and X+dX is,

$$\frac{d\dot{M}}{dX} = \dot{M}_{a,T} + \dot{M}_{a,E} \qquad (2.6.9)$$

where the mass of air entrained at the top of the plume per unit length in the axial direction is:

$$\dot{M}_{a,T} = \rho_a \alpha W \mid U_{wind}(H) - U_c \mid \qquad (2.6.10)$$

and the mass of air entrained on the two sides of the plume per unit length in the axial direction is:

$$\dot{M}_{a,E} = 2\,\rho_a\,\alpha\,H\,|\,U_{wind}(H) - U_c\,| \qquad (2.6.11)$$

The parameters in the above equations are: ρ_a is the density of the entrained air, α is the entrainment factor for a turbulent jet (related to the semi-angle of the plume), W is the width of the plume, H is the height of the plume, $U_{wind}(H)$ is the wind velocity at height H, $\overline{U_{wind}}(H)$ is the average wind velocity over the height of the plume, and U_c is the plume axial velocity.

Momentum Equation

$$\frac{d(\dot{M}U_c)}{dX} = U_{wind}(H)*\dot{M}_{a,T} + U_{wind}(H)*\dot{M}_{a,E} + W*\tau_{w\to p} - W*\tau_0 \qquad (2.6.12)$$

where the shear stress induced by the wind on the plume is:

$$\tau_{w\to p} = c_1\,\rho_a\,|U_{wind}(H) - U_c|\,(U_{wind}(H) - U_c) \qquad (2.6.13)$$

and the ground friction shear stress is:

$$\tau_0 = \rho_c\,(c_2\,U_c)^2 \qquad (2.6.14)$$

c_1 and c_2 are constants and ρ_c is the density of the plume at X.

Equation 2.6.12 can be re-written using equations 2.6.9, 10, 11, 13, and 14 and noting that:

$$\dot{M}_c = \rho_c\,U_c\,W_c\,H_c \qquad (2.6.15)$$

giving:

$$U_c\frac{dU_c}{dX} = \frac{\rho_a}{\rho_c}\frac{1}{H}\,(\alpha + c_1)\,(U_{wind}(H)-U_c)\,|U_{wind}(H)-U_c| +$$

$$\frac{2\alpha H}{W}[U_{wind}(H)-U_c]\,|U_{wind}(H)-U_c| - \frac{c_2^2\,U_c^2}{H} \qquad (2.6.16)$$

This equation for U_c is solved for all values of X with the initial conditions:

$$\begin{aligned} U_c &= U_{c_i} \\ H_c &= H_{c_i} \\ W_c &= W_{c_i} \end{aligned} \qquad \text{at } X = 0 \qquad (2.6.17)$$

Lateral Plume Expansion due to Gravity

The rate of lateral expansion due to heavy gas effects is given by:

$$\frac{dW_c}{dX} = \frac{k\sqrt{g\,H_c\,\Delta'}}{U_c} \qquad (2.6.18)$$

where k is the Froude number, taken as a constant approximately equal to 1 and the fractional density deviation, Δ', is:

$$\Delta' = (\rho/\rho_a - 1) \qquad (2.6.19)$$

It should be noted that the flow area of the jet increases not only because of the increase in mass flow due to air entrainment, but also due to the reduced jet velocity caused by ground friction and the stream mixing shear force. The lateral gravity spread does not change the flow cross sectional area; it changes the ratio of the width to the height of the plume. This ratio, or shape factor, changes with distance from the source.

The velocity in the plume at all downwind locations X can be determined by integrating the differential equation above (2.6.16). This was done using the Runge-Kutta method in the computer program. In addition, the equations above were non-dimensionalized before being implemented in the programs.

2.6.3 Results from the Jet Model

The results obtained using this model are shown in Figure 2.6.3. The values of the coefficients chosen for use in the computer model were selected by comparing model predictions with the data from the Desert Tortoise 4 Ammonia release field test. The two sets of coefficients which were used to generate the figure are listed in Table 2.6.1. The second set was implemented in the computer model.

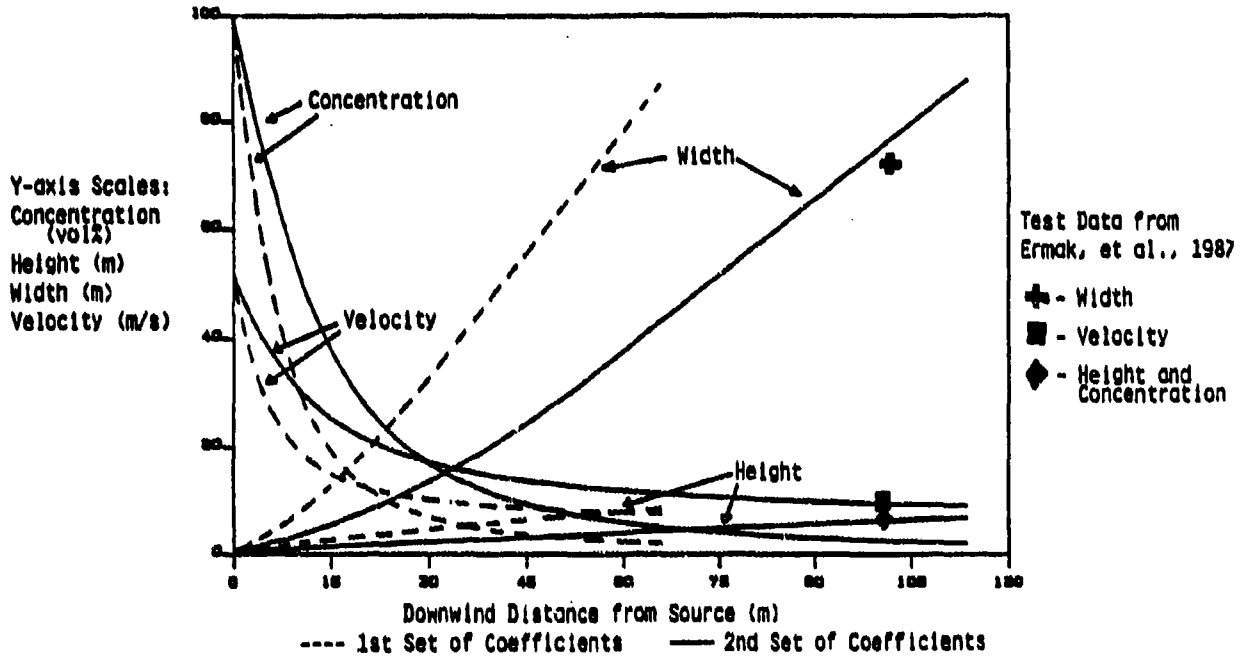

FIGURE 2.6.3 Comparison of Jet Dilution for Different Coefficients with Desert Tortoise 4 Ammonia Release Field Test Data

TABLE 2.6.1 Entrainment Coefficients Used in the Jet Models to Generate Figure 2.6.3.

Coefficient	Set No. 1	Set No. 2
α	0.16	0.065
C_1	0.006	0.006
C_2	0.1	0.05
k	1.07	0.85

CHAPTER 3

THERMODYNAMIC MODELING

3.1 INTRODUCTION

Many different types of behavior are possible for a chemical vapor cloud containing aerosols. Reactions may occur with the air or with the water vapor in the air, for example. The physical and chemical states of the air-chemical vapor cloud depend on parameters such as: the quantity, state, and temperature of the chemical initially present; the quantity, temperature, and relative humidity of the entrained air; the quantity of heat exchanged between the cloud and its surroundings (ambient air, ground); etc. The chemical state of the vapor cloud also depends on the extent to which possible chemical reactions (dissociation, reaction with water, etc.) take place. The physical state of the cloud, after equilibrium with the entrained air is reached, is characterized by its temperature, average density, total volume, and chemical composition. The various chemical species in the cloud may exist in different phases. Depending on the chemical released, some of the reactions may be so slow that they may be neglected in the dispersion calculations. Other reactions may be fast compared to the dispersion time scales, so that chemical equilibrium can be expected to prevail and the distribution of the various species in the resulting cloud can be calculated using thermodynamic calculations.

This chapter deals with such considerations. The role of chemical reactions in a vapor-air cloud is determined by the final thermodynamic equilibrium state of the system, which depends on the initial conditions of the system (mass and nature of chemical present; quantity, temperature, and relative humidity of entrained air; heat exchange with the surroundings; etc.). The cloud is treated as a closed system and allowed to come to thermodynamic equilibrium (except, as noted above, for very slow reactions), and the final state of the cloud is therefore determined. By this approach, we assume that the turbulence characteristics and the resulting mixing that might prevail in the cloud do not influence the extent of chemical reactions and vice versa. Since this approach can be adopted for any chemical (reactive or otherwise), we follow, as outlined in the next section, a generic approach applicable for chemicals under consideration in this study, namely nitrogen tetroxide, ammonia, chlorine, phosgene, sulfur dioxide, and hydrogen sulfide.

Depending on the environmental conditions prevailing at the spill location, the chemical is stored under one of many possible states (pressurized or non-pressurized, gas or liquid, etc.). The spill can result in the formation of either: a vapor cloud containing all of the chemical stored (instantaneous release), or a vapor plume (continuous release). As the chemical vapor cloud is moved downwind, it is diluted by entrained air. The thermodynamic state of the cloud at every instant is assumed to be determined by the equilibrium calculations. These calculations are also used in the estimation of the source strength of the chemical following its release.

3.2 CLASSIFICATION OF CHEMICAL REACTIVITY

The role of chemical reactions possible with the mixture consisting of the released chemical and atmospheric air and water vapor must be considered in conjunction with the dispersion mechanisms prevailing in the gas cloud. Important parameters in such atmospheric chemical reactions are the extent and effect of solar insolation, air (and water) temperatures, presence of large pools of water (such as lakes and oceans) in contact with the cloud, the nature of the cloud itself (aerosol fraction and its associated liquid-vapor interface area), and the time scales of motion and chemical reactions. There is a vast amount of information collected in the field of atmospheric chemistry, but these deal with chemical reaction time scales much larger (days, months) than those of interest in dispersion calculations (hours, minutes). Thus, the types of chemical reactions pertinent for dispersion are only a subset of those considered in the field of atmospheric chemistry.

The cloud formed may be heavier than air and contain liquid aerosols. The chemical may not react with the air or water vapor and its liquid aerosols may not dissolve appreciably in liquid water (e.g. chlorine). In this case, the entrainment of air into the cloud lowers the vapor concentration and consequently lowers the chemical partial pressure. The aerosols evaporate at the expense of the sensible heat of the cloud and, in the absence of any external heating, depress the cloud temperature. The density of the cloud may increase due to the lowering of temperature.

Other chemicals may behave this way under certain circumstances, but they may also behave differently if liquid water drops are present in the cloud (due to rain, fog, snow, or water droplets from a fireman's hose). A classic example of such a chemical is phosgene. If no liquid water is present in the cloud, phosgene vapor and phosgene liquid aerosols are not reactive with moisture vapor in the atmosphere. If liquid water drops are present due to condensation or other reasons, however, phosgene liquid aerosols readily dissolve in water forming hydrochloric acid drops and carbon dioxide vapor. This type of behavior obviously has a profound influence on dispersion predictions.

A second type of chemical behavior is exemplified by the release of a chemical whose vapor is quite soluble in water (e.g., anhydrous ammonia). In this case, the cold vapor-aerosol cloud formed after release condenses moisture from the atmosphere. The anhydrous aerosols dissolve in the condensed water forming aqueous liquid aerosols. These liquid droplets can persist for a long time if the partial pressure of the chemical over a dilute aqueous mixture is low.

The third type of behavior involves spontaneous dissociation and/or reaction of a chemical with the moisture in the atmosphere to produce new chemical species. These new species may condense, depending on their partial pressure, and form liquid chemical aerosols. These formations have profound effects on the vapor cloud temperature, density and, of course, cloud size. Hazards may be posed by the secondary product chemicals as well as by the primary chemical. The

aerosols formed may be stable and persist for a considerable distance. In addition, the aerosols may extend the region over which the cloud behaves as a heavy gas. An example chemical for this type of behavior is nitrogen tetroxide (N_2O_4). It forms nitrogen dioxide by dissociation and it forms nitric acid aerosols due to reaction with the moisture in the atmosphere. The nitric acid further interacts with water and forms aqueous nitric acid aerosols which may persist until considerable dilution of the cloud has occurred.

It is clear from the above brief discussion that chemicals which form liquid aerosols and/or react influence the physical make up of the dispersing cloud and have effects on the density, temperature, and species concentrations. A significant number and volume of the chemicals used, stored, and transported by chemical and other industries are reactive and stored under pressure (therefore, producing liquid aerosols when released into the air by accident). Unfortunately, most of the tests conducted and the theoretical analyses developed have been concerned with the dispersion of chemical clouds that are non-reactive and/or do not contain evaporating aerosols. The reason for this is the complexity of the dispersion phenomenon and the difficulty in understanding even simple of cases. Non-reactive dispersion models may not always provide reasonable estimates of the area of hazard and the type of hazard. Very few modeling efforts have been undertaken which include the effects of chemical reaction and/or aerosol presence.

Based on the interactions of relevant chemical reactions and dispersion, it is thus possible to classify the chemical released in one of three categories: (I) The first type, termed 'passive', involves chemicals that have no significant chemical transformations within the time scales of interest. The released chemical in vapor form and aerosol, if present, is transported in a downstream direction as a passive tracer, its concentration decreasing with distance and time due to the increasing entrainment of ambient air. Liquid aerosols, if any, will evaporate due to air entrainment. Examples of such chemicals are chlorine, phosgene, sulfur dioxide and hydrogen sulfide etc. (II) The second type, termed '(water) soluble', involves those chemicals that have a strong solubility in water condensed from the atmosphere. The presence of liquid aerosols in such systems will serve to dissolve some of the chemical vapor into the condensed water. An example of such a case is ammonia. (III) The third type, termed 'reactive' involves significant chemical and phase transformations with atmospheric water vapor and thus the production of chemical species very different from that released. Examples of such chemicals are nitrogen tetroxide and silicon tetrafluoride. This type, which includes both physical and chemical changes, is clearly the most complex to analyze.

3.3 GENERIC CLOUD CONCENTRATION (CLUDCC) MODULE

In order to decouple the chemical reactions from the dispersion processes, we have developed a generic approach. At each stage of dispersion, the closed system consisting of initial mass of chemical

released and the total amount of air entrained from the time of release up to the time of interest, is allowed to come to thermodynamic equilibrium in the presence of the prescribed heat exchange with the surroundings. These concepts are implemented in a generic program module called CLUDCC (for CLoUD ConCentration), which defines the thermodynamic equilibrium state of the system consisting of a given set of initial conditions (mass and temperature of the chemical and the entrained air, net amount of heat input etc.). The final state of the system is characterized by the concentration of all the reactants and products in various phases (solid, liquid and vapor) as well as the final mixture temperature and density. The equations that govern this final thermodynamic state are dependent on the chemical released. For type I chemicals (discussed above), which do not undergo any physical or chemical transformations, the final temperature is altered by the sensible heat effects, and the final material composition will be identical to that of the initial state. For type II chemicals, one should consider the effects of solubility and associated energetics, and for type III chemicals, both mass and energy conservation laws must be solved to determine the final state. Of the chemicals considered in this study, chlorine, phosgene, hydrogen sulfide and sulfur dioxide are of type I, ammonia is of type II, and nitrogen tetroxide is of type III.

The generic CLUDCC is defined as a subroutine with a prescribed input and output specification list. The input parameters are:

CH	a three character chemical code
MCH	the total mass of chemical vapor and aerosol (kg)
FLI	the mass fraction of liquid aerosol in cloud or plume
TCH	temperature of chemical before mixing with air (K)
MAIR	the mass of air entrained in the cloud or plume (kg)
TAIR	the dry bulb temperature of the air (K)
RH	the relative humidity of the air (%)
Q	net heat input (+) to or extraction (-) from the chemical-air mixture from/to the surroundings (J)

The output parameters are:

TMIX	temperature of the mixture after reaction (K)
RHOMIX	overall density of the mixture (kg/m^3)
VOLMIX	volume of mixture at 1 atm pressure (m^3)
NSPECS	number of chemical species in the final mixture
SPLIST	an array of three letter chemical species names
CSOL	an array of mass fractions of each species in the solid phase
CLIQ	an array of mass fractions of each species in the liquid phase
CVAP	an array of mass fractions of each species in the vapor phase

The last three arrays include the mass fractions of all the individual species present in the system as well as the total mass and moles present in each phase. The first species in the array is water, the

is very low (10^{-14} atm^2), and thus the extent of the chlorine hydrolysis reaction is essentially zero. The reverse of 3.4.1, known as the Deacon process, is commercially used to produce chlorine.

Chlorine dissolves in and reacts with liquid water as follows:

$$Cl_2\ (g) = Cl_2\ (aq)$$
$$Cl_2\ (aq) + H_2O = Cl^- + H^+ + HOCl \qquad (3.4.2)$$

The physical absorption step is usually described by Henry's Law,

$$[Cl_2, aq] = Hp \qquad (3.4.3)$$

where p is the partial pressure (bar) of chlorine over the aqueous phase, [] denotes concentration (gmole/ℓ), and H is Henry's Law constant(gmole/ℓ-bar).

If reaction 3.4.2 attains equilibrium and water is in excess,

$$K = [Cl^-]\ [H^+]\ [HOCl] / [Cl_2, aq] = [Cl^-]^3 / [Cl_2, aq] \qquad (3.4.4)$$

The total concentration of chlorine in the aqueous phase [C] is comprised of the dissolved form $[Cl_2, aq]$ and chlorine in the reacted forms. If there is no other source of Cl^- or H^+, then,

$$[Cl^-] = [H^+] = [HOCl] = [C] - [Cl_2, aq] \qquad (3.4.5a)$$

or

$$K = (\ [C] - [Cl_2, aq]\ )^3 / [Cl_2, aq] \qquad (3.4.5b)$$

Using equation 3.4.3,

$$[C] = Hp + (KHp)^{1/3} \qquad (3.4.6)$$

Whitney and Vivian (1941) reported the values of K and H at 293 K to be

$$H = 0.0753 \quad (gmoles/\ell\ bar)$$
$$K = 2.75 \times 10^{-4} \quad (gmoles/\ell)^2 \qquad (3.4.7)$$

The second term on the RHS of equation 3.4.6 indicates the increase in the equilibrium solubility of chlorine due to the chemical reaction (3.4.2).

The kinetics of liquid phase hydrolysis reaction are rapid (Sherwood, et al., 1975; Eigen and Kustin, 1962), and normally diffusional processes within the liquid phase control the rate of chlorine absorption. For small water droplets in a cloud of chlorine and air, it is reasonable to assume a conservative situation where all droplets are saturated. We note, however, that the solubility of chlorine in water is low and little chlorine would be lost from a vapor cloud.

second is air, the third is the primary chemical released, and then follow any other chemical species formed by the chemical reactions.

In the following sections, the detailed thermodynamic analysis of the six chemicals under consideration and the results obtained are presented. The case of passive type I chemical releases are considered first, followed by ammonia (type II) which displays considerable solubility with water. The case of nitrogen tetroxide release (type III) is treated last.

3.4 PASSIVE CHEMICAL (TYPE I)

In this section, we consider the thermodynamic equilibrium associated with the passive chemical-wet air mixture. The chemicals treated here are chlorine, phosgene, sulfur dioxide and hydrogen sulfide. For each of these chemicals, the relevant chemical reactions are described in detail. In all these cases, it is observed that the solubility of the chemical in water and the possible chemical reactions are not significant. The treatment of thermodynamic calculations involves the energy changes associated with condensation of the chemical or the atmospheric water. This treatment is detailed in a common section following the description of each of the chemicals. Finally, the cloud temperatures and densities calculated for various conditions encountered in practice are discussed.

3.4.1 Chlorine

Background

Chlorine is a gas at normal ambient conditions, but it is transported as a pressurized liquid. The normal boiling point is 239.1 K and at 293 K, the vapor pressure is about 6.9 atm. The pressurized liquid chlorine will, upon release, flash to ambient pressure in essentially an adiabatic manner. An enthalpy balance for the flashing process indicates that about 20% of the liquid flashes into vapor. Some liquid may be entrained as an aerosol while the remaining would pool in the immediate area and subsequently evaporate. Thus, the source strength of a spill is determined by the quantity of chlorine in the flash cloud (with entrained aerosol) and the quantity in the vapor from the evaporating pool. The chlorine, vapor and aerosol, is mixes with air at ambient temperature. This mixing of the cold (239 K) chlorine saturated vapor cloud with the warmer ambient air could cause water vapor in the air to condense and/or freeze. Thus, in addition to any chemical reactions, we must consider the energetics due to phase transformations when dealing with chlorine spills.

Chemical Reactions

Chlorine and water do not react in the vapor phase at ambient temperatures, even in the presence of light (Cline and Forbes, 1938). The equilibrium constant for the gas phase reaction:

$$2H_2O + Cl_2 = 4HCl + O_2 \qquad (3.4.1)$$

For example, consider pure chlorine mixed with saturated air (RH=100%) at 293 K. Each kg of this saturated air at 293 K would contain about 0.014 kg of water. If all of this water condensed, and equilibrium solubility were achieved, only 0.0001 kg of chlorine would be removed from the cloud. Also, the low concentration of Cl_2 (aq) and the reaction products would not significantly affect the properties (density, etc.) of a water mist.

Thus, it can be concluded that the chemical reactions in the chlorine-water system do not significantly affect the overall process. Due to the low temperatures however, the energetics involved in the various phase transformations of chlorine and water are important.

3.4.2 Phosgene

Background

Phosgene ($COCl_2$) is normally stored as a pressurized liquid. Its normal boiling point is 281.4 K. Since its boiling point is near normal ambient temperatures, a phosgene vapor cloud which mixes with air is not expected to decrease the temperature of the mixture significantly. Therefore the water in the air would not condense under most conditions.

Reaction with water

The only reference found in the literature for gas phase hydrolysis of phosgene involved relatively high temperatures and low concentrations (Gaisinovich and Katov, 1969). They suggest that the reaction order is about unity for both phosgene and water for the hydrolysis reaction:

$$COCl_2 + H_2O = CO_2 + 2HCl \qquad (3.4.8)$$

The rate constant (k) is given by:

$$k\ (\ell/\text{gmole-min}) \quad (3.6 \times 10^5)\ e^{(-6010/T)} \qquad (3.4.9)$$

The reaction is very slow at or near ambient temperature. Thus, for our purposes, we can assume that phosgene does not react with water vapor.

Few investigations have been conducted to measure the reaction rate between phosgene and liquid water. Böhme (1941) states that the decomposition in liquid water is very rapid. Rona (1921) discusses its use as a war gas and states that liquid water "practically at once" destroys phosgene. Kirk and Othmer (1982) note that it reacts with liquid water and that care must be taken to keep the storage cylinders dry.

Manogue and Pigford (1960) reported on the quantitative aspects of the phosgene-liquid water system by absorbing phosgene gas into a laminar water jet. They were primarily interested in the mass transfer aspects

of the problem, but they had to correct the phosgene concentration in the aqueous phase to allow for decomposition by:

$$COCl_2\,(aq) + H_2O \leftrightarrow CO_2\,(g) + 2H^+ + 2Cl^- \qquad (3.4.10)$$

They assumed a pseudo-first order reaction since water was in great excess:

$$d\,C_{COCl2}/dt = -k_l\,C_{COCl2} \qquad (3.4.11)$$

Where concentration (C_{COCl2}) is for the aqueous phase.

Values of k_l and phosgene solubility reported for one atmosphere pressure are given in Table 3.4.1. Also shown are estimated solubilities of phosgene in water under one atmosphere pressure.

TABLE 3.4.1 Values of k_l and Phosgene Solubility at One Atmosphere

Temperature (°C)	K_l (1/s)	Solubility (gmoles/ℓ atm)
15	≈ 3	0.109
25	≈ 6	0.069
35	22	0.046
45	75	0.027

The values of k_l indicate that the reaction is very rapid, and thus, the controlling effect is probably due to mass transfer. For example, at 1 minute following the contact of phosgene with liquid water (at 25°C), the concentration of the remaining phosgene in the aqueous phase, $C \approx C^*_{\ell(\sim 360)}$, is very small. (In the absorption experiments, the contact time was probably on the order of or less than one second.)

The solubility values indicate that the quantity of phosgene which would dissolve into water condensed from air is small. At 25°C, 1 kg of wet air at 100% relative humidity contains 0.02 kg of water. If this water were to condense, the mass of phosgene that would dissolve into the liquid would be 0.0014 kg. In addition, since the normal boiling point of phosgene (280.7 K) is near ambient temperatures, there is little chance that the contact with phosgene would condense as much water from the atmosphere as chemicals with lower boiling points. Thus, it can be concluded that while the phosgene-water reaction is very fast, the total quantity of phosgene removed by water in the atmosphere would be quite small. It should be noted that this conclusion may not hold if the environment contains a sufficient quantity of liquid water, if for example, the spill occurred in a rain

storm, or if there was water spray from fog nozzles, or if the spill was on a lake or ocean, etc.

3.4.3 Sulfur Dioxide

Background

Sulfur dioxide (SO_2) is transported as a pressurized liquid. Its normal boiling point is 263.2 K. Due to the fact that the boiling point is low and the molecular weight is higher than air (64 compared to 29), the saturated vapor density is about 3 kg/m^3 (2.5 times that of ambient air). Thus, SO_2 clouds would be dense and difficult to disperse.

Chemical Reactions

Sulfur dioxide is quite stable. It does not react with oxygen or water in the vapor phase unless temperatures exceed ≈ 700 K and a catalyst is present. If liquid water is present, some SO_2 will dissolve. In solution, SO_2 is believed to exist in two forms, non-ionized and ionized, both of which are in equilibrium, according to reaction (3.4.12).

$$SO_2 + H_2O = H_2SO_3 = H^+ + HSO_3^- \qquad (3.4.12)$$

For the ionization,

$$K = [H^+]\,[HSO_3^-]/\,[H_2SO_3]\,\gamma^2 \qquad (3.4.13)$$

and, since $[H^+] = [HSO_3^-]$,

$$[HSO_3^-] = (\,K\,[H_2SO_3]\,)^{1/2}/\gamma \qquad (3.4.14)$$

where γ is the mean ionic activity coefficient for the hydrogen and bisulfite ions. We define

C_u = concentration of non-ionized SO_2, i.e., H_2SO_3, [g SO_2/kg H_2O]
C_i = concentration of ionized SO_2, i.e., HSO_3^-, [g SO_2/kg H_2O]

and assume

$$C_u = Hp \qquad (3.4.15)$$

where H is the Henry's law constant (gmole/ℓ-Pa) and p the partial pressure (Pa) of SO_2 over the solution.

The total dissolved SO_2, C (g SO_2/kg H_2O), is then given by

$$C = C_u + C_i \qquad (3.4.16)$$

Accounting for the conversion of concentration, [], from molar units to mass units,

$$C = Hp + 8(HpK)^{1/2}/\gamma \qquad (3.4.17)$$

Pearson et. al. (1951) suggest correlations for H, K, and γ as

$$\begin{aligned} \ln H &= 3150.93/T - 17.7170 \\ \ln K &= 1941.84/T - 10.8569 \\ \gamma &= 1 - 0.56\,(KHp)^{1/2} \quad \text{when } (KHp) < 0.1 \\ \gamma &= 0.82 \quad \text{when } (KHp) > 0.1 \end{aligned} \tag{3.4.18}$$

As an example, consider the case where the partial pressure of SO_2 is 1.013×10^5 Pa (1 atm) and the temperature is 273.2 K. At this temperature, H = 0.00206 and K = 0.0235. The value of (KHp) = 4.92, and thus γ = 0.82. With these parameters, we get

$$\begin{aligned} C_u &= Hp = 209.0 \text{ g } SO_2/\text{kg } H_2O \\ C_l &= 21.64 \text{ g } SO_2/\text{kg } H_2O \\ C &= 230.67 \text{ g } SO_2/\text{kg } H_2O \end{aligned} \tag{3.4.19}$$

To place the sulfur dioxide solubilities in perspective, assume the cold SO_2 cloud mixes with air at 293 K and 100% relative humidity. At this temperature, the wet air contains about 14.6 g H_2O/kg air. If this water were to condense and be cooled to the lowest possible temperature possible (273.2 K, where the SO_2 solubility is the highest), then, with a partial pressure of SO_2 = 1.0132×10^5 Pa, C_u = 209, C_l = 21.6, and C = 230 g SO_2/kg H_2O. Thus (230)(14.6/1000) = 3.4 g SO_2 would be dissolved in the water. This result corresponds to an extreme case. As more air is entrained (with its additional water), the partial pressure of SO_2 would drop so that the total SO_2 lost to the condensed water would not vary appreciably.

It is also interesting to note that the vapor pressure of water over solutions with dissolved SO_2 is essentially the same as for pure water. This fact allows one to treat the water condensation step independently from the SO_2 dissolution step in any calculation of the final state after mixing with wet air.

Pearson et al. (1951) also quote values of 409 J/g SO_2 as the heat of solution for non-ionized SO_2, and 252 J/g SO_2 for the heat of solution of ionized SO_2. For the case discussed above, the heat of solution of SO_2 is 1274.8 J, with 1198.3 J due to non-ionized SO_2, and 76.5 J due to ionized SO_2. It can also be noted that for the temperatures involved in dispersion analysis, the ionization, as described by the reaction is not a significant component of the overall solubility. This is evident from the data shown in Table 3.4.2. In addition, the amount of SO_2 dissolved in water is seen to decrease as the temperature increases. Thus, the thermodynamic state of the sulfur dioxide-water-air mixture can be estimated from energetics considerations alone.

TABLE 3.4.2 Distribution of SO_2 Dissolved in Water

Temperature (K)	Non-Ionized SO C_u	Ionized SO_2 C_I	Total SO_2 C
	g SO_2/kg H_2O		
250	609.6	51.4	661.0
270	239.6	24.2	263.8
290	107.2	12.6	119.8
310	53.1	7.15	60.25
330	28.7	4.3	33.0

3.4.4 Hydrogen Sulfide

Background

Hydrogen sulfide is stored as a pressurized liquid. The normal boiling temperature is 212.4 K and, at 293 K, the vapor pressure is about 1.78×10^6 Pa (17.6 atm). Thus, in spills, this material would flash vaporize and form a cold, dense cloud.

A phase diagram for the hydrogen sulfide-water system is shown in Figure 3.4.1 (Sellick et al., 1952). A majority of studies have emphasized the high pressure domain of H_2S and water. Using limited data, we have, however, expanded the low-pressure region in Figure 3.4.2. The quadruple point denotes the state where gas (G) is in equilibrium with an aqueous phase (L_A) and two solid phases, a hexahydrate (S_B) and water ice (S_A). This point is at 272.9 K and 9.3×10^4 Pa pressure (of H_2S). Depending upon the conditions after mixing a cold H_2S cloud with water vapor, various equilibrium states could be achieved. But, with air dilution, the pressure of H_2S would certainly be well below 10^5 Pa, so except for unusual situations, only a gas phase with water ice would be present.

Chemical Reactions

H_2S does not react with water vapor at the temperatures and pressures of interest. It is, however, flammable so fire is always a possibility. It is also soluble in liquid water. Again, most studies have been conducted at high H_2S pressures where several investigators have detailed the properties of the H_2S-H_2O system (Pohl, 1961; Burgess and Germann, 1969). Linke (1958) has, however, presented solubilities at lower H_2S partial pressures. To correlate these data, the following mechanism is assumed.

$$H_2S\ (g) = H_2S\ (aq) \qquad (3.4.20)$$

$$H_2S\ (aq) = HS^- + H^+ \qquad (3.4.21)$$

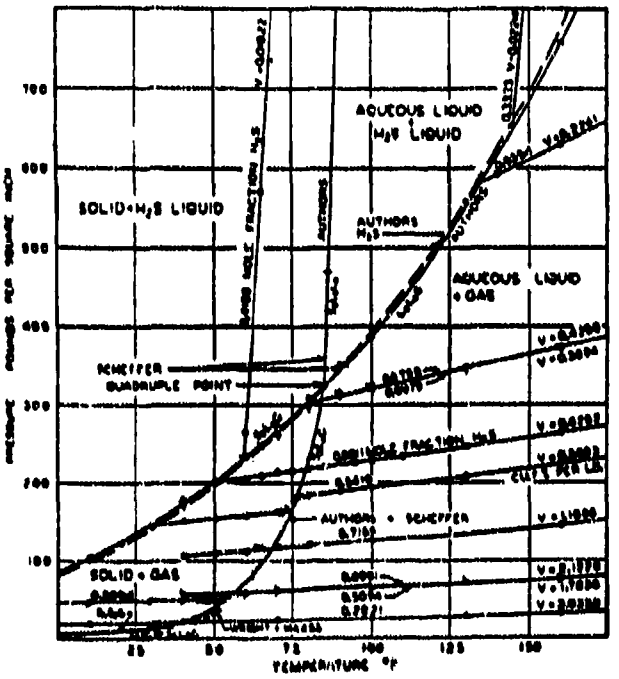

Figure 3.4.1: Pressure-Temperature Diagram for Hydrogen Sulfide-Water System at Low Pressures

Ref. Source: Selleck, et al., 1952

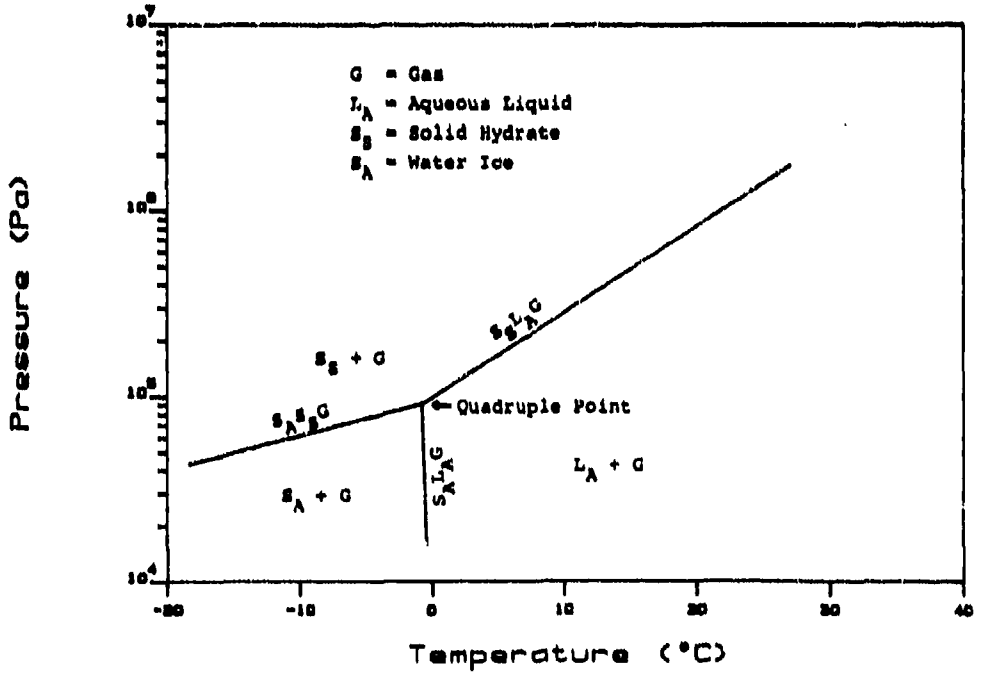

Figure 3.4.2: Low Pressure Region for H_2S-H_2O Phase Diagram

For reaction 3.4.20, a Henry's law treatment is employed,

$$[H_2S,aq] = Hp \qquad (3.4.22)$$

where $[H_2S,aq]$ represents the concentration of molecular H_2S dissolved in the solution. p is the partial pressure of H_2S and H is Henry's law constant.

For reaction 3.4.21,

$$K = [HS^-][H^+] / [H_2S,aq] \qquad (3.4.23)$$

Assuming no other source of H^+ or HS^- than from the dissociation of H_2S,

$$[HS^-] = [H^+] = ([S] - [H_2S,aq]) \qquad (3.4.24)$$

where [S] is the total sulfur concentration in the solution. From the above, we can derive,

$$[S] = Hp + (HKp)^{1/2} \qquad (3.4.25)$$

Thus experimental data may be correlated by plotting $[S]/p^{1/2}$ vs. $p^{1/2}$. Using this analysis and Linke's data, we obtained the constants at various temperatures. While this technique provides good estimates of H, it is not particularly accurate for determining K, as the values obtained are very sensitive to the exact manner in which the data correlation lines are drawn. The values of H and K obtained in this manner are shown in Table 3.4.3.

TABLE 3.4.3 Henry's Law (H) and Equilibrium (K) Constants for H_2S-H_2O system

Temperature °C	H (gmole $x10^6$/ℓ-Pa)	K (gmole/ℓ) x 10^4
5	1.68	1.9
10	1.40	4.2
20	1.06	7.4
30	0.89	~ 0
40	0.72	0.3

The K values at 5, 10 and 20°C appear reasonable, but the results at higher temperatures are probably low. The ratio $(HKp)^{1/2}/[S]$ indicates the enhancement of the H_2S solubility due to the ionization reaction (3.4.21). As the ionization reaction becomes more important, however, the non-ionized H_2S solubility decreases, and, thus, the overall solubility decreases. This is shown in Figure 3.4.3. For the peak

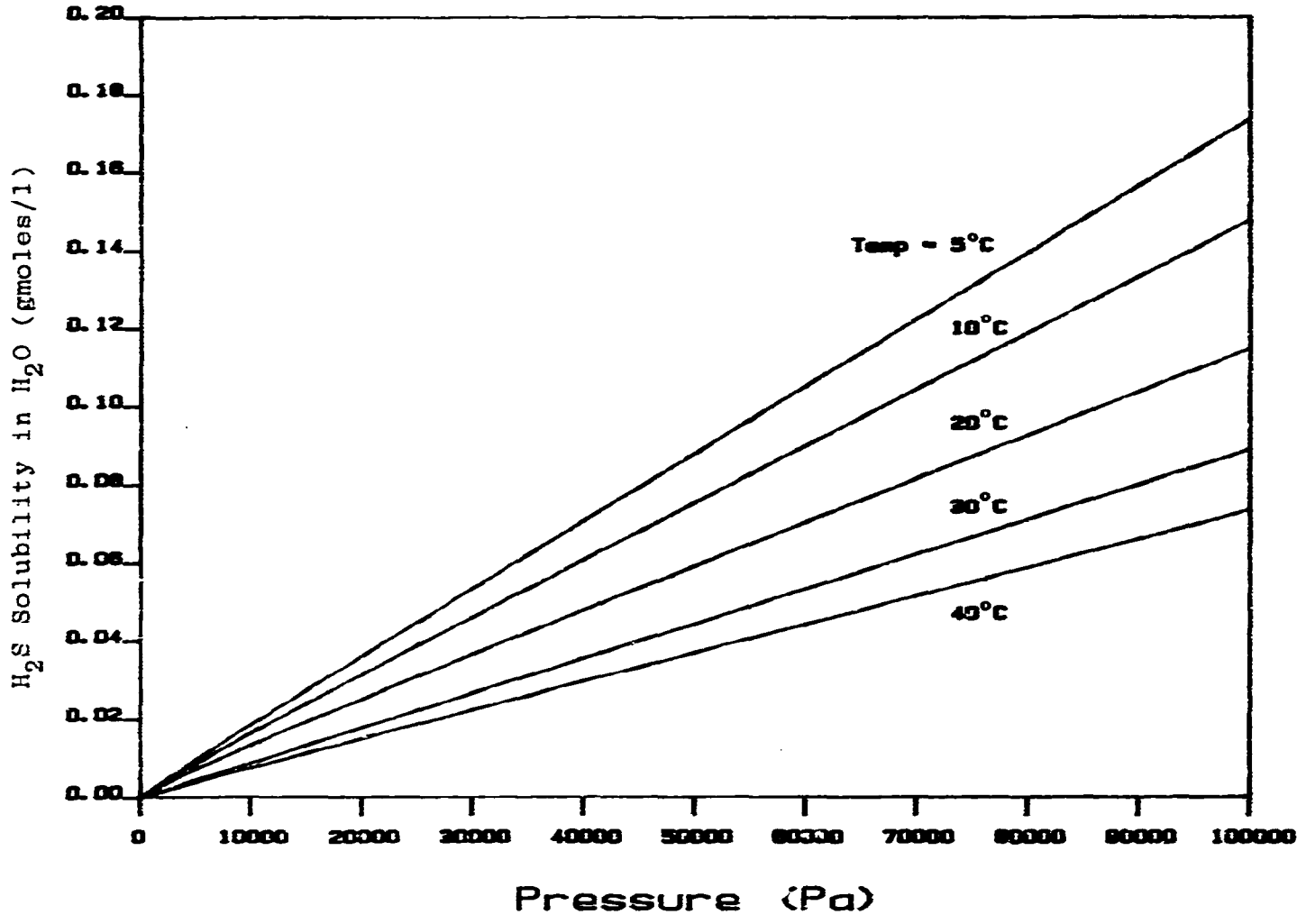

FIGURE 3.4.3: Solubility of Hydrogen Sulfide (Ionized and Non-Ionized) in Water as a Function of H_2S Partial Pressure and Temperature

solubility shown (5°C and 1 bar H_2S partial pressure) the solubility is 0.17 gmole/ℓ or 5.8 g H_2S/kg H_2O.

In summary, H_2S flashing after a spill would most probably freeze the water in the entrained air, humid air. Under conditions of extreme dilution in the vapor phase due to added air, the liquid phase is usually absent, thus eliminating the dissolution of H_2S. Thus, in most cases, the problems in the estimation of K do not lead to significant errors in the calculation of H_2S dissolution. It can be concluded that the chemical reactions in the hydrogen sulfide-water system do not significantly affect the overall process.

3.4.5 Thermodynamic Considerations

The final state of the passive chemical-air-water cloud depends upon the relative quantities of these components and the energy exchange with the surroundings. We consider the case where a specified quantity M_{CH} (kg) of chemical is mixed with a specified quantity of wet air M_{AIR} (kg) with a given relative humidity RH (%), and with a specified energy input Q (J). From an overall net enthalpy balance for the isobaric mixing process, we can determine the final state. Using equilibrium relationships and partial pressures of the various species, we can ascertain whether condensed phases (liquid chemical, liquid water, or water ice) are present. Since the final temperature of the system is unknown at the outset, we determine the enthalpy of the system at various end states. These end states can be characterized by considering the mixing process of the chemical-wet air mixture. The thermodynamic calculations are illustrated here for the case of the representative chemical chlorine mixed with ambient wet air. The analysis is identical for other passive chemicals.

Initially, the liquid chlorine flashes to produce a cloud of chlorine vapor with entrained liquid chlorine aerosols. Before any air is mixed in, the liquid and vapor chlorine are in equilibrium. For ambient pressure (1 atm), the temperature of the cloud (T_{CH}) would be chlorine's normal boiling point of 239 K. As air is entrained, the partial pressure of chlorine decreases and, if liquid chlorine is present, evaporation occurs. These two processes have opposing effects. The inclusion of warmer air and the condensation and freezing of water tend to increase the temperature, the chlorine evaporation decreases the temperature. Initially, the latter step is dominant, and the cloud temperature decreases. This trend continues as additional air is entrained until all the liquid chlorine is completely evaporated. The cloud temperature is then below 239 K and all water is in the form of ice.

When no liquid chlorine remains, the temperature increases as more warm air is entrained into the cloud. As this continues, some ice sublimes so as to maintain its equilibrium vapor pressure. When the temperature reaches 273.2 K, the ice converts to liquid water, and above this temperature, water is present in liquid and vapor forms.

The scheme adopted here allows for various final domains from a given initial state, depending on the circumstances and the extent of energy

transfer with the surroundings. We define the inlet conditions by specifying: a) the quantity, temperature, and relative humidity of the ambient air; b) the quantity of chlorine flashed, its liquid aerosol fraction, and its temperature; and c) the quantity of energy input into the cloud from the surroundings. We use these data, with appropriate equations representing the enthalpies of chlorine (vapor and liquid), water (vapor, liquid, and solid) and air (vapor) as functions of temperature, to calculate the "initial stream enthalpy", H_I (Joules). No mixing is assumed to have occurred yet, so the property values of pure chlorine and air are used in the computations. We add to H_I, the given energy input, Q (J). The sum $H_I + Q$ represents the total stream enthalpy at any time, and thus is equal to H_f, the final mixed stream enthalpy.

When carrying out a calculation, one does not know (at the start) which condensed phases are present. To overcome this difficulty, we first bracket the domains and compute HF values at the extreme conditions of each domain. This allows us to determine the appropriate temperature range for the final mixture. The cloud temperature and the state of the system can be obtained by a numerical iteration process. Based on the earlier discussion, we can identify several domains as shown in Table 3.4.4.

TABLE 3.4.4 Species Phases in a Humid Air-Chlorine Mixture at Various Temperatures

Domain	Temperature Range (K)	Phases Present
I	273.2 to $T^{SAT}(P_{vp,W})$	Cl_2 (g), H_2O (g,ℓ)
II	273.2	Cl_2 (g), H_2O (g,ℓ,s)
III	$T^{SAT}(P_{vp,CH})$ to 273.2	Cl_2 (g), H_2O (g,s)
IV	Below $T^{SAT}(P_{vp,CH})$	Cl_2 (g,ℓ), H_2O (s)

where

$T^{SAT}(P_{vp,CH})$ = Saturation temperature for the chemical vapor partial pressure $P_{vp,CH}$

$T^{SAT}(P_{vp,W})$ = Saturation temperature for the water vapor partial pressure $P_{vp,W}$

We begin with domain I and calculate H_f at both extremes. If $H_I + Q$ lies between these extremes, we know the solution lies in domain I. Otherwise, we repeat this procedure for other domains. Identification of the domain defines the final physical state of the cloud, the temperature, cloud density, etc., can then be obtained by numerical iteration.

3.4.6 Thermodynamic Properties

In this section, we include the relationships used to compute the specific heats air and of water in the vapor, liquid, and solid phases and the vapor pressure of liquid and solid water. The thermodynamic properties of the six chemicals modeled are calculated using the property database functions which are discussed in detail in Appendix A.

To calculate the enthalpy of air at a given temperature T_{AIR} (K), we assume that air consists of 79 mole % N_2 and 21 mole % O_2. The heat capacity of air was taken as the mole fraction average of the pure component values. These pure component C_p° (in J/mole-K) values are given in Table 3.4.5 (Reid, et al., 1987). The molecular weight of air is taken to be 28.9 kg/kgmole. Thus the C_p° in (J/kg-K) can be found by multiplying the per mole values by (1000/28.9). The enthalpy of air is obtained by integrating $C_p^\circ dT$, with 273.2 K as the reference temperature.

To calculate the enthalpy of water vapor, the equation for C_p° (in J/kg-K) given in Table 3.4.5 (Reid, et al., 1987) is integrated as $C_p^\circ dT$. The reference temperature was chosen to be 273.2 K, liquid water. The enthalpy of vaporization is chosen as 2.5×10^6 J/kg. For the enthalpy of liquid water, the relationship used for integration was obtained by fitting the data given by (Horvath, 1975). This relation is also in Table 3.4.5 and 273.2 K liquid water was used as the reference state.

For solid water, the data from steam tables (Keenen and Keyes, 1936) was fitted to provide a relationship. The reference state used was liquid water at 273.2 K. The enthalpy of fusion was 3.339×10^5 J/kg. The enthalpy H(T) is:

$$H(T) = -6.3490 \times 10^5 + 98.85\ T + 3.671\ T^2 \quad \text{(J/kg)} \qquad (3.4.26)$$

Another property that is needed in the calculations is the vapor pressure, P_{vp} (N/m^2), of liquid and solid water. Correlations for this property are given in Table 3.4.6.

TABLE 3.4.5 Heat Capacities of Air and Its Component Species

	C_p° Equation $(a+bx10^{-2}T+cx10^{-5}T^2+dx10^{-8}T^3)$				
Chemical	a	b	c	d	units
N_2	31.15	-1.357	2.680	-1.168	J/gmole K
O_2	28.11	-3.680	1.746	-1.065	J/gmole K
Air	30.51	-1.072	2.484	-1.146	J/gmole K
Air	1058	-37.16	86.11	-39.73	J/kg K
H_2O_{vap}	1790	-10.68	58.58	-19.97	J/kg K
H_2O_{liq}	5420	-1281.	1982.		J/kg K

TABLE 3.4.6 Vapor Pressures of Liquid and Solid Water

Water Phase	$\ln P_{vp} = a - b/T$ a	P_{vp} in Pascals, T in K b
Liquid	25.7710	5288.39
Solid	28.8078	6118.05

3.4.7 Calculation Scheme

The actual thermodynamic calculation steps for a chemical release are outlined in this section.

Consider the situation wherein M_{AIR} kg of wet air at temperature T_{AIR}, atmospheric pressure P_A, and relative humidity RH_i (containing M_A kg of dry air and M_W kg of water), is mixed with M_{CH} kg of chemical at temperature T_{CH} with a mass fraction f as liquid aerosol. In addition, we define the following terms:

H_{AF} = enthalpy of dry air in the final mixture (J)
$H_{CH\ell F}$ = enthalpy of the liquid chemical in the final mixture (J)
H_{CHVF} = enthalpy of the chemical vapor in the final mixture (J)
H_{WSF} = enthalpy of the solid water in the final mixture (J)
$H_{W\ell F}$ = enthalpy of the liquid water in the final mixture (J)
H_{WVF} = enthalpy of the water vapor in the final mixture (J)
MW_A = molecular weight of air (kg/kgmole)
MW_W = molecular weight of water (kg/kgmole)
MW_{CH} = molecular weight of the chemical (kg/kgmole)
$P_{vp,W}$ = vapor pressure of water at a given temperature (Pa)
$P_{vp,CH}$ = vapor pressure of the chemical at a given temperature (Pa)
P_a = atmospheric pressure = 101325 Pa
RH_f = relative humidity of the equilibrium mixture
N_{TOT} = total number of moles in the vapor
T_{MIX} = final mixture (equilibrium) temperature (K)
M_{WVF} = mass of water vapor in the final mixture (kg)
$M_{W\ell F}$ = mass of water liquid in the final mixture (kg)
M_{WSF} = mass of water ice in the final mixture (kg)
M_{CHVF} = mass of chemical vapor in the final mixture (kg)
$M_{CH\ell F}$ = mass of chemical liquid in the final mixture (kg)
y_{wi} = mole fraction of water in the vapor initially
y_{wf} = mole fraction of water in the vapor at equilibrium

Given the initial mass of wet air and relative humidity, the mass of dry air and water present initially are given as

$$y_{wi} = RH_i * [P_{vp,w}(T_{AIR})/P_a]$$

$$M_A = M_{AIR} * (1-y_{wi})/[1 + y_{wi} * [(MW_w/MW_A) - 1]] \quad (3.4.27)$$

$$M_w = M_{AIR} - M_A$$

The relative humidity of the final mixture is given by:

$$N_{TOT} = [(M_{CH}/MW_{CH}) + (M_A/MW_A) + (M_w/MW_w)] * 1000$$

$$y_{wf} = (M_w/MW_w)*1000/N_{TOT} \quad (3.4.28)$$

$$RH_f = y_{wf} * (P_a/P_{vp,w}(T_{MIX}))$$

If the calculated RH_f is greater than 1, then we have water present in condensed form as well. In such a case, saturation of water in the vapor requires the following relation to hold:

$$y_{wf}*P_a = P_{vp,w}$$

$$P_{vp,w} = (M_{WVF}/MW_w)*P_a/[(M_{CH}/MW_{CH})+(M_A/MW_A)+(M_{WVF}/MW_w)] \quad (3.4.29)$$

Rearrangement gives

$$M_{WVF} = [P_{vp,w}/(P_a-P_{vp,w})]*[(M_{CH}/MW_{CH})*MW_w+(M_A/MW_A)*MW_w] \quad (3.4.30)$$

and

$$M_{wlf} = M_w - M_{WVF} \quad (3.4.31)$$

where $P_{vp,w}$ is evaluated at the system temperature. Similarly, in order to calculate the distribution of chlorine in liquid and vapor phases,

$$P_{vp,CH} = [(M_{CHVF}/MW_{CH})*P_a]/[M_{CHVF}/MW_{CH})+(M_A/MW_A)] \quad (3.4.32)$$

Rearrangement gives,

$$M_{CHVF} = [(M_A/MW_A)*MW_{CH}] * P_{vp,CH}/(P_a-P_{vp,CH}) \quad (3.4.33)$$

and

$$M_{CHlf} = M_{CH} - M_{CHVF} \quad (3.4.34)$$

where $P_{vp,CH}$ is calculated at the system temperature.

The general enthalpy balance equation becomes,

$$H_I + Q = H_F \quad (3.4.35)$$

where the final enthalpy is given by

$$H_f = M_A * H_{AF} + M_{CHVF} * H_{CHVF} + M_{CH\ell F} * H_{CH\ell F} + M_{WVF} * H_{WVF} + M_{W\ell F} * H_{W\ell F} + M_{WSF} * H_{WSF} \quad (3.4.36)$$

Depending upon which domain the final mixture is in, one or the other terms in the above equation will be zero. In domain I, all chlorine is in vapor form, while water is in liquid and vapor forms ($273.2 < T_{MIX} < T^{SAT}(P_{VP,W})$). Thus, $M_{CH\ell F}$ and M_{WSF} are zero. In domain II, chlorine is a vapor, while water is present in gas, liquid and solid forms. The temperature is 273.2 K. In this case, $M_{CH\ell F} = 0$. In domain III, chlorine is a vapor, and water is present as solid ice and vapor ($T^{SAT}(P_{VP,CH}) < T_{MIX} < 273.2$). Thus, $M_{CH\ell F}$ and $M_{W\ell F}$ are zero. In domain IV, chlorine is present both as liquid and vapor, and all water is present as vapor and solid ice. ($T_{MIX} < T^{SAT}(P_{VP,CH})$). Here, $M_{W\ell F}$ is zero. We first calculate H_f at the temperatures that divide the domains. By comparing these calculated H_f's with the value $H_I + Q$ we can identify in which domain the final mixture lies. Then, numerical temperature iterations are done until H_f is close to $H_I + Q$ (within 5%) and the final temperature and other cloud parameters (density, etc.) are found.

3.4.8 Results and Discussion

Figures 3.4.4 (a) and (b) illustrate the effects of increased entrainment of ambient wet air and the initial chlorine aerosol fraction on the final system temperature and density. One kg of saturated chlorine with aerosol fraction, f, (0%, 20%, and 50%) is mixed with increasing amounts (0.001 kg to 1000 kg) of wet air at 300 K and relative humidity of 75%. Adiabatic conditions are assumed (Q = 0).

Figure 3.4.4a indicates that with 0% aerosol fraction (only chlorine vapor in the mixture initially) the final system temperature increases monotonically with increased entrainment of warm, humid air. At $(M_{AIR}/M_{CH}) = 1$, the system temperature is about 285 K. If liquid chlorine is present initially, entrainment of ambient air results in liquid evaporation and thus the system temperature decreases. For an aerosol fraction of 20%, the system temperature falls to as low as 230 K. For f = 50%, the minimum temperature is about 215 K ($M_{AIR}/M_{CH} \approx 1$). This decrease in cloud temperature is due to the evaporation of the liquid aerosol, and the cloud temperature reaches a minimum when the last drop of the liquid chlorine aerosol evaporates. The temperature subsequently increases rapidly as more warm, humid air is entrained into the cloud. At (M_{AIR}/M_{CH}) above 100, the temperature of the system is essentially that of the ambient air. The condition $(M_{AIR}/M_{CH}) > 10$ is typically achieved relatively quickly after a chemical vapor cloud is released. Thus, for practical purposes, one might be able to assume that the final temperature of the system to be the same as that of the ambient air in the dispersion region and simplify the calculations.

Figure 3.4.4b shows that the density of the cloud decreases (for f = 0%) monotonically from about 3.5 kg/m^3 ($M_{AIR}/M_{CH} = 0.001$) to 1.2 kg/m^3 for large entrainment values. The behavior is similar for other

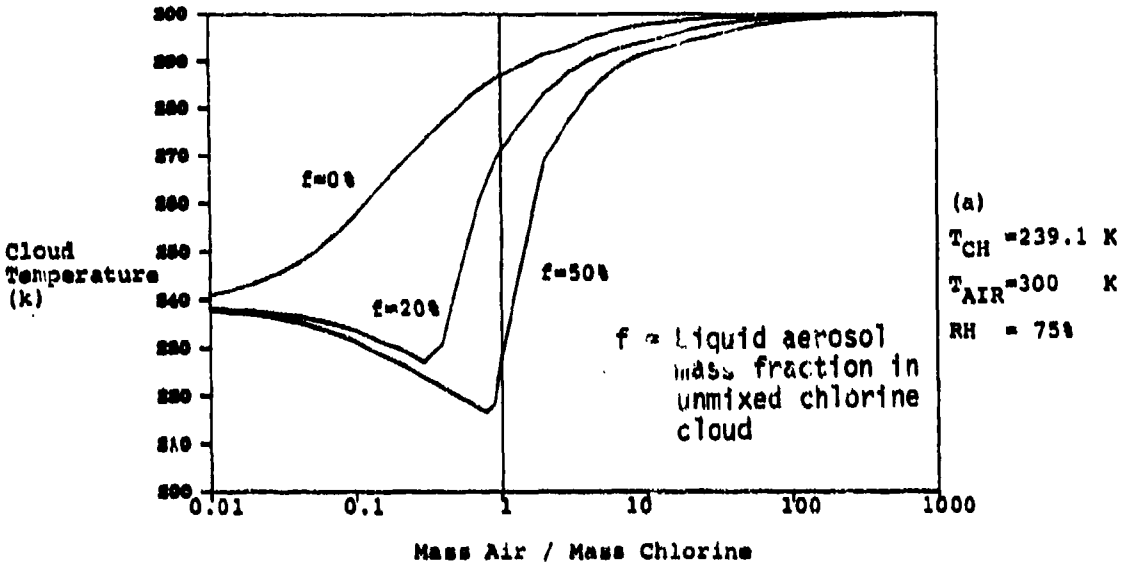

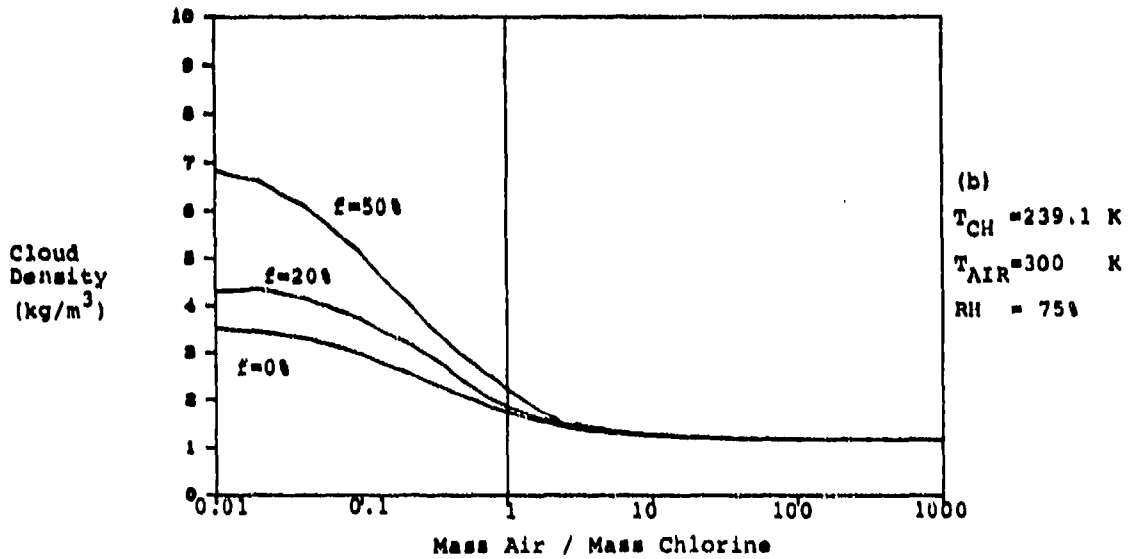

FIGURE 3.4.4: Cloud Temperature (K) and Cloud Density (kg/m^3) as a function of mass of air entrained, mass of chlorine initially present

aerosol fraction values as well, but the cloud densities are higher due to the presence of significant liquid in the system. Again, for $(M_{AIR}/M_{CH}) > 10$, the cloud density is very close to that of ambient air.

Figures 3.4.5 (a) and (b) illustrate the effects of lowering the relative humidity of the entrained air on the results shown in Figures 3.4.4 (a) and (b). The relative humidity here is 25%, versus 75% in previous case; the other conditions are identical. The cloud temperature and density show similar behavior, although the cloud temperature is slightly lower than that for the previous case. There is no significant change in the cloud density since the fraction of water in ambient air is not very large (most of the mass of wet air is due to dry air).

Figures 3.4.6 (a) and (b) illustrate the effects of lowering the temperature of the entrained air on the results shown in Figures 3.4.4 (a) and (b). The air temperature is decreased to 260 K, versus 300 k in the previous case; the other conditions are identical. The cloud temperature and cloud density show similar behavior, i.e., for f = 0% the cloud temperature increases monotonically from T_{CH} to T_{AIR}. For higher values of f, the temperature decreases first and then increases as more wet air is entrained, because of increasing liquid evaporation. Again, there is no significant change in the cloud density.

Figures 3.4.7 (a) and (b) illustrate the effects of lowering the temperature and relative humidity of the entrained air on the results shown in Figures 3.4.4 (a) and (b). The variations in cloud temperature and density are similar to those discussed in the previous cases.

Figures 3.4.8 (a) and (b) illustrate these results for a release of phosgene at its normal boiling point. The initial conditions are 1 kg phosgene at 281.4 K, mixed with air at 300 K, RH = 75%. The general behavior of the system is similar to that of chlorine release. With f = 0%, the cloud temperature rises and cloud density declines monotonically with increased entrainment. At higher f values, the cloud temperature drops initially, followed by an increase. The cloud density decreases, as it did for the chlorine release. Similar behavior is also seen for the cases of other chemicals as well (Figures 3.4.9 (a) and (b) for sulfur dioxide and Figures 3.4.10 (a) and (b) for hydrogen sulfide). Differences in the actual temperatures and densities arise due to the differences in their thermodynamic properties.

The passive (type I) chemicals behave similarly as shown above. When the ratio of the mass of entrained air to the mass of released chemical is large ($M_{AIR}/M_{CH} >> 10$), as is usually encountered in atmospheric dispersions, the cloud temperature and density approach those of the ambient air. Furthermore, all of the chemicals have a higher (than air) density at low M_{AIR}/M_{CH} ratios, indicating that these chemicals behave as heavy gases, at least initially. The higher

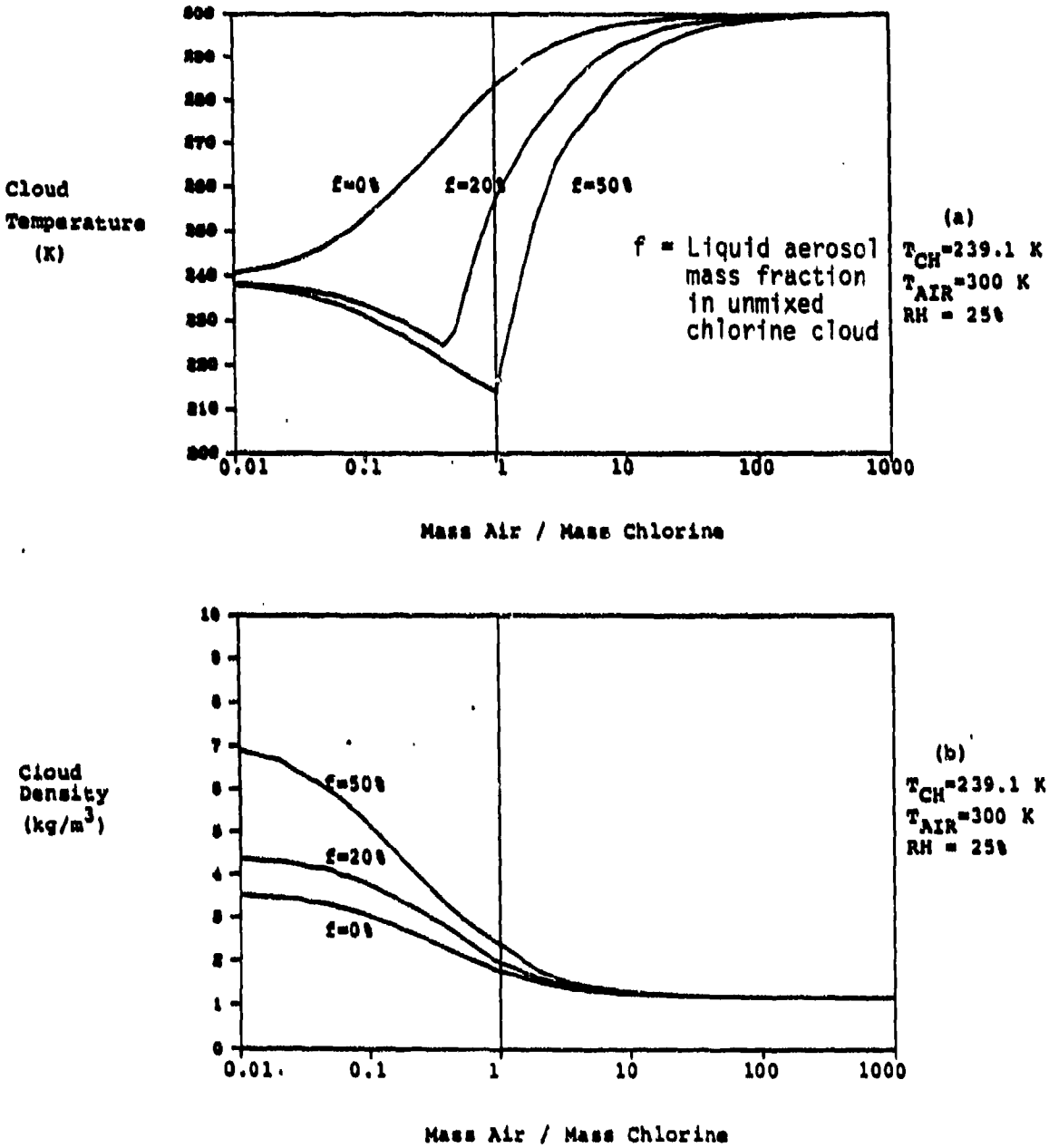

FIGURE 3.4.5: Cloud Temperature (K) and Cloud Density (kg/m^3) as a function of mass of air entrained/mass of chlorine initially present

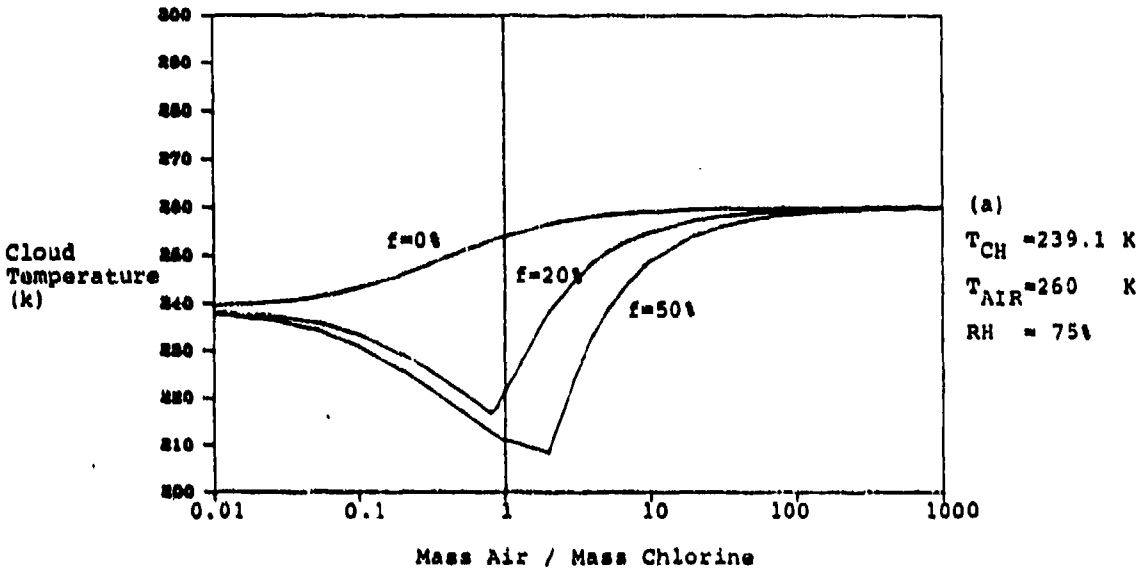

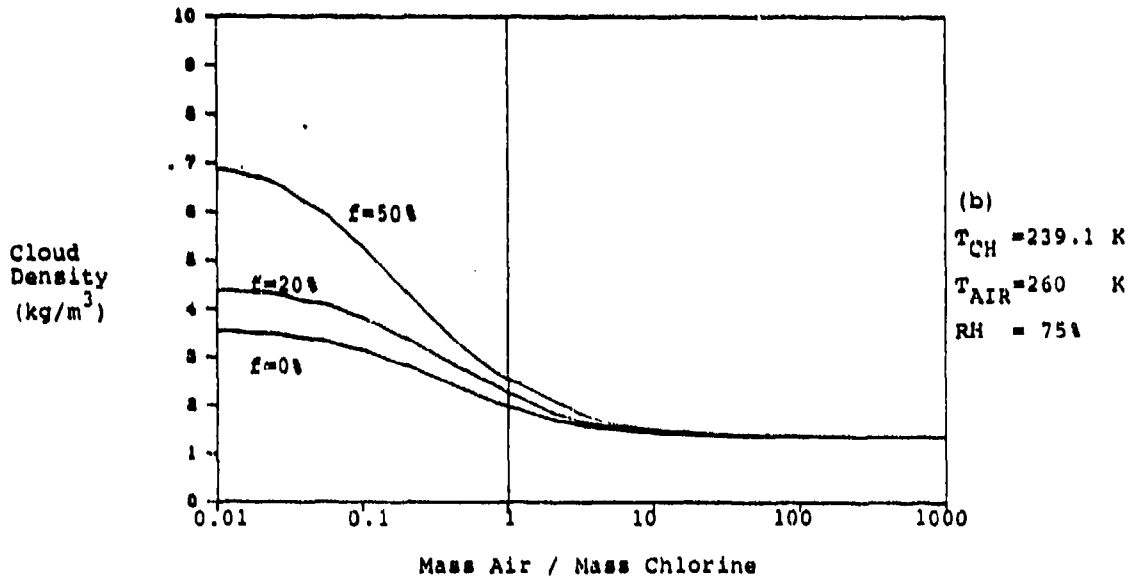

FIGURE 3.4.6: Cloud Temperature (K) and Cloud Density (kg/m^3) as a function of mass of air entrained/mass of chlorine initially present

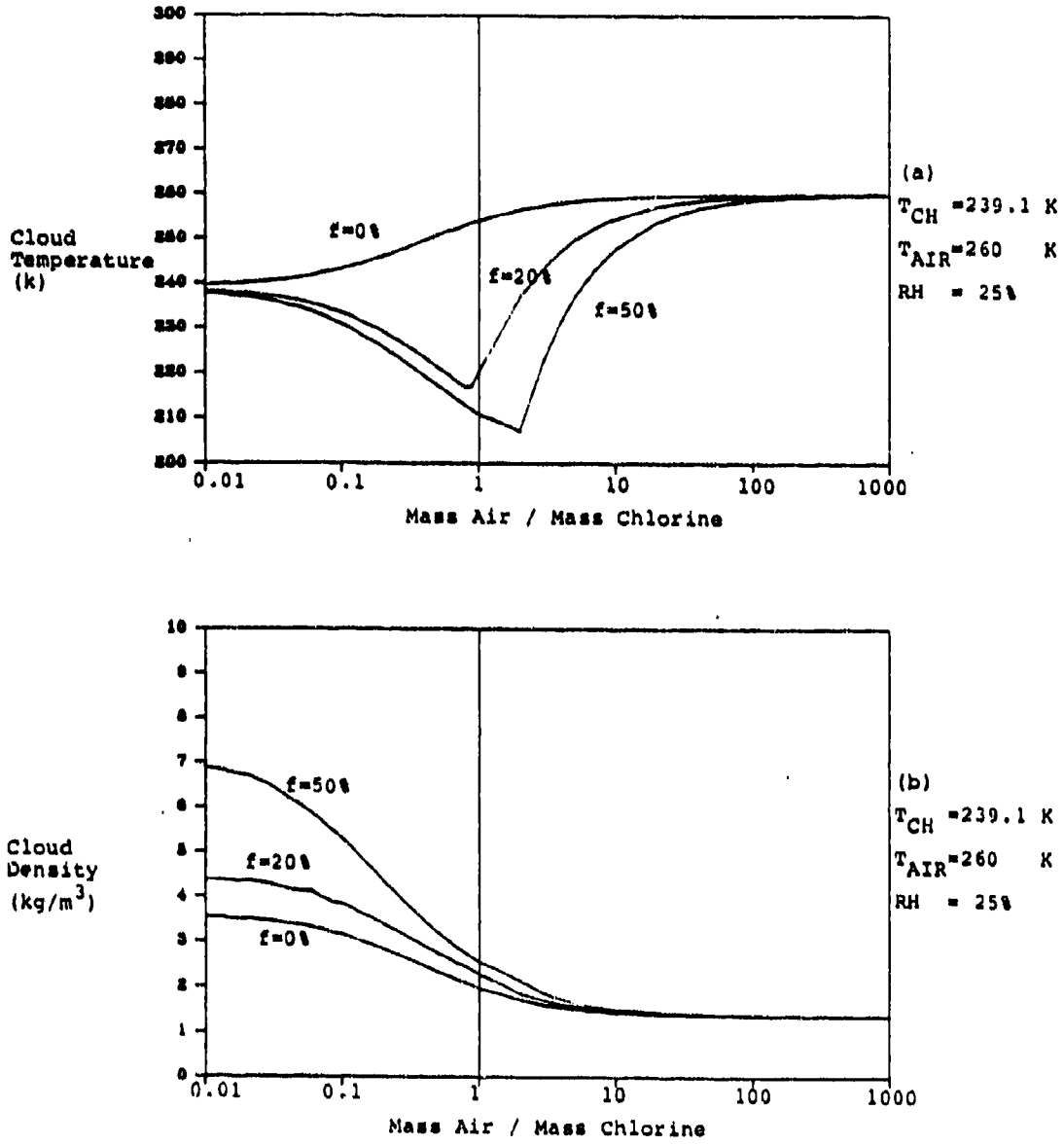

FIGURE 3.4.7: Cloud Temperature (K) and Cloud Density (kg/m^3) as a function of mass of air entrained/mass of chlorine intitially present

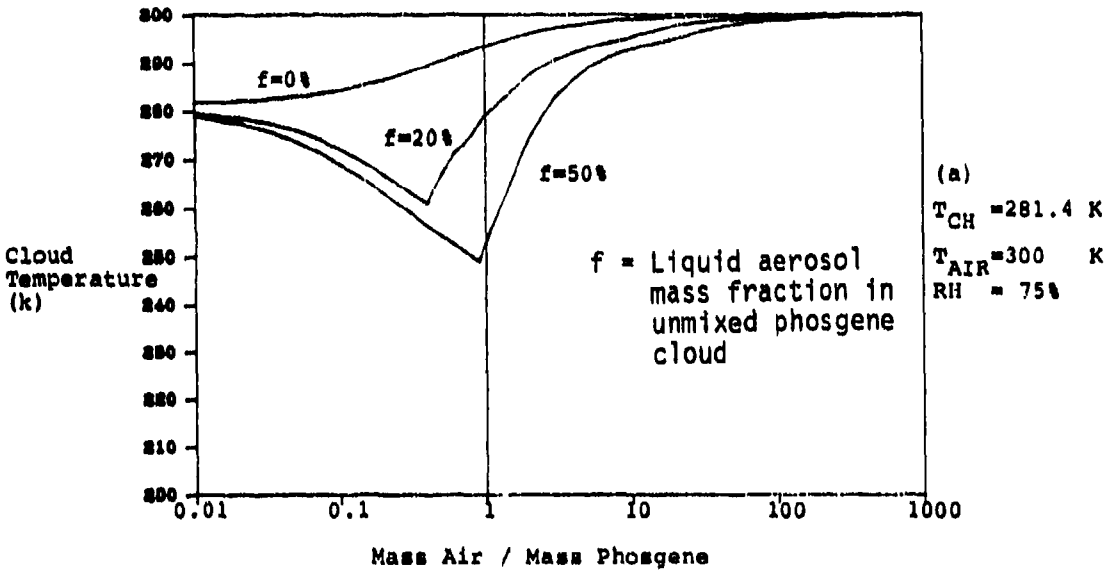

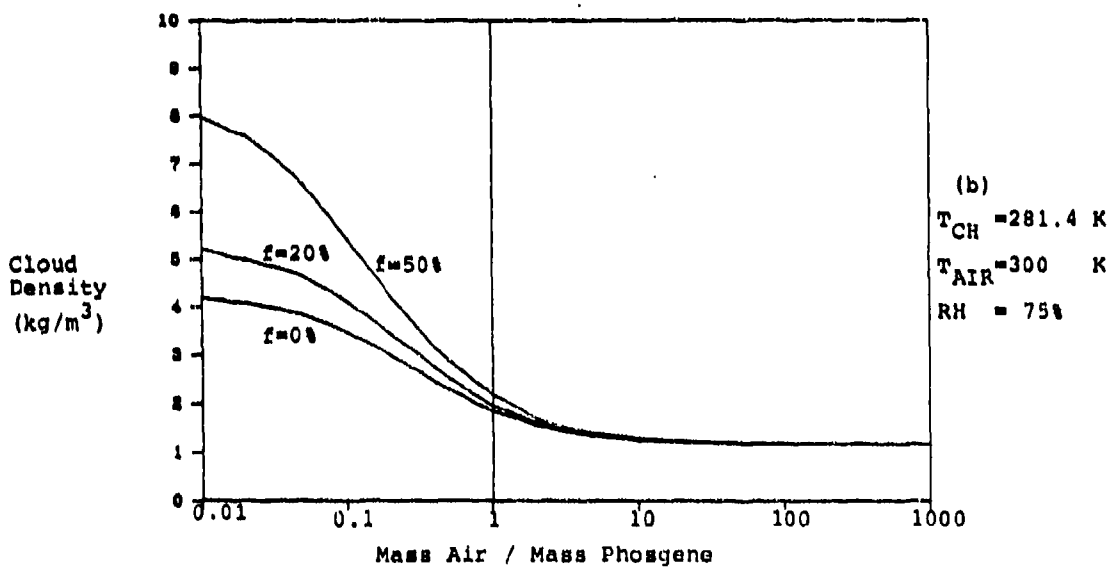

FIGURE 3.4.8: Cloud Temperature (K) and Cloud Density (kg/m^3) as a function of mass of air entrained/mass of phosgene initially present

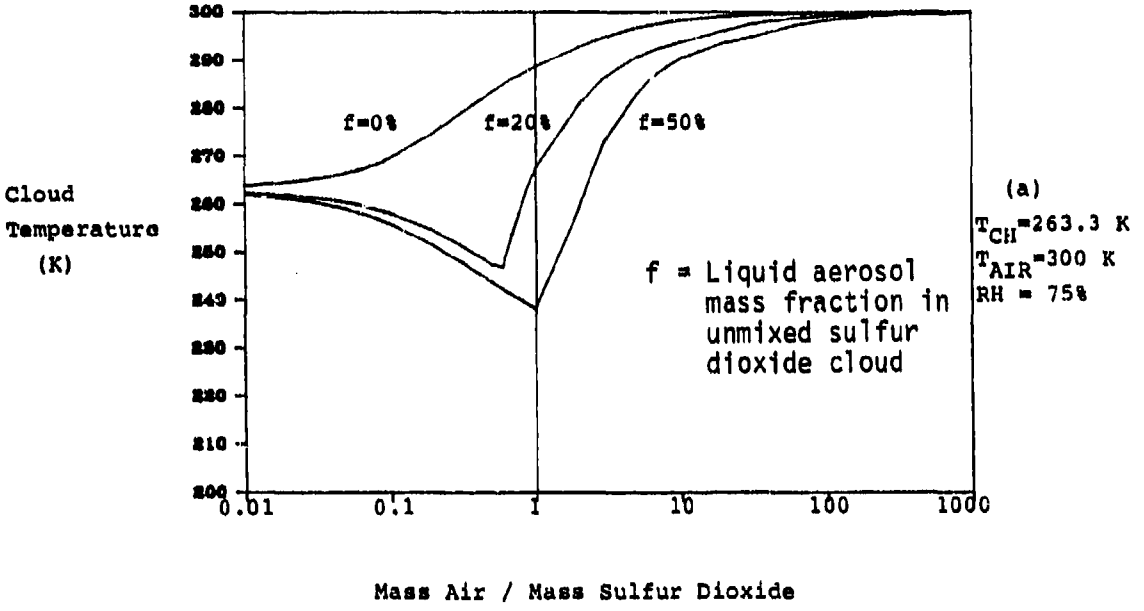

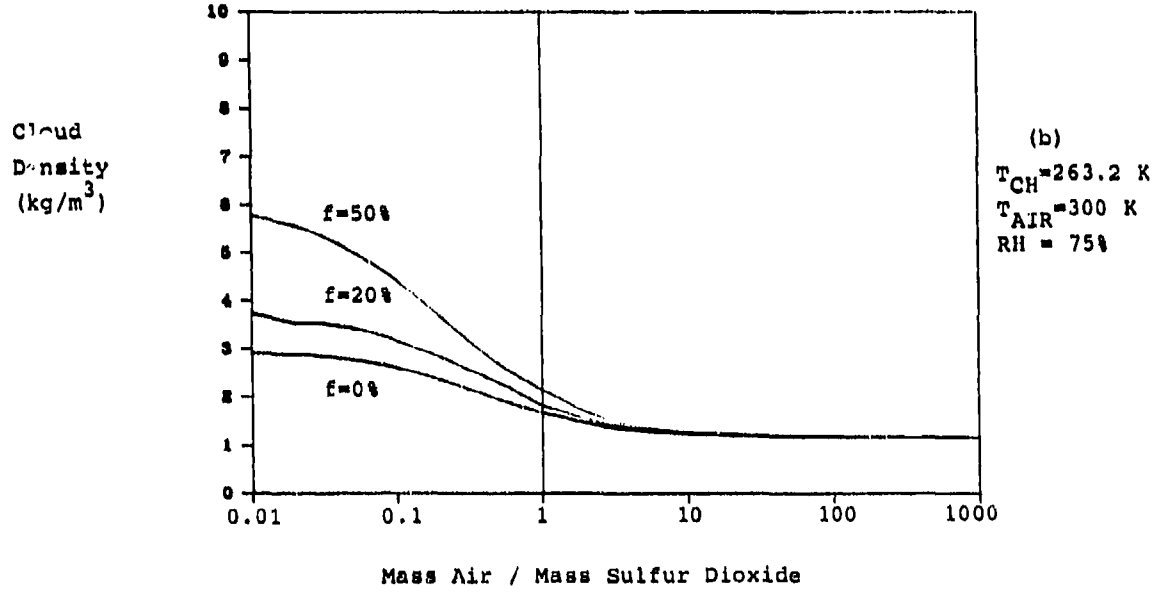

FIGURE 3.4.9: Cloud Temperature (K) and Cloud Density (kg/m^3) as a function of mass of air entrained/mass of sulfur dioxide initially present

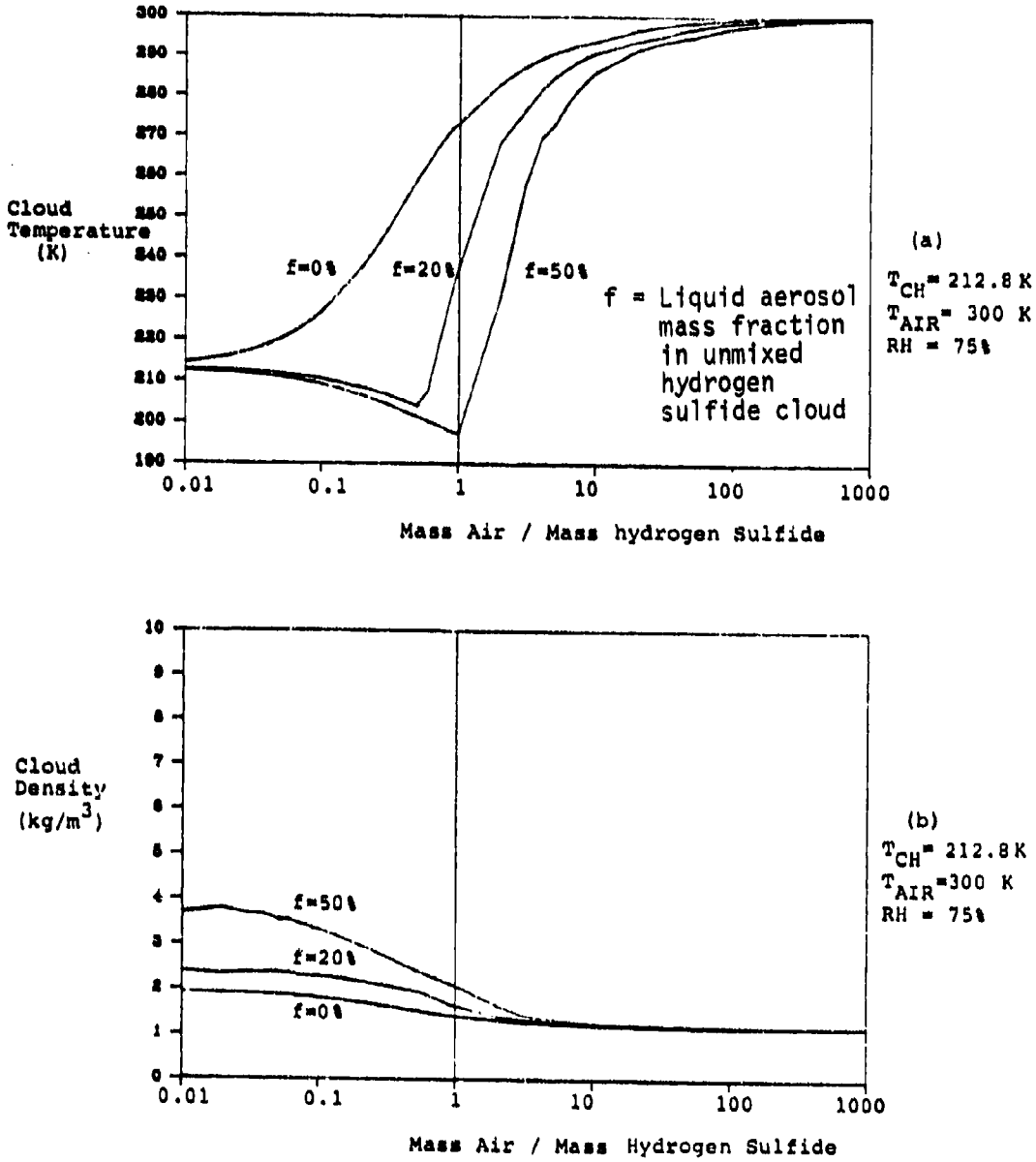

FIGURE 3.4.10: Cloud Temperature (K) and Cloud Density (kg/m^3) as a function of mass of air entrained/mass of hydrogen sulfide initially present

densities are due to entrained aerosols, decreased temperature due to aerosol evaporation, and higher molecular weights than air.

3.5 AMMONIA (TYPE II)

3.5.1 Background

Ammonia (NH_3), a very widely used chemical, is transported and stored as a pressurized liquid. Its normal boiling point is 239.8 K and the liquid has a vapor pressure of 10.4 atm. at 300 K (7.6 atm. at 290 K). Due to the relatively high vapor pressure of ammonia stored at ambient temperatures, liquid ammonia escaping from a pressurized tank will vigorously flash and much of the liquid released will be in the form of fine aerosols (Raj, 1982).

Ammonia is quite soluble in liquid water. At 293 K, for example, with a partial pressure of ammonia = one atm., the weight fraction of ammonia in solution is about 0.33. The solubility increases as the temperature is lowered.

Kaiser and Walker (1978) modeled the consequences of mixing ammonia aerosols with air. Based on computations by Haddock and Williams (1978), they assumed that the effect of water in the entrained air could be neglected when the aerosol fraction was large. They do state, however, that this assumption is invalid at low aerosol fractions. Raj and Aravamudan (1980) did account for the reaction chemistry between ammonia aerosols and water condensed from the entrained air.

3.5.2 NH_3 - Water Reaction Model

If humid air is mixed with a cold ammonia and water condenses, a significant quantity of ammonia is found in the water. Also, the solution process is exothermic with some 700 kJ evolved for the dissolution of 1 kg of ammonia to form a 20-40 weight percent solution. To treat the equilibrium and energetic aspects of the ammonia-water (vapor-liquid) system, detailed property correlations are necessary. The partial pressures of both ammonia and water in equilibrium with an aqueous solution depend upon the temperature and liquid composition. The specific solution enthalpy is also a function of the same two variables. Therefore, an enthalpy balance employed to calculate the final state after mixing ammonia (vapor plus aerosol) with humid air must allow for the dissolution process as well as the enthalpy changes to form ammonia solutions. If no water condenses, then the final thermodynamic state of the cloud is relatively easy to compute. The calculations done are the same as for the passive (type I) chemicals described in Section 3.4.

One conceptual question for the ammonia-water solution is if a solid phase (water or water-ammonia) would exist. Water-ammonia solutions have low freezing points, e.g., from about 30 weight percent ammonia to pure liquid ammonia, the solution freezing point is ≈ 190 K. Equilibrium considerations would dictate that solutions would appear

in the temperature region 273 K > T_{MIX} > 190 K, but shock cooling could well form some solid water ice. Without definitive data, we have opted for the "equilibrium" case and, thus, have assumed cold (<273K) solutions of water and ammonia exist as a liquid solution.

In our thermodynamic analysis, M_{CH} kg of NH_3 is released with a mass fraction, f, of aerosol at temperature T_{CH}. The ammonia vapor-aerosol is in vapor-liquid equilibrium at 1 atmosphere pressure. This is mixed with M_{AIR} kg of wet air consisting of M_A kg of dry air with an absolute humidity AH (kg H_2O/kg dry air). Energy input from the environment is specified as Q (J).

In the calculations of the state after mixing ammonia (vapor and aerosol) with humid air, one should consider if (i) pure, liquid ammonia exists, and (ii) if a condensed aqueous water and ammonia solution is present. To show that liquid ammonia is present, one must demonstrate that the partial pressure of ammonia in the vapor is greater than the vapor pressure of pure ammonia at the system temperature. Similarly, to show that water is present in the liquid phase, one must prove that the partial pressure of water in the vapor is greater than the partial pressure over saturated ammonia-water solution at the system temperature. The system temperature is itself determined from an enthalpy balance wherein one equates the total initial enthalpy of ammonia plus humid air to the final mixture enthalpy plus any energy input from the environment.

We begin by calculating the temperature ($T^{SAT}(P_{VP,W})$) above which no condensed phase exists. This is the dew point for water, assuming that the more volatile component (ammonia) will be the first to evaporate. At the dew point, the partial pressure of water, $P_{VP,W}$, is:

$$P_{VP,W} = P_a*(AH*M_A/MW_W)/[(AH*M_A/MW_W)+(M_A/MW_A)+(M_{CH}/MW_{CH})] \quad (3.5.1)$$

where the parameters are the same as described in Section 3.4.7 above.

An overall enthalpy balance is then computed where the total initial enthalpy (H_I) plus the energy added (Q) is equal to the final total enthalpy (H_F).

$$H_I + Q = H_F \quad (3.5.3)$$

where H_F is calculated at $T^{SAT}(P_{VP,W})$ and the properties of ammonia-air-water vapor mixtures are used. If $H_F > H_I + Q$, then we conclude that the actual final temperature lies below $T^{SAT}(P_{VP,W})$ and a condensed phase is present. Otherwise, the final state is a homogeneous vapor mixture.

In the case where liquid a phase exists, we need to solve the material and energy balances by an iterative process. The initial enthalpy of the system is given by

$$H_I = M_{CH}*(1-f)*H_{CHVI}+M_{CH}*f*H_{CHLI}+M_A*C_A*T_{AIR}+M_A*AH*H_{VVI} \quad (3.5.4)$$

where

$H_{CH\ell I}$ = Initial specific enthalpy of the ammonia liquid (J/kg)
H_{CHVI} = Initial specific enthalpy of the ammonia vapor (J/kg)
H_{WVI} = Initial specific enthalpy of the water vapor (J/kg)
C_A = Specific heat of air (J/kg-K)
T_{AIR} = Initial air temperature (K)

The final enthalpy is given by

$$H_F = (M_{CH\ell F}+M_{W\ell F})*H_{\ell F} + (M_{CHVF}+M_{WVF})*H_{VF} + M_A*C_A*T_{MIX} \qquad (3.5.5)$$

where

$H_{\ell F}$ = enthalpy of liquid in the final mixture
H_{VF} = enthalpy of vapor in the final mixture
T_{MIX} = final system temperature

The ammonia vapor and water vapor specific enthalpies and the liquid ammonia, liquid water, and aqueous ammonia specific enthalpies, are found using a special subroutine (H2ONH3). This subroutine contains data for the enthalpies of saturated water-ammonia mixtures at various (ammonia + water) partial pressures and ammonia mass fraction in the liquid phase. When the partial pressure of the ammonia and/or water vapor ($P_{vp,CH}+P_{vp,W}$) and the mass fraction of the liquid that is ammonia ($M_{CH}/(M_{CH}+M_W)$)are input into the subroutine, the enthalpies of the liquid and vapor phases ($H_{\ell F}$ and H_{VF}), the temperature (T_{MIX}), and the mass fraction of the vapor that is ammonia ($M_{CHVF}/(M_{CHVF}+M_{WVF})$) are calculated by interpolating stored data.

By using the subroutine H2ONH3, and an iterative procedure, one is able to solve the energy balance equation to obtain the final system temperature as well as the final thermodynamic state.

3.5.3 Results

Figure 3.5.1 shows the variation of density of ammonia vapor and entrained liquid aerosol mixture when saturated liquid is released from various storage temperatures. This shows that the density of ammonia and entrained aerosols can be greater that the density of air ($\rho_{AIR} \approx 1.2$ kg/m^3). Thus, heavy gas effects must be considered in the dispersion of such releases.

Figures 3.5.2 (a) and (b) illustrate the computed results for the ammonia-humid air thermodynamic analysis. M_{CH} kg of ammonia (50 wt% of the liquid remaining after the flash is entrained as liquid in the vapor and aerosol mixture) at 239.8 K is mixed with M_{AIR} kg of humid air at 300 K and relative humidities of 0, 50, and 100%. The mass of humid air/mass of ammonia is shown on the abscissa. This ratio is varied from 0.01 to 10000; increasing the ratio corresponds to more dilution by air. In Figure 3.5.2 (a) the calculated cloud temperatures are shown. The temperature decreases initially as the liquid ammonia evaporates. After the liquid ammonia has evaporated, the system temperature increases and approaches that of the ambient air. This

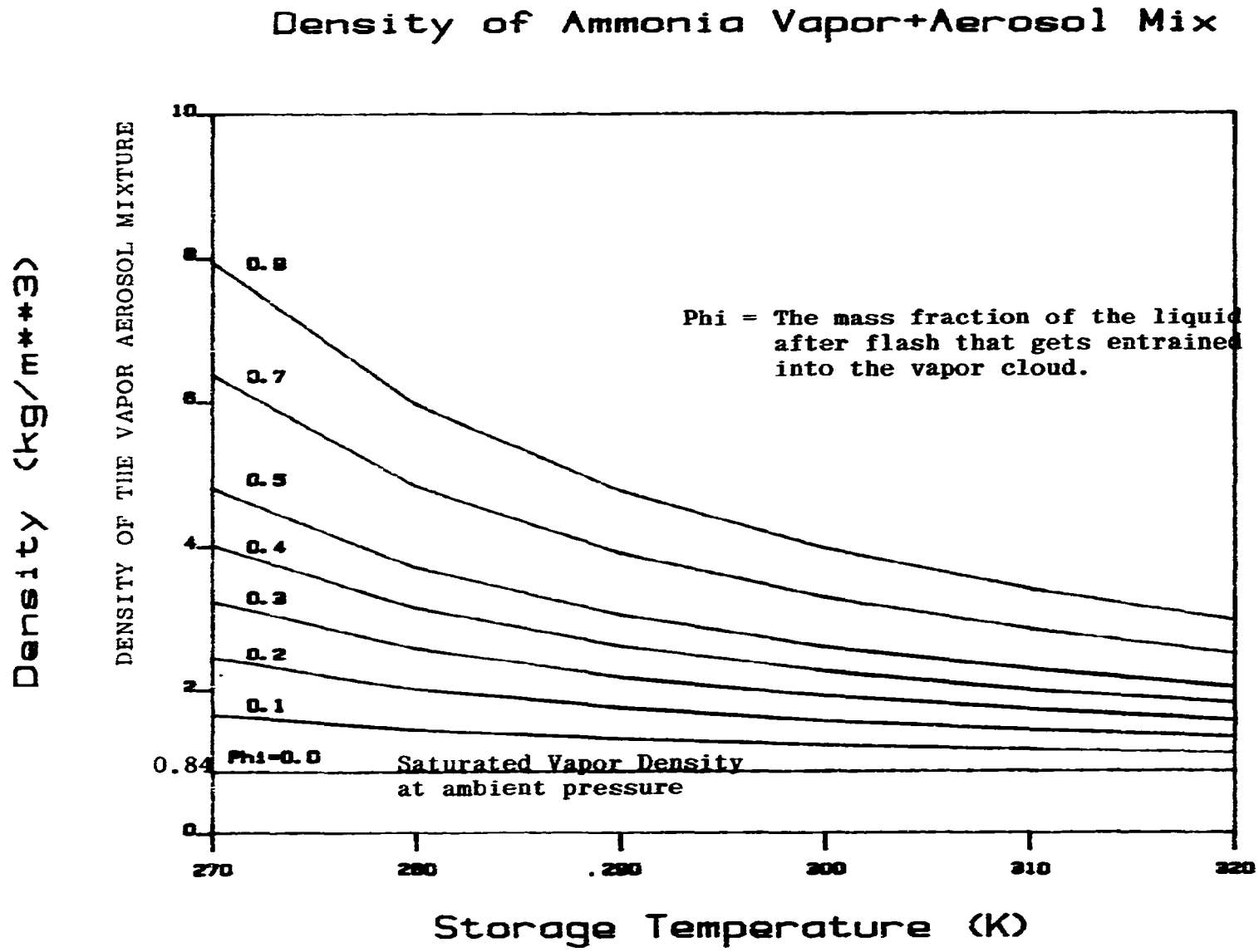

FIGURE 3.5.1: Variation of Density of Ammonia Vapor+ Entrained Liquid Aerosol Mixture When Saturated Liquid is Released From Various Storage Temperatures

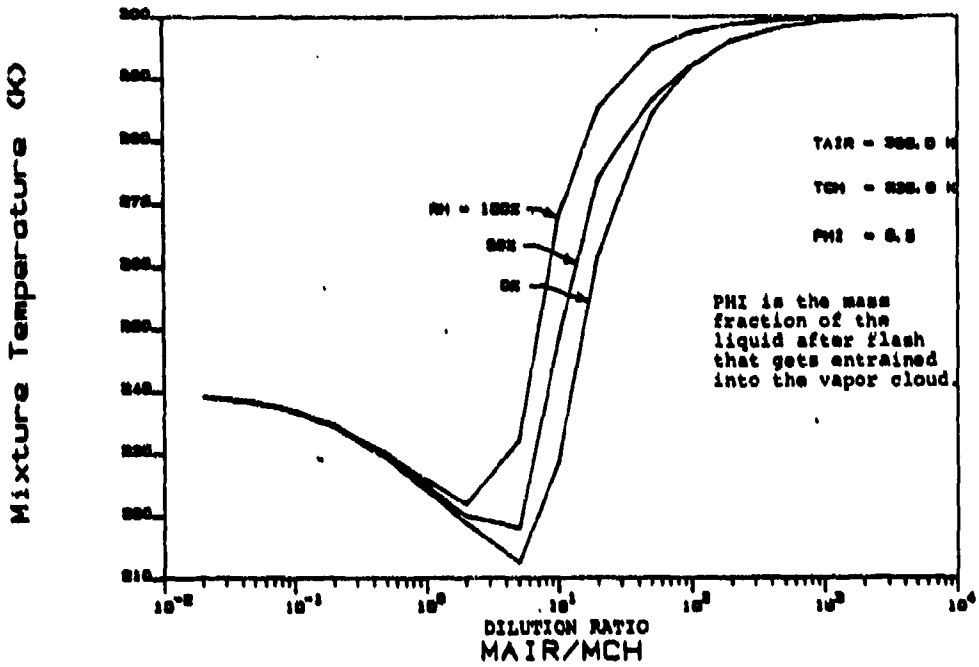

FIGURE 3.5.2a: Variation of Ammonia Vapor+Aerosol & Air Mixture Temperature with Air Dilution Ratio

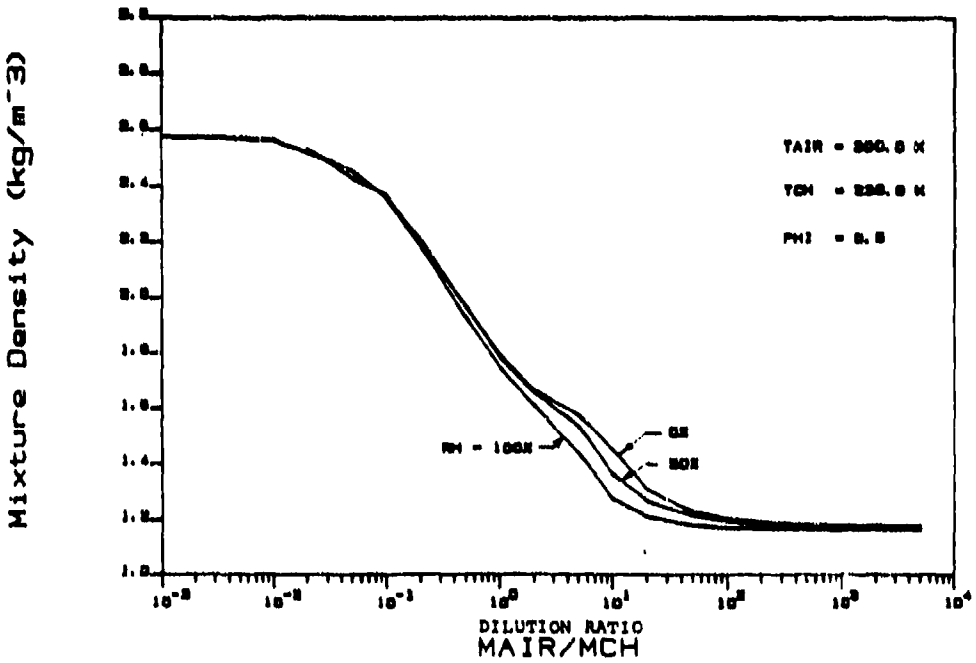

FIGURE 3.5.2 b: Variation of Ammonia Vapor + Aerosol + Humid Air Mixture Density with Dilution Ratio

FIGURE 3.5.2: Variation of Ammonia Air Mixture Temperature and Density With Air Dilution

behavior is similar for all three relative humidities shown. The cloud temperature is higher for mixtures that have higher ambient air relative humidities. At the higher humidities, more water is present in the air, and, thus, more heat is released into the cloud from the ammonia dissolution in the water. This results in a higher cloud temperature.

In Figure 3.5.2 (b), the corresponding cloud densities are plotted. As shown, the densities is initially around 2.6 kg/m^3 and it decreases as air is entrained. Thus, heavy gas effects must be considered in the dispersion analysis.

Figure 3.5.3 shows the computed results for the ammonia-humid air thermodynamic analysis. M_{CH} kg of ammonia (90 wt% vapor and 10 wt% aerosol) at 239.8 K was mixed with M_{AIR} kg of wet ambient air at 300 K and relative humidity of 100%. The mass ratio of humid air to ammonia (M_{AIR}/M_{CH}) was varied from 0.01 to 10000, as shown on the abscissa. On the ordinate, the mass fractions of the various components present at equilibrium are shown, with the sum of the mass fractions for each phase equal to one. The mass fraction of ammonia in the vapor phase decreases as the quantity of air entrained increases. The mass fraction of liquid ammonia also decreases during this process. This is clearly due to the increasing effect of dilution of the ammonia in the system.

The mass fraction of the liquid phase components are also shown in the figure. For low ratios of air to ammonia, most of the water condenses, and thus, there is a negligible water vapor component. As the quantity of air entrained increases, however, the water also begins to evaporate, and as $(M_{AIR}/M_{CH}) > 100$, all the water is in vapor form. It can also be seen that the liquid ammonia mass fraction decreases during the time the water concentration increases in the range $(M_{AIR}/M_{CH}) = 0.01$ to 10. This indicates that the dilution effect of the entrained air is much more pronounced than the tendency of ammonia to be soluble in liquid water. This is consistent with our earlier assumption that the water will be the last to evaporate from the liquid phase. In addition, as M_{AIR}/M_{CH} approaches 100, the dew point of the water is reached and all of the liquid evaporates, as shown by the nearly vertical H_2O (aq) line at that point.

3.6 NITROGEN TETROXIDE (TYPE III)

3.6.1 Background

There is an overwhelmingly large body of literature dealing with the oxides of nitrogen. Most papers, however, are concerned with the role these oxides play in air pollution or in the production of nitric acid.

The air pollution literature was examined primarily to ascertain if any of the well-studied reactions were pertinent to the current problem. It was concluded that the air-pollution time-scales are much longer. Also, photochemical reactions play a key role in air

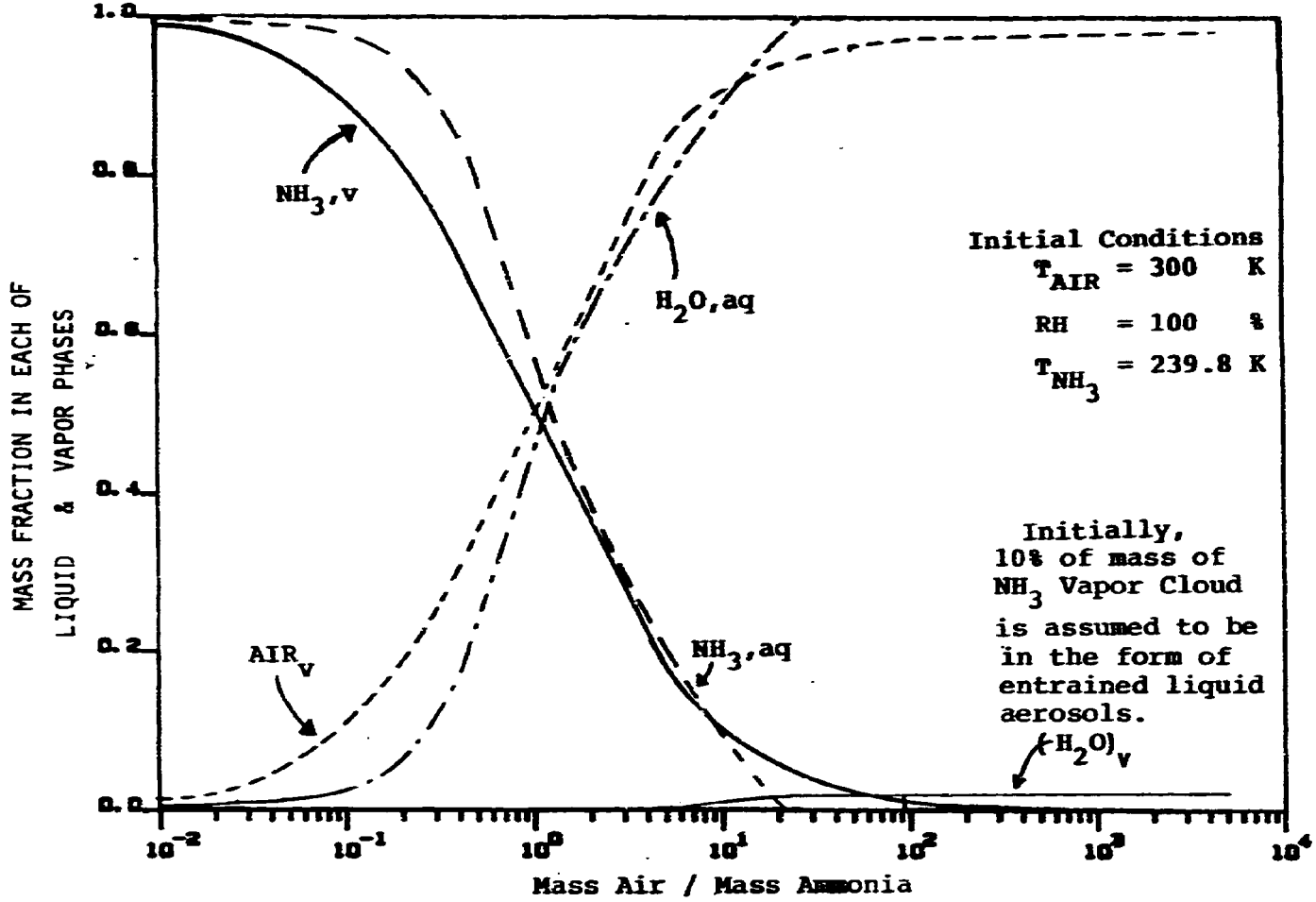

FIGURE 3.5.3: Composition of Equilibrium Mixtures of NH_3 and Humid Air

pollution studies, but such are not relevant here. An excellent review of the air pollution literature is, however, available (Seinfeld, 1980) and the topic is discussed in American Petroleum Institute's report (API Manual, 1977).

The second major area is concerned with the system O_2-NO-NO_2-liquid water and the concomitant reactions and mass transfer aspects in producing liquid nitric acid. While such material is not directed to reactions between vaporized (spilled) N_2O_4 and humid air, some of the research conducted in gas-phase reactions are indeed pertinent to the present study.

3.6.2 Nitrogen Oxides Involved

Many oxides of nitrogen have been studied. By various techniques they are all interconvertable from one to another. The principal oxide of interest here is the tetroxide, N_2O_4. The properties of N_2O_4 are detailed in a publication from Hercules Chemical Company (1968).

In the liquid - or vapor, N_2O_4 is always considered to be in equilibrium with nitrogen dioxide, e.g.,

$$2NO_2 = N_2O_4 \qquad (3.6.1)$$

The time constant for reaction (3.6.1) is less than one microsecond. Often one speaks of the "chemical" NO_2 in a mixture of NO_2 and N_2O_4. This is interpreted to mean $[NO_2 + 2(N_2O_4)]$ as though all material were in the dioxide form.

The oxides N_2O, NO_3, and N_2O_5 are either unstable or difficult to form from N_2O_4 and are not considered in this study. The last oxide, NO, plays a role in the NO_2-N_2O_4 reactions with water.

3.6.3 Chemical Reactions Relevant to the N_2O_4-NO_2-H_2O System

N_2O_4 and NO_2 form an equilibrium mixture which freezes at -11.2°C and boils at 21.2°C at atmospheric pressure. At the freezing point, the solid is essentially all N_2O_4, but the liquid contains 0.03 percent NO_2 by wt. At the normal boiling point, the liquid contains 0.13 weight percent NO_2, and the vapor contains 16 weight percent NO_2. The dissociation of gaseous N_2O_4 to NO_2 increases from 20 percent at 27°C to around 90 percent at 100°C. Above about 60°C, secondary reactions begin, for example:

$$2NO_2 = 2NO + O_2 \qquad (3.6.2)$$

Since these temperatures are not characteristic of ambient conditions, such secondary reactions are not considered here. In addition, for the time scales of interest, temperatures, and concentration levels expected after an N_2O_4 spill, oxidation reactions (either chemical with O_2 or photochemical) are neglected.

The principal reactant, therefore, is water (present as a vapor) in the entrained air. There is considerable controversy concerning the

reactions that do occur with water as well as to the macroscopic behavior of the system following the addition of humid air to an N_2O_4 cloud.

In a simplistic sense, the following reaction may be written

$$3NO_2(g) + H_2O(g) = NO(g) + 2HNO_3(g) \qquad (3.6.3)$$

As shown, reaction (3.6.3) applies to the gas phase. If the nitric acid concentration increases to a sufficiently high level, a liquid HNO_3 phase should form. At 20°C, the vapor pressure of pure HNO_3 is 5600 Pa (42 torr), thus the partial pressure would, presumably, have to exceed this value to form a liquid phase of pure acid. England and Corcoran (1974), however, state "about 50 ppm of HNO_3 at atmospheric pressure and ambient temperature" are necessary for the threshold of a two-phase region. This translates to only 5 Pa partial pressure HNO_3. Clearly if HNO_3 nucleates, then water (and perhaps N_2O_4) would dissolve in the acid mist droplets.

One of the early studies of reaction (3.6.3) was made by Goyer (1963). His work was, however, more qualitative than quantitative. He saturated a N_2 stream by bubbling it through liquid N_2O_4. If equilibrium were indeed attained, the stream would have been essentially pure "chemical" NO_2 since the vapor pressure of liquid N_2O_4 at 20 °C is ≈ 96,000 Pa (720 torr). This stream was mixed with humid air. He usually observed the formation of an acid mist-although this mist often disappeared if the relative humidity (RH) of the entrained air were low. It is difficult to interpret his few graphs, but he does show that reaction (3.6.3) is rapid, with time constants of only a few minutes. Christini (1965) also noted that mists readily formed when mixing wet air with NO_2-N_2O_4 at 50 °C. Similarly Cathala and Weinreich (1952) reported mists when gaseous NO_2-N_2O_4 was combined with water and oxygen gases. They suggested an oxidation occurred, but this is not certain.

In contradistinction to the above studies, Kuzminykh and Udintseva (1954), Harris (1951), and Simon (1948) conducted experiments wherein humid air was mixed with NO_2-N_2O_4. In no case was any reaction [i.e., (3.6.3)] noted either from a drop in pressure (constant volume system) or by the formation of NO or acid mists. It has been suggested that their concentrations were too low to cause HNO_3 nucleation (England and Corcoran, 1974).

England and Corcoran (1974) were particularly interested in studying only the gas phase reaction (3.6.3), thus they kept their NO_2-N_2O_4 and water concentrations very low (partial pressure of NO_2 < 45 ppm and less than 1.2 mole percent H_2O). At such low concentrations, their rates were slow and it often required a day or so to approach equilibrium. They showed that the order of reaction (3.6.3) with respect to water was 1.000 +/- 0.003. The order with respect to NO_2 was much larger and ranged between 3 and 4. They proposed a complex mechanism to explain their rate data. Involved was an intermediate species, nitrous acid, HNO_2. Addition of oxygen had little effect although there was a slow oxidation of product NO. [The addition of NO

inhibited the reaction as expected since it is a product in reaction (3.6.3).] From these rate studies, they concluded that if the concentration of NO_2 exceeded ≈ 100 Pa, then the reaction would achieve equilibrium in a matter of a few seconds.

We conclude, therefore, that if an N_2O_4 spill occurs, the vapors are an equilibrium mixture of NO_2 and N_2O_4. The exact composition depends upon temperature and upon the extent of dilution. Contact with humid air will lead to a rapid formation of HNO_3 and NO - the extent being governed by chemical equilibrium. If the HNO_3 concentration exceeds some critical value (which is now in doubt), HNO_3 mist will form and, then, N_2O_4 and water will dissolve in the droplets.

Figure 3.6.1 illustrates schematically these physical processes occurring in a NO_2-N_2O_4 vapor cloud released from a storage tank. The initial system consists of 1 kg mass of NO_2-N_2O_4 mixture at T_{NO2}, mixing with M_{AIR} kg of humid air at temperature T_{AIR} and relative humidity RH. The two vapor phase reactions described above (3.6.1 and 3.6.3) lead to the formation of the products NO and HNO_3. The final mixture, therefore, contains the species NO_2, N_2O_4, NO, H_2O, HNO_3, and air. The formation of the condensed phase, if any, leads to a distribution of all these species, except air, into both of these phases. In practice, however, one can expect the condensed phase to contain predominantly H_2O and HNO_3. The detailed mathematical formulation of this system and the discussion of the computed results are given in the following sections.

3.6.4 Chemical Equilibria - Overview

The determination of the thermodynamic state of the NO_2-N_2O_4 humid air system is dependent on how the chemical equilibrium mass balance and the enthalpy balance equations are solved. These, in turn, depend on the specification of the initial state of the system; i.e., the quantities and temperatures of the reactants.

The properties of NO_2-N_2O_4 mixtures suggest that below 20°C, the N_2O_4-NO_2 mixture is mostly in the form of a liquid (or solid). In such a case, very little vapor NO_2 or N_2O_4 is expected. On the other hand, at temperatures above 20°C, most of the NO_2-N_2O_4 released will be in the vapor phase. As described in the earlier sections, we neglect the liquid phase chemical reactions, and consider the reactions between the NO_2-N_2O_4 mixture and the atmospheric water vapor.

Consider the reactions (gas phase only):

$$2NO_2 = N_2O_4 \qquad (3.6.4)$$

$$3NO_2 + H_2O = NO + 2HNO_3 \qquad (3.6.5)$$

Table 3.6.1 contains the standard heats of formation, standard Gibbs energies of formation, and the molecular weights of species involved in the above set of reactions.

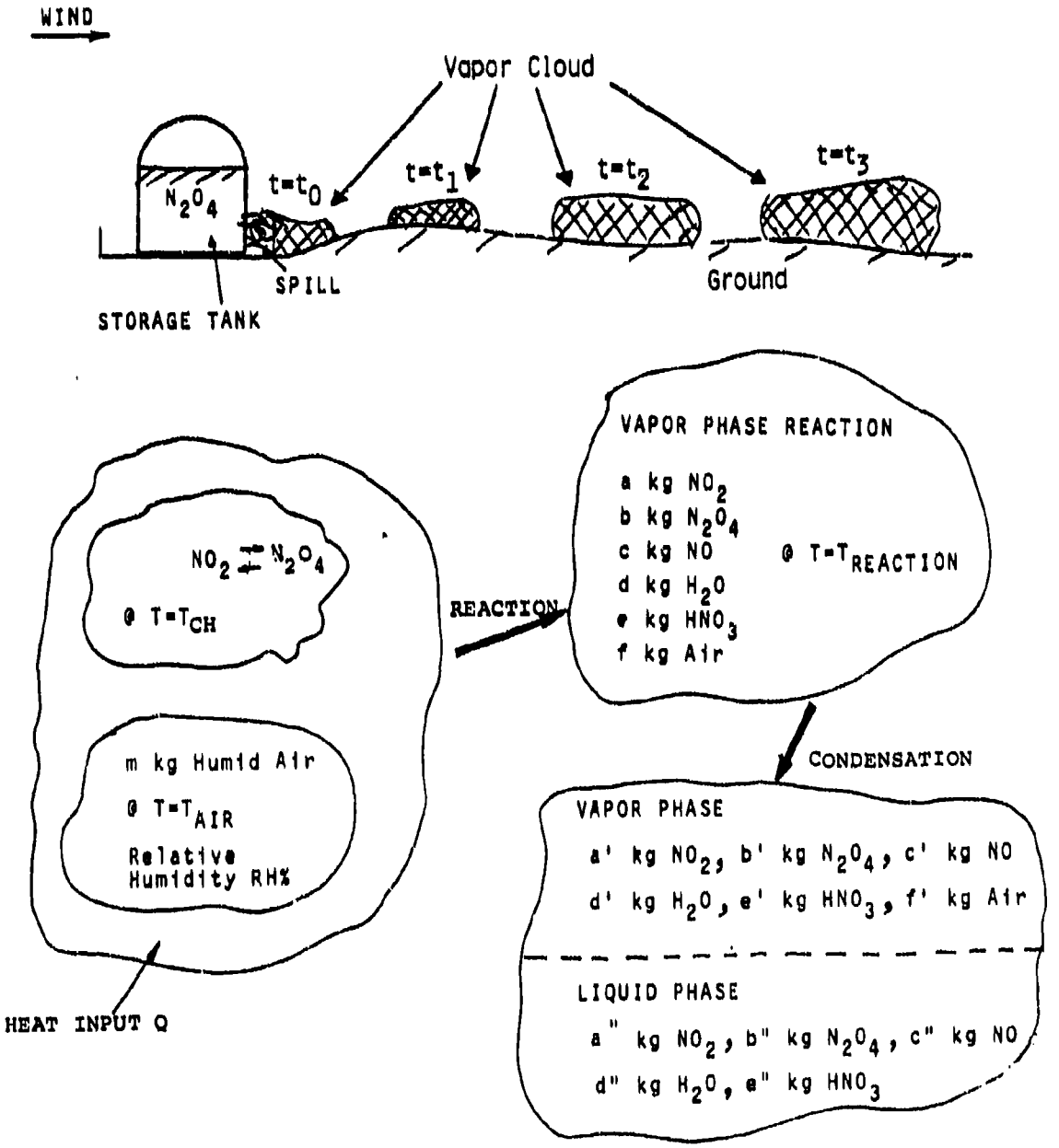

Figure 3.6.1 Nitrogen Tetroxide Reaction Modeling

TABLE 3.6.1 Properties of N_2O_4-Humid Air Reactants and Products

Component	$\Delta G_f°$ (kJ/mole at 298K)	$\Delta H_f°$ (kJ/mole at 298K)	Molecular Weight (kg/kmole)
NO_2 (g)	51.32	33.19	46.0
H_2O(g)	-228.68	-241.95	18.0
H_2O(ℓ)	-285.99	-237.30	18.0
NO(g)	86.51	90.29	30.0
HNO_3 (g)[1]	-74.80	-174.18	63.0
HNO_3 (ℓ)	-80.83	-135.12	63.0
N_2O_4 (g)	97.87	9.17	92.0

1England and Corcoran (1974) suggest a value of -18.58 kcal/gmole for $\Delta G_f°$ at 298 K.

The equilibrium constants K_A and K_B (1/atm), for reactions 3.6.1 and 3.6.3 are defined as:

$$K_A = (Y_{N_2O_4}/Y_{NO_2}^2)*(1/P) \quad (3.6.6)$$

$$K_B = \left[(Y_{NO}*Y_{HNO_3}^2)/(Y_{NO_2}^3*Y_{H_2O})\right]*(1/P) \quad (3.6.7)$$

where Y_i is the mole fraction (at equilibrium) of component i. To a first approximation (assuming ΔHr to be independent of temperature), the variation of K_A and K_B with temperature can be calculated as:

$$\ln K_A = -21.161 + 6879.7/T(K) \quad (3.6.8)$$

$$\ln K_B = -51.408 + 13910/T(K) \quad (3.6.9)$$

The composition of the various species present at equilibrium conditions can be obtained by a simple mass balance, with the definition of the equilibrium constant indicated above. Such a scheme, for a system consisting of an equilibrium mixture of $Z_{NO2}°$ moles of NO_2, and $Z°_{N2O4}$ moles of N_2O_4, as well as $Z°_{H2O}$ moles of H_2O and $Z°_{AIR}$ moles of air initially at temperature T_{AIR} and pressure P_a is outlined in Table 3.6.2. For a system with a prescribed heat input Q (Q = 0 for an adiabatic system), we need to solve the energy balance equations to obtain the reaction temperature T_{MIX}. The two equations need to be solved in an iterative manner. This is discussed in more detail in Section 3.6.6.

TABLE 3.6.2
EQUILIBRIUM MOLE FRACTIONS OF SPECIES
IN AN N_2O_4 - NO_2 - H_2O REACTION

SPECIES #	CHEMICAL SPECIES	INITIAL VALUE OR REACTANT MOLES	MOLES OF SPECIES AT EQUILIBRIUM	MOLE FRACTIONS AT EQUILIBRIUM
1	N_2O_4	$Z^o_{N_2O_4}$	$(Z^o_{N_2O_4} + Z_{N_2O_4})$	$X_{N_2O_4} = (Z^o_{N_2O_4} + Z_{N_2O_4})/Z_T$
2	NO_2	$Z^o_{NO_2}$	$(Z^o_{NO_2} - 3Z_{NO} - 2Z_{N_2O_4})$	$X_{NO_2} = (Z^o_{NO_2} - 3Z_{NO} - 2Z_{N_2O_4})/Z_T$
3	NO	0	Z_{NO}	$X_{NO} = (Z_{NO}/Z_T)$
4	HNO_3	0	$2\,Z_{NO}$	$X_{HNO_3} = (2\,Z_{NO}/Z_T)$
5	H_2O	$Z^o_{H_2O}$	$Z^o_{H_2O} - Z_{NO}$	$X_{H_2O} = (Z^o_{H_2O} - Z_{NO})/Z_T$
6	AIR (DRY)	Z^o_{AIR}	Z^o_{AIR}	$X_{AIR} = (Z^o_{AIR}/Z_T)$
	TOTAL	Z^o_T	Z_T	$X_{TOTAL} = 1$

$Z^o_T = Z^o_{N_2O_4} + Z^o_{NO_2} + Z^o_{H_2O} + Z^o_{AIR}$ = Total Moles of Reactants

$Z_T = [Z^o_T - Z_{NO} - Z_{N_2O_4}]$ = Total Moles in the Mixture After Reaction

$K_A = (X_{N_2O_4} / X^2_{NO_2}) * (1/P)$

$K_B = [(X_{NO} * X^2_{HNO_3}) / (X^3_{NO_2} * X_{H_2O})] * (1/P)$

Z represents the actual moles of species.
X represents the mole fractions of species.

3.6.5 N_2O_4 - NO_2 Reaction Equilibrium

Consider the N_2O_4-NO_2 vapor phase reaction system indicated earlier (Reaction 3.6.1). Starting with a given quantity of NO_2-N_2O_4, the equilibrium constant determines the composition of the mixture at equilibrium. The specification of the reaction temperature and pressure (1 atm) specifies the equilibrium constant and thus the equilibrium composition of the NO_2-N_2O_4 system.

Figure 3.6.2 shows the computed mole and mass fractions of N_2O_4 in the equilibrium vapor NO_2-N_2O_4 system at various temperatures and 1 atm pressure. It can be seen that at lower temperatures, most of the chemical is N_2O_4.

3.6.6 N_2O_4 - NO_2 - H_2O Gas Phase Reaction Equilibrium

In formulating the final equilibrium conditions when the vapor emanating from a nitrogen tetroxide spill mixes with humid ambient air, we must satisfy the conditions of chemical equilibria for reactions 3.6.4 and 3.6.5, energy balance (taking into consideration energy exchange with the environment) and phase equilibria relationships. In this subsection, we consider only gas phase reactions.

Specification of Vapor Initial Condition

Consider the release into the atmosphere of 1 kg of vapor from a nitrogen tetroxide spill. This vapor will mix with the ambient humid air. Before we analyze this situation we need to specify, carefully, the initial conditions of the vapor prior to mixing with air. We assume that (i) the vapor temperature is T_{CH}, (ii) there are no liquid (aerosols) in the vapor, and (iii) the total pressure is atmospheric.

The vapor under equilibrium conditions will have both nitrogen tetroxide (N_2O_4) molecules and molecules of nitrogen dioxide (NO_2). The objective of the calculations indicated below are to determine the mole fractions of the two species in 1 kg of vapor, at temperature T_{CH} and 1 atmosphere pressure. Let,

$X^{o}_{N_2O_4}$ - Mole fraction of N_2O_4 in the vapor (before air mixing)

and,

$X^{o}_{NO_2}$ - Mole fraction of NO_2 in the vapor (before air mixing)

The equilibrium reaction between these two species is given by 3.6.4 and the equilibrium constant is given by equation 3.6.6. Noting that

$$X^{o}_{N_2O_4} + X^{o}_{NO_2} = 1 \qquad (3.6.10)$$

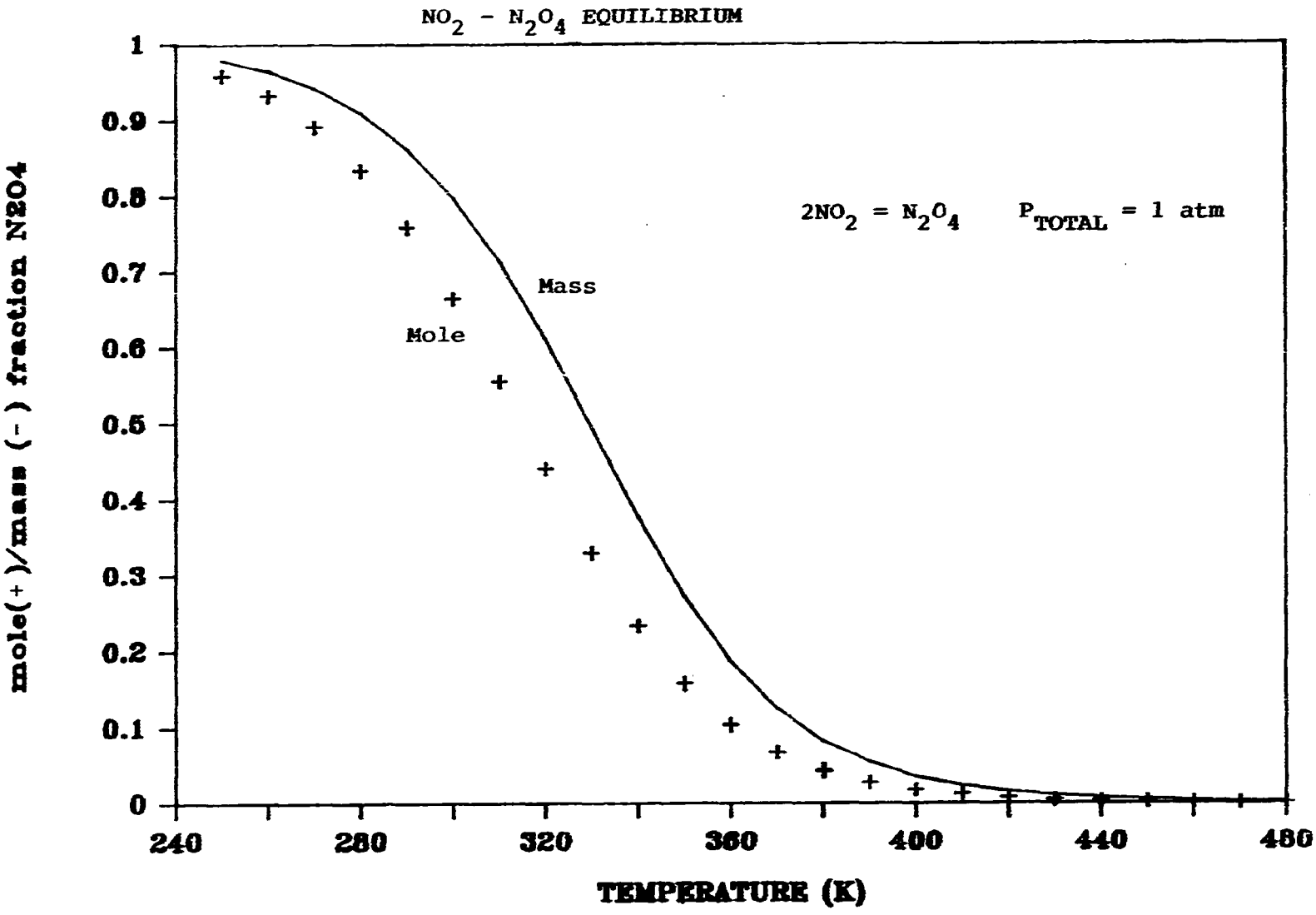

FIGURE 3.6.2: Mole and Mass Fractions of N_2O_4 in NO_2-N_2O_4 Equilibrium

and using equation 3.6.6, we write

$$X^{o}_{N_2O_4} = \left(1 + \frac{1}{2\,K_A}\right) - \left(1 + \frac{1}{2\,K_A}\right)^2 - 1 \qquad (3.6.11)$$

where K_A is a function of temperature and is calculated using equation 3.6.8.

The mass fractions (Y^{o}) of the species (i.e., N_2O_4 and NO_2) before mixing with the ambient air can be shown to be:

$$Y^{o}_{N_2O_4} = \frac{1}{1 + (X_{NO_2} / X_{N_2O_4})\,(M_{NO_2} / M_{N_2O_4})} \qquad (3.6.12a)$$

and

$$Y^{o}_{NO_2} = 1 - Y^{o}_{N_2O_4} \qquad (3.6.12b)$$

Mixing with Humid Air

Consider now the mixing of the (above 1 kg of) vapor at temperature T_{CH} with "r" kgs of humid air at dry bulb temperature T_A and relative humidity RH %. Let the temperature of the mixture of vapor and air be T_{MIX} at equilibrium.

Let,

$$Z^{o}_{N_2O_4} = Y^{o}_{N_2O_4} / M_{N_2O_4} \qquad (3.6.13a)$$

$$Z^{o}_{NO_2} = Y^{o}_{NO_2} / M_{NO_2} \qquad (3.6.13b)$$

Z^{o}_{AIR} = Total moles of dry air at T_A

$Z^{o}_{H_2O}$ = Total moles of water vapor at T_A

be the moles of various species brought into the mixture by the mixing 1 kg of vapor at T_{CH} with of r (kgs) of humid air. In the above equations M is the molecular weight of the specie. It can then be shown that,

$$Z^{o}_{H_2O} = r\,\frac{(P_w / P)}{(P_w / P)\,M_w + [1 - (P_w / P)]\,M_A} \qquad (3.6.13c)$$

$$Z^{o}_{AIR} = r\,\frac{1 - (P_w / P)}{(P_w / P)\,M_w + [1 - (P_w / P)]\,M_A} \qquad (3.6.13d)$$

We assume that after the reaction is complete and is in equilibrium, $Z_{N_2O_4}$ additional moles of N_2O_4 and Z_{NO} moles of NO are formed. The additional unknown is the equilibrium temperature of the mixture, T_{MIX}. In order to solve for these three unknowns, we apply the equations for K_A and K_B (at T_{MIX}) in Table 3.6.2. The dependencies of K_A and K_B on temperature are given in equations 3.6.8 and 3.6.9. In addition, the enthalpy balance equation is used. That is,

$$H_i + Q = H_f \qquad (3.6.14)$$

where H_i and H_f are respectively the total enthalpies of the reactants and of the mixture of air vapor. Q is the energy <u>input</u> into the mixture <u>from</u> the environment.

The initial total enthalpy of the system of mixing gases is given by,

$$H_i = Z^o_{N_2O_4}\, h_{N_2O_4}(T_{ch}) + Z^o_{NO_2}\, h_{NO_2}(T_{ch}) + Z^o_{AIR}\, h_{AIR}(T_A) + Z^o_{H_2O}\, h_{H_2O}(T_A) \qquad (3.6.15)$$

where the Z's represent the moles of the species and h's are the enthalpies per unit mole of the species. The enthalpy of the final equilibrium mixture of the gases at T_{MIX} is written as

$$H_f = Z_T \sum_{i=1}^{6} X_i\, h_i(T_{MIX}) \qquad (3.6.16)$$

where Z_T is the total number of moles in the mixture, X_i and h_i are, respectively, the mole fraction and enthalpy per mole at the mixture temperature of the "i"th specie. The specie numbers ("i"s) are indicated in Table 3.6.2. Substituting equations 3.6.15 and 3.6.16 in equation 3.6.14 and using the relationships indicated in Table 3.6.2, we can show that

$$Z_{N_2O_4}\, \Delta H_{r,A}(T_{MIX}) + Z_{NO}\, \Delta H_{r,B}(T_{MIX}) + Z^o_{AIR} \int_{T_{AIR}}^{T_{MIX}} C_{P,Air}\, dT + Z^o_{H_2O} \int_{T_{AIR}}^{T_{MIX}} C_{P,H_2O}\, dT + \left(Z^o_{N_2O_4} + \frac{1}{2} Z^o_{NO_2}\right) \int_{T_{CH}}^{T_{MIX}} C_{P,N_2O_4}\, dT - \frac{Z_{N_2O_4}}{2} \left[\Delta H_{r,A}(T_{MIX}) - \Delta H_{r,A}(T_{CH})\right] = Q \qquad (3.6.17)$$

where $\Delta H_{r,A}$ is the enthalpy of reaction A per mole of N_2O_4 and $\Delta H_{r,B}$ is the enthalpy of reaction of reaction B, per mole of NO. The values of ΔH's can be obtained from equation 3.6.8 using the relationship

$$\frac{d}{d(1/T)} \ln (K_A) = - \frac{\Delta H}{R_u T} \qquad (3.6.18)$$

where R_u is the universal gas constant (8314 J/mole K). At 298 K, the enthalpies of reaction have the following values

$$\Delta H_{r,A} = -57,230 \text{ J/mole of } N_2O_4$$
$$\Delta H_{r,B} = -115,700 \text{ J/mole of NO}$$

If it is assumed that the reaction enthalpy is independent of temperature (as is the case by virtue of equation 3.6.8), the last term on the LHS of equation 3.6.17 drops out.

The value of C_{p,N_2O_4} in equation 3.6.17 refers to the "frozen" heat capacity of N_2O_4. It may be expressed as

$$C_{p,N_2O_4} = 66.8 + 0.03875\ T \qquad \text{(J/K Mole of } N_2O_4\text{)}$$

where T is in degrees Kelvin.

The three unknowns, namely $Z_{N_2O_4}$, Z_{NO} and T_{MIX} are then solved using the two equilibrium equations of Table 3.6.2 and equation 3.6.17.

Procedure for Calculating the Final Conditions of the Mixture

Assume 1 kg of vapor and r kgs of humid air,

1. Calculate $Y^o_{N_2O_4}$ and $Y^o_{NO_2}$ from equations 3.6.12a and 3.6.12b.
2. Specify r, T_{AIR}, RH and Q.
3. Calculate Z^o values from equation 3.6.13a through 3.6.13d.
4. Assume a mixture temperature T_{CH} (guess value).
5. Calculate K_A and K_B values from equations 3.6.8 and 3.6.9.
6. This gives two equations in two unknowns, namely $Z_{N_2O_4}$ and Z_{NO}, using an iterative method solve for $Z_{N_2O_4}$ and Z_{NO}.
7. Substitute these values in the energy equation 3.6.17 and see if it is satisfied.
8. Repeat the steps 4 through 7 until the energy equation is satisfied.

Result of N_2O_4 Vapor Mixing with Humid Air

Figure 3.6.3 shows the variation of final mixture temperature for various masses of air mixed per unit mass of chemical vapor (this ratio is termed the "dilution ratio") for the case when no external heat is added to the mixture. The relative humidity of the air is also varied. It is seen that there is virtually no difference between the 0% relative humidity and 100% relative humidity case (within the temperature scale of the plots). First, we notice that the gaseous mixture temperature decreases as the mass of air added is increased. This is because the dilution process decreases the partial pressure of NO_2 causing the N_2O_4 to NO_2 dissociation reaction to occur. Since this reaction is endothermic, the temperature of the mixture drops. However, as the mass of air added is increased substantially, the heat liberated by dissociation has less effect on the mixture (i.e., the temperature decrease becomes smaller). At very large dilutions, the enthalpy of the air dominates the system enthalpy and hence the mixture temperature approaches that of air.

It is interesting to see that the mixture temperature is not discernibly affected by varying the relative humidity (under adiabatic conditions). This is because, first, the mass of water vapor per unit mass of air even at 100% relative humidity is very small (about 1%). Because of this low water vapor concentration, very small quantities of NO are produced at low dilution ratios. Therefore, the heat liberated is very small. For example, the total moles of NO produced with an initial 1 kg of N_2O_4 vapor and a dilution ratio of 0.1 is about 10^{-6} (see Figure 3.6.4). This amount of NO production will result in the liberation of about 0.12 J. This is sufficient to raise the temperature of the gas mixture by 10^{-4} K! Clearly, at high dilution ratios, the overall effect of the exothermic reaction (equation 3.6.5) is even smaller.

In Figure 3.6.4 we show the variations in the molar concentrations of different species with increasing dilution ratio, for the case of a 100% humid air mixing. It is seen that the concentrations of NO and HNO_3 are relatively small (never exceeding 500 ppm). Also plotted in the same figure is the water vapor concentration in the mixture of gases. The effect of different levels of water vapor concentration in the mixture on the possible condensation of nitric acid is discussed later.

The variation of mixture density with dilution is indicated in Figure 3.6.5. The density of the mixture decreases continuously with increase in dilution. The effect of relative humidity on the mixture density is negligible. It is, however, to be noted that we have assumed no condensation of vapors in developing the results presented in Figure 3.6.5.

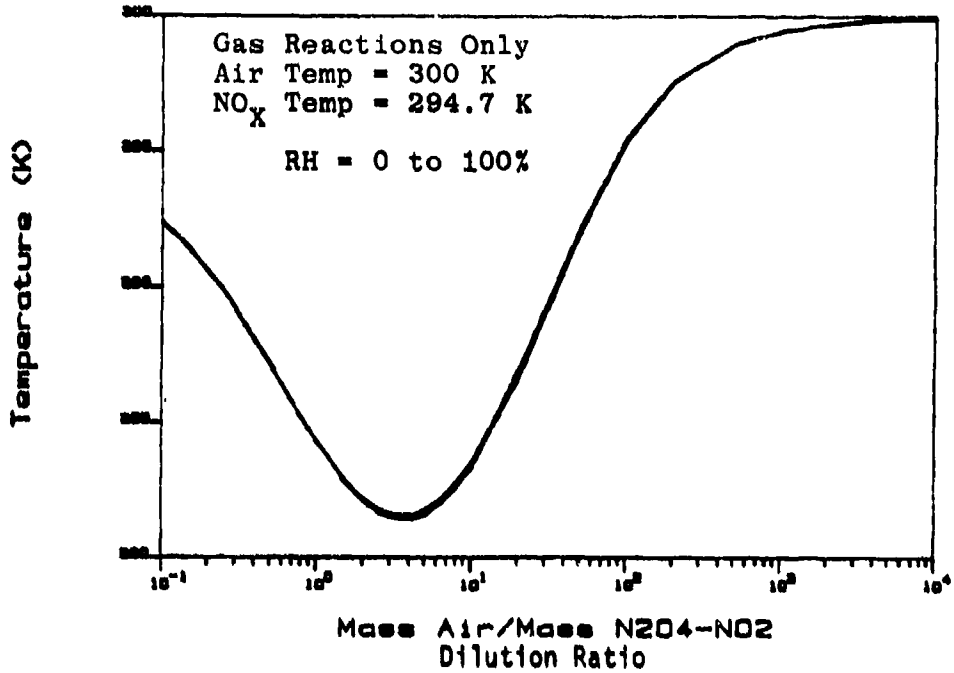

FIGURE 3.6.3 Reaction Temperature of N_2O_4-Humid Air System

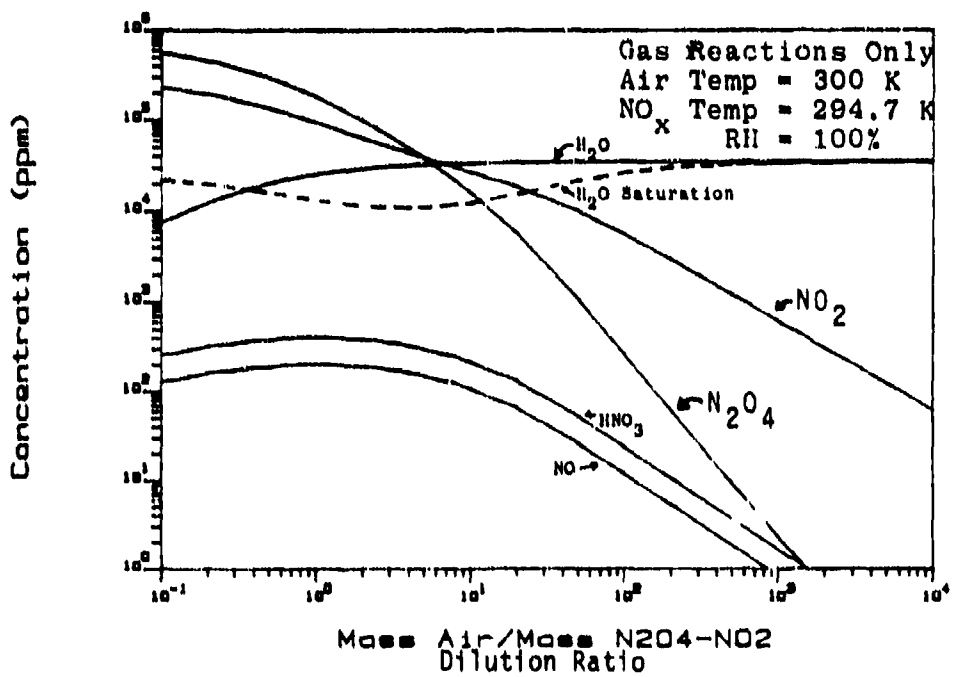

Air is by Difference

FIGURE 3.6.4 Concentrations of Various Species in an Equilibrium Mixture of N_2O_4-NO_2 and Humid Air

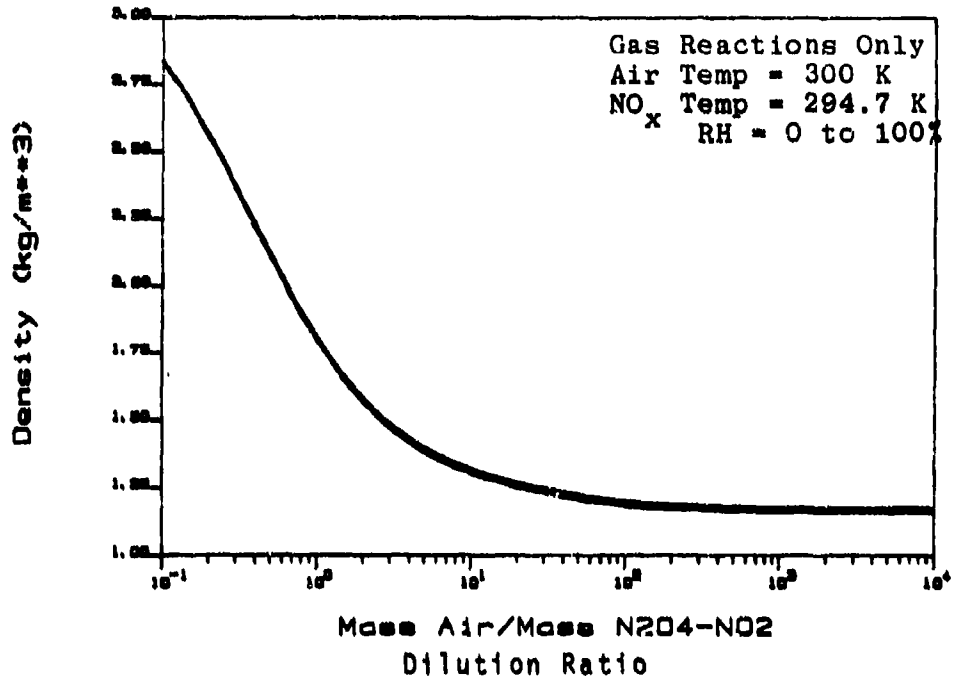

FIGURE 3.6.5 Density of an Equilibrium Mixture of N_2O_4-NO_2 and Humid Air

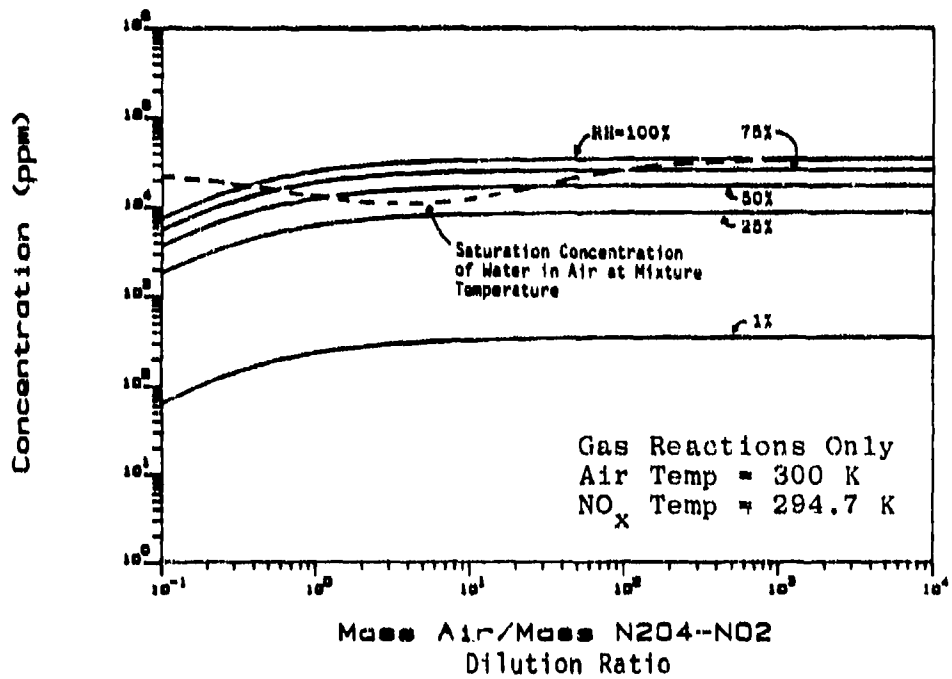

FIGURE 3.6.6 Concentration of Water in Equilibrium Mixtures of N_2O_4-NO_2 and Humid Air for Various Air Humidities

3.6.7 Nitric Acid Condensation

To determine the distribution of the various species in the vapor and liquid phase, if the presence of a condensed phase is assumed, we need to solve the coupled equations of energy, reaction equilibrium and the phase equilibrium. This process of obtaining the solution to these coupled equations is extremely complex. It can be argued, however, that condensed phase will result once the partial vapor pressure of water or that of the nitric acid vapor exceeds its respective saturation pressure at the mixture temperature. Figure 3.6.6 shows the partial vapor pressure of water vapor in the N_2O_4-NO_2 vapor-air mixture for various relative humidities and dilution ratios. Also plotted on the same figure is the saturated water vapor pressures at mixture temperatures given in Figure 3.6.3. It is seen that at relative humidities in excess of about 30%, there is a range of dilution ratios over which the water vapor will condense. Once water condenses, it is logical to assume that HNO_3 dissolves in it forming aqueous nitric acid.

The condition under which nitric acid vapor condenses is not very clear from data available in the literature. For example, at 20°C the vapor pressure of HNO_3 is 5600 Pa and presumably when HNO_3 partial vapor pressure exceeds this value, the vapors will condense. However, Koopman, et al. (1984), McRae (1985) indicate that nitric acid aerosols were formed in a field test conducted by the Lawrence Livermore National Laboratories. They also allude to the laboratory test results from the literature (England and Corcoran, 1974) and suggest that when the partial vapor pressure of HNO_3 vapor exceeds 50 ppm aqueous nitric acid would be formed. In our opinion, the observed aerosol formation in the field tests conducted by Koopman, et al., is probably due to water condensing in the cloud because of the 35% RH ambient condition prevailing during the test. Also, the conditions of the test were such that a cold plume (at a temperature of - 12°C) of nitrogen tetroxide vapor (together with its equilibrium mixture of nitrogen dioxide vapor) would have been released into the atmosphere from the frozen liquid pool of nitrogen tetroxide. This cold vapor plume would have condensed the moisture from the ambient air. In fact, this observation confirms our theoretical finding as to when HNO_3 condensation will occur (see Figure 3.6.6).

One approach to simplifying the analysis of "condensed phase" problem is to assume ideal solutions (H_2O-HNO_3 aqueous mixtures). We have tried this approach. The results from this approach indicate that even at very low dilution ratios (less than 10^{-2}), all liquid phase will evaporate if the relative humidity is low (< 20%). The results for higher relative humidities are not available at this time.

3.7 SUMMARY AND CONCLUSIONS

The chemicals studied for this project undergo a variety of reactions and interactions with air, especially with the water in the air. The reactions for each chemical and humid air were examined, with the result that three types of behavior were assumed to occur. The first type (I) of chemicals (Cl_2, $COCl_2$, SO_2, and H_2S) were those for which reactions or interactions with the water and/or air did not occur or were not significant. The calculations done for this type of chemicals considered only the energetics of the mixtures. For the second type (II) of chemical (NH_3) the dissolution of the ammonia in condensed atmospheric water was determined to be significant, and thus, the model for this chemical accounts for the dissolution reaction energy. For the third type (III) of chemical (N_2O_4), the reactions play an important role in determining the composition and properties of the air and chemical mixtures. The model for this chemical type accounts for the reactions and their effects on the equilibrium mixtures.

We conclude that:

1) For all of the chemicals, the densities of equilibrium mixtures are insensitive to the humidity of the entrained air since the quantity of water in the air is only a small percentage of the total air mass.

2) The densities are, however, strongly dependent on the mass of liquid chemical entrained as aerosols in the initial mixture. Ammonia, for example, is less dense than air (both at the same temperature) unless there is liquid ammonia aerosol present in the mixture. It behaves as a heavy gas because of this entrained aerosol.

3) The temperature of the chemical vapor+aerosol and air mixture drops below the normal boiling point of the chemical as the liquid aerosols evaporate. This evaporative cooling enhances the heavy gas affects since the gases become more dense as they cool.

4) The heats of fusion are relatively unimportant for the energetics of the mixtures since only small quantities of water will freeze in most cases. For the case of ammonia, the model developed assumes the ammonia water solutions do not freeze, since these aqueous solutions have very low (190 K) freezing points. The effects of freezing are considered in the other models.

CHAPTER 4

CHARACTERIZATION OF ATMOSPHERIC CONDITIONS

4.1 INTRODUCTION

The passive dispersion of a chemical in the atmosphere is described using dispersion parameters (σ_y and σ_z) whose values are dependent on the atmospheric stability and the distance from the source. The method used for calculating the stability parameter used in the calculations is taken from the AFTOX model and it is described in the "User's Guide to AFTOX" by Kunkel (1985, 1986). This is discussed in Section 4.2. The actual determination of the dispersion parameters using the calculated stability parameter is discussed in Section 4.3.

A continuous stability parameter ranging from 0.5 to 6.0 is used in the model. The numbering scheme is based on the Pasquill stability categories, which range from A (extremely unstable) to F (moderately stable), as shown in Table 4.1.1 from Kunkel (1986).

In addition to the stability parameter, other parameters that are calculated by the atmosphere characterization module of the model are the friction velocity (u_*) and the wind speed at a height of 10 meters (U_{10}).

4.2 MODELS DESCRIBING ATMOSPHERIC STABILITY

Two methods are used in the model to calculate the stability parameter based on the type of input data that is available. One method (Option 1) uses wind speed, cloudiness, surface roughness, time and date, location, and other data to determine the stability using Golder's nomogram (1972), which relates the stability to the surface roughness (Z_0) and the Monin-Obukov length (L). The second method (Option 2) is the Modified Sigma Theta approach introduced by Mitchell and Timbre (1979) and presented by Mitchell (1982) which uses the locally measured wind statistical data to calculate the stability. The two methods are described in the following sections.

4.2.1 OPTION 1: Golder's Nomogram Method for Determining the Stability of the Atmosphere

This method uses the Monin-Obukov length, L (m), and the surface roughness, Z_0 (m), to determine the stability parameter. The relationship between the three is shown in Golder's nomogram (see Figure 4.2.1 based on Figure 1 from Kunkel (1986)). The numeric stability parameter determined using this nomogram can be found using the following mathematical expressions:

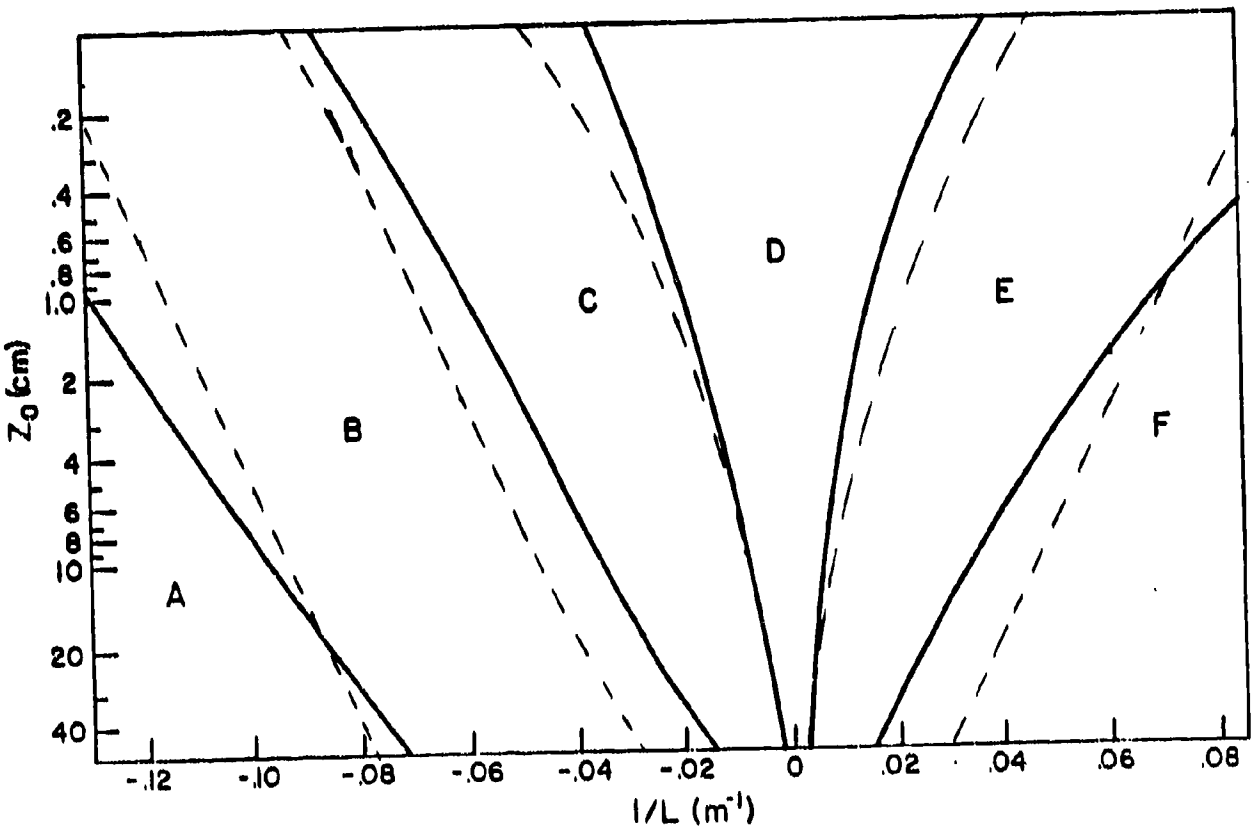

Golder's Nomogram Stability Catagories

Calculated Stability Catagories Using Eq. 4.2.1

Figure 4.2.1 1/L as a Function of Pasquill Stability Classes and Aerodynamic Roughness Length (Z_0)

Ref. Kunkel, 1986

$$SP = A + B \, \mathrm{Log}_{10} (Z_0 * 100) \qquad (4.2.1)$$

where:

$$A = 3.5 + 21.67/L \qquad (4.2.2)$$

$$B = 0.48 \quad \text{when } | 1/L | > 0.015 \qquad (4.2.3)$$

$$B = 43.63 \, | 1/L |^{1.08} \quad \text{when } | 1/L | < 0.015 \qquad (4.2.4)$$

$$B = -B \quad \text{when } 1/L < 0.0 \qquad (4.2.5)$$

The results obtained with these equations are shown in Figure 4.2.1 also, as the dashed lines.

The Monin-Obukov length is calculated as follows:

$$L = - \frac{\rho_a \, C_p \, T_a \, u_*^3}{k \, g \, H} \qquad (4.2.6)$$

where ρ_a is the ambient air density (kg m^{-3}), C_p is the specific heat of air (J kg^{-1} K^{-1}), T_a is the air temperature (K), k is the von Karman constant (0.41), g is gravity (9.8 m s^{-2}), and H is the sensible heat flux from the ground to the lower atmosphere boundary layer (W m^{-2}).

The value for u_* is an unknown, however, so an iterative approach, similar to that described by Koo, et al., (1984), is used to calculate both L and u_*. The other equations used in the iterations are the surface layer wind profile equations for neutral, unstable and stable conditions, as summarized by Ragland and Dennis (1975):

neutral conditions ($L = \infty$):

$$\frac{k \, U_Z}{u_*} = \ln \frac{Z}{Z_0} \qquad (4.2.7)$$

unstable conditions ($L < 0$):

$$\frac{k \, U_Z}{u_*} = 2(\tan^{-1}x - \tan^{-1}x_0) + \ln \frac{x - 1}{x_0 - 1} - \ln \frac{x + 1}{x_0 + 1} \qquad (4.2.8)$$

where:

$$x = \left[1 - \frac{15Z}{L} \right]^{.25} \quad \text{and} \quad x_0 = \left[1 - \frac{15Z_0}{L} \right]^{.25} \qquad (4.2.9a,b)$$

stable conditions (L > 0):

$$\frac{k\,U_Z}{u_*} = \ln\frac{Z}{Z_0} + 5.2\,\alpha \qquad (4.2.10)$$

where U_Z is the wind speed (m s^{-1}) at anemometer height Z (m), and $\alpha = Z/L$ when $Z < L$ and $\alpha = 1$ when $Z > L$.

To start the iterations, an initial guess value for u_* is used and the values for L and u_* are found. U_{10} is then calculated using the iterated value of u_*, from equation 4.2.7, 4.2.8, or 4.2.10.

The other parameter that must be calculated to find L and u_* is the sensible heat flux from the ground to the lower atmosphere boundary layer (H). The appropriate equation for the surface layer wind profile (4.2.7, 4.2.8, 4.2.10) is also selected using the value for H. Unstable conditions are defined by a heat flux greater than 1 W m^{-2}, stable conditions are for a heat flux less than -1 W m^{-2} and neutral conditions are defined by a heat flux between 1 and -1 W m^{-2} (heat flux from the ground into the atmosphere is defined to be positive). For the daytime, the heat flux is calculated using a method described by DeBruin and Holtslag (1982):

$$H = \frac{(1-\alpha) + (\gamma/s)}{1 + (\gamma/s)}\,(Q-G) - \beta \qquad (4.2.11)$$

where $\alpha = 1.0$ and $\beta = 20$ W m^{-2} for wet conditions, and 0.65 and 20 W m^{-2} for dry conditions. The soil heat flux, G, is 0.1*Q unless there is a snow cover, in which case G = 0.0. The value for (γ/s) is presented as a function of ambient air temperature, T_a (K), by:

$$(\gamma/s) = 119.56 - 0.7843*T_a + 1.2887\times10^{-3}*T_a^2 \qquad (4.2.12)$$

The net solar radiation, Q (W m^{-2}), is found as presented by Holtslag and Van Ulden (1983) using:

$$Q = \frac{(1-r)\,K + C_1\,T^6 - \sigma\,T^4 + C_2\,N}{1+C_3} \qquad (4.2.13)$$

where r is the earth's albedo (r = 0.23 except for when there is a snow cover, r = 0.75), σ is the Stefan-Boltzmann constant (5.67 x 10^{-8} W m^{-2} K^{-4}), and N is the fraction of the sky covered by clouds. The constants C_1, C_2, and C_3 are equal to 5.31×10^{-13} W m^{-2} K^{-6}, 60 W m^{-2}, and 0.12 respectively. The net incoming solar radiation at ground level, K (W m^{-2}), is found using the following expression, by Kasten and Czeplak (1980):

$$K = K_0\,(1 - (1-T)\,N^{b2}) \qquad (4.2.14)$$

where b_2 is an empirical coefficient equal to 3.4, and T is the transmittance of the cloud cover, depending on the type of cloud (cirrus = 0.61, altus = 0.27, cumulus = 0.25, stratus = 0.18, and nimbostratus = 0.16). The incoming solar radiation at ground level (K_0) is found using:

$$K_0 = a_1 \sin \phi + a_2 \qquad (4.2.15)$$

where a_1 and a_2 are turbidity coefficients which describe the average atmospheric attenuation of K_0 by water vapor and dust for a given site. Average values of $a_1 = 990$ W m^{-2} and $a_2 = -30$ W m^{-2} are used in the model. The solar elevation angle (ϕ) is found using the method described by Wolfe (1980):

$$\sin \phi = \sin LA \sin D + \cos LA \cos D \cos SHA \qquad (4.2.16)$$

where LA is the latitude, D is the solar declination, and SHA is the solar hour angle. The solar declination is found using:

$$\sin D = \sin 23.4438 \sin \sigma \qquad (4.2.17)$$

where

$$\sigma \text{ (deg)} = a + 279.9348 + 1.914827 \sin a - 0.079525 \cos a + 0.019938 \sin 2a - 0.00162 \cos 2a \qquad (4.2.18)$$

The angular fraction of the year (a) is found by:

$$a = 360 (JU - 1) / 365.242 \qquad (4.2.19)$$

where JU is the Julian date.

The solar hour angle (SHA) is given by:

$$SHA \text{ (deg)} = 15 (GMT - M) - LO \qquad (4.2.20)$$

where GMT is the Greenwich mean time, LO the longitude and M the time of meridian passage (true solar noon). M is found by:

$$M = 12 + 0.12357 \sin a - 0.004289 \cos a + 0.153809 \sin 2a + 0.06078 \cos 2a \qquad (4.2.21)$$

Smith's (1972) formula for sensible heat flux is used for nighttime:

$$H = -40 (1-N) \qquad (4.2.22)$$

where, again, N is the fraction of the sky covered by clouds.

4.2.2 OPTION 2: Modified Sigma Theta Approach for Determining the Stability of the Atmosphere

When the standard deviation of the wind direction is known (σ_Θ), the Modified Sigma Theta method of Mitchell can be used to determine the atmospheric stability. The stability category relationship outlined in the NRC Regulatory Guide 1.23 (1972) is used except that at night, any $\sigma_\Theta \geq 12.5^\circ$ is attributed to meandering, not to instability. Table 4.2.1 (from Kunkel (1986)) shows the relation of σ_Θ to the stability.

For all daytime conditions and for nighttime conditions when $\sigma_\Theta < 12.5^\circ$, the following equation is used to calculate SP:

$$SP = 6.46 - 0.341\ \sigma_\Theta + 0.0045\,\sigma_\Theta^2 \qquad (4.2.23)$$

The values for SP in Table 4.2.1 are for σ_Θ's which were measured at a height of 10 meters and for a 60 minute averaging time. To use the equation (4.2.23) derived from the data in the table, the σ_Θ must measured the same way. If σ_Θ is for other than 10 meters and 60 minutes, the following is used:

$$(\sigma_\Theta)_{10,60} = \sigma_\Theta\ (10/Z)^{-0.2}\ (60/t)^{0.2} \qquad (4.2.24)$$

where Z is the height at which σ_Θ was measured and t is the averaging time used.

For nighttime conditions when $\sigma_\Theta \geq 12.5^\circ$, the stability parameter is computed using the relations in Table 4.2.2 (from Kunkel (1986).

The values of the wind speed at 10 meters (U_{10}) and the friction velocity (u_*) are found in option 2 assuming the wind velocity profile is logarithmic:

$$U_{10} = U_Z \frac{\ln \frac{10}{z_0}}{\ln \frac{z}{z_0}} \qquad (4.2.24)$$

$$u_* = U_Z \frac{k}{\ln \frac{z}{z_0}} \qquad (4.2.25)$$

TABLE 4.1.1 Relationship Between Pasquill Stability Categories (SC) and the Continuous Stability Parameter (SP)

Stability Category	A	B	C	D	E	F
Stability Parameter	0-1	1-2	2-3	3-4	4-5	5-6

TABLE 4.2.1 Modified Sigma Theta Method for Determining Atmospheric Stability

σ_θ* (degrees)	Daytime stability	Wind speed ($m\ s^{-1}$ at 10 m)	Nighttime** stability
$\sigma_\theta \geq 22.5$	A	$u < 2.4$	G
		$2.4 \leq u < 2.9$	F
		$2.9 \leq u < 3.6$	E
		$3.6 \leq u$	D
$22.5 > \sigma_\theta \geq 17.5$	B	$u < 2.4$	F
		$2.4 \leq u < 3.0$	E
		$3.0 \leq u$	D
$17.5 > \sigma_\theta \geq 12.5$	C	$u < 2.4$	E
		$2.4 \leq u$	D
$12.5 > \sigma_\theta \geq 7.5$	D	all wind speeds	D
$7.5 > \sigma_\theta \geq 3.8$	E	all wind speeds	E
$3.8 > \sigma_\theta \geq 2.1$	F	all wind speeds	F
$2.1 > \sigma_\theta$	G	all wind speeds	G

* at 10 meter height, 60 minute averaging time

** Nighttime is defined as the period from 1 hour before sunset to 1 hour after sunrise.

4.3 DETERMINATION OF DISPERSION COEFFICIENTS

For given values of the down wind distance from the source and atmospheric stability (or σ_θ and downwind distance), the values of the horizontal (σ_y) and vertical (σ_z) Gaussian dispersion parameters can be calculated. This is done using the relation of atmospheric stability to the dispersion coefficients described originally by Pasquill and Meade and represented by the graphs in Figures 4.3.1 and 4.3.2, from Slade, 1968. This relation is implemented in the model using correlations of the curves shown. Interpolation is performed if the stability falls between curves, as the continuous stability parameter calculations described above allow.

4.4 RESULTS AND DISCUSSION

The equations described in Section 4.2 are used to calculate the numeric stability parameter, the wind speed at 10 meters height and the friction velocity which are used in later calculations to describe the dispersion of chemical vapors in the atmosphere. With limited variable input data, such as air temperature, time, wind speed at any height, and cloud cover, the stability of the atmosphere can be correctly computed and prediction of hazard distances and areas can begin.

The predictions from the model are valid for a wide range of conditions as Table 4.4.1 shows [based on Table 3.3 from Slade (1968)]. In the upper half of this table are indicated the relationships between weather parameters and the Pasquill stability categories. In the bottom half, the calculated stability parameters (calculated using the models discussed above) are indicated in terms of alphabetic stability categories.

In this chapter we have described a method by which the value of the atmospheric stability and the dispersion coefficients corresponding to this stability, can be determined. The principal difference between the method described here and those available in the literature has to do with the definition of the stability values. We have assumed, justifiably, that the atmosphere goes through continuous states of stability over a diurnal cycle. The Pasquill-Gifford method, on the other hand, describes the atmospheric stabilities in six unique classes with no continuum of states in between. The latter method can lead to substantially different values of the dispersion coefficient, especially at large distances from the source. This in turn will result in erroneous concentration predictions. The method described here is superior to the Pasquill-Gifford method.

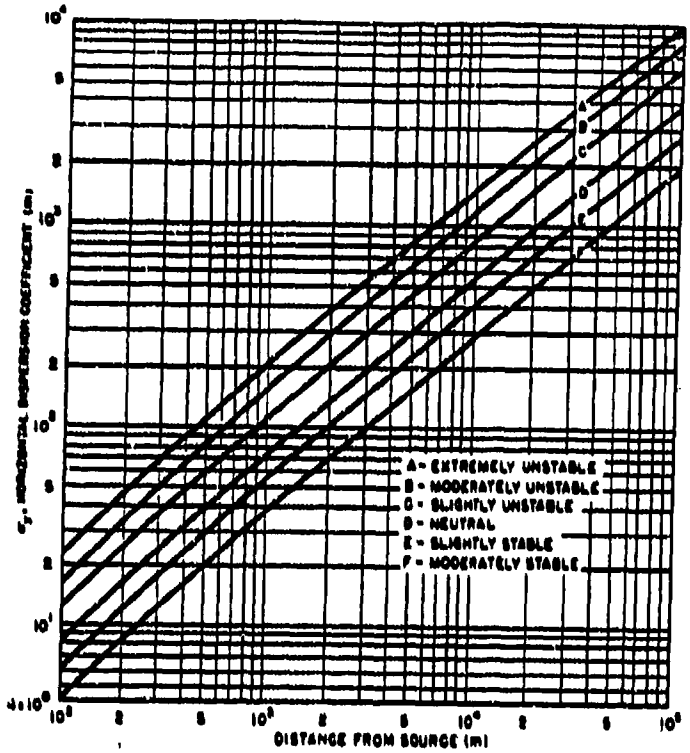

Figure 4.3.1 Lateral Diffusion, σ_y, vs. Downwind Distance from Source for Pasquill's Turbulence Types.
Ref. source: Slade, 1968

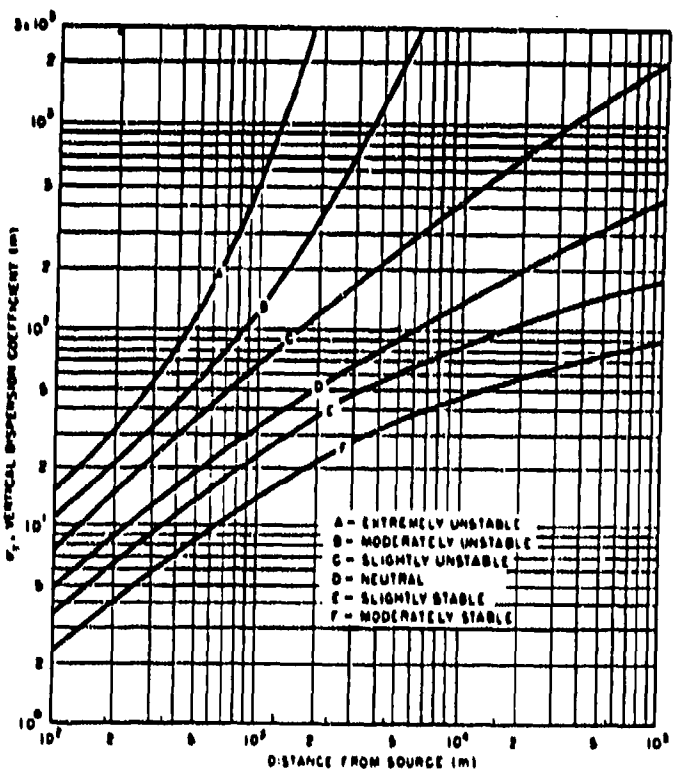

Figure 4.3.2 Vertical Diffusion, σ_z, vs. Downwind Distance from Source for Pasquill's Turbulence Types.
Ref. source: Slade, 1968

TABLE 4.2.2 Nighttime Stability Parameter as a Function of and Wind Speed for $\sigma_\theta \geq 12.5^o$.

σ_θ* (degrees)	Wind speed (m s^{-1} at 10 m)	Stability parameter
$\sigma_\theta \geq 22.5$	$4.1 \leq u$	SP = 3.5
	$2.4 \leq u < 4.1$	SP = 14.44/u
	$u < 2.4$	SP = 6.0
$22.5 > \sigma_\theta \geq 17.5$	$3.4 \leq u$	SP = 3.5
	$2.0 \leq u < 3.4$	SP = 12.00/u
	$u < 2.0$	SP = 6.0
$17.5 > \sigma_\theta \geq 12.5$	$2.7 \leq u$	SP = 3.5
	$1.9 \leq u < 2.7$	SP = 9.60/u
	$u < 1.9$	SP = 5.0

* at 10 meters, 60 minute averaging time

TABLE 4.4.1 Relation of Stability Categories to Weather Conditions - Calculated Values Compared to Pasquill's Values.

Wind speed (m s^{-1})	Daytime insolation			Nighttime conditions	
	Strong	Moderate	Slight	Thin overcast or > 4/8 cloudiness	< 3/8 cloudiness
			Pasquill's values		
< 2	A	A - B	B		
2	A - B	B	C	E	F
4	B	B - C	C	D	E
6	C	C - D	D	D	D
> 6	C	D	D	D	D
			Calculated values		
< 2	A	A	A	F	F
2	A	A - B	B - C	F	F
4	C	C	C - D	D	F
6	C - D	D	D	D	D
> 6	D	D	D	D	D

The second important difference between the calculations indicated in this section and those in the traditional dispersion literature is the corrections that are applied (in our method) to the dispersion parameter values for concentration averaging time and aerodynamic roughness. When they are different than the standard values (10 minute averaging time and 10 centimeters roughness) for which the dispersion parameters are correlated, they are adjusted to account for the differences.

CHAPTER 5

DISPERSION MODEL DEVELOPMENT

In this chapter we discuss the approach to describing the dispersion of a heavy vapor cloud and heavy vapor plume and then present models in the form of mathematical equations. The description of the vapor cloud* includes its geometrical size, variation of ground level concentration with distance, distribution of chemical concentration within the cloud, the location of the center of the cloud with respect to the chemical release point, etc. Also indicated are the procedures to calculate the lateral extent of the cloud (with respect to the cloud center) for a given concentration.

The physical processes occurring after a heavy gas cloud is released are discussed in section 5.1. In section 5.2 the instantaneous dispersion model is discussed. The continuous dispersion model is analyzed in section 5.3.

5.1 PHYSICAL PROCESSES IN THE DISPERSION OF A HEAVY GAS CLOUD

When a vapor cloud which is heavier than air (due to its vapor density or the combined density of vapor and any aerosols) is released** into the atmosphere, it undergoes dilution in different stages. Depending on the nature of release (explosive, passive, jet, etc), there may be an initial rapid entrainment of air into the cloud. Subsequently, the cloud goes through a gravitational slumping stage due to its excess density. During this second stage the lateral dimensions of the cloud increase due to gravity induced flows and the cloud is accelerated downwind due to momentum transfer from the wind. The entrainment of air during this stage is primarily controlled by the density stratification in the cloud and by the lateral spread rate. When the cloud density is within a few percent of the density of air, a third stage of dispersion occurs in which the dilution of the cloud depends on both the atmospheric turbulence characteristics and the cloud density. In the fourth and final stage, the cloud dilution is principally due to atmospheric turbulence. These stages of dispersion of a heavy vapor cloud are illustrated schematically in Figure 5.1.1

Air is entrained into the cloud at the edges and at the top. Therefore, the concentration of the chemical decreases first at

---

* The term "vapor cloud" used in this report is assumed to mean both a puff of vapor and a plume.

** As described in Chapter 2 a variety of chemical release modes and sources result in the formation of liquid aerosols which may be entrained into the vapor cloud and disperse with the cloud.

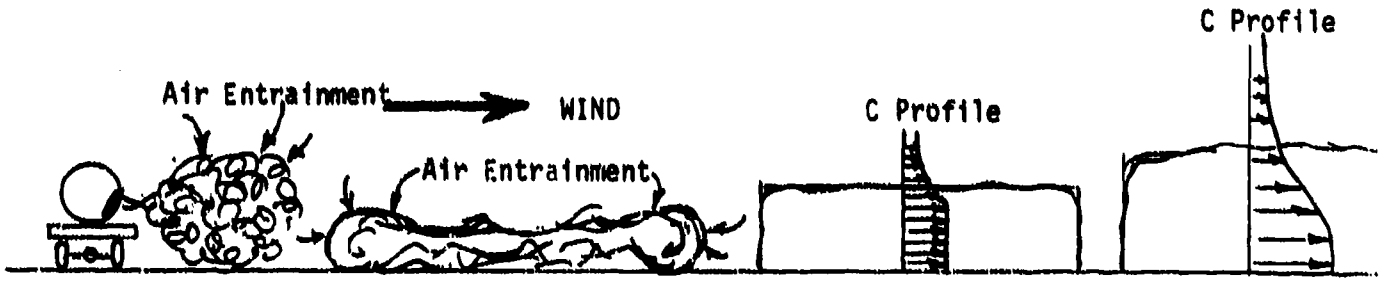

REGIME I	REGIME II	REGIME III	REGIME IV
Explosive Release of Vapor and its rapid mixing with atmospheric air	Slumping of the heavy gas cloud and its radial expansion. Entrainment predominantly from the edges.	Transition Regime in which the gravity flow induced turbulence and atmospheric turbulence are instrumental in air into the cloud	Atmospheric turbulence is the only important mechanism for air mixing.
	Concentration profile in the cloud is "Top Hat"	Concentration Profile is a combination of Gaussian & Top Hat	Profile of concentration is a fully developed Gaussian

FIGURE 5.1.1: Schematic illustration of the Four Regimes of Dispersion of a Heavy Gas Vapor Cloud.

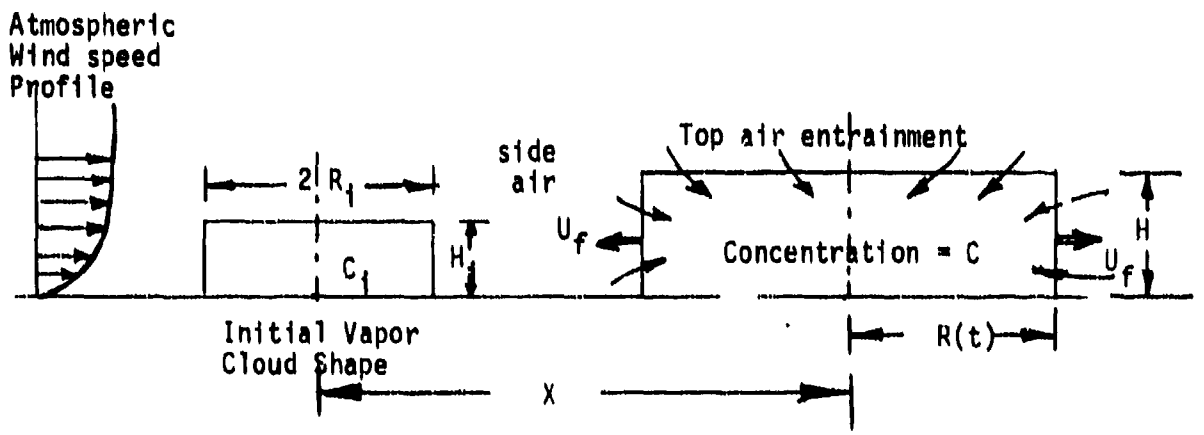

FIGURE 5.2.1: Heavy Gas Cloud Dispersion Model Features ("Box Model")

the edges and the top. The chemical concentration at the core remains high until sufficient air has diffused into the central regions. If there is chemical reaction, the concentrations of the products of reaction are high at the edges and the top. In effect, in a real cloud the concentrations within the cloud are non-uniform and may show distinct bi-modal distributions in the lateral direction for reaction products. However, as the dilution continues, it can be argued that the reaction product distributions will show a more uniform or modified Gaussian type distributions.

The primary assumption in our dispersion model is that the chemical-with-air reaction phenomenon, if any, and the dispersion process can be decoupled. The only coupling between the two phenomena occurs through the overall density of the cloud. The air entrainment rate is determined by the overall density of the cloud and the atmospheric meteorological conditions. The overall density of the cloud and the mean concentration of the species in the cloud at any instant of time are determined solely by: (i) the mass, phase, and thermodynamic conditions of the chemical at release, (ii) the mass of air mixed, its temperature and humidity, and (iii) the total net heat input into the cloud from external sources.

Our second assumption is that any reaction between air and the chemical ceases when the concentration of the primary chemical is very low. In fact, we assume that no reaction occurs after the transition from the heavy gas dominated dispersion to the atmospheric dominated dispersion.

The third assumption in our model is that the initial stages of dispersion can be described by a modified "box" model and the atmospheric dispersion stage is described using a modified, volume source based, Gaussian model. The details of these are described in the appropriate sections below.

5.2 DISPERSION OF INSTANTANEOUSLY RELEASED HEAVY VAPOR CLOUD ("PUFF")

5.2.1 Assumptions

In developing the puff dispersion model we make the following assumptions:

1. The initial geometry of the cloud is a circular cylinder with specified physical dimensions.

2. The initial thermodynamic condition of the cloud is prescribed. That is, the temperature, concentration of chemical both in the liquid and gaseous phase (and if other species are present their concentrations), and the total volume of the cloud are known initially.

3. The initial property distributions within the cloud are assumed to be uniform.

4. The air entrained is assumed to be mixed within the cloud in a very short time. That is, the time of mixing is very short compared to the time for the cloud to move a distance equal to its diameter.

5. During the initial gravity dominated dispersion phase the concentration and other intensive properties within the "box" are assumed to be uniform. In other words, we assume a top hat distribution for the various parameters within the cloud.

6. The cloud is assumed to be in thermodynamic equilibrium at all times. This state is consistant with the total air entrained and the total heat exchanged with the surroundings up to any given time. In effect, this is equivalent to assuming that the reaction time constants are much smaller than the time constant for mixing of air and the cloud.

7. No rain out of the liquid aerosol is assumed.

8. The initial cloud depth is equal to the initial cloud radius.

The initial state of the cloud is calculated by noting the quantity of material released (using the source models described in Chapter 2), the amount of air mixed initially and using the thermodynamic models described in Chapter 3. The initial thermodynamic state of the cloud is specified by the overall volume of the cloud, the mass of the various species, the temperature, and the overall density.

Assuming that,

V_i = Initial cloud volume

we calculate the initial radius of the cloud and initial cloud depth by the following equations:

$$R_i = \left(\frac{V_i}{\pi} \right)^{1/3} \qquad (5.2.1)$$

$$H_i = R_i \qquad (5.2.2)$$

5.2.2 Modeling the Heavy Gas Dispersion Phase

The cylindrical cloud, shown schematically in Figure 5.2.1, moves downwind and expands radially. At any downwind position, X, of the ground level center of the cloud the concentration distribution within the cloud will be essentially uniform within a core along with "tails" at the edges. The classical "box" models described in the literature (Wheatley and Webber, 1984; Carpenter, et al., 1986; Raj, 1986) do not provide the facility to calculate the tail distributions outside the cloud. To take into account the presence of Gaussian tail distributions outside the "box", we model the heavy gas dispersion phase in two parts.

Let us assume that the concentration distribution in the cloud at a downwind location X (i.e, the location of the ground level center of the cloud) is needed. In the part one calculation we assume that the cloud disperses as a classical "box", i.e., the air entrainment occurs at the top and edges and that there is momentum transfer from the wind to the cloud. From this box type description, the total air entrained up to the downwind distance X is determined. The cloud dilution, vaporization of aerosols, reaction, etc., are now determined using the thermodynamic and reaction kinetic models described in Chapter 3 and using the total air entrained up to the position X. This gives the mean concentration of the primary chemical, secondary species, if any, temperature, etc. In the box model description, all of the material released is within the box at all times.

The side dilution caused by atmospheric turbulence is taken into account in part two of the heavy gas model. In this part of the model, the results obtained from the exercise of the model in part one are used to determine the actual concentration distribution at position X as follows:

- We assume that a cylindrical volume source of vapor exists at the release point (i.e., at X = 0). The physical dimensions of this cylindrical cloud and the thermodynamic state are the same as that of the "box" at X calculated using the part one model.

- The dispersion of this volume source is now calculated using the volume source Gaussian model approach (see section 5.2.4 below). The dispersion coefficient values correspond to the stability of the atmosphere and the distance X.

The result from this latter calculation yields the actual concentration profile at position X of the cloud.

Part 1: Model Formulation for Box Type Dispersion.

We follow very closely the formulation of the box dispersion model described by Raj (1985, 1986), Carpenter, et al., (1986) and others with minor variations in the recipe for the entrainment velocities. The various equations describing the radial spread rate, the air entrainment rate and the acceleration of the vapor cloud by the wind are indicated below:

$$V = \pi R^2 H \quad : \text{Volume of the Box cloud} \quad (5.2.3)$$

$$U_f = \frac{dR}{dt} = k\sqrt{g H \Delta'} \quad : \text{Radial spread velocity} \quad (5.2.4a)$$

$$\text{with} \quad \Delta' = (\rho/\rho_a - 1) = \text{fractional density excess over air density} \quad (5.2.4b)$$

$$M = M_c + M_a \quad : \text{Total mass in the cloud} \quad (5.2.5)$$

$$\frac{dM_a}{dt} = \frac{dM_E}{dt} + \frac{dM_T}{dt} \quad : \text{Air Entrainment Rate} \quad (5.2.6)$$

where, M_E and M_T represent, respectively, the total mass of air entrained on the edge and on the top of the cloud from the release point up to the present location of the cloud.

The rate of air mass entrainment into the cloud can be represented by the equations:

$$\frac{dM_E}{dt} = \rho_a u_E \; 2\pi R H \quad \text{and} \quad \frac{dM_T}{dt} = \rho_a u_T \pi R^2 \quad (5.2.7)$$

where u_E and u_T are, respectively, the entrainment velocity for edge entrainment and for top entrainment.

The momentum equation is given by:

$$M \frac{dU}{dt} = (f \bar{u}_H - U) \frac{dM_E}{dt} + [u(H) - U] \frac{dM_T}{dt} + D - F \quad (5.2.8)$$

where the frontal drag force on the cloud due to the wind is given by D and the ground friction is given by F. In the above equation the total horizontal momentum brought into the cloud due to side entrainment of air is assumed to be a fraction of the mean horizontal momentum of the entrained air over the height of the cloud. In the above equation this fraction is represented by the symbol f.

The wind-to-cloud drag force is calculated assuming that the dynamic pressure at every vertical position is due to the difference in the wind velocity at the position and the mean translation speed of the cloud, U.

That is,

$$D = \rho_a C_D R \int_{z=0}^{z=H} |u(z) - U| [u(z) - U] \, dz \qquad (5.2.9)$$

where,

$$C_D = \frac{F_D / A}{1/2 \, \rho_a \, U^2} \qquad (5.2.9a)$$

and

$$F = \pi R^2 \rho_a u^{*2} \qquad (5.2.10)$$

Entrainment velocities.

Many correlations have been proposed in the literature to express the entrainment velocities as functions of cloud parameters and atmospheric meteorological conditions. These correlations have been reviewed and presented by Raj (1986). Based on the recent findings from the Thorney Island test data (Carpenter, et al., 1986), we use the following description of the entrainment velocities:

$$u_E = \alpha U_f \qquad \text{Edge Entrainment velocity} \qquad (5.2.11)$$

and

$$u_T = \frac{u_1}{\sqrt{\frac{1}{\beta_2^2} + (Ri/\beta_1)^2}} \qquad \text{Top Entrainment velocity} \qquad (5.2.12)$$

where,

u_1 = the longitudinal rms turbulent velocities in the air

Ri = Richardson number based on atmospheric turbulence and the atmospheric eddy size at box cloud height. This is defined in equation 5.2.16.

The form of the top entrainment velocity used in equation (5.2.12) has the proper limit in the heavy gas phase as well as in the atmospheric turbulence limit. The choice of the turbulent velocity scale used in this equation and in the definition of the Richardson number is based on the argument that the entrainment at the cloud top is due to "local turbulence" characteristics in the atmosphere at cloud height modified by the presence of a stratified layer below. The longitudinal turbulence velocity scale u_1 is related to the friction velocity u^* by the equation,

$$u_1 = u^* [3.12 - 0.233\ SP] \qquad (5.2.13)$$

where SP is the atmospheric stability number on the continuous scale described in Chapter 4. The ambient turbulent eddy size L (or turbulent length scale) at the top of the cloud is given by,

$$(L/H_r) = 1.776\ (H/H_r)^{0.48} \qquad (5.2.14)$$

in which H_r is a reference height generally taken to be 10 meters (Taylor, 1970). Equation 5.2.14 has been correlated by us using the values of the ratio of u_1 and u^* for the six Pasquill stability classes indicated in the report by Wheatley, et al., (1987).

Starting with the specified initial conditions of the cloud the extent of radial expansion of the cloud over a short duration can be obtained from equation 5.2.4. The mass of air entrained during the same short time can be estimated using equation 5.2.7. However, in order to use this equation the entrainment velocities are calculated using equations 5.2.11 through 5.2.14. The momentum equation, 5.2.8, is integrated over the same short duration of time to obtain the cloud velocity at the new time. Knowing the total mass of air in the cloud and utilizing the thermodynamic models described in Chapter 3, the concentration, temperature, volume and the density of the cloud at the new time (and therefore the new spatial position downwind) can be obtained.

Using the above procedure we calculate the conditions of the heavy gas box cloud at any specified downwind position X of the ground level center of the cloud. However, in order to calculate the actual concentration distributions and the "proper" extent of the cloud at X, we allow the cloud edges to be affected by the atmospheric turbulence. The details of this model are indicated in the following sub section.

Part 2: Model for the Volume Source Dispersion.

We assume in this model that a cylindrical cloud of radial dimension R_X, height H_X, and uniform chemical concentration C_X is released at the origin (X = 0). The concentration distribution within the cloud is desired when the ground level center of the cloud is at downwind position X. For this model, we assume that the initial cylindrical source can be treated as a volume source and the volume source Gaussian dispersion equations can be applied to each and every packet of vapor within the source. We also assume that no chemical reaction or chemical phase modifications take place in this "pseudo" dispersion.

Under the above conditions it can be shown that the concentration distribution at the downwind position X is given by (Slade,1968):

$$C(X,r_p,z_p) = \frac{C_X}{(2\pi)^{3/2}\,\sigma_y^2\,\sigma_z}\int_{r=0}^{R_X} r\,dr \int_{\Theta=0}^{2\pi} e^{-\frac{(r_p^2 + r^2 - 2r\,r_p\cos\Theta)}{2\,\sigma_y^2}}\,d\Theta$$

$$* \int_{z=0}^{H_X} \left[e^{-\frac{(z_p - z)^2}{2\,\sigma_z^2}} + e^{-\frac{(z_p + z)^2}{2\,\sigma_z^2}} \right] dz \qquad (5.2.15)$$

where, r_p and z_p are, respectively, the relative radial and vertical coordinate positions of a point relative to a cylindrical coordinate system located at X, the ground level center of the cloud. The dispersion coefficients, σ_y and σ_z, are functions of the downwind distance X and the stability of the atmosphere. In this model, these parameters are calculated using the approach of Kunkel (1986) in which a system of continuous atmospheric stability classes is employed and the variations due to the surface aerodynamic roughness and concentration integration times are accounted for. The determination of the dispersion coefficients is described in Chapter 4.

The details of the derivation of equation 5.2.15 and the simplifications under several conditions are given in Appendix B. The second integral of equation 5.2.15 can be expressed in terms of the modified Bessel function of the second kind and zeroth order. The third integral (over z) is the sum of two error functions.

The result of application of the box model superimposed with the modified Gaussian model is shown, schematically, in Figure 5.2.2. The concentration distributions within the "box" are still very much uniform but the cloud has Gaussian tail distributions at the edges and at the top. The extent of tail penetration into the box is dependent on the distance X and the atmospheric stability.

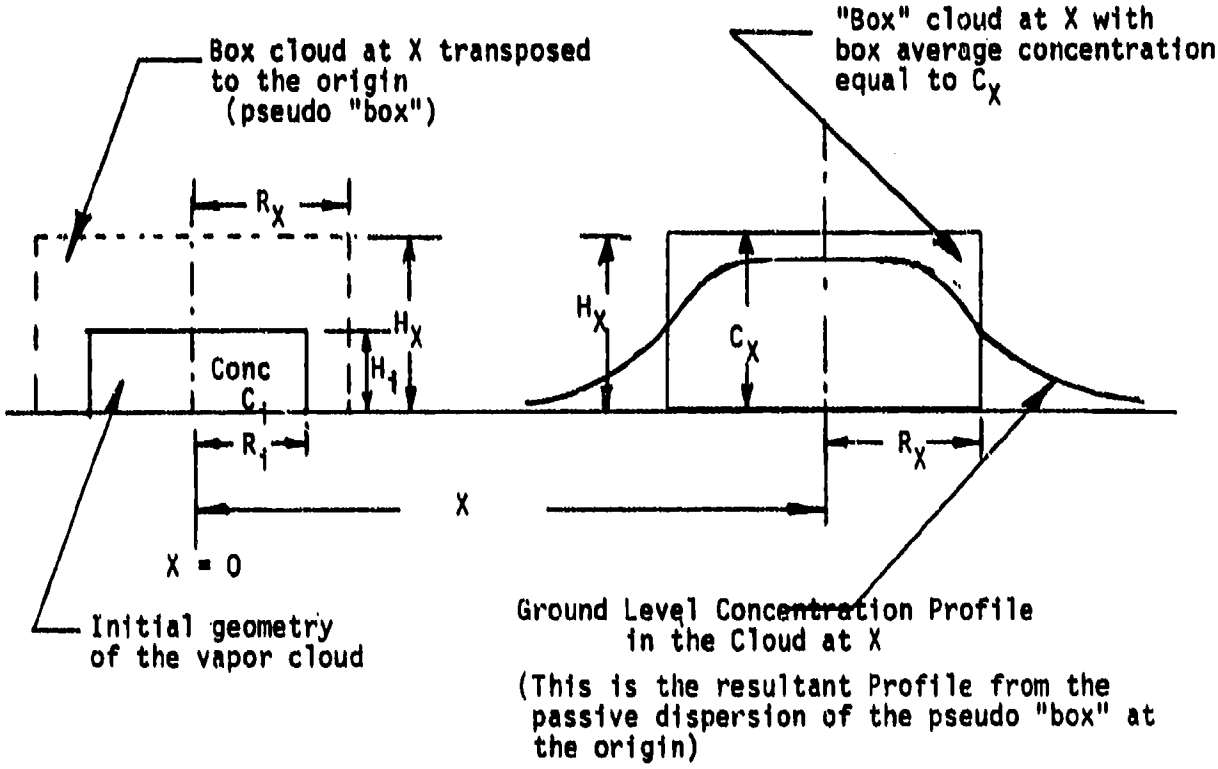

FIGURE 5.2.2: Schematic Illustration of the Hybrid Dispersion Model Using the "Box" Model and the "Volume Source Gaussian" Model.

Transition to Passive Dispersion

The negative buoyancy effects become less important as the cloud gets very dilute. That is, the gravity induced radial expansion velocity becomes very small. Correspondingly, the influence of this gravity induced flow velocity in generating turbulence for mixing air into the cloud becomes negligible. The importance of the gravity induced flow relative to the external flow is expressed by the Richardson number. There are several definitions of the Richardson number depending on the velocity and length scales used in the definition. The definition used in our model is as follows.

$$Ri = \frac{g \Delta' L}{u^2_1} \qquad (5.2.16)$$

where Δ' is the fractional density excess (Equation 5.2.4b) and U_1 the longitudinal turbulent velocity (Equation 5.2.13). Other definitions of the Richardson number include the use of the instantaneous cloud depth (H) for the length scale and the turbulent friction velocity (u^*) for the velocity scale. Various other definitions of the Richardson number used in the literature have been reviewed by Raj (1985). In our model we use the definition given in equation 5.2.16 based on the argument that the rate of mixing induced by atmospheric turbulence is a function of the mean square fluctuating velocity in the turbulent eddy (over the depth of the cloud). The gravity induced flow over the same depth scale (L) forms the numerator of equation 5.2.16. We assume that transition occurs when the atmospheric turbulence effects begin to be important in the mixing of air into the cloud.

Various criteria have been presented in the literature for the "transition" from the heavy gas dominated dispersion to the passive mode of dispersion. Havens (1982) has reviewed the transition criteria used by different researchers. While there are differences in the models there seems to be agreement in that most transition criteria are in the range of Richardson number between 1 and 10. However, the definitions of the Richardson numbers are different in different models.

In our model, we have investigated the following transition criteria.

$$Ri = 10 \quad \text{and} \quad Ri = 1 \qquad (5.2.17a)$$

and

$$\Delta' = 10^{-3} \quad \text{and} \quad \Delta' = 10^{-4} \qquad (5.2.17b)$$

In all of the models discussed in the literature the transition is treated as occurring at a specific location downwind. The models used for describing the dispersion after the transition are essentially Gaussian models. For example, in the SRD model

(Jagger, 1983; Wheatley, et al., 1986) it is assumed that the lateral and vertical edges of the box at transition are equivalent to the width and height of the vapor concentration which is 10% of the peak concentration as calculated by using a point source Gaussian model originating at the virtual sources. To match the conditions at transition, two separate virtual sources are used. The post transition horizontal dispersion is calculated assuming that the vapor originates from one virtual source and the vertical dispersion is calculated by assuming that the vapor originates from the other virtual source. Other models use similar "virtual source" approaches.

Inherent in all of the current models in the literature which describe the post transition dispersion regime are the following difficulties.

- Not all cloud parameters (concentration distributions, physical size, etc.) can be matched at the transition point. There is always a mismatch of other parameters when only one criterion is used for matching. Multiple parameter matching is impossible because of the completely different modeling approaches in the pre and post transition regimes.

- In some cases, the matching of one parameter (say the physical size) will result in either more or less mass of chemical in the passive dispersion regime. This artificial mass loss or gain is unacceptable from the standpoint of continuity of mass.

- Abrupt changes exist in the slopes of wind peak concentration, cloud width, and cloud height with down wind distance.

- Mass loss of the primary chemical due to reaction, dissociation, deposition, etc., cannot be accounted for properly.

5.2.3 Model for the Passive Dispersion Phase

The model we have discussed below has none of the above limitations. It provides for smooth transition from the box type dispersion to the passive dispersion. All parameters are matched and are continuous through the transition region.

Let X_T be the distance from the release point to the ground level center of the cloud at which any one of the transition criteria indicated in equations 5.2.17a or 5.2.17b is satisfied.

The detailed derivation of the equations describing dispersion of vapor from a cylindrical volume source is indicated in Appendix B. In this model the concentration distributions at any point down wind of the transition point are calculated as follows:

1. The volume source of vapor is assumed to be a cylindrical vapor cloud at the origin (i.e., the spill point)

2. The physical dimensions of this pseudo vapor cloud at the origin are the same as that of the "box" vapor cloud when the cloud center is at the transition point (X_T).

3. The concentration, temperature, and density of the cylindrical cloud at the origin are the same as that in the "box" cloud at the transition point.

4. The dispersion coefficients σ_y and σ_z are calculated for the atmospheric stability and the distance (from the origin) at which the concentration values are desired.

5. Cloud concentrations are calculated using equation 5.2.15 and other equations given in Appendix B.

In this model, the post transition dispersion is handled in exactly the same way as in the initial phase of dispersion, described in section 5.2.2., except that the radial spread and entrainment induced by the density effects are turned off. In addition, we assume that since the transition occurs at very low density deviations (from that of air) chemical reactions and aerosol evaporations, if any, are completed before the transition. This approach ensures that in the post transition region, the mass of the chemical is conserved and that the continuity and smoothness of concentration-with-distance and cloud size-with-distance are ensured.

From the equations presented in Appendix B it can be easily seen that at large distances (large compared to the transition distance or distances at which the values of the dispersion parameters are of the same order of magnitude as the respective dimensions of the box cloud at transition) the concentration distribution given by equation 5.2.15 tends towards a Gaussian profile in the horizontal and vertical directions.

The results of application of the above equations to several test cases and the sensitivity of the results to perturbations in the values of the parameters are discussed in Chapter 6.

5.3 DISPERSION OF CONTINUOUSLY RELEASED HEAVY VAPOR ("PLUME")

A plume results when the chemical vapor is released continuously from the source. This may arise due to the slow evaporation of a volatile chemical or due to the long term release of a flashing chemical. The "plume" model for a heavy vapor is in most respects similar to that of the "puff" model. However there are a few important differences. We list below the assumptions made in the model discussed in this section.

5.3.1 Assumptions

In the model presented below it is assumed that the:

1. geometry of the source of vapor is always rectangular.
2. mass flow rate of vapor through the source "window" is constant.
3. dispersion in the longitudinal direction is negligible.
4. entrainment rate is not affected by the presence of liquid aerosol particles.
5. dispersion of the plume can be modeled as a heavy gas "slab" moving down wind and diluting, together with a superposed passive dispersion of the slab edges.

5.3.2 Modeling the Plume Dispersion in the Heavy Gas Phase

In our model for describing the dispersion of a plume of vapor two simultaneously acting phenomena are considered. These are the heavy gas effects which induce lateral expansion of the plume and the air entrainment and passive dispersion effects which result in the plume edge dilution. We model the dispersion in the heavy gas plume in two parts, similar to the model for the puff dispersion.

In part 1 the dilution of a heavy gas "slab" is modeled. In this part the density effects are considered in both the lateral expansion of the "slab" and the rate of entrainment of air into the plume. In part 2 the passive dispersion using a modified Gaussian model is superimposed on the slab dispersion. This superposition is performed as follows. First, the plume is allowed to disperse as a slab. The result of this is that at any down wind position (say, X) the cross section of the plume is still a rectangle. The overall dispersion results for location X are now calculated by transposing the slab conditions at X (as calculated by the heavy gas "slab" model) to the origin of the plume and letting this pseudo slab disperse as a neutral density area source. The conditions at X are now calculated using an area source Gaussian model described in section 5.3.5. Once the heavy gas effects become small only the area Gaussian model is used to describe the down wind concentrations.

Part 1: Formulation of the Model for the "SLAB" type Dispersion

The schematic representation of plume dispersion in this phase is indicated in Figure 5.3.1. At the origin (X = 0), the vapor flow characteristics are known. That is, the window geometry (W_i, H_i), vapor density, mass flow rate of chemical and air, aerosol fraction in the vapor stream, vapor temperature, etc., are known. These values are calculated using the appropriate source models discussed in Chapter 2. For example, if the initial source is a jet of vapor/aerosol the amount of air entrained into the jet before the jet velocity reduces to the local wind speed value is calculated. Using the thermodynamic models discussed in Chapter 3 the thermodynamic condition of the vapor flow at the beginning of the dispersion regime (i.e., at the "window") is calculated. A similar approach is used if the source of vapor is from a vaporizing liquid pool. A wind uptake model described in Chapter 2 is used to determine the downwind vapor mass flow rate, the air flow rate and the size of the initial "window" for dispersion. In this case, the dispersion regime starts very close to the down wind edge of the pool.

The mass flow rate at X = 0 is given by:

$$\dot{M}_i = \rho_i \; 2 \; W_i \; H_i \; U_{tr,i} \qquad (5.3.1)$$

and the volume flow rate is given by

$$V_i = 2 \; W_i \; H_i \; U_{tr,i} \qquad (5.3.2)$$

Also, the mass flow rate is related to the chemical vapor flow rate and the air flow rate at the origin by the equation:

$$\dot{M}_i = \dot{M}_{ch} + \dot{M}_{a,i} \qquad (5.3.3)$$

where,

$\dot{M}_{ch}$ = The constant mass flow rate of the chemical

$\dot{M}_{a,i}$ = The mass flow rate of air at the source

Consider a plume "slab" of width 2 W, height H and longitudinal extent dX located at the down wind distance X from the origin (see Figure 5.3.1). We now write the following equations.

$$\frac{dW}{dX} = U_f/U_{tr} = [k\sqrt{g \, \Delta' \, H}\,]/\, U_{tr} \quad ; \text{ Lateral Expansion Velocity} \qquad (5.3.4)$$

$$\frac{d\dot{M}}{dX} = \dot{M}_a' = 2 \rho_a [\, W \, u_T + H \, u_E \,] \quad ; \text{ Mass continuity} \qquad (5.3.5)$$

where $\dot{M}_a'$ is the mass rate of entrainment of air per unit distance (along the wind direction).

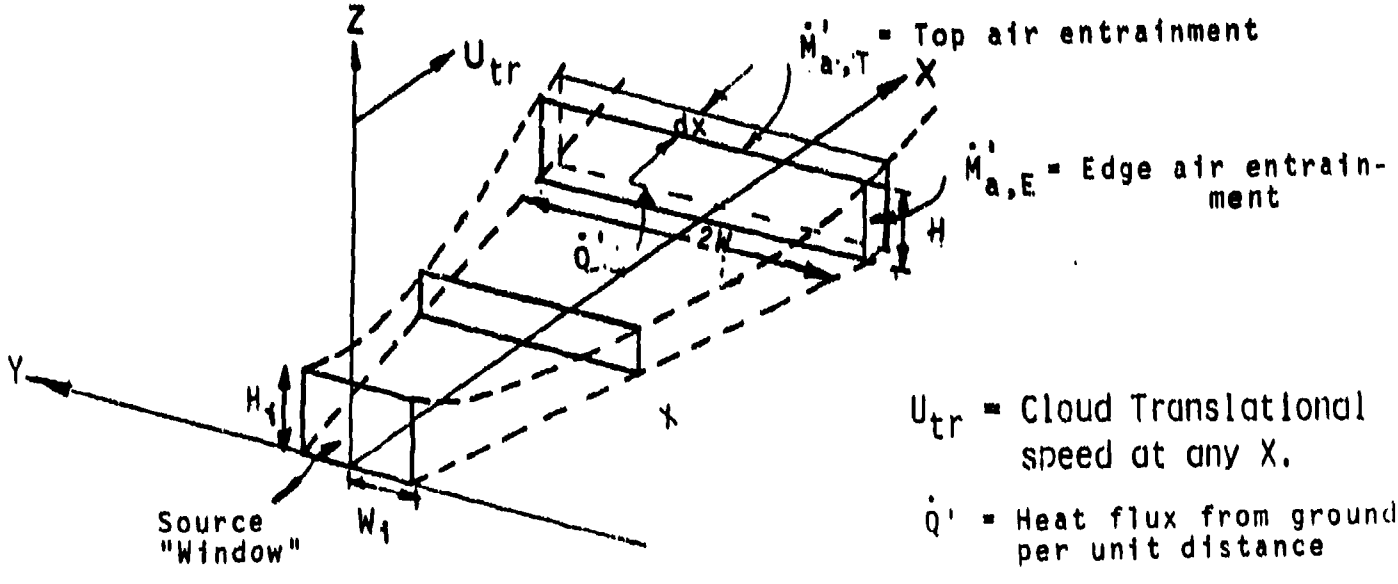

Figure 5.3.1: Schematic Diagram Showing the Dispersion of a Heavy Gas Plume

The entrainment velocity equations are the same as for puff dispersion. These are equations 5.2.11 and 5.2.12 in Section 5.2.2.

The rate of heat exchange between the ground and the plume is given by

$$\dot{Q}_G' = h\,(T_G - T)\;\; 2\,W \qquad (5.3.6)$$

where the left hand side of the equation represents the heat flux from the ground into the cloud per unit distance along the wind direction.

The translational speed of the plume is assumed to be the mean wind speed over the depth of the plume. This is represented by the following equation.

$$U_{tr} = \bar{U}(H) \qquad (5.3.7)$$

This is different than is some models where the translational speed of the plume is defined to be some fraction of the wind speed at the top of the plume. The representation we have used is based on the physical situation.

Part 2: Model for the Area Source Passive Dispersion

The characteristics of the "slab" plume at any down wind location X can be obtained by solving the equations 5.3.1 through 5.3.7 and using the thermodynamic models described in Chapter 3. Let, C_X = slab mean concentration of the chemical, W_X = Semi width of the slab, and H_X = Plume depth, be the parameters at X calculated using the "slab" model described above. The actual concentration distribution in the plume in the Y and Z directions at the down wind location X is now given by,

$$C(X,Y,Z) = C_X\; B_Y\; B_Z \qquad (5.3.8)$$

where,

$$B_Y = 0.5 * \left[\mathrm{erf}\left(\frac{W_X - Y}{2\,\sigma_y(X)}\right) + \mathrm{erf}\left(\frac{W_X + Y}{2\,\sigma_y(X)}\right) \right] \qquad (5.3.9)$$

and

$$B_Z = 0.5 * \left[\mathrm{erf}\left(\frac{H_X - Z}{2\,\sigma_z(X)}\right) + \mathrm{erf}\left(\frac{H_X + Z}{2\,\sigma_z(X)}\right) \right] \qquad (5.3.10)$$

In the above equations σ_y and σ_z are the Pasquill dispersion parameter values (discussed in Chapter 4) for the distance X under the prevailing atmospheric stability.

The equations in Part 1 are solved numerically to calculate the "slab" plume parameters downwind. The results are then used in equation 5.3.8 to calculate the concentration distribution at the down wind location. The sequence of calculations is indicated in Table 5.3.1. These calculations determine the following parameters at any downwind cross section of the plume.

(a) Lateral extent of the plume and the plume depth in the "slab" model.

(b) The plume translational velocity and the mean mass flow rate at the section.

(c) The mean density of the vapor cloud and its mean temperature.

(d) The cross section averaged vapor concentration and liquid aerosol concentration, if any.

(e) The distribution of concentration both horizontally and vertically.

Transition to Passive Dispersion Phase

As in the heavy gas puff dispersion model we assume that the effects of density driven lateral flows are relatively insignificant when the Richardson number (Ri, defined in equation 5.2.16) is of the order of unity. The heavy gas "slab" model is exercised until one of the conditions indicated in equations 5.2.17a or 5.2.17b is satisfied. The applicable transition criterion is determined by comparing the model results with test results. This is discussed in Chapter 6.

TABLE 5.3.1: SEQUENCE OF CALCULATIONS IN THE PLUME MODEL

Step #	Calculation
1	Using the initial conditions of mass flow rate, vapor density and the width of the "window", the height of the window is calculated by a process of iteration using equation 5.3.7 and the known wind speed characteristics.
2	The lateral spread rate at X = 0 is calculated using the initial conditions given and equation 5.3.4.
3	The entrainment velocities are calculated using equations 5.2.11 and 5.2.12. Substituting these in equation 5.3.5 gives the mass flow rate in the plume at location X + dX.
4	The heat flux into the cloud is calculated using equation 5.3.6.
5	Knowing at section X + dX the mass flow rate of air, the mass flow of the chemical, and the total heat added into the system from X = 0, the new thermodynamic condition of the plume is calculated using the models described in Chapter 3. This gives the density, temperature, and the concentration (C_{X+dX}) of the cloud.
6	With the known mass flow and width (from step 2) at X+dX, the value of plume depth, H_{X+dX}, is calculated as in step 1.
7	Equations 5.3.8 through 5.3.10 are now applied to calculate the true concentration distribution within the plume at position X+dX.
8	The value of X is now incremented and steps 2 through 7 are repeated.

A stable numerical integration results if the step size dX is chosen to be sufficiently small.

5.3.3 Passive Phase Dispersion Model

The dispersion in the post transition phase is characterized by no heavy gas effects and dilution dominated by atmospheric turbulence. We model the plume behavior in this phase by assuming that the vapor concentration in the post transition regime is significantly small so as to neglect any chemical reaction effects.

The model used to describe the concentration distribution in the plume is the area source Gaussian model. The area source of vapor is assumed to be at the origin (i.e., at the location of the original source of vapor). The size and vapor concentration of this area source are the same as the "slab" model values at the transition point. This approach ensures that the concentration and other property and geometrical parameters are continuous at the transition point.

The vapor concentration in the passive dispersion phase is determined by,

$$C(X,Y,Z) = C_T \; B_Y \; B_Z \qquad (5.3.12)$$

where,

$$B_Y = 0.5 * \left[\operatorname{erf}\left(\frac{W_T - Y}{2\,\sigma_y(X)}\right) + \operatorname{erf}\left(\frac{W_T + Y}{2\,\sigma_y(X)}\right) \right] \qquad (5.3.13)$$

and

$$B_Z = 0.5 * \left[\operatorname{erf}\left(\frac{H_T - Z}{2\,\sigma_z(X)}\right) + \operatorname{erf}\left(\frac{H_T + Z}{2\,\sigma_z(X)}\right) \right] \qquad (5.3.14)$$

where C_T, W_T and H_T represent, respectively, the slab model concentration, semi width, and plume depth at the transition point (X_T). The derivation of equations 5.3.12 thru 5.3.14 is indicated in Appendix B.

At large distances from the source, or more precisely, when the following conditions are satisfied,

$$\frac{2\;\sigma_y(X)}{W_T} > 5 \quad \text{and} \quad \frac{2\;\sigma_z(X)}{H_T} > 5 \qquad (5.3.15)$$

it can be shown that the maximum concentration within the plume is given by,

$$C_{max} = C_T \; \frac{2\;W_T\;H_T}{\pi\;\sigma_y(X)\;\sigma_z(X)} \qquad (5.3.16)$$

However, when $Y>>W_T$ and $Z>>H_T$ the concentration in the plume is given by the Gaussian equation,

$$C(X,Y,Z) = C_{max} \exp\left(-\frac{Y^2}{2\sigma_y^2}\right) \exp\left(-\frac{Z^2}{2\sigma_z^2}\right) \quad (5.3.17)$$

The models derived in chapters 2, 3, 4 and 5 are coded into a comprehensive computer code written in FORTRAN. The details of the computer code, the names of the various subroutines and the general calculation flow chart are described in Appendix C.

The application of the dispersion models derived in sections 5.2 and 5.3 to specific release conditions is discussed in Chapter 6. Also discussed in Chapter 6 are the sensitivity of the results from the models to the values chosen for the various parameters. The models are also applied to the conditions of different field experiments and the results from the models are compared with the test data.

CHAPTER 6

COMPARISON OF FIELD TEST DATA WITH MODEL RESULTS

The model developed in this project, henceforth called the "model", was validated by comparing its predictions with field test data. These comparisons are discussed in section 6.1. One set of values for the entrainment coefficients and transition criteria was used for all of the validation exercises. These values, obtained from the literature, were also varied to determine the sensitivity of the results to the values chosen. In section 6.2 this sensitivity analysis is discussed. An overall discussion of the model results is given in Chapter 7.0.

6.1 Model Validation

6.1.1 Introduction

The field test data with which the model results are compared include a variety of release rates, weather conditions, and four of the six chemicals reviewed in Chapter 3. The release conditions for these tests are summarized in Table 6.1.1 (additional test details can be found in the references cited in each of the sections below). The specific field test data used are from: 1) Eagle 3 and 6 (E3 and E6) nitrogen tetroxide releases, 2) Desert Tortoise 2 and 4 (DT2 and DT4) ammonia releases, 3) Lyme Bay V and VI (LBV and LBVI) chlorine releases, 4) U.S. Army Phosgene Test 1 (PT1), and 5) Thorney Island 8, 9, 11, 13, 45, and 47 (TI08, 09, 11, 13, 45, and 47) freon releases.

As shown in Table 6.1.1, the first three sets of tests are continuous spill tests. A major reason for including the Thorney Island freon tests is that they include both instantaneous and continuous releases. The freon was assumed to be a non-reacting chemical; in addition, it was released at ambient temperature and pressure and thus no aerosols were present.

Model comparisons with the field test data are complicated because the test data are presented in a mixture of formats. Some data have been presented as average centerline concentrations at ground level as a function of downwind distance from the source. Other data are peak concentrations recorded or area averaged concentrations. The model predictions shown are for time average centerline concentrations at ground level. The relation of this type of concentration data to the various test data is discussed in the appropriate sections below. In addition, in many of the tests the exact source strength is unknown causing more uncertainties in the comparisons.

The entrainment coefficient and transition criteria parameter values were constant for all of the model results shown. Entrainment coefficient values used in the models are based on values from Carpenter, et al., 1986 (the definition and value of C_D and the value of top entrainment coefficient have been changed) and are shown in

TABLE 6.1.1 Experimental Conditions for Field Tests

Trial	Chemical	Spill mass kg	Spill rate kg/s	T_{air} K	RH %	Wind speed m/s*	Pasquill stability
E3	N_2O_4	6350	33.7	295	45	3.9	E
E6	N_2O_4	5000	16.9	296	35	6.2	D
DT2	NH_3	29900	117	304	18	7.2	D
DT4	NH_3	41100	108	306	21	5.6	D-E
LBV	Cl_2	(15 min. @)	11.5	286	82	4.1	B
LBVI	Cl_2	(15 min. @)	7.0	286	88	3.6	D
PT1	$COCl_2$	236	Inst.	289	15	1.0	F
TI08	Freon	1890	Inst.	290	88	2.4	D
TI09	Freon	1890	Inst.	292	87	1.7	F
TI11	Freon	3180	Inst.	285	74	5.1	D
TI13	Freon	3150	Inst.	286	77	7.5	D
TI45	Freon	3370	7.4	286	100	2.3	E-F
TI47	Freon	3290	7.1	287	97	1.5	F

* At 10 meters height: measured or calculated assuming a logarithmic profile (see Equation 4.2.24).

TABLE 6.1.2 Entrainment Coefficient Values and Transition Criteria Values

Entrainment Coefficients:

$k = 1.07$ $\quad C_D = 0.50$

$\alpha = 0.7$ $\quad \beta_1 = 0.08$

$f = 0.55$ $\quad \beta_2 = 0.3$

Transition Criteria:

$(\rho_c/\rho_a - 1) < 10^{-3}$ $\quad Ri < 1.0$

Table 6.1.2. Also listed are the two transition criteria used and their values, based on the review by Raj, 1983.

The following subsections contain discussions on the various field tests. In the first subsection, Figure 6.1.1 is discussed in detail as an example of the figures that are presented for each test case.

6.1.2 Eagle Nitrogen Tetroxide (N_2O_4) Field Tests and Model Results Comparisons

In September and October of 1983, Lawrence Livermore National Laboratory conducted a series of large-scale (3-5 m^3) nitrogen tetroxide (N_2O_4) spill tests at the Frenchman Flat area of the Department of Energy's Nevada Test Site for the US Air Force Engineering and Services Laboratory, Tyndall AFB. These tests were designed to provide source strength characteristics and heavy gas dispersion aspects of large N_2O_4 spills under various conditions (Koopman, et al., 1984; Ermak, et al., 1987; Goldwire, et al, 1986).

Eagle 3 (E3)

As reported in the above references, in both this test and Eagle 6 the N_2O_4 was spilled in a multiexit, unconfined configuration to distribute the chemical over a large area in order to evaporate it as quickly as it was spilled. The N_2O_4 is reported to have soaked into the lakebed playa surface, however, and outgassed for several hours after the spill terminated. The surface vapor temperature measurement indicated that the N_2O_4 became frozen. HNO_3 mist formed near the source due to reactions between the N_2O_4 and the water vapor in the air (humidity was 45%). No data for the HNO_3 concentrations were given, so no estimate of this effect can be made. Estimating the source strength was difficult due to non-availability of direct measurements of the vapor source strength. Downwind flux calculations based on the measured concentrations account for only 20% or less of the chemical released. Other uncertainties in concentration were caused by: 1) Using gas sensor instruments that were optimized for liquefied natural gas (LNG) detection and which did not perform as expected during all of the Eagle tests. 2) Using the measured N_2O_4 concentrations at 25 meters downwind to derive the NO_2 concentration using a temperature dependent rate constant. 3) Assuming the gas sensors at 25 meters downwind would only detect N_2O_4 and not NO_2. The downwind average centerline volume percent concentrations ($C(x,0,0)$) were calculated from weighted Gaussian fits of concentration contour data (Ermak, et al., 1987).

The model was run with the release conditions shown in Table 6.1.1. The source strength was assumed to be 20% of the spill rate, based on the results of the downwind flux calculations cited above. A one minute concentration averaging time was used, since time averaged contours over approximately a one minute period were used to reduce the data. The concentrations used for comparisons were the total NO_2 and N_2O_4 present at each measurement location, as reported by Ermak. The comparison of the model results and the test data is in Figure 6.1.1.

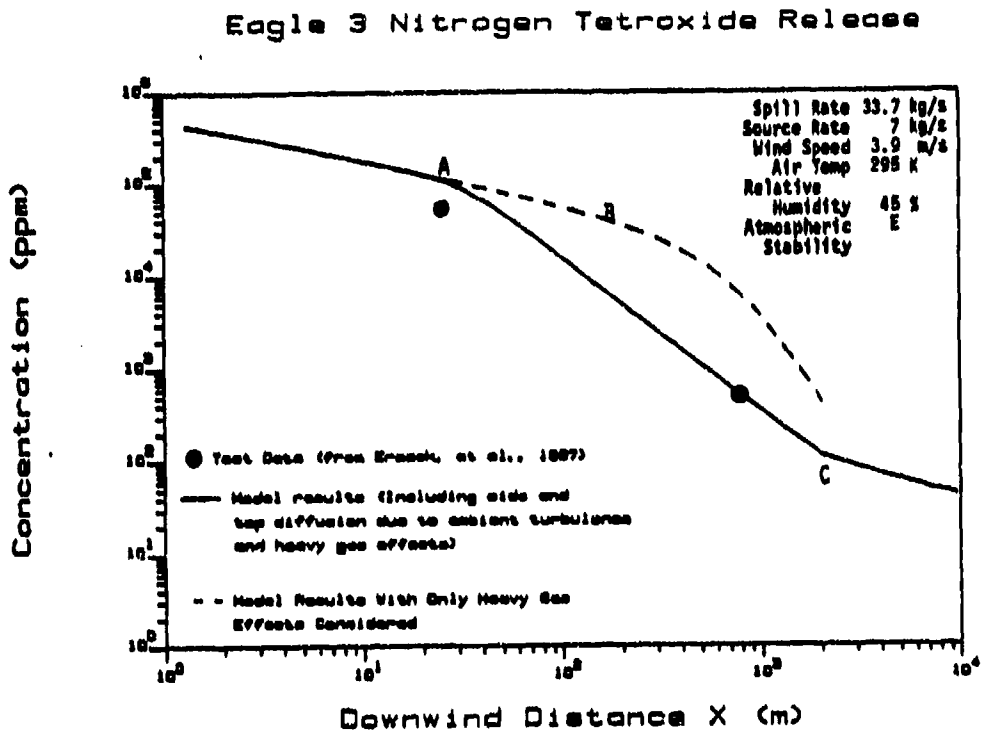

Figure 6.1.1: Comparison of Model Predictions for Downwind Centerline Concentration with Test Data from Eagle 3 Nitrogen Tetroxide Release

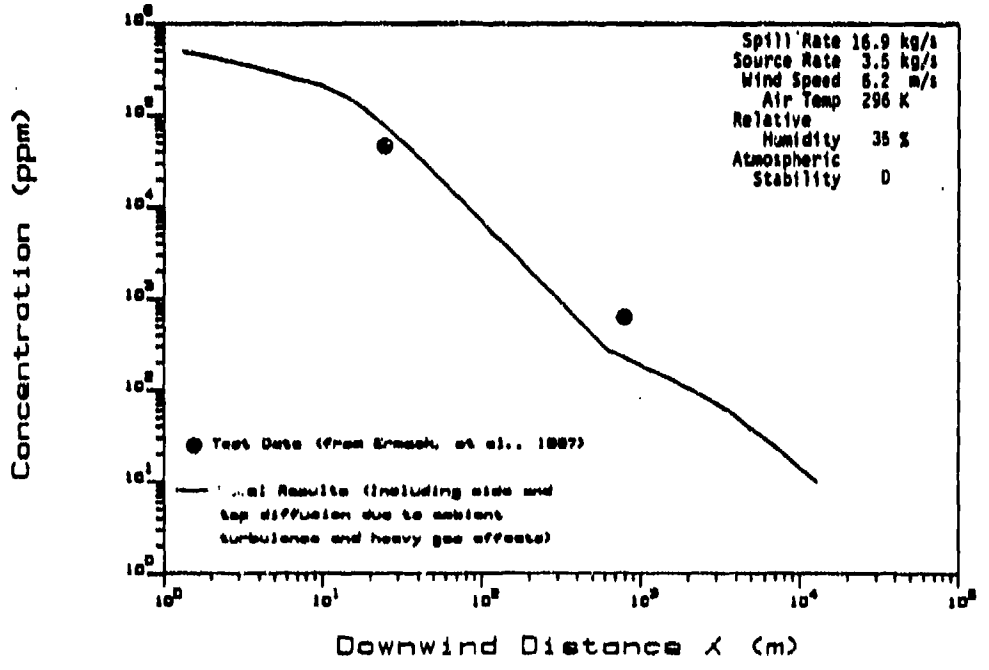

Figure 6.1.2: Comparison of Model Predictions for Downwind Centerline Concentration with Test Data from Eagle 6 Nitrogen Tetroxide Release

The model results are in good agreement with the measured test data, as the figure shows. There are several important general points to note in this figure, as similar characteristics are evident in all of the model / data concentration comparison graphs. The first is that the data are presented as pluses (+) and the model results as solid lines (——); in addition, the graphs are drawn on $\log_{10}$ scales. The concentrations are all presented in ppm units; the x axis, however, can have units of either downwind distance or time since release, depending on the test.

The first slope change in the line denoting the model results (marked by the A) is in the heavy gas dispersion region and is due to the increased vertical mixing that results (in the model) due to atmospheric turbulence. As an example, if this mixing is turned off, leaving only heavy gas effects, the concentration would decrease as shown by the dashed line (- - -), which is marked with a B. The second slope change (marked with a C) occurs at the point where transition from heavy gas to passive dispersion occurs. The slope changes since the heavy gas effects in the model are turned off, leaving only the vertical and horizontal passive mixing effects.

Eagle 6 (E6)

The release conditions for this test were very similar to those for Eagle 3, discussed above. This test had a smaller spill rate; again, the data presented only account for 20% or less of the amount of chemical released. The source strength used in the model was, therefore, only 20% of the spill rate. A one minute averaging time was used. The data for the 25 m position were derived from measured concentrations contours averaged over more than one minute; but the data for the 785 meter position were derived from only one time contour due to a lifting of the plume from the ground during most of the spill duration. The comparison of the model results and the measured data is in Figure 6.1.2. Again, the model results agree well with the measured data. For this test, one of the data points falls after the model transition point.

Unfortunately, the Lawrence Livermore group that has published the test data has not indicated "error bars" on the data reported. It is generally known in dispersion physics that the concentration at a given location in a test varies with time even when all conditions are seemingly steady. A peak to mean ratio of 2 for concentrations is generally accepted for center line concentrations and larger values have been found for locations at the off center line locations of plumes and puffs. Therefore, if we assume "error bars" of $\pm$ 2 factors around the mean, it is seen that the data and the model predictions agree remarkably well.

6.1.3 Desert Tortoise Ammonia (NH_3) Field Tests and Model Results Comparisons

Four (4) large scale (15-60 m^3) pressurized anhydrous liquid ammonia (NH_3) spill tests were conducted at the Frenchman Flat area of the Department of Energy's Nevada Test Site in August and September 1983 by the Lawrence Livermore National Laboratory (LLNL) for the US Coast Guard, The Fertilizer Institute, and Environment Canada as a joint Government and Industry study. Ammonia was released at a constant pressure from a 0.094 m diameter orifice forming a horizontal jet. The release pressure was held constant by external pressurization of the ammonia tanks with nitrogen. The released ammonia flashed and formed a radially expanding two-phase jet. The effective velocity of the jets were > 20 m/s at the release point and velocities greater than the ambient wind speed persisted for several hundred meters downwind. The velocity of the plume, as it passed through a sensor array at 100 meters downwind, was estimated to be 10 m/s (Goldwire, et al., 1986; Ermak, et al., 1987).

Desert Tortoise 2 (DT2)

Concentration data are given in the above references at each of the downwind sensor array locations (100, 800, and 1400 m). The released ammonia was still a jet at the first line of sensors (100 m) with an estimated velocity of 10 m/s (wind speed was 5.76 m/s at 2 meters height). The average centerline concentrations were calculated by LLNL using a weighted Gaussian fit of the averaged centerline concentration contours. Downwind flux calculations accounted for only 70% or less of the released ammonia. No error bars on the concentration data have been reported.

The release conditions for this test are shown in Table 6.1.1. A one minute concentration averaging time was used to generate the model results. The source strength was taken to be 70% of the spill rate, due to the flux calculations above. The comparison of the test data and the model predictions is shown in Figure 6.1.3. The model predictions are below the data during the initial phase of the dispersion. This is due to an over-prediction of the air entrainment during the jet phase of the dispersion. Again, as before, we contend that the model and experimental results agree very well. However, as can be seen from Figure 6.1.3, there is not much distance resolution in the data. It is not possible to state whether the concentration predicted for 10 km distance was indeed realized in the test.

Desert Tortoise 4 (DT4)

This test is very similar to DT2, and thus the details are similar. The differences are: data are available at 2800 m downwind instead of 1400 m and three minute averaging times were used for the data calculations and the model results. The comparison of the average centerline concentrations calculated from measured data with the model predictions is shown in Figure 6.1.4. The model predictions are

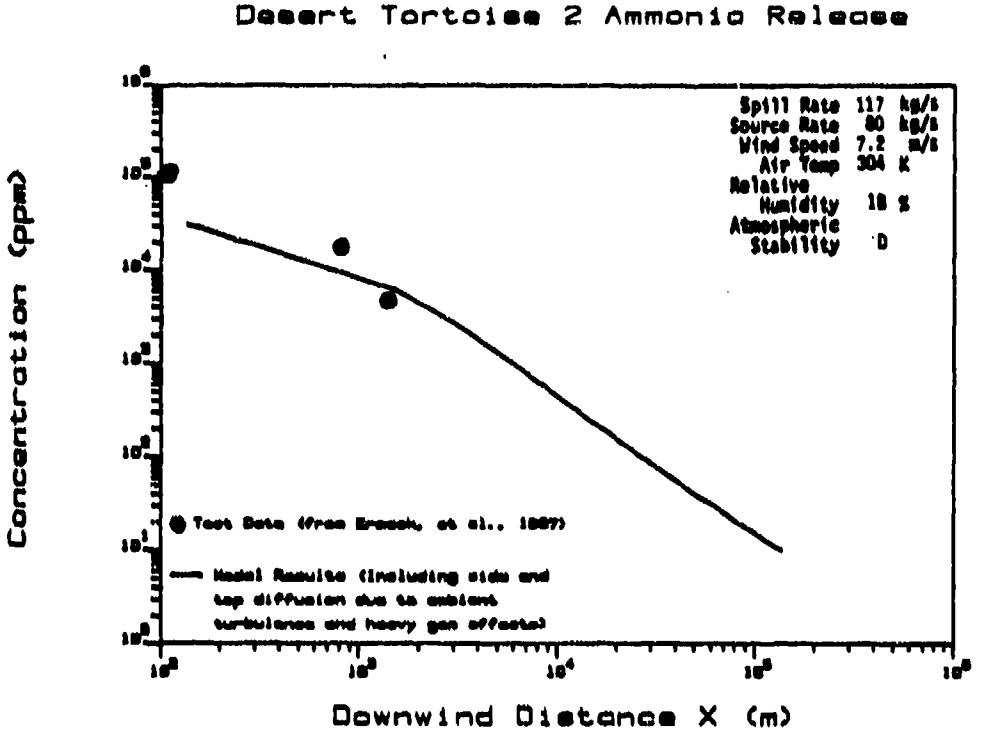

Figure 6.1.3: Comparison of Model Predictions for Downwind Centerline Concentration with Test Data from Desert Tortoise 2 Ammonia Release

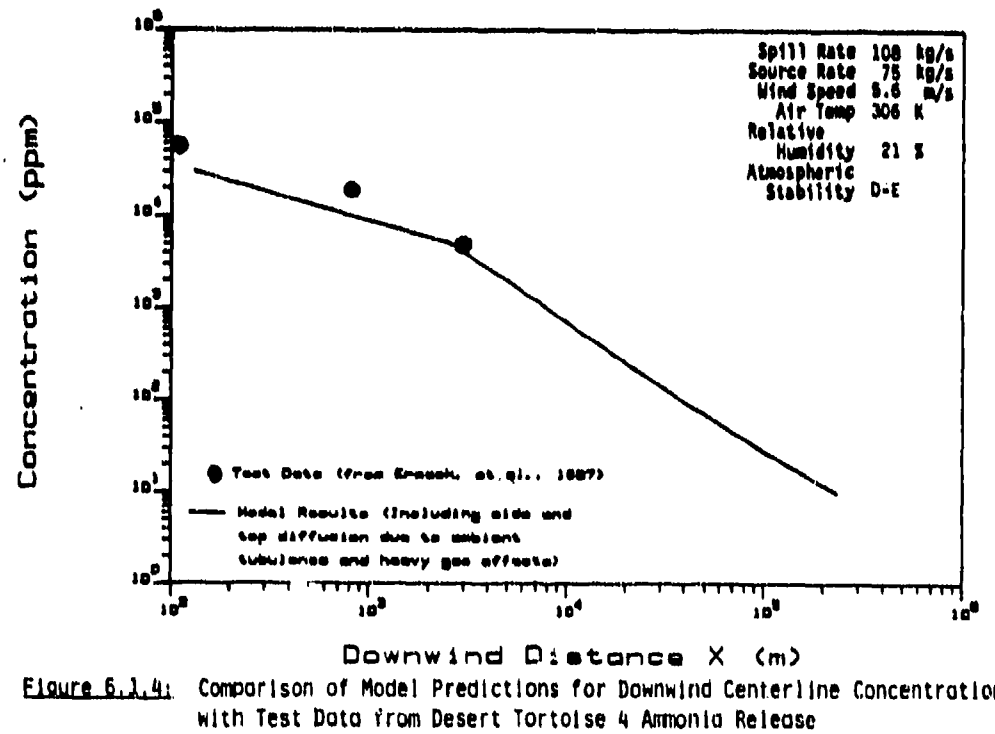

Figure 6.1.4: Comparison of Model Predictions for Downwind Centerline Concentration with Test Data from Desert Tortoise 4 Ammonia Release

closer to the measured data for this test, due to a better prediction of the jet air dilution.

It is to be noted, however, that the predicted concentrations are consistently lower than those observed in the test. We are unsure of the precise reasons; however, we can discuss several possibilities. First, the diffusion of air in our model may be overestimated. The effect of varying the entrainment coefficients are discussed in Section 6.2. The second explanation could be that the test data are subject (or at least incomplete because of lack of error estimates). However, notwithstanding all of the above possibilities, it is gratifying to note that the agreement between measured and predicted concentration values are within a factor of 2.

6.1.4 Lyme Bay Chlorine (Cl_2) Field Tests and Model Results Comparisons

A series of trials of continuous releases of pressurized liquid chlorine was conducted by the Chemical Defence Establishment of Great Britain in 1927. Data from these trials and their analyses have been indicated by Wheatley, et al. (1987) in a recent report. The report on the trials is detailed enough to allow comparisons of the measured data with dispersion models. The trials were conducted at sea by having a ship release chlorine as it steamed perpendicular to the wind. Four submarines with sensors on masts were positioned at different crosswind distances from the ship and also sailed perpendicular to the wind keeping the masts in the smoke colored chlorine cloud (see Figure 6.1.5).

Model comparisons with the chlorine concentrations for two of the trials are discussed below. There are several uncertainties in the comparisons including:

1) There is insufficient information on the initial conditions of the release

2) There is insufficient information on the atmospheric conditions at sea during each trial; in fact, the applicability of the land based stability parameters to the atmosphere over the sea is questionable.

Lyme Bay V (LBV)

The release conditions for this test are shown in Table 6.1.1. The comparison of the measured concentrations with the model predictions is shown in Figure 6.1.6. The model results are one minute time average centerline concentrations, C(x,0,0). The model predictions for this post transition dispersion data agree well with these data.

Uncertainties in the exact relative position of the submarines with respect to the ship are covered by the horizontal data range. For the vertical concentration range shown: 1) the lower concentration value

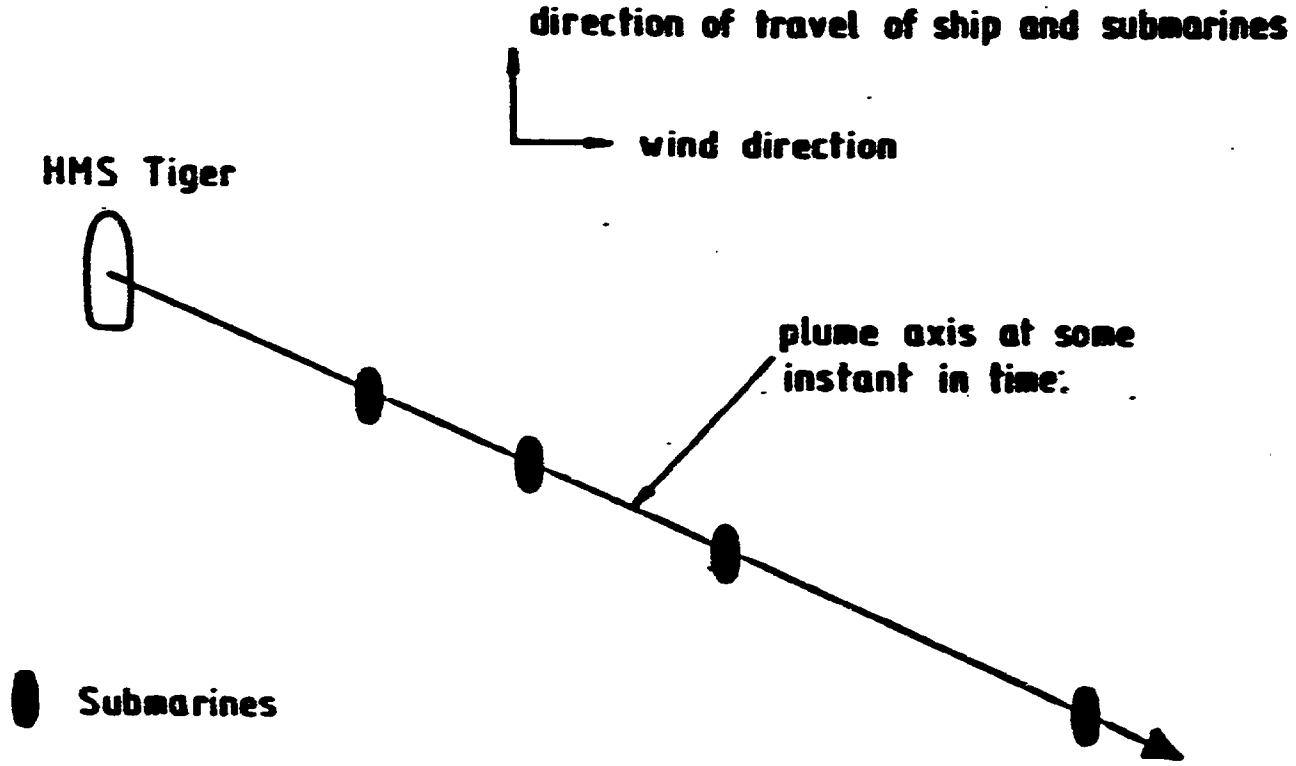

FIGURE 6.1.5 SCHEMATIC DIAGRAM SHOWING THE PRESCRIBED RELATIVE POSITIONS AND DIRECTION OF TRAVEL OF THE SHIP AND SUBMARINES DURING A TRIAL.

REFERENCE SOURCE: WHEATLEY, ET AL., 1987

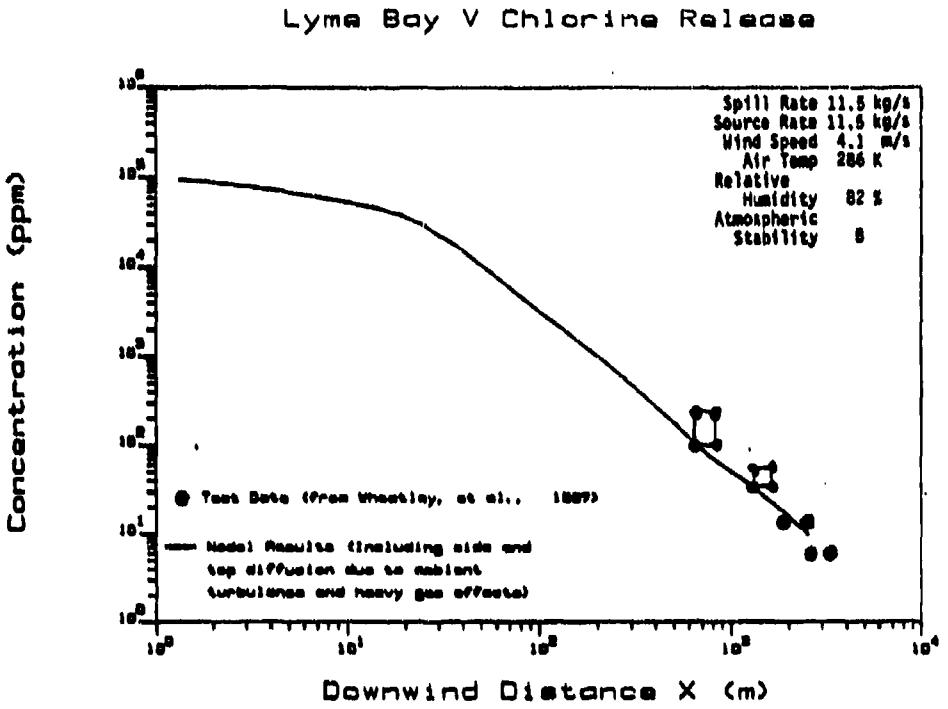

Figure 6.1.6: Comparison of Model Predictions for Downwind Centerline Concentration with Test Data from Lyme Bay V Chlorine Release

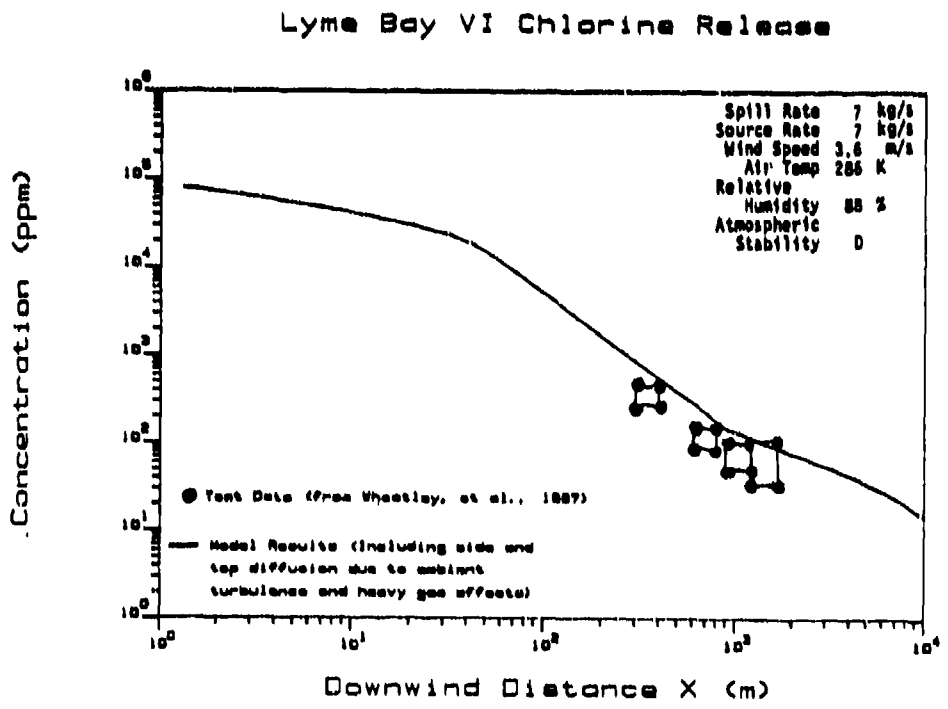

Figure 6.1.7: Comparison of Model Predictions for Downwind Centerline Concentration with Test Data from Lyme Bay VI Chlorine Release

at each downwind distance is the mean of all one-minute averaged concentrations for all sensors on the submarine (3 sensors at 3.0 m, 1 at 6.1 m and 1 at 9.1 m) and 2) the upper concentration value is the peak one minute average concentration. For two stations only the continuous concentrations data are available and thus no peak one minute average data are shown.

The atmospheric stability parameter for this trial is reported as Pasquill stability B based on the reported conditions. As stated above, the use of the SP scheme over water is questionable. The possibility of having moderately unstable conditions over the sea is also questionable. If a D stability had been used in the model, the predicted concentrations at each distance would have been higher.

Lyme Bay VI (LBVI)

The release data for this test are shown in Table 6.1.1. The comparison of the measured concentrations with the model predictions is shown in Figure 6.1.7. The model results are one minute time average centerline concentrations, C(x,0,0). Here, the model predictions are very near the measured data.

The data shown are similar to those described above. For this test, peak one minute average concentrations for all downwind distances were reported by Wheatley, et al. The stability parameter for this trial is D based on the reported conditions.

A comparison by Wheatley of these data and the data from trial LBV showed there was no change in the mixing rate of the air in the atmosphere between the two trials. The atmospheric stability parameter value is dependent on the air mixing rate, however, and thus it should have been the same for the two trials. They are reported as being different in the original trial report. This may be due to the inapplicability of the land based stability determination scheme to over sea atmospheric conditions (Wheatley, et al., 1987). The model predictions for the two trials seem to confirm this, since for LBV the predictions are lower than the data, and for LBVI, they are slightly above the data.

6.1.5 U.S. Army Phosgene ($COCl_2$) Field Test and Model Results Comparison

Field releases of chemical agents, including phosgene, were conducted by the U.S. Army in the 1940's. The declassified results from some of the tests were communicated to TMS by the Army Chemical Systems Laboratory (CSL) in 1983 (CSL, 1983; Raj, 1983).

Phosgene Trial 1 (PT1)

Phosgene was released from a 0.2 m^3 drum using 0.45 kilograms of dynamite. The initial source cloud was estimated by Raj, 1983, to be a cylinder 40 meters in diameter and 2 meters high. The concentrations were measured by observers working in the visible cloud

with injector and bubblers and with snap sampling equipment. The measured data used for comparisons were the highest observed concentrations at 0.7 m height. The results from the use of the instantaneous release model are for one minute average centerline ground level concentrations, C(x,0,0). The comparison of the test data with the model results is shown in Figure 6.1.8. Here, the model and data are in excellent agreement.

6.1.6 Thorney Island Freon (CCl_2F_2) Field Tests and Modal Results Comparisons

Extensive field trials on the dispersion of heavy gas clouds at ground level in the atmosphere were performed by a consortium of groups from 10 countries lead by the Health and Safety Executive in Great Britain (Ermak, et al., 1987; McQuaid, 1985; Brighton, et al., 1985; Brighton, 1985; Spicer and Havens, 1985; Pfenning and Cornwell, 1985; Wheatley, et al., 1986; Carpenter, et al., 1986; Puttock, 1986).

Numerous gas clouds (fixed volume, isothermal) of varying density (ρ_c/ρ_a) Freon and Nitrogen mixtures were instantaneously released in the atmosphere and gas concentrations were carefully monitored using sensors placed in the downwind range of the clouds. In the instantaneous releases, a nearly cylindrical bag with a volume of 2000 m^3 was filled with a mixture of Freon and Nitrogen. The top and sides of the bag were quickly removed releasing the entire contents at once. The mixture immediately started a gravity slumping expansion.

Additional trials having continuous releases of the gas mixtures were also performed. In these trials, the gas mixture was stored in the bag but then conveyed through an underground duct to the release point. The discharge end of the duct was designed so that the material was released with no vertical and relatively small radial momentum.

The extensive sensor and visual records of the trials provides a reliable data base for use in validating physical and mathematical models of heavy gas dispersion.

The model results are compared with data from six of the Thorney Island trials in the discussion below. Four of the trials compared were instantaneous releases and two were continuous.

6.1.6.1 Thorney Island Instantaneous Releases

The initial conditions of the four instantaneous release trials compared are listed Table 6.1.1. Individual trials are discussed in greater detail in the following sections. For all instantaneous releases, the lowest and highest time data points are not entirely reliable due to tailing off of the concentration at the edges of the clouds and sensor lower limit resolution (Brighton, 1985). In addition, the transition from heavy gas dispersion to passive dispersion as predicted by the model occurs at a distance larger than

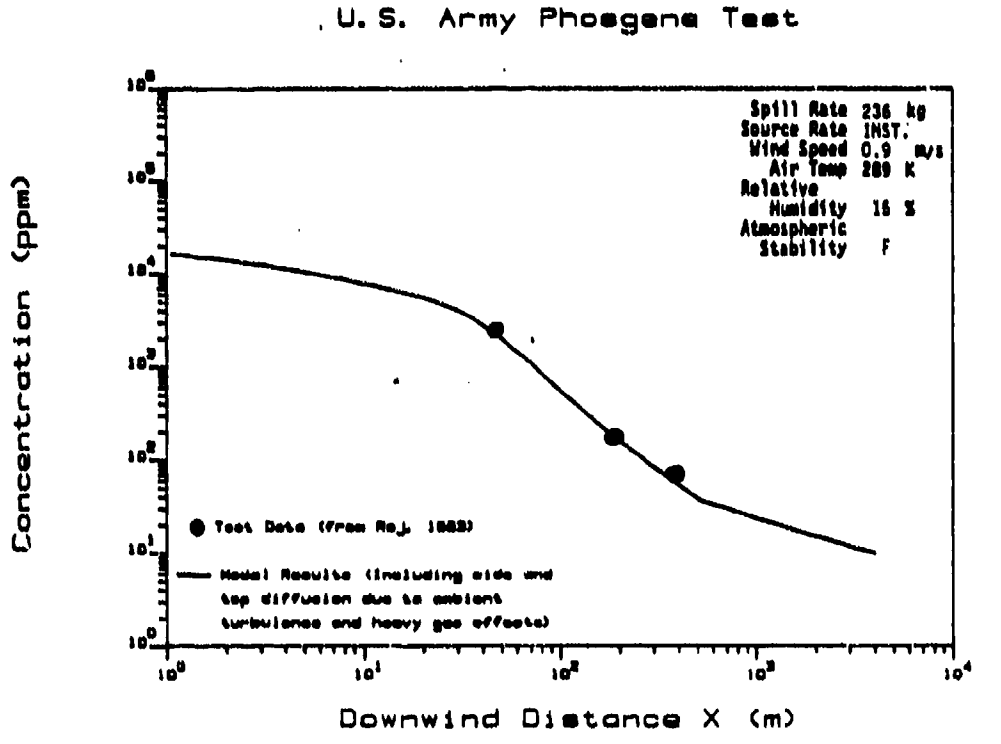

Figure 6.1.8: Comparison of Model Predictions for Downwind Centerline Concentration with Test Data from U.S. Army Phosgene Test

the farthest data sensor array making validation of predicted far field concentrations with the available data impossible.

Thorney Island Trial 8 (TI08)

This trial, TI08, and TI09 are similar except for the stability of the atmosphere and the wind speed. The comparison of the trial's gas sensor data with the model prediction is shown in Figure 6.1.9. The model predictions and data agree very well.

Comparisons of photographically derived data for cloud location, height, and area in the initial collapse of the gas cloud and the model predictions for this period are shown in Figures 6.1.10a, 10b, and 10c. The model predictions for cloud height were very good for this time period, as the figure shows. The cloud area predictions have the correct slope, but are offset from the data resulting in overpredictions. This offset may be due in part to the initial period of cloud dispersion when the stationary cylindrical cloud is accelerated and becomes horseshoe shaped as the edges are eroded by the wind. The cloud centroid locations are predicted with the least accuracy for this trial.

Thorney Island Trial 9 (TI09)

This trial, TI09, and TI08 are similar except for the stability of the atmosphere and the wind speed. The comparison of this trial's gas sensor data with the model prediction is shown in Figure 6.1.11. The model predictions are in good agreement with the data.

Comparisons of photographically derived data for cloud location, height, and area in the initial collapse of the gas cloud and the model predictions for this period are shown in Figures 6.1.12a, 12b, and 12c. The cloud height predictions are in excellent agreement with observed data for this period, as the figure shows. Here, the cloud centroid location is more accurately predicted. Again, the cloud are predictions are offset from the observed data, but they do have the correct slope.

Some additional uncertainty in the data for this trial exists due to the extreme stableness of the atmosphere during this test; it is believed that some gas was trapped in the grass at the test site and it dispersed more slowly than would be predicted. The cloud remained in the sensor field for the longest time of any of the trials, and the cloud was very flat. None of the upper sensors in the field (4.4 and 6.4 meters high) detected gas; only the two lower sensors (0.4 and 2.4 meters) detected any. This test also was run during high humidity conditions which could have caused erratic behavior of the sensors.

Thorney Island Trial 11 (TI11)

The comparison of the trial's gas sensor data with the model prediction is shown in Figure 6.1.13. In this figure, the transition from heavy gas dispersion to passive dispersion is shown - it occurs at the end of the available data, thus no validation of far field

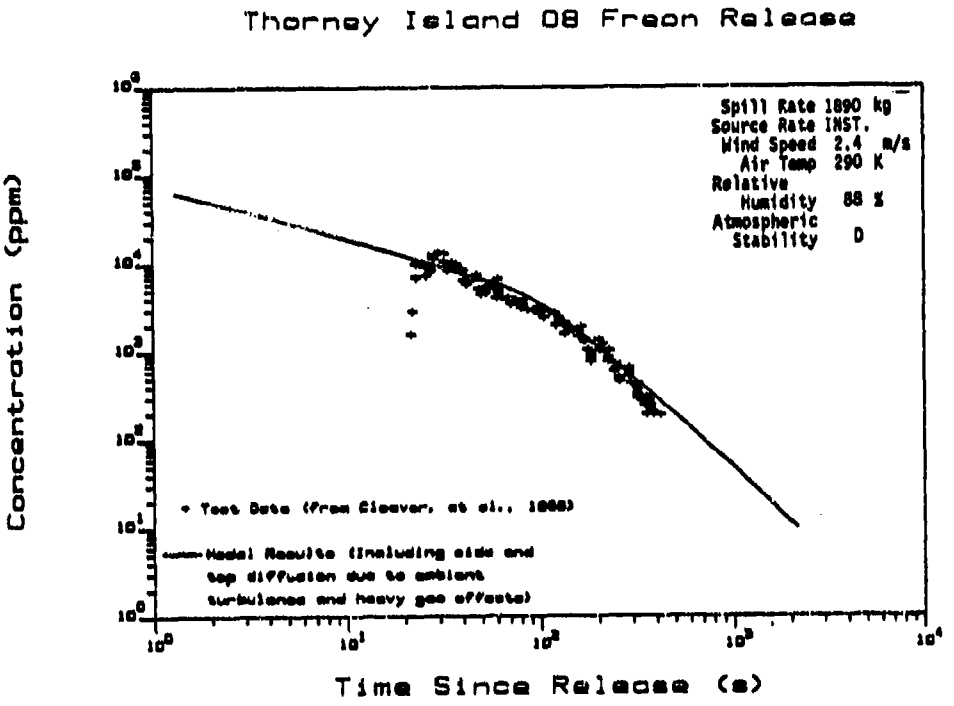

Figure 6.1.9: Comparison of Model Predictions for Downwind Centerline Concentration with Test Data from Thorney Island 08 Freon Release

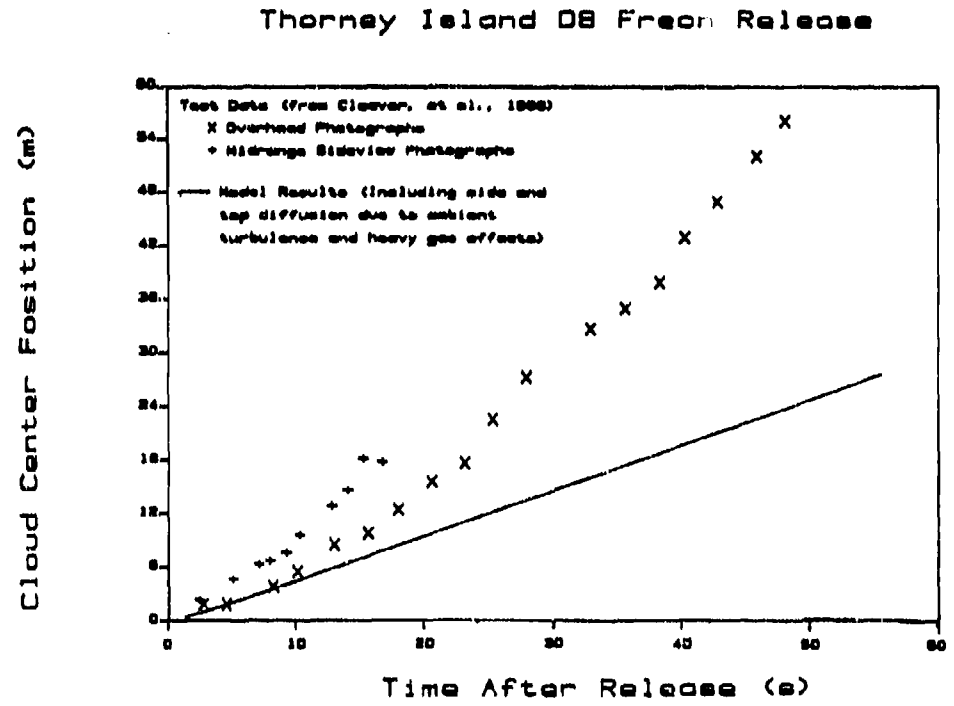

Figure 6.1.10a: Comparison of Model Predictions for Downwind Cloud Position with Test Data from Thorney Island 08 Freon Release

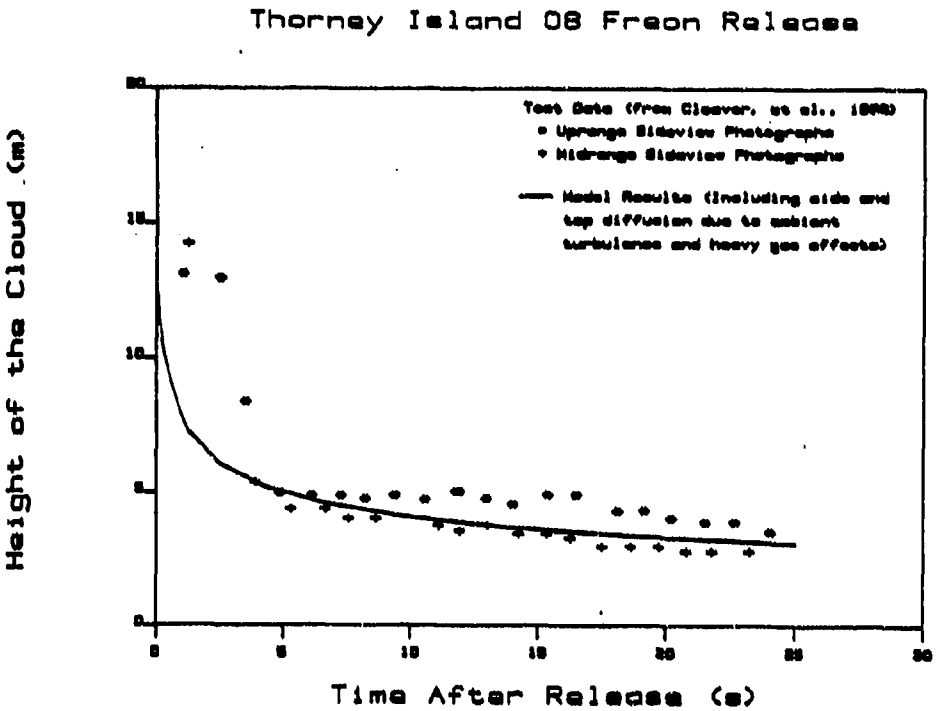

Figure 6.1.10b: Comparison of Model Predictions for Cloud Height with Test Data from Thorney Island 08 Freon Release

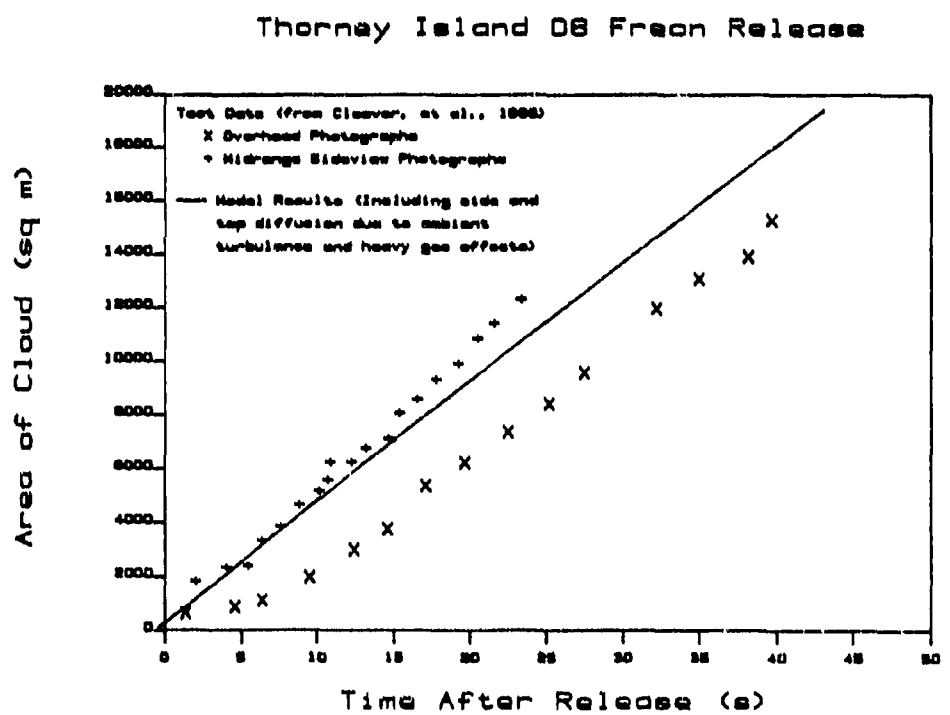

Figure 6.1.10c: Comparison of Model Predictions for Cloud Area with Test Data from Thorney Island 08 Freon Release

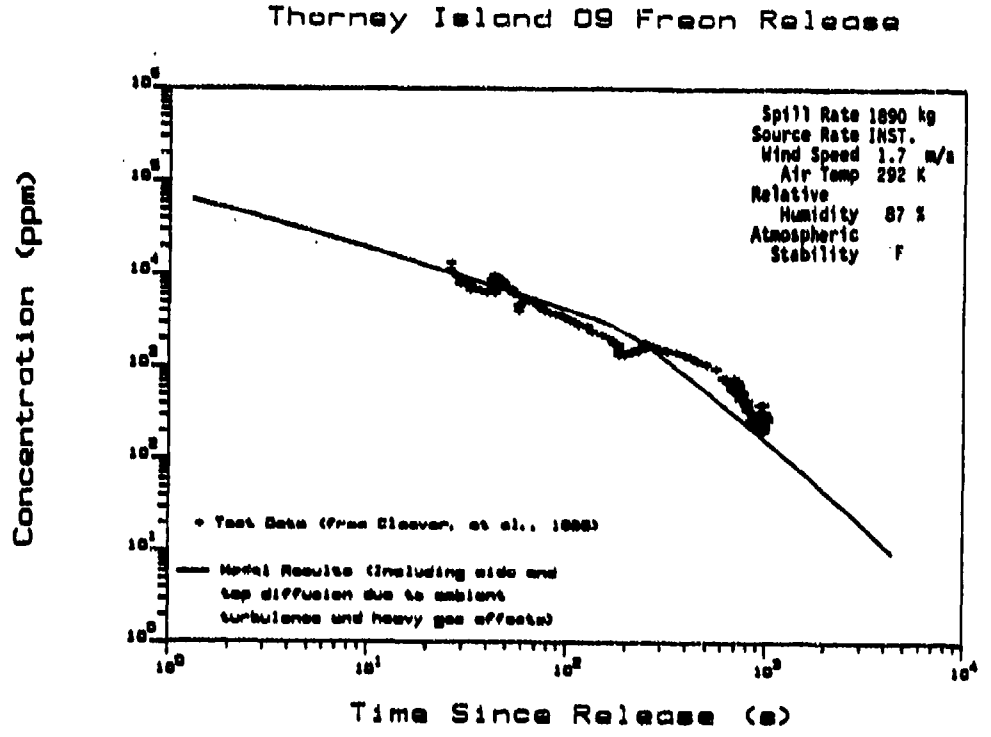

Figure 6.1.11: Comparison of Model Predictions for Downwind Centerline Concentration with Test Data from Thorney Island 09 Freon Release

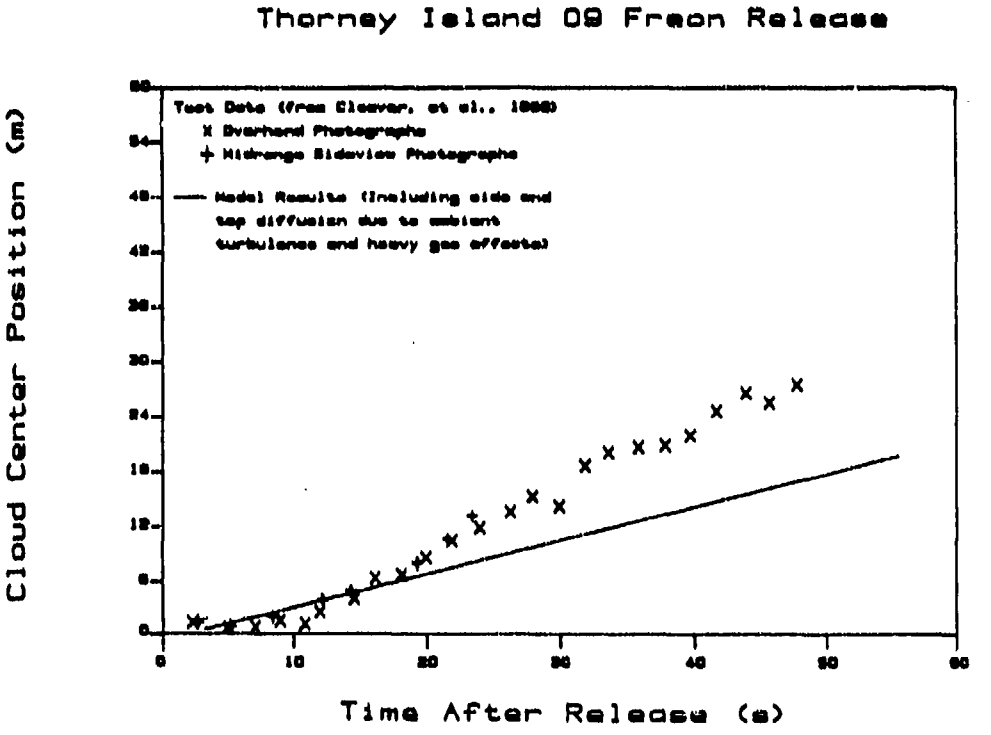

Figure 6.1.12a: Comparison of Model Predictions for Downwind Cloud Position with Test Data from Thorney Island 09 Freon Release

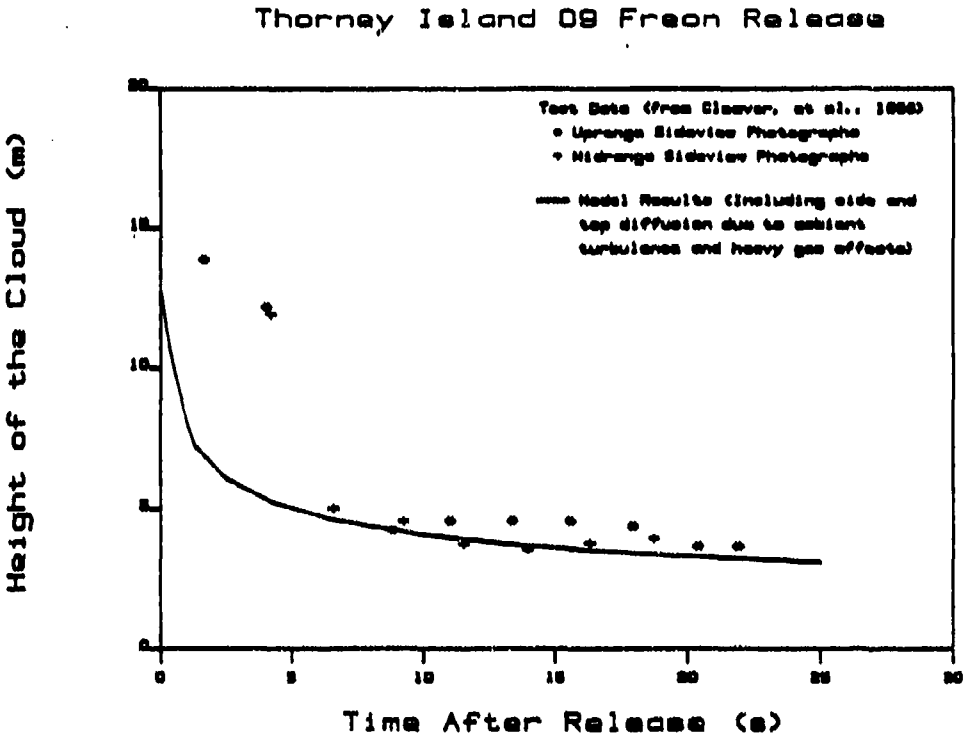

Figure 6.1.12b: Comparison of Model Predictions for Cloud Height with Test Data from Thorney Island 09 Freon Release

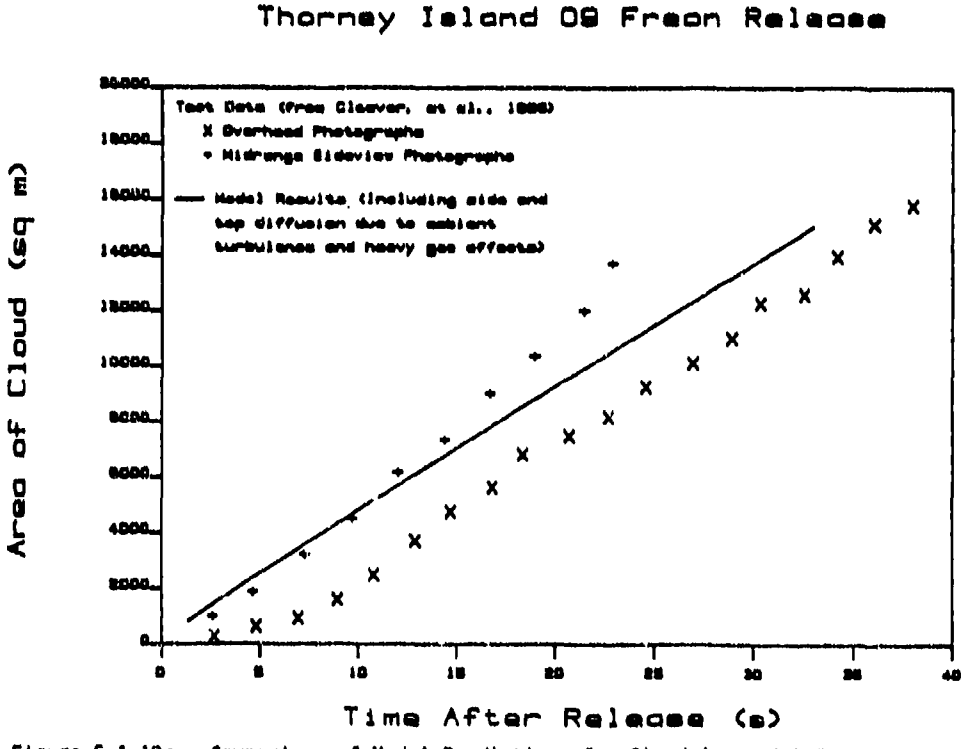

Figure 6.1.12c: Comparison of Model Predictions for Cloud Area with Test Data from Thorney Island 09 Freon Release

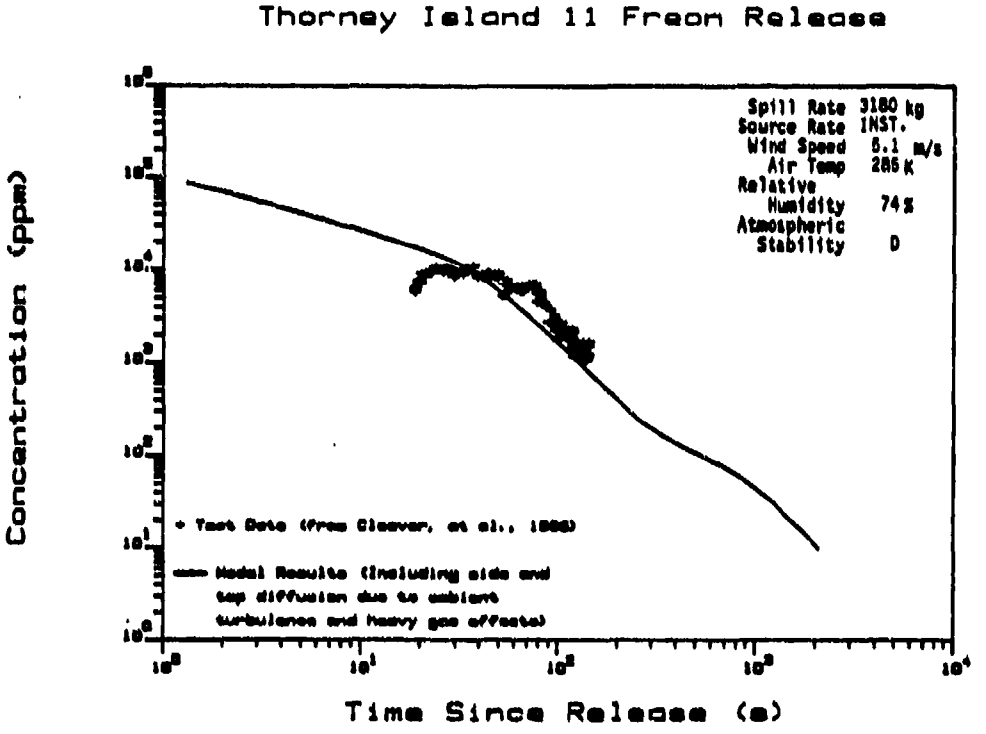

Figure 6.1.13: Comparison of Model Predictions for Downwind Centerline Concentration with Test Data from Thorney Island 11 Freon Release

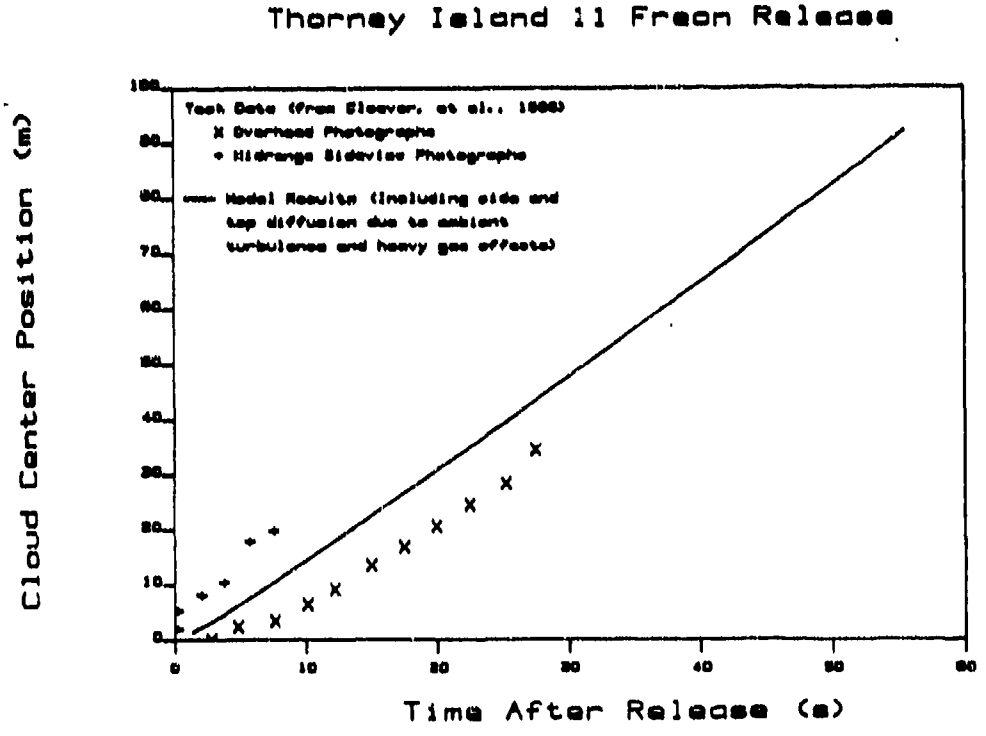

Figure 6.1.14a: Comparison of Model Predictions for Downwind Cloud Position with Test Data from Thorney Island 11 Freon Release

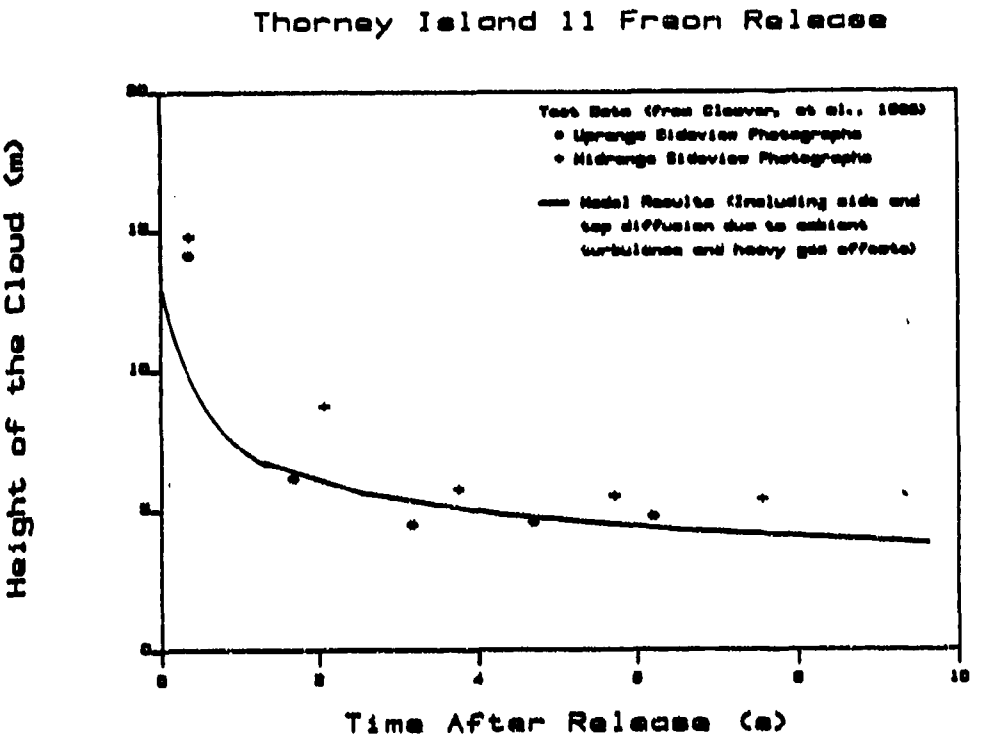

Figure 6.1.14b: Comparison of Model Predictions for Cloud Height with Test Data from Thorney Island 11 Freon Release

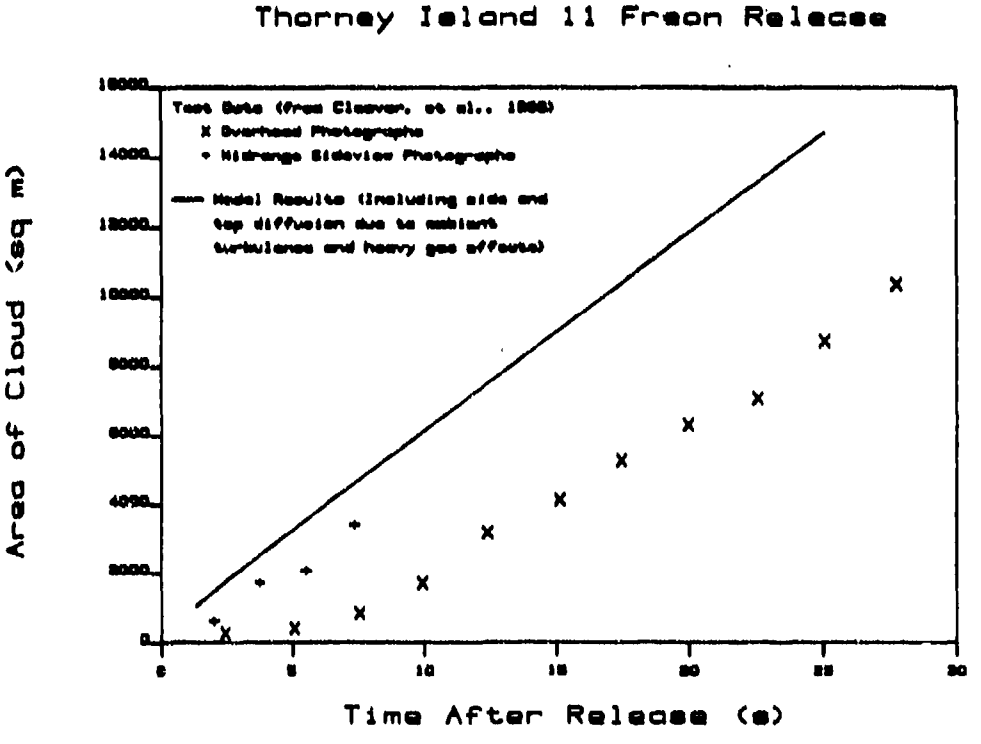

Figure 6.1.14c: Comparison of Model Predictions for Cloud Area with Test Data from Thorney Island 11 Freon Release

model predictions are possible. The model and data agree well, however.

Comparisons of photographically derived data for cloud location, height, and area in the initial collapse of the gas cloud and the model predictions for this period are shown in Figure 6.1.14a, 14b, and 14c. The downwind position and cloud height model predictions were good for this time period; as the figures show. The cloud area predictions are, again, offset from the data but they have the correct slope. For this trial, the cloud area data do not increase until after 5 seconds.

This release and TI13 are similar since they were both quickly dispersed and pushed out of the sensor field due to the high wind speed when the trials were run. In addition, the wind direction changed in trial 11 before release, so the cloud traveled to the side of the sensor field (Pfenning and Cornwell, 1985).

Thorney Island Trial 13 (TI13)

The comparison of the trial's gas sensor data with the model prediction is shown in Figure 6.1.15. In this figure, the transition from heavy gas dispersion to passive dispersion is shown - it occurs at the end of the available data, so no validation of far field model predictions are possible. Some differences between the model and the data may be caused by the wind speed increasing during the trial (Pfenning and Cornwell, 1985). The data and model predictions are in close agreement.

Comparisons of photographically derived data for cloud location, height, and area in the initial collapse of the gas cloud and the model predictions for this period are shown in Figure 6.1.16a, 16b, and 16c. The downwind position model predictions of the data are very good for this time period, as the figure shows. Cloud heights are slightly underpredicted by the model. The cloud area predictions have the correct slope, but are offset from the data. The data do not start increasing until after 5 seconds after release.

6.1.6.2 Thorney Island Continuous Releases

The initial conditions of the two (2) continuous release trials compared are listed in Table 6.1.1. The two trials are discussed in greater detail in the following sections. The transition from heavy gas dispersion to passive dispersion as predicted by the model occurs after the farthest position data reported making validation of far field model concentration predictions impossible.

Thorney Island Trial 45 (TI45)

The comparison of the trial's gas sensor data with the model prediction is shown in Figure 6.1.17. The concentration data were presented as the peak concentration (measured). The model results are time averaged values at ground level. This accounts for at least a part of the discrepancy between the model results and the data.

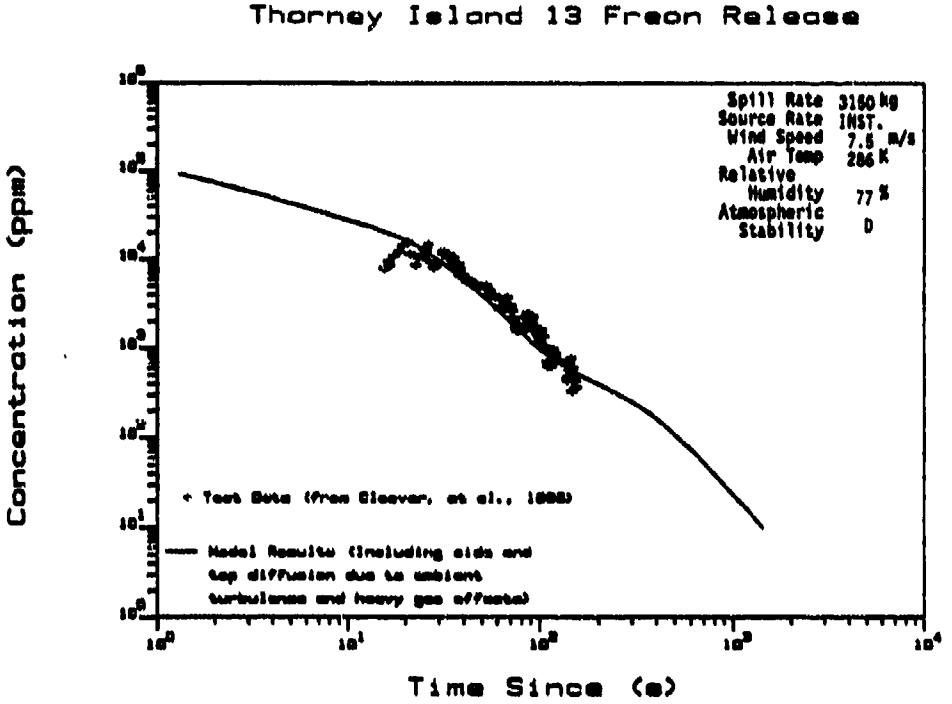

Figure 6.1.15: Comparison of Model Predictions for Downwind Centerline Concentration with Test Data from Thorney Island 13 Freon Release

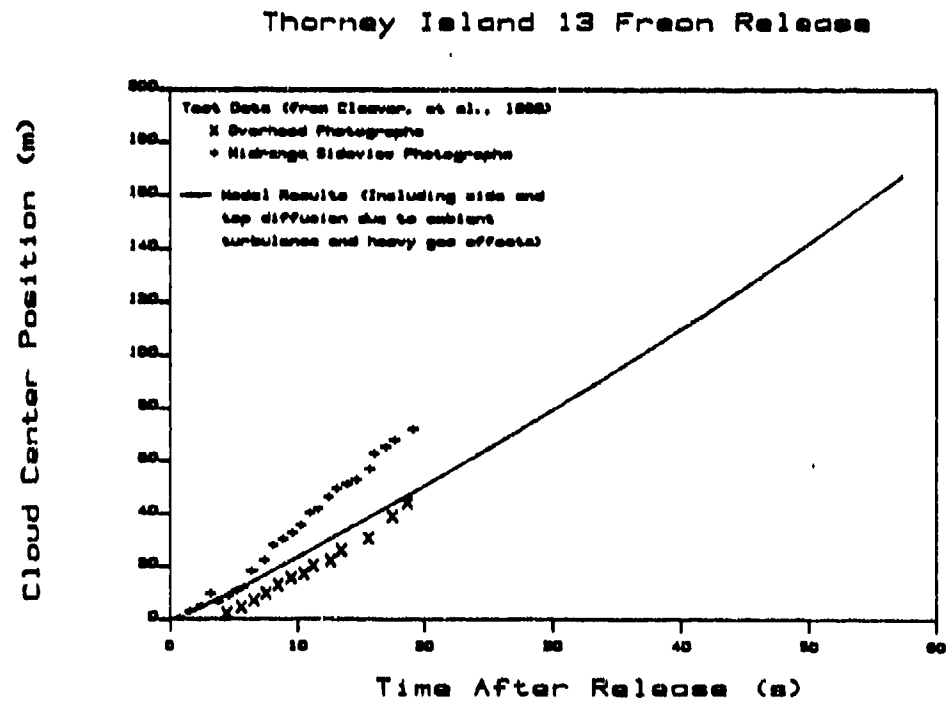

Figure 6.1.16a: Comparison of Model Predictions for Downwind Cloud Position with Test Data from Thorney Island 13 Freon Release

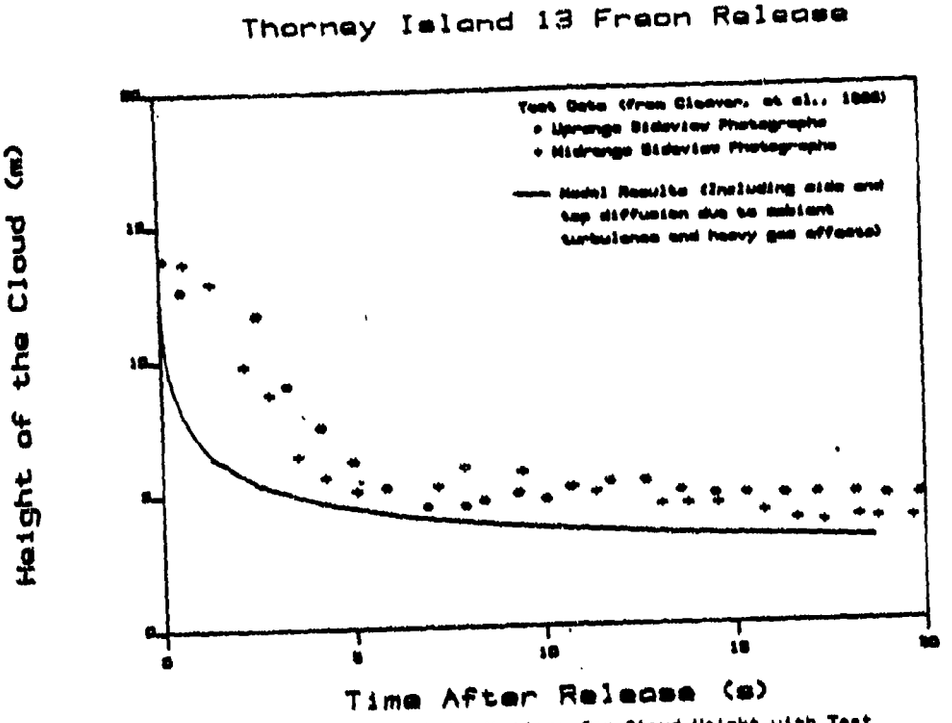

Figure 6.1.16b: Comparison of Model Predictions for Cloud Height with Test Data from Thorney Island 13 Freon Release

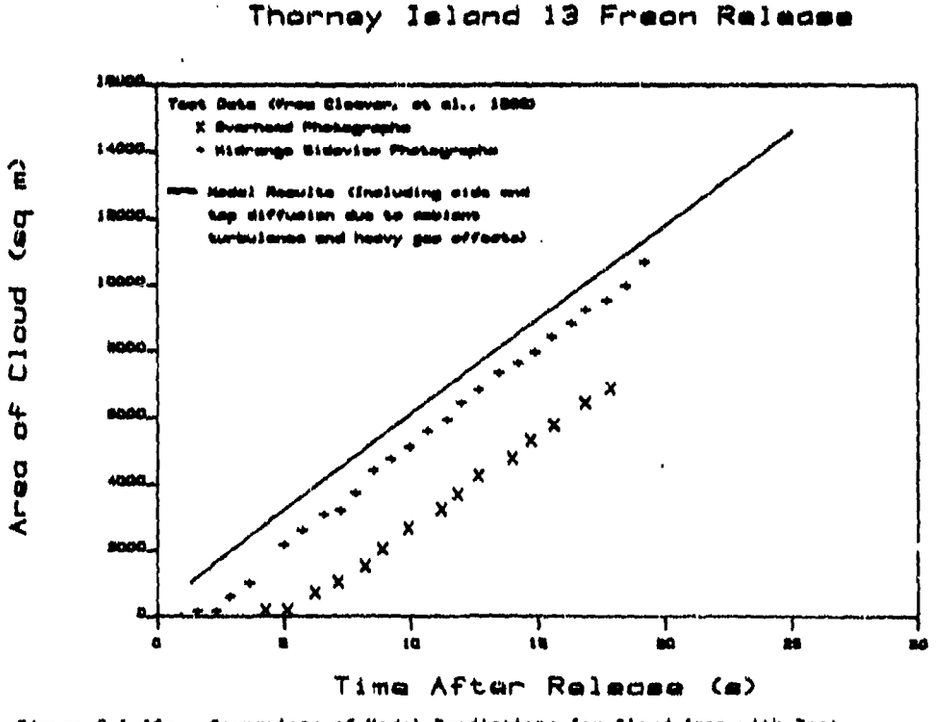

Figure 6.1.16c: Comparison of Model Predictions for Cloud Area with Test Data from Thorney Island 13 Freon Release

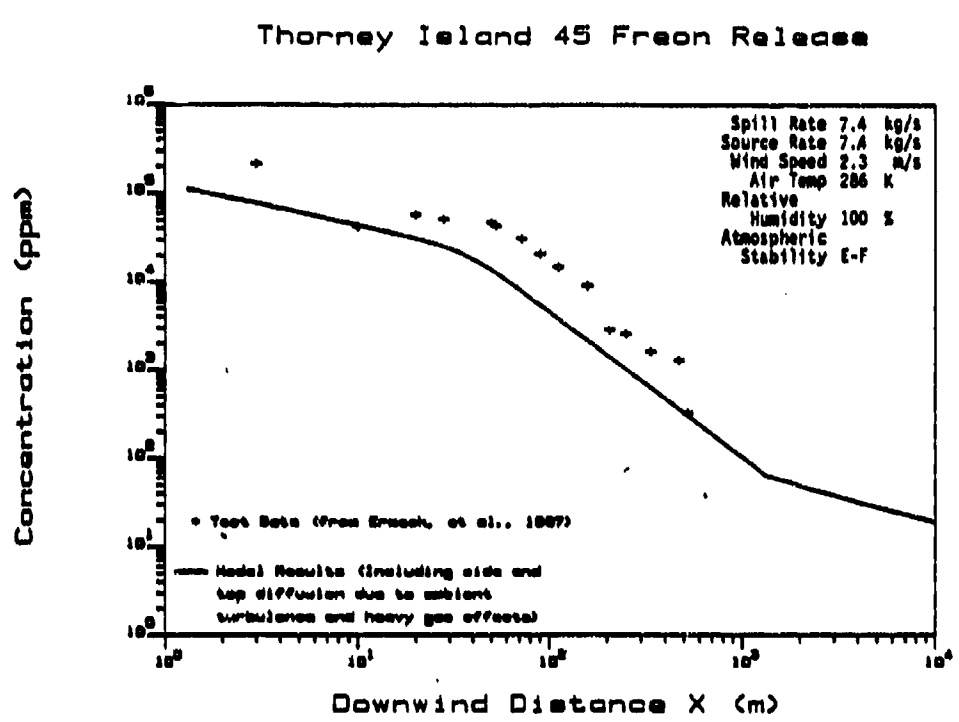

Figure 6.1.17: Comparison of Model Predictions for Downwind Centerline Concentration with Test Data from Thorney Island 45 Freon Release

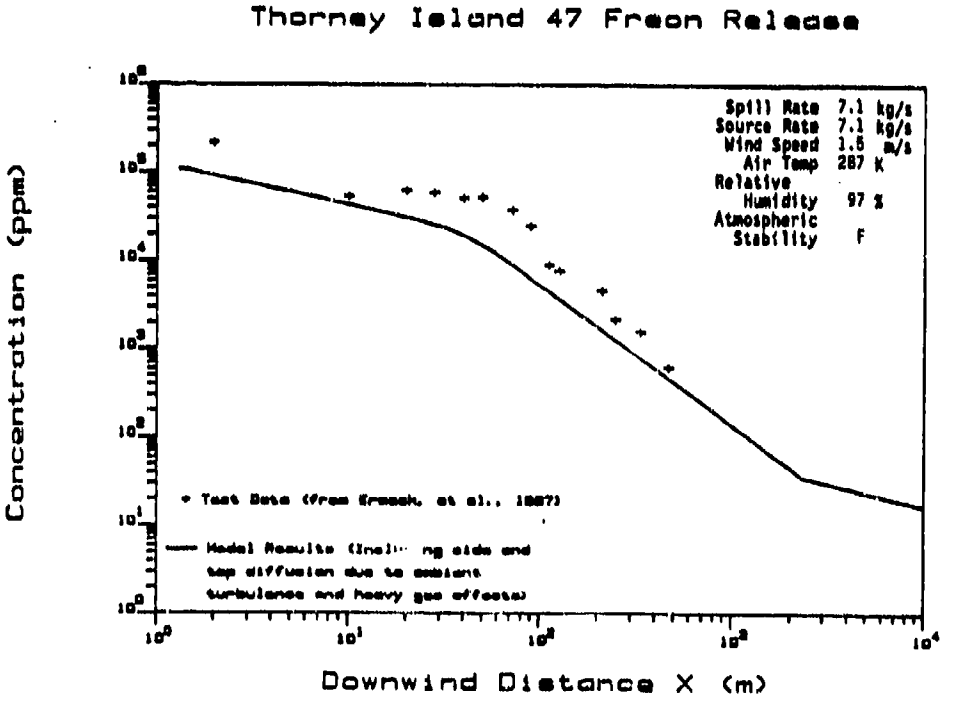

Figure 6.1.18: Comparison of Model Predictions for Downwind Centerline Concentration with Test Data from Thorney Island 47 Freon Release

Thorney Island Trial 47 (TI47)

The comparison of the trial's gas sensor data with the model prediction is shown in Figure 6.1.18. In this figure, the transition from heavy gas dispersion to passive dispersion is shown - it occurs at the end of the available data, thus no validation of far field model predictions are possible. Again, the concentration data is for peak concentration measured while the model predictions are for average centerline concentrations.

6.1.7 Conclusions from the Comparison of Field Test Data with Model Results

Model results have been compared to data from field tests for five different chemicals released under a wide variety of conditions. For all of the model results, the same entrainment coefficients, transition criteria, and other internal values were used. This was true for both instantaneous and continuous sources. The concentrations predicted agree, for the most part, within factors of two. Other data (jet velocity, size, area, height, etc.) are also predicted remarkably well. Hence, we conclude that the model developed is exceedingly good.

6.2 Sensitivity Analysis

The entrainment coefficients, drag coefficients, and transition criteria values used in the model were perturbed to test the sensitivity of the results to changes of these parameters. In addition, the user input parameters for atmospheric stability, aerodynamic roughness length, and concentration averaging time were perturbed to show the effects of changing user inputs. A listing of the entrainment coefficients, drag coefficients, and transition criteria parameters perturbed is given in Table 6.2.1. The equations (discussed in Chapter 5) in the model that these parameters are used in are given in the second column. The recommended values for each parameter are in the last column, based on the results of the sensitivity analysis. Each of the parameters that was perturbed is discussed in Sections 6.2.1 and 6.2.4 below. Data from the Thorney Island 13 freon release test were used for comparison in sensitivity analysis. The sensitivity analysis conclusions are in Section 6.2.5.

6.2.1 Entrainment Coefficient Perturbations

Froude Number (k) Perturbation

The Froude number (k), used in Equations 5.2.4 and 5.3.4, was varied from a value of 0.5 to 2.0. The results of this perturbation are shown in Figure 6.2.1. In all of the figures, the middle value of the parameter is the recommended value. The model results using the value for k obtained from the literature, k = 1.07 (the recommended value in Table 6.2.1), fit the data much better than the model results for the k values of 0.5 and 2.0. The effects of changing k are seen in the

TABLE 6.2.1 Entrainment Coefficient and Transition Criteria Value Sensitivity Analysis

Parameter	Equation Number	Possible Range of Values	Recommended Values
Transition Criteria			
Ri_{tr}	5.2.17a	1 - 10	1
$(\rho_s/\rho a-1)$	5.2.17b	10^{-4} - 10^{-3}	1 x 10^{-3}
Entrainment Coefficients			
α	5.2.11 5.3.6a	0.5 - 1.5	0.7
β_1	5.2.12	0.05 - 0.15	0.08
β_2	5.2.12	0.1 - 0.4	0.3
k	5.2.4 5.3.4	0.8 - 1.3	1.07
Drag Coefficients			
f	5.2.8	0 - 1	0.55
C_D	5.2.9	0 - 1	0.5

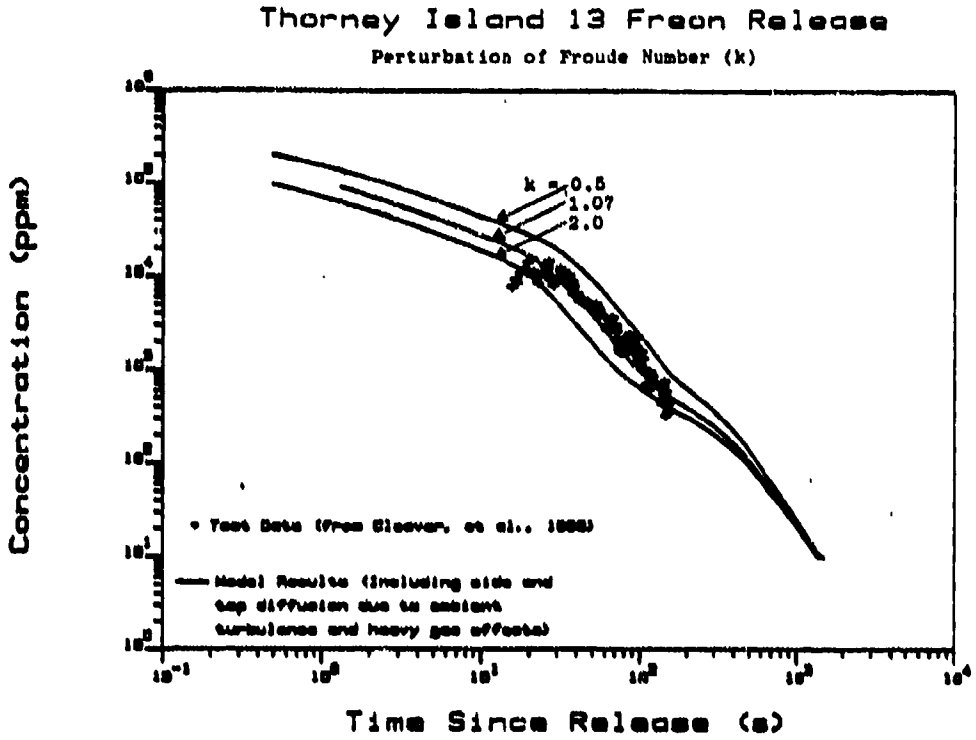

FIGURE 6.2.1: Comparison of Model Predictions for Downwind Centerline Concentration with Test Data from Thorney Island 13 Freon Release Using Several Values for the Froude Number (k)

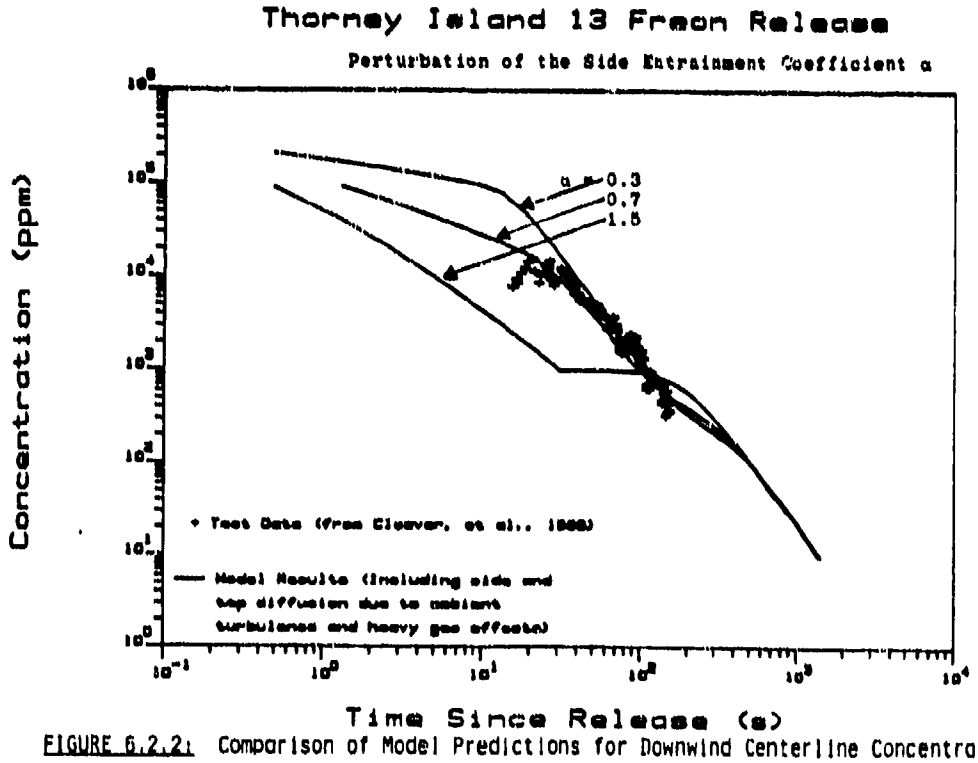

FIGURE 6.2.2: Comparison of Model Predictions for Downwind Centerline Concentration with Test Data from Thorney Island 13 Freon Release Using Several Values for the Side Entrainment Coefficient α

initial heavy gas region of the dispersion since the equation in which k is used describes the radial spread velocity of the heavy gas cloud. After transition to passive, Gaussian dispersion, the model predictions are nearly identical for all values of k chosen.

Edge Entrainment Coefficient (α) Perturbation

The edge entrainment coefficient, α, was varied from 0.3 to 1.5. The model results from this perturbation are shown in Figure 6.2.2. Changing this parameter has a great effect on the initial centerline concentration since it helps determine the mass of air entrained by the gravity spreading cloud during the heavy gas phase. The value obtained from the literature, $\alpha = 0.7$, gave results that best modeled the test data. The model results using the α value of 2.0 flatten out because this value gives a transition to passive dispersion after only 30 seconds when the cloud is approximately 80 meters downwind from the release point. The effects of passive dispersion are not significant until the cloud has traveled several hundred meters, which is where the concentration curve again slopes downward in the figure.

Top Entrainment Coefficients (β_1 and β_2) Perturbation

The top entrainment coefficients, β_1 and β_2, were independently varied from 0.004 to 0.15 and 0.1 to 0.6, respectively. The model results from these perturbations are shown in Figures 6.2.3 and 6.2.4. There is very little effect on the model results if changes are made to either of these parameters, although there are different reasons for the lack of effect. Changes in β_2 affect the model results only when the Richardson number (Ri) falls below 1. Since it is above 1 for this test, changing it has no effect on the dispersion (See Figure 6.2.4). The changes to β_1 have some effect on the model results, though not nearly as great as changes to α, or k. This is due to lesser importance of top entrainment than edge entrainment in the heavy gas phase of dispersion.

6.2.2 Transition Criteria (Ri) Perturbation

The transition from heavy gas dominated dispersion to Gaussian dispersion occurs in the model when the Richardson number (Ri) is of the order of 1. The model results obtained using Richardson number transition criteria values of 5, 1, and 0.5 are shown in Figure 6.2.5. The model results using the recommended value for Ri of 1 predict the test data the best.

6.2.3 Momentum Transfer Coefficient Perturbations

Edge Momentum Transfer Coefficient (f) Perturbation

The total horizontal momentum brought into the cloud due to side entrainment of air is assumed to be a fraction (f) of the mean horizontal momentum of the entrained air. The model results using values for f of 0.2, 0.55, and 1.5 are shown in Figure 6.2.6. Using the recommended value, f = 0.55, the model predicts the test data very well.

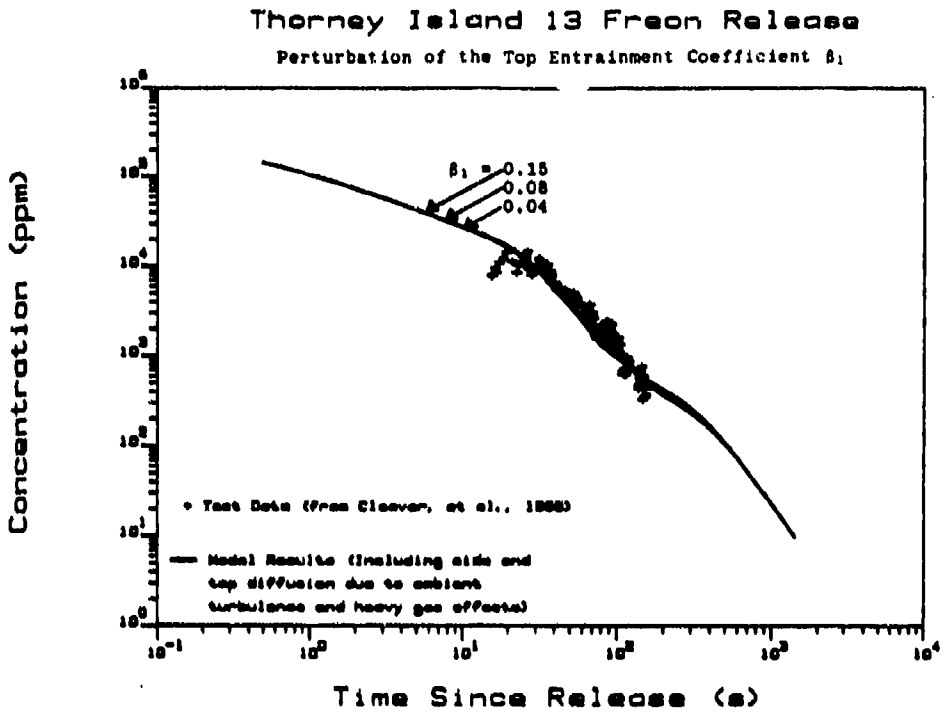

FIGURE 6.2.3: Comparison of Model Predictions for Downwind Centerline Concentration with Test Data from Thorney Island 13 Freon Release Using Several Values for the Top Entrainment Coefficient β_1

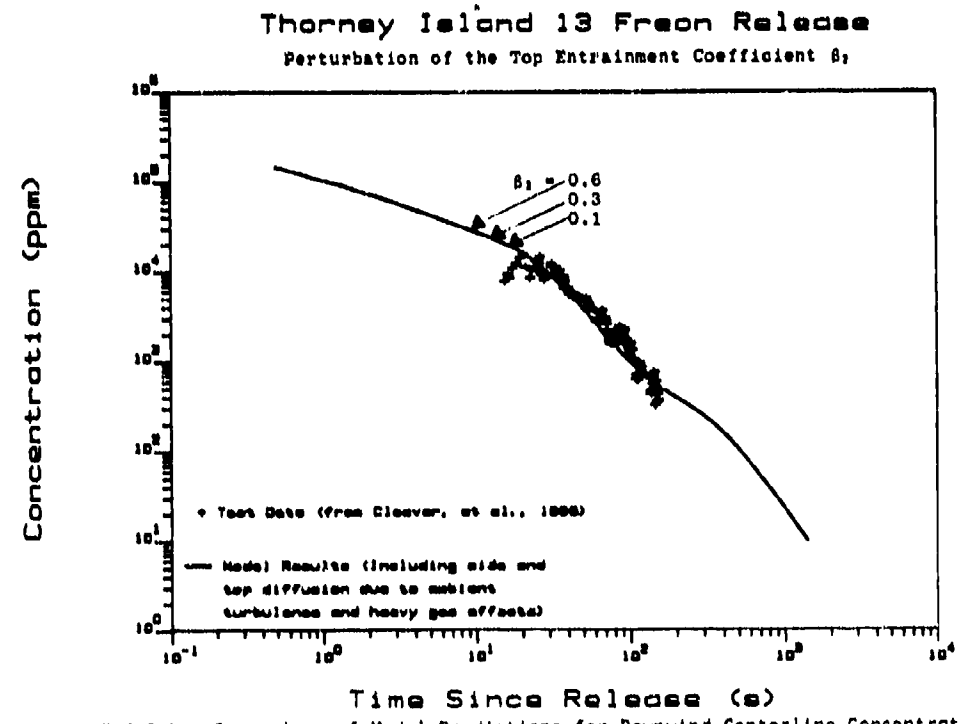

FIGURE 6.2.4: Comparison of Model Predictions for Downwind Centerline Concentration with Test Data from Thorney Island 13 Freon Release Using Several Values for the Top Entrainment Coefficient β_1

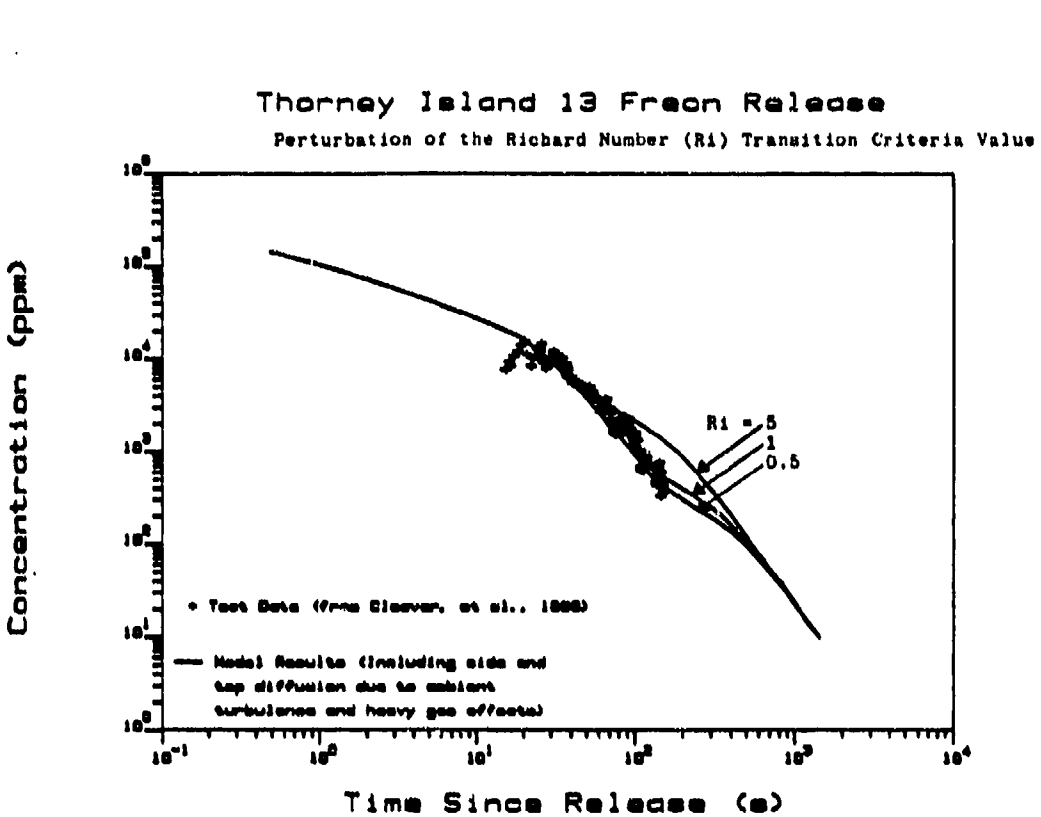

FIGURE 6.2.5: Comparison of Model Predictions for Downwind Centerline Concentration with Test Data from Thorney Island 13 Freon Release Using Several Values for the Richardson Number (Ri) Transition Criteria Value

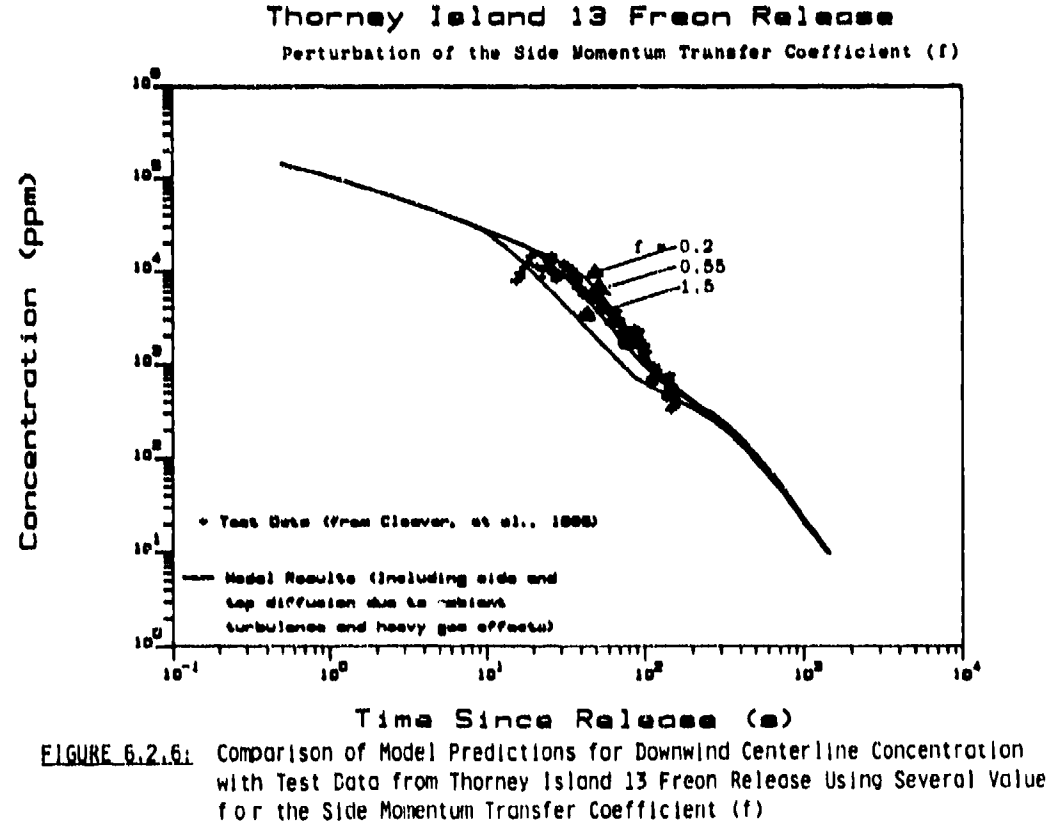

FIGURE 6.2.6: Comparison of Model Predictions for Downwind Centerline Concentration with Test Data from Thorney Island 13 Freon Release Using Several Values for the Side Momentum Transfer Coefficient (f)

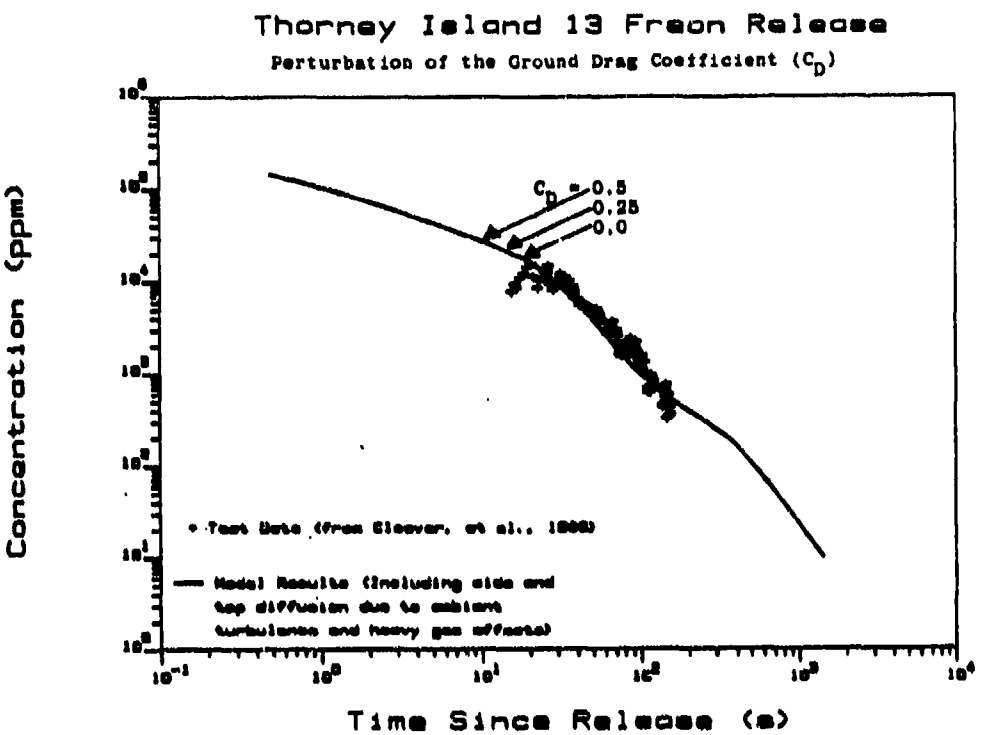

FIGURE 6.2.7: Comparison of Model Predictions for Downwind Centerline Concentration with Test Data from Thorney Island 13 Freon Release Using Several Values for the Ground Drag Coefficient (C_D)

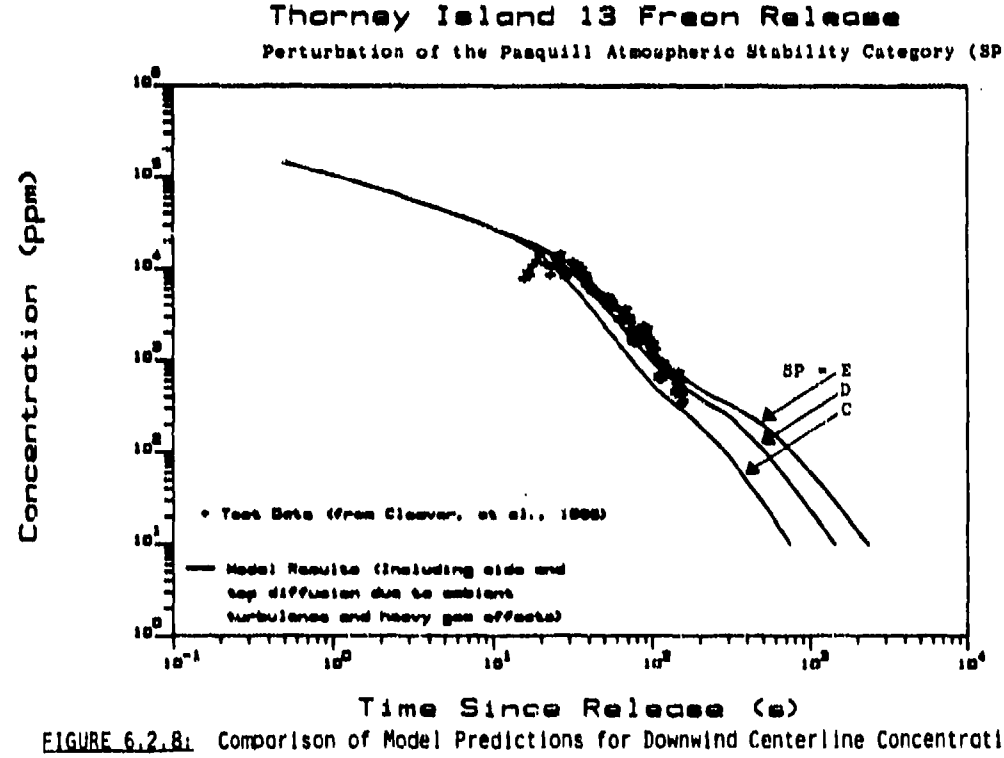

FIGURE 6.2.8: Comparison of Model Predictions for Downwind Centerline Concentration with Test Data from Thorney Island 13 Freon Release Using Several Values for the Pasquill Atmospheric Stability Category (SP)

Ground Drag (C_0) Coefficient Perturbation

The ground drag coefficient (C_0) was varied from 0 to 1.0. The model results using these values are shown in Figure 6.2.7. There is very little effect on the dispersion results, since the ground drag term in the momentum transfer equation is, in general, smaller than the air entrainment momentum transfer terms.

6.2.4 User Input Parameter Perturbations

Pasquill Atmospheric Stability Category (SP) Perturbation

The atmospheric stability class greatly affects the hazard area, as shown in Figure 6.2.8. The value recorded for the test, SP = D, yields model results that predict the test data very well. A slightly more stable atmosphere, SP = E, also yields model results that compare well with the data, however, a less stable atmosphere, SP = C, yields results that are not consistent with the data. As shown, the hazard distances for all concentrations decrease as the atmosphere becomes less stable. This is consistent with the fact that less stable atmospheres have greater mixing and thus dilute the cloud more quickly.

Aerodynamic Roughness Length (Z_0) Perturbation

The aerodynamic roughness length was varied from 0.1 cm to 10 cm; the model results for these values are shown in Figure 6.2.9. The results are consistent with the fact that a smaller Z_0 results in less mixing and thus a longer time until a given concentration is reached.

Concentration Averaging Time ($t_{a,v}$) Perturbation

The concentration averaging time, $t_{a,v}$, was varied from 6 sec. to 10 min. The results are shown in Figure 6.2.10. Again, the results are consistent with the fact that longer averaging times produce lower concentration measurements at a given time. This only affects the post transition dispersion, as shown, since the Gaussian model predictions are sensitive to averaging time.

6.2.5 Sensitivity Analysis Conclusions

The model coefficients which are internal to the program, and thus not user changeable, were perturbed to see the effects of such changes on the predicted centerline concentrations. The parameters and the range of their values tested are indicated in Table 6.2.1. The values tested for the parameters were over a wide range. It was found that downwind concentration predictions were quite sensitive to the value of the edge entrainment coefficient (α) in the heavy gas dispersion regime; however, variation in this coefficient value had no effect in the far field concentration values. The effect of variation in the transition Richardson number is significant only in a narrow region of the concentration-distance plot. The effect of variation in the values of other parameters (k, β_1, β_2, and C_0) on predictions of downwind

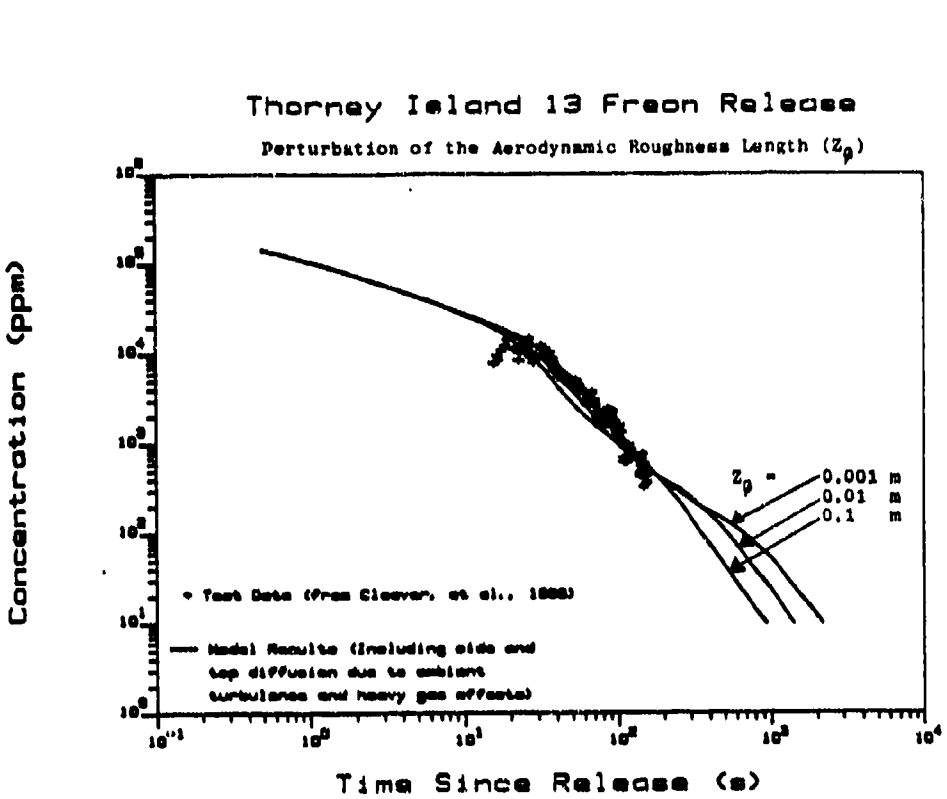

FIGURE 6.2.9: Comparison of Model Predictions for Downwind Centerline Concentration with Test Data from Thorney Island 13 Freon Release Using Several Values for the Aerodynamic Roughness Length (Z_0)

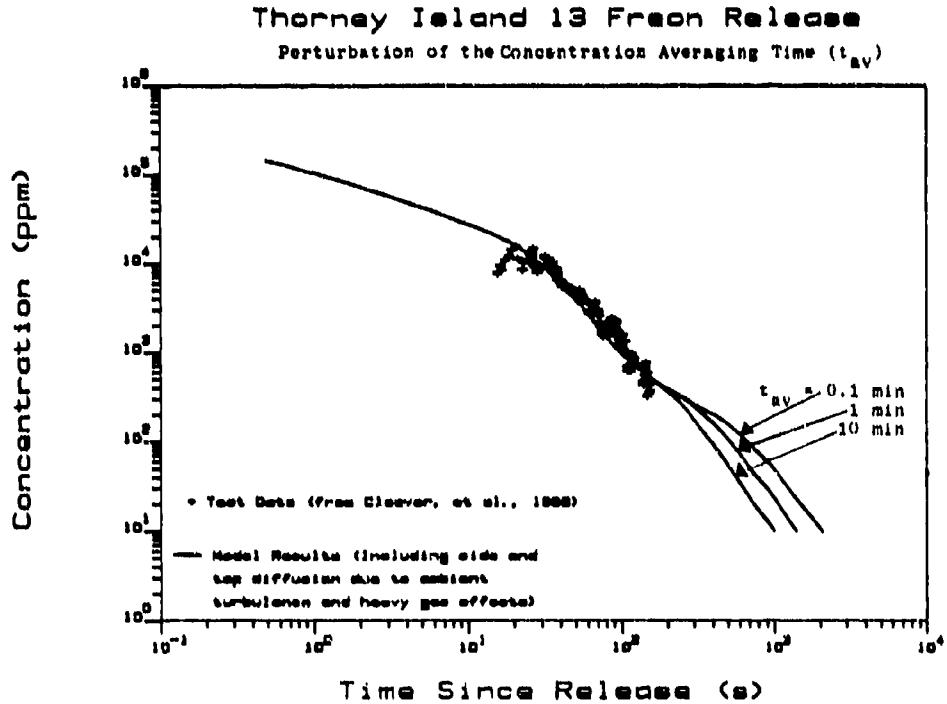

FIGURE 6.2.10: Comparison of Model Predictions for Downwind Centerline Concentration with Test Data from Thorney Island 13 Freon Release Using Several Values for the Concentration Averaging Time (t_{av})

concentration is quite small. The model is, therefore, relatively insensitive to the exact values chosen for these parameters. The recommended values for these coefficients (which give the best agreement with data from many tests) are indicated in Table 6.2.1. These values are used in our computer program.

Several user input parameters were also perturbed to show the effects of such changes on the dispersion predictions. These changes showed that the model results are very dependent on the user input values for the parameters studied.

CHAPTER 7

PROJECT ACHIEVEMENTS

A comprehensive toxic chemical vapor dispersion analysis system has been developed. This computerized system consists of several mathematical models for estimating the source strength, atmospheric parameters, chemical reactions and for describing the dispersion in the atmosphere. The system predicts the hazard area resulting from the release of heavier-than-air chemical vapors. To compile this dispersion analysis system, we have developed the following models:

1. A database of properties relevant to dispersion for the following six chemicals: nitrogen tetroxide, phosgene, ammonia, chlorine, hydrogen sulfide, and sulfur dioxide. The database was designed to i) allow additions, changes, and deletions of individual chemical properties, ii) allow additional chemicals to be added easily, and iii) provide thermodynamic and other properties quickly to programs needing the data.

2. Models to characterize various source types needed to provide source strength data for dispersion predictions. These include: single source, confined and unconfined source, instantaneous and continuous source, liquid and/or gas release, cryogenic or non-cryogenic liquid release sources, etc.

3. Thermodynamic models for describing the mixing of humid air and the chemical vapor and liquid aerosols resulting from the chemical release. The models predict thermodynamic conditions at equilibrium resulting from the mixing of a known mass of humid air with a specific mass of chemical vapor/aerosol cloud.

4. Dispersion models for predicting the hazard areas resulting from heavier-than-air toxic chemical vapor releases. The dispersion is controlled by heavy gas effects initially (if the density of the released vapor/aerosols is greater than that of the air) resulting in rapid lateral expansion and a low, ground hugging cloud. As additional air is entrained, the turbulent mixing of the atmosphere becomes the dominant dispersion force and the heavy gas effects become negligible. This is modeled by using a new, modified Gaussian technique whereby "tails" are added to the heavy gas "boxes". Once the dispersion is entirely atmosphere turbulence driven, a smooth transition from the modified Gaussian models to Gaussian models occurs.

In addition, we have:

1. Coded the models into computer programs that can be executed on microcomputers. The programs provide output in both graphical and tabular forms, and execution time is reasonable.

2. Compared model predictions with data from several field tests. The chemicals used in the field tests included nitrogen tetroxide, phosgene, ammonia, chlorine and freon. The agreement of the predictions and data is exceedingly good.

3. Performed a sensitivity analysis to determine the importance of various parameter values on the dispersion hazard area. The model results are relatively insensitive to changes in parameter values.

CHAPTER 2 NOMENCLATURE

a	Sonic velocity	(m/s)
A	Cross sectional flow area of orifice or plume	(m^2)
	Also pool area for evaporation	
C	Concentration of vapor in air	(kg/m^3)
C_D	Coefficient of discharge	
D	Diameter	(m)
	Also the diffusivity of gases & vapors	(m^2/s)
f	Mass fraction of vapor or liquid	
g	Acceleration due to gravity	(m/s^2)
h	Depth of liquid in the tank	(m)
	Also heat transfer coefficient	($W/m^2 K$)
h_m	Mass transfer coefficient	(m/s)
H	Plume depth	(m)
k	Ratio of specific heats of vapor	
	Also the coefficient in gravity spread equation	
l_p	Characteristic pool length	(m)
$\dot{m}$	Mass flow rate of liquid or vapor	(kg/s)
M	Mass of chemical	(kg)
M_w	Molecular weight of the chemical	(kg/kmole)
NU	Nusselt number	
P	Pressure	(N/m^2)
Pr	Prandtl number	
q	Heat flux from various sources	(W/m^2)
r	Ratio of ambient pressure to the storage pressure	
R	Radius of a pool or orifice	(m)
	Also the individual gas constant	(J/kg K)
R_U	Universal gas constant	(J/kmol K)
Re	Reynolds number	
Sc	Schmidt number	
t	Time	(s)
T	Temperature	(K)
U	Velocity of liquid or vapor plume	(m/s)
V	Volume of tank or vapor cloud	(m^3)
W	Width of plume	(m)
x	Down wind distance	(m)
y	Cross wind distance	(m)
Y	Expansion factor (see equations 2.3.16 & 17)	
z	Vertical distance	(m)

SUPERSCRIPTS

Sat	Saturation condition of the chemical
'	Denotes non dimensional parameter
.	Denotes "per unit time"

SUBSCRIPTS

a	Refers to the condition of atmospheric air
c	Refers to the value of the parameter at plume center Also convective heat transfer condition Also critical condition
ch	Refers to the characteristic parameter
e	Exit condition (a few diameters down wind of orifice)
G	Refers to the ground conditions
H	Refers to the hole characteristics
i	Initial value of the plume parameter
m	Mass transfer related
o	Initial condition
P	Liquid pool condition
REL	Release condition (of the chemical outside the tank after release
s	Source condition
sat	Saturation condition of the chemical
spill	Spill condition (after release from tank)
tr	Translational
T	Conditions inside the storage tank
Th	Condition at the throat of a nozzle or orifice
v	Vapor condition
wind	Wind value
x	Value of parameter in the x coordinate direction
y	Value of parameter in the y coordinate direction
z	Value of parameter in the z coordinate direction
∞	At a distance far from the liquid pool surface

GREEK LETTERS AND OTHER SYMBOLS

ℓ	Liquid condition	
α	Thermal conductivity	(m^2/s)
Δ'	Fractional density deviation = $(\rho/\rho_a - 1)$	
ϵ	Emissivity of pool or atmosphere	
λ	Heat of vaporization of liquid	(J/kg)
ν	Kinematic viscosity of air or vapor	(m^2/s)
ρ	Density	(kg/m^3)
σ	Stefan-Boltzmann Constant	$(W/m^2 K^4)$
τ	Dimensionless time Also the shear stress between wind and plume and ground and plume.	

CHAPTER 3 NOMENCLATURE

AH	Absolute Humidity (kg H_2O/kg dry air)
aq	Aqueous phase
C	Concentration (gmoles/ℓ)
C	Total dissolved SO_2 (gSO_2/kg H_2O)
C°	Initial concentration (gmoles/ℓ)
[C]	Total concentration in the aqueous phase (gmoles/ℓ)
C_{COCl2}	Concentration of phosgene in aqueous solution (gmoles/ℓ)
CH	Three letter HACS Chemical Code (Chlorine = 'CLX')
C_I	Concentration of ionized SO_2 (gSO_2/kg H_2O)
$[Cl_2,aq]$	Concentration of dissolved chlorine gas in aqueous phase (gmoles/ℓ)
CLIQ	A vector of mass fractions of each species in the liquid phase
CLUDCC	Cloud Concentration Computer Program
Co	Initial concentration (gmoles/ℓ)
$C_p°$	Pure component heat capacity (J/gmole K)
$C_{p,AIR}$	Mass specific heat of air (J/kg-K)
$C_{p,NO2}$	Mass specific heat of NO_2 (J/kg-k)
$C_{p,W}$	Mass specific heat of water (J/kg-K)
CSOL	A vector of mass fractions of each species in the solid phase
C_U	Concentration of unionized SO_2 (gSO_2/kg H_2O)
CVAP	A vector of mass fractions of each species in the vapor phase
f	Mass fraction of liquid aerosol in the initial mixture of pure vapor and liquid of the chemical before mixing with air
FLI	The mass fraction of liquid aerosol in the released chemical vapor/aerosol cloud
G	Gas
g	Gas phase
H	Henry's law constant
H_{AF}	Enthalpy of dry air in the final mixture (J/kg)
$H_{CH\ell F}$	Enthalpy of the liquid chemical in the final mixture (J/kg)
H_{CHVF}	Enthalpy of the chemical vapor in the final mixture (J/kg)
H_I	Initial enthalpy of a chemical and air mixture (J)
H_F	Final enthalpy of a chemical and air mixture (J)
$H_{W\ell F}$	Enthalpy of liquid water in the final mixture (J/kg)
H_{WSF}	Enthalpy of solid water in the final mixture (J/kg)
H_{WVF}	Enthalpy of water vapor in the final mixture (J/kg)
H(T)	Specific enthalpy at temperature T (J/kg)
K	Equilibrium constant (gmoles/ℓ)^2
k	Equilibrium constant (ℓ/atm s)
K_A	Equilibrium constant (1/atm)
K_B	Equilibrium constant (1/atm)
k_L	Equilibrium constant for phosgene (1/s)
L_A	Aqueous phase
M	Molecular weight of air (g/gmole)
M_A	Mass of dry air (kg)
M_{CH}	Total mass of chemical vapor and aerosol present (kg)
$M_{CH\ell F}$	Mass of chemical liquid in the final mixture (kg)
M_{CHVF}	Mass of chemical vapor in the final mixture (kg)
M_W	Mass of water in wet air (kg)
MW_A	Molecular weight of air (kg/kgmole)

CHAPTER 3 NOMENCLATURE (Continued)

MW_{CH}	Molecular weight of chemical (kg/kgmole)
$M_{W\ell F}$	Mass of water liquid in the final mixture (kg)
M_{WSF}	Mass of water ice in the final mixture (kg)
M_{WVF}	Mass of water vapor in the final mixture (kg)
MW_W	Molecular weight of water (kg/kgmole)
NSPECS	Number of chemical species present after reaction
N_{TOT}	Total number of moles in the vapor (kgmoles)
p	Partial pressure (Pa)
P	Partial pressure (Pa)
P_a	Atmospheric pressure (101325 Pascals)
Phi	The mass fraction of the liquid left after the flash which is entrained into the vapor cloud
P_{vp}	Vapor pressure (N/m^2)
$P_{vp,CH}$	Vapor pressure of chemical at a given temperature (Pa)
$P_{vp,W}$	Vapor pressure of water at a given temperature (Pa)
Q	Heat input to (+) or extraction (-) the chemical air mixture (kg)
RH	Relative Humdity (%)
RH_i	Initial relative humidity of the air (%)
RH_f	Relative humidity of the equilibrium mixture (%)
RHOMIX	Density of the final mixture after reaction (kg/m^3)
SPLIST	A vector list of species names
s	Solid phase
S_A	Water ice solid of hydrogen sulfide-water system
S_S	Hexahydrate solid of hydrogen sulfide-water system
T	Temperature (K)
t	Time (s)
T_{AIR}	Air Temperature (K)
T_{CH}	Chemical temperature (K)
T_{MIX}	Final mixture (equlilibrium) temperature (K)
T_{NH3}	Temperature of NH_3 (K)
T_{NO2}	Temperature of NO_2 (K)
T_{SAT}	Saturation temperature (K)
X_i	Mole fraction of equilibrium component i
X_{NO}	Moles of NO at equilibrium
X_{N2O4}	Moles of N_2O_4 at equilibrium
Y_{AIR}°	Initial number of moles of air
Y_{H2O}°	Initial number of moles of H_2O
Y_{NO2}°	Initial number of moles of NO_2
Y_{N2O4}°	Initial number of moles of N_2O_4
Y_{TOTAL}°	Initial number of total moles of components
Y_{wi}	Mole fraction of water in the vapor initially
Y_{wf}	Mole fraction of water in the vapor at equilibrium
[]	Concentration (gmoles/ℓ)
[]	$Y_{TOTAL}^\circ - X_{NO} - X_{N2O4}$
ℓ	Liter
ℓ	Liquid
γ	Mean ionic activity coefficient for hydrogen bisulfate ions
ΔH_r	Heat of reaction (J/kg)
$\Delta H_{r,1}$	Heat of reaction for 3.6.4 (J/kg N_2O_4)
$\Delta H_{r,2}$	Heat of reaction for 3.6.5 (J/kg NO)
ρ_{AIR}	Air density (kg/m3)

CHAPTER 4 NOMENCLATURE

a	Angular fraction of the year
a_1	Turbidity coefficient (W/m^2)
a_2	Turbidity coefficient (W/m^2)
b_2	Empirical solar radiation exponent constant
C_p	Air specific heat (J/kg-K)
C_1	First solar radiation constant (W/m^2-K^6)
C_2	Second solar radiation constant (W/m^2)
C_3	Third solar radiation constant
D	Solar declination (deg)
g	Gravity (m/s^2)
G	Soil heat flux (W/m^2)
GMT	Greenwich mean time (24 hr decimal clock)
H	Sensible heat flux (W/m^2)
JU	Julian date
k	Von Karman constant
K	Net incoming solar radiation at ground level (W/m^2)
K_0	Incoming solar radiation at ground level (W/m^2)
L	Monin-Obukov length (m)
LA	Latitude (deg)
LO	Longitude (deg)
M	Time of meridian passing (24 hr decimal clock)
N	Fraction of the sky covered by clouds
Q	Net solar radiation (W/m^2)
q_s	Saturation specific humidity
r	Earth's albedo
s	Change in saturation specific humidity per change in air temp
SHA	Solar hour angle (deg)
SP	Pasquill stability category (continuous scale, 0.5 to 6)
t	Concentration averaging time (s)
T	Transmittance of the cloud cover
T_a	Air temperature (K)
U_z	Wind velocity at height Z (m/s)
U_{10}	Wind velocity at 10 meters height (m/s)
u*	Wind friction velocity (m/s)
Z	Anemometer height (m)
Z_0	Aerodynamic roughness length (m)
α	Anemometer height to aerodynamic roughness length ratio Also Sensible heat flux empirical constant for wet/dry conditions
β	Sensible heat flux empirical constant (W/m^2)
γ/s	Ratio of air specific heat/latent heat of water vaporization
ρ_a	Air density (kg/m^3)
σ	Angular fraction of the year Also Stefan-Boltzmann constant (W/m^2-K^4)
σ_y	Horizontal standard deviation of a Gaussian distribution (m)
σ_z	Vertical standard deviation of a Gaussian distribution (m)
σ_θ	Standard deviation of the wind direction (deg)
ϕ	Solar elevation angle (deg)

CHAPTER 5 NOMENCLATURE

B_Y	Plume horizontal dispersion factor
B_Z	Plume vertical dispersion factor
C_D	Cloud drag coefficient
C_i	Initial box cloud concentration (kg/m_3)
C_{max}	Maximum concentration within the plume at X (kg/m^3)
C_T	Chemical concentration of cloud at transition (kg/m_3)
C_X	Chemical concentration of cloud at position X (kg/m_3)
D	Frontal drag force on the cloud ($kg\ m/s^2$)
f	Fraction of mean horizontal momentum of entrained air
F	Ground friction force on cloud ($kg\ m/s^2$)
g	Gravity (m/s^2)
h	Heat transfer coefficient for ground to plume ($J/K\ m^2$)
H	Box cloud height (m)
H_i	Initial box cloud height (m)
H_l	Height of plume source (m)
H_r	Turbulence length scale reference (m)
H_T	Height dimension of cloud at transition (m)
H_X	Height dimension of cloud at position X (m)
k	Froude number
L	Ambient air turbulent eddy size (m)
M	Mass in the cloud (kg)
M_a	Mass of air in the cloud (kg)
M_a'	Mass rate of entrainment of air per unit distance (kg/m s)
$M_{a,E}$	Edge air entrainment rate for plume (kg/m s)
$M_{a,I}$	Mass flow rate of air at the source for the plume (kg/s)
$M_{a,T}$	Top air entrainment rate for plume (kg/m s)
M_c	Mass of chemical in the cloud (kg)
M_{ch}	Initial mass flow rate of chemical in the plume (kg/s)
M_I	Initial mass flow rate in plume (kg/s)
M_E	Air entrainment rate at the cloud edge (kg/s)
M_T	Air entrainment rate at the cloud top (kg/s)
Q_G	Heat flux from ground per unit distance (J/m)
r	Radial position in cloud (m)
R	Box cloud radius (m)
R_i	Initial box cloud radius (m)
Ri	Richardson number
r_p	Radial coordinate position of a point relative to a cylindrical coordinate system at X (m)
R(t)	Box cloud radius as a function of time (m)
SP	Numeric Pasquill stability category
T	Plume temperature (K)
T_G	Ground Temperature (K)
U	Cloud translation velocity (m/s)
u_E	Edge entrainment velocity (m/s)
U_f	Radial spread velocity (m/s)
u_H	Mean wind velocity over height H (m/s)
u_H	Wind velocity at height H (m/s)
u_l	Logitudinal RMS turbulent velocity of the air (m/s)
u_T	Top entrainment velocity (m/s)
U_{tr}	Translation velocity of plume at any X (m/s)
$U_{tr,i}$	Initial translation velocity of plume (m/s)

CHAPTER 5 NOMENCLATURE (Continued)

$u(z)$	Wind velocity at height z (m/s)
u^*	Wind friction velocity (m/s)
V	Volume of the box cloud (m^3)
V_1	Source volume flow rate of the plume (m^3/s)
V_I	Initial box cloud volume (m^3)
W_I	Width of plume source (m)
W_T	Radial dimension of cloud at transition (m)
W_X	Radial dimension of cloud at position X (m)
X	Cloud position relative to intial position (m)
z	Vertical position in cloud (m)
z_p	Vertical coordinate position of a point relative to a cylindrical coordinate system at X (m)
α	Edge mixing coefficient
β_1	First top mixing coefficient
β_2	Second top mixing coefficient
Δ	Fractional density deviation (ρ_c/ρ_a -1)
θ	Angle from source cloud to position (X, r_p, z_p)
ρ_a	Air density (kg/m^3)
ρ_c	Cloud density (kg/m^3)
ρ_I	Initial density of plume (kg/m^3)
σ_y	Horizontal standard deviation of a Gaussian distribution (m)
σ_z	Vertical standard deviation of a Gaussian distribution (m)

CHAPTER 6 NOMENCLATURE

C_D	Cloud drag coefficient
f	Fraction of mean horizontal momentum of entrained air
k	Froude number
Ri	Richardson number
Ri_{tr}	Transition Richardson number
RH	Relative humidity (%)
T_{AIR}	Air temperature (K)
α	Edge mixing coefficient
β_1	First top mixing coefficient
β_2	Second top mixing coefficient
ρ_a	Air density (kg/m^3)
ρ_c	Cloud density (kg/m^3)

APPENDIX B NOMENCLATURE

B_y	Plume horizontal dispersion factor
B_z	Plume vertical dispersion factor
B_z^{max}	Plume vertical dispersion factor
C_{max}	Maximum concentration within the plume at X (kg/m^3)
dM_s	Vapor mass flux through the plume elemental vapor source (kg/s)
f_1	Function used to replace the Bessel function
f_2	Function used to replace the Bessel function
H_T	Height dimension of cloud or plume window at transition (m)
I_0	Modified Bessel function of the first kind and zeroth order
P	Point at which the effects of the volume source are measured
Q	Point at which the infinitesimal volume source is located
q_e	Dimensionless radial position of the elemental source (m)
r	Radial coordinate of a point (m)
r_p	Dimensionless radial coordinate position of an observation point relative to a cylindrical coordinate system (m)
r_s	Radial coordinate of the infinitesimal source volume (m)
R_T	Radial dimension of cloud at transition (m)
S_y	Dimensionless Y direction dispersion coefficient
S_z	Dimensionless Z direction dispersion coefficient
t	Time (s)
U	Wind velocity (m/s)
U_T	Cloud translation velocity (m/s)
W_T	Width of plume at transition (m)
x	Downwind coordinate of point (m)
x_c	Downwind coordinate of cloud center (m)
x_p	Downwind coordinate of plume observation point (m)
x_s	Downwind coordinate of infinitesimal volume source (m)
X_T	Cloud or plume window position relative to initial source position (m)
y	Horizontal coordinate of point (m)
y_c	Horizontal coordinate of cloud center (m)
y_p	Horizontal coordinate of plume observation point (m)
y_s	Horizontal coordinate of infinitesimal volume source (m)
z	Vertical coordinate of point (m)
z_c	Vertical coordinate of cloud center (m)
z_p	Vertical coordinate of plume observation point (m)
z_s	Vertical coordinate of infinitesimal volume source (m)
ζ	Dimensionless vertical coordinate position of the point at which the concentration is to be calculated
ζ_s	Dimensionless Z coordinate of elemental source
η	Dimensionless Y coordinate of observation point
η_s	Dimensionless Y coordinate of elemental source
θ	Angle between the r vector and the downwind axis X (deg)
σ_x	Downwind standard deviation of a Gaussian distribution (m)
σ_y	Horizontal standard deviation of a Gaussian distribution (m)
σ_z	Vertical standard deviation of a Gaussian distribution (m)
ϕ	Angle between the r_s vector and the downwind axis X (deg)

CHAPTER 1 REFERENCES

AIChE; Proceedings of the International Conference on Vapor Cloud Modeling, Cambridge, MA, November 1987.

Blewitt, D.N., J.F. Yohn, R.P. Koopman, and T.C. Brown, "Conduct of Anhydrous Hydrofluoric Acid Spill Experiments", International Conference on Vapor Cloud Modeling, Proceedings, Cambridge, MA, November 1987.

Ermak, D.L., R. Chapman, H.C. Goldwire, F.J. Gouveia, H.C. Rodean, "Heavy Gas Dispersion Test Summary Report", Air Force Engineering and Services Laboratory, Draft Summary Report, 1987.

Haas, W., E. Simon and J. McDonald, "Propellant Spill Source Strength", Final Engineering Report, Martin Marietta Aerospace, Denver, to Hill AFB Contract # F42600-80-D-0974, Nov. 1981.

JHM: Journal of Hazardous Materials, V. II, 1985. Special issue on "Heavy Gas Dispersion Trials at Thorney Island, Proceedings of a Symposium held at the University of Sheffield, Great Britain, 3-5, April 1985".

Kahler, Jon P., Lt. Col. R.G. Curry and Maj. R.A. Kandler, "Calculating Toxic Corridors", Air Weather Service (MAC), Scott AFB, IL 62225, Nov. 1980.

Kaiser, G.D. and B.C. Walker, "Releases of Anhydrous Ammonia from Pressurized Containers - The Importance of Denser-than-Air Mixtures", Atm. Env., V. 12, 1978.

Kansa, E.J., D.L. Ermak, S.T. Chan and H.C. Rodean, "Atmospheric Dispersion of Ammonia: An Ammonia Fog Model", LLNL Report #UCRL-88649, Jan. 1983.

Koopman, R.P., T.G. McRae, H.C. Goldwire, Jr., D.L. Ermak, and E.J. Kansa, "Results of Recent Large Scale NH_3 and N_2O_4 Dispersion Experiments", LLNL Report # UCRL-91830, Nov. 1984.

Kunkel, B.A., "A Comparison of Evaporative Source Strength Models for Toxic Chemical Spills", Report # AFGL-TR-83-0307, AFGL, Hanscom AFB, ADA139431, Nov. 1983.

Raj, P.K., "Heavy Gas Dispersions; A State-of-the-Art Review of the Experimental Results and Models", Heavy Gas Dispersal Lecture Series, von Karmann Institute, Brussels, Belgium, May 1982.

Raj, P.K., "Atmospheric Dispersion of Chemical Agents: A Model Including Thermodynamic and Heavy Gas Effects", Report to Chemical Systems Laboratory, U.S. Army Aberdeen Proving Grounds, 1983.

Raj, P.K., "Models for Cryogenic Liquid Spill Behavior on Land and Water", J. Haz. Mat., V.5, p.111-130, 1981.

CHAPTER 1 REFERENCES (Continued)

Raj, P.K., "On the Near Field Dispersion of Heavy Vapor/Aerosol Plume Generated by the Release of Pressurized Liquid Ammonia", Report to U.S. Naval Weapons Center, China Lake, CA, 1980.

Raj, P.K., "Summary of Heavy Gas Spills Modeling Research", Proc. Heavy Gas (LNG/LPG) Workshop, Toronto, Ontario, Jan. 1985.

HSE: Proceedings of the Second Symposium on Heavy Gas Dispersion Trials at Thorney Island, held at University of Sheffield, Great Britain, organized by the Health & Safety Executive, 23-25 September, 1986.

Webber, D.M., "The Physics of Heavy Gas Cloud Dispersal", UKAEA Report, SRD-R243, Sheffield, England, 1983.

Wheatley, C.J., B. Crabol, R.J. Carpenter, S.F. Jagger, C. Nussey, R.P. Cleaver, R.D. Fitzpatrick, and A.J. Prince, "Comparison and Test of Models for Atmospheric Dispersion of Continuous Releases of Chlorine", SRD Report R438, 1987.

CHAPTER 2 REFERENCES

Fay, J.A., "The Spread of Oil SLicks on a Calm Sea", in Oil on the Sea, (D.P. Hoult, Ed.), p.53, Plenum Press, NY, 1969.

Ille, G. and C. Springer, The Evaporation and Dispersion of Hydrazine Propellants From Ground Spills, CEEDO-TR-78-30, AD A059407, 1978.

Kunkel, B.A., "A Comparison of Evaporative Source Strength Models for Toxic Chemical Spills", Report # AFGL-TR-83-0307, AFGL, Hanscom AFB, ADA139431, Nov. 1983.

Liepmann, H.W. and A. Roshko, Elements of Gasdynamics, J. Wiley & Sons, Inc., Eighth Printing, NY, May 1967.

Perry, R.H. and C.H. Chilton, "Chemical Engineer's Handbook", McGraw-Hill Book Co., 5th Edition, NY, 1973.

Raj, P.K., "Models for Cryogenic Liquid Spill Behavior on Land and Water", J. Haz. Mat., V.5, p.111-130, 1981.

Reid, R.C. and P.K. Raj, "Evaluation of LNG Vapor Control Methods", Report to the American Gas Association, Arlington, VA, 1974.

TRC, Inc., "Evaluation and Assessment of Models for Emergency Response Planning", Report to CMA, 1986.

CHAPTER 3 REFERENCES

API: "Manual on Disposal of Refinery Wastes; Volume on Atmospheric Emissions", API Publication 931, American Petroleum Institute, Washington, DC, 1977.

Böhme, H., "The Influence of Oxygen and Sulfur Atoms in the α-Position on the Hydrolysis Velocity of the Carbon-Halogen Bond", Ber. 74B, 248 (1941).

Burgess, M.P., and R.P. Germann, "Physical Properties of Hydrogen Sulfide-Water Mixtures", AIChE J. 15, 272 (1969).

Cathala, J. and G. Weinreich, Compt. Rend. 244, 1502 (1952).

Christini, J.N., M.S. Thesis, Univ. of Delaware, 1965.

Cline, J.E. and G.S. Forbes, J. Am. Chem. Soc. 60, 1699 (1938).

Eigen, M., and K. Kustin, J. Am. Chem. Soc. 84, 1355 (1962).

England, C. and W.H. Corcoran, Ind. Eng. Chem. Fundam. 13, 373 (1974).

Gaisinovich, M.S. and A.N. Ketov, "High-Temperature Hydrolysis of Carbon Tetrachloride and Phosgene in the Gaseous Phase", Russ. J. Phys. Chem. 14, 1218 (1969).

Goyer, G.G., J. Colloid. Sci. 18, 616 (1963).

Haddock, S.R. and R.J. Williams, "The Density of an Ammonia Cloud in the Early Stages of Its Atmospheric Dispersion", United Kingdom Atomic Energy Authority Report SRD R103, 1978.

Harris, G.E., B.S. Thesis, Univ. of Delaware, 1951.

Hercules Chemical Co., "Nitrogen Tetroxide", 1968.

Horvath, A.L., Physical Properties of Inorganic Compounds, Edward Arnold, London, 1975.

Kaiser, G.D., and B.C. Walker, "Releases of Anhydrous Ammonia from Pressurized Containers - The Importance of Denser than Air Mixtures", Atm. Env. 1, 2289 (1978).

Keenan, J.H. and F.G. Keyes, "Thermodynamic Properties of Steam", Wiley & Sons, Inc., NY, 1936.

Kirk and Othmer, "Phosgene", Ency. Chem. Tech., 3rd Ed., 1982.

Koopman, R.P, T.G. McRae, H.C. Goldwire, Jr., D.L. Ermack, and E.J. Kansa, "Results of Recent Large-Scale NH_3 and N_2O_4 Dispersion Experiments", UCRL-91830, Lawrence Livermore National Laboratory,

Kuzminykh, I.N. and V.S. Udintseva, Khimatroi. 6, 523 (1954).

Linke, W.F., "Solubilities of Inorganic and Metal-Organic Compounds", D. Van Nostrand Co., Princeton, NJ, 1958.

Manogue, W.H. and R.L. Pigford, "The Kinetics of the Absorption of Phosgene into Water and Aqueous Solutions", AIChE J. 3, 494 (1960).

McRae, T.G., "Evaluation of Source Strength and Dispersion Model Predictions with Data from Large Nitrogen Tetroxide Field Experiments", UCRL-91402/ESL-TR-85-06, Lawrence Livermore National Laboratory, April, 1985.

Pearson, D.A., L.A. Lundberg, F.B. West, and J.L. McCarthy, "Absorption of Sulfur Dioxide in Water in a Packed Tower", Chem. Eng. Prog. 47, 257 (1951).

Pohl, H.A., "Thermodynamics of the Hydrogen Sulfide-Water System Relevant to the Dual Temperature Process for the Production of Heavy Water", J. Chem. Eng. Data 6, 515 (1961).

Raj, P.K., "Ammonia", in Hazardous Materials Spills Handbook, edited by G.F. Bennett, F.S. Feates, and I. Wilden, McGraw-Hill Book Co., NY, 1982.

Raj, P.K., and K. Aravamudan, "Theoretical Models Supporting the Design of Ammonia Spill Experiments", Report to the Fertilizer Institute, Washington, DC, 1980.

Reid, R.C., J.M. Prausnitz and B.E. Poling, The Properties of Gases and Liquids, McGraw-Hill Book Co., NY, 1987.

Rona, P., "The Destructive Action of Water on War Gases", Z. exp. Med. 13, 16 (1921).

Seinfeld, H.H., "Lectures in Atmospheric Chemistry", AIChE Monograph Series, 12, 76, 1980.

Selleck, F.T., L.T. Carmichael, and B.H. Sage, "Phase Behavior in the Hydrogen Sulfide-Water System", Ind. Eng. Chem. 44, 2219 (1952).

Sherwood, T.K., R.L. Pigford, and C.R. Wilke, Mass Transfer, McGraw-Hill Book Co., New York, 1975, Chapter 8.

Simon, R.H.M., B.S. Thesis, Univ. of Delaware, 1948.

Whitney, R.P. and J.E. Vivian, Ind. Eng. Chem. 33, 741 (1941).

CHAPTER 4 REFERENCES

DeBruin, H.A.R., and A.A.M. Holtslag, "A Simple Parameterization of the Surface Fluxes of Sensible and Latent Heat During Daytime Compared with the Penman-Monteith Concept, J. Appl. Meteor., 21: 1610-1621, (1982).

Golder, D., "Relations Between Stability Parameter in the Surface Layer", Boundary Layer Met., 3, 46-58, (1972).

Holtslag, A.A.M., and A.P. Van Ulden, "A Simple Scheme for Daytime Estimates of the Surface Fluxes from Routine Weather Data, J. Climate Appl. Meteor., 22: 517-529, (1983).

Kastan, F. and G. Czeplak, "Solar and Terrestrial Radiation Dependent on the Amount and Type of Cloud", Solar Energy, 24: 177-189, (1980).

Koo, E., W.L. Chang, and B.Y. Lee, An Alternative Stability Classification Scheme for Air Quality Modeling, Fourth Joint Conference on Applications of Air Pollution Modeling, Portland, OR, 95-98, (1984).

Kunkel, B.A., Private Communication.

Kunkel, B.A., Development of an Atmospheric Diffusion Model for Toxic Chemical Releases, AFGL-TR-85-0338, Hanscom AFB, ADA169135, 1985.

Mitchell, A.E., Jr., "A Comparison of Short-Term Dispersion Estimates Resulting from Various Atmospheric Stability Classification Methods", Atmos. Environ., 16, 765-773, (1982).

Mitchell, A.E., Jr., and K. Timbre, Atmospheric Stability Class from Horizontal Wind Fluctuation, Paper 79-29.2, Air Pollution Control Association Annual Meeting, Cincinnati, OH, 1979.

Ragland, K.W., and B.L. Dennis, "Point Source Atmospheric Diffusion Model with Variable Wind and Diffusivity Profiles", Atmos. Environ., 9, 175-189, (1975).

Slade, D.H., ed., Meteorology and Atomic Energy 1968, U.S. Atomic Energy Commission, 1968.

Smith, F.B., A Scheme for Estimating the Vertical Dispersion of a Plume from a Source Near Ground Level Proceedings of the Third Meeting of the Expert Panel on Air Pollution Modeling, NATO Committee on the Challenges of Modern Society, Paris, France, 1972.

USNRC, Onsite Meteorological Programs Regulatory Guide 1.23, U.S. Nuclear Regulatory Commission, 1972.

Wolf, H.M., On the Computation of Solar Elevation Angles and the Determination of Sunrise and Sunset Times. National Meteorological Center, Environmental Sciences Services Administration, Hillcrest Heights, MO, 1980.

CHAPTER 5 REFERENCES

Carpenter, R.J., R.P. Cleaver, M.A. English, and P.J. Waite, "The Calibration of a Simple Model for Dense Dispersion Using the Thorney Island Phase I Trials Data", presented at the Second Symposium on Heavy Gas Dispersion Trials at Thorney Island, held at the University of Sheffield, Great Britain, 23-25 September, 1986.

Havens, J.A., "Dispersion of Dense Vapors", LNG Safety and Research Workshop, March 22-24, 1982.

Jagger, S.F., "Development of CRUNCH: A Dispersion Model for Continuous Releases of a Denser-Than-Air Vapour into the Atmosphere", UKAEA, SRD R229, 1983.

Kunkel, B.A., Private Communication.

Raj, P.K., "Dispersion of Hazardous Reactive Chemical Vapors in the Atmosphere", Proceedings form the 1986 Hazaroudous Materials Spills Conferance, May 5-8, 1986.

Raj, P.K., "Summary of Heavy Gas Spills Modeling Research", Proceedings of the Heavy Gas (LNG/LPG) Workshop, Toronto, Ontario, Jan. 1985, p.51.

Slade, D.H., ed., Meteorology and Atomic Energy 1968, U.S. Atomic Energy Commission, 1968.

Taylor, R.J., et al., "Scale Length in Atmosphere Turbulence as Measured from an Aircraft", Quart. J. R. Met. Soc., 96, pp750- , 1970.

Wheatley, C.J., P.W.M. Brighton, and A.J. Prince, "Comparison Between Data From the Heavy Gas Dispersion Experiments at Thorney Island and Predictions of Simple Models", presented at the Second Symposium on Heavy Gas Dispersion Trials at Thorney Island, held at the University of Sheffield, Great Britain, 23-25 September, 1986.

Wheatley, C.J., B. Crabol, R.J. Carpenter, S.F. Jagger, C. Nussey, R.P. Cleaver, R.D. Fitzpatrick, A.J. Prince, "Comparison and Test of Models for Atmospheric Dispersion of Continuous Releases of Chlorine", SRD Report R438, 1987.

Wheatley, C.J. and D.M. Webber, "Aspects of the Dispersion of Denser-Than-Air Vapours Relevent to Gas Cloud Explosions", Final Report to the UKAEA and EAEC, 1984.

CHAPTER 6 REFERENCES

Brighton, P.W.M., "Area-Averaged Concentrations, Height-Scales and Mass balances", J. Haz. Matls., 11 (1985) 189-208.

Brighton, P.W.M., A.J. Prince, D.M. Webber, "Determination of Cloud Area and Path from Visual and Concentration Records", J. Haz. Matls., 11 (1985) 155-178.

Carpenter, R.J., R.P. Cleaver, M.A. English, and P.J. Waite, "The Calibration of a Simple Model for Dense Dispersion Using the Thorney Island Phase I Trials Data", presented at the Second Symposium on Heavy Gas Dispersion Trials at Thorney Island, held at the University of Sheffield, Great Britain, 23-25 September, 1986.

CSL (May 1983), Chemical Systems Laboratory, Aberdeen Proving Grounds; "Unclassified data from past field trials with agent", Communicated to Technology and Management Systems, Inc.

Ermak, D.L., R. Chapman, H.C. Goldwire, F.J. Gouveia, H.C. Rodean, "Heavy Gas Dispersion Test Summary Report", Air Force Engineering and Services Laboratory Draft Summary Report, 1987.

Goldwire, H.C, Jr., "Large-Scale Ammonia Spill Tests", Chem. Eng. Prog., Vol. 82, No. 4 (1986) 35-41.

Goldwire, H.C, Jr., T.G. McRae, G.W. Johnson, D.L. Hipple, R.P. Koopman, J.W. McClure, L.K. Morris, R.T. Cederwall, "Desert Tortoise Series Data Report: 1983 Pressurized Ammonia Spills", Lawrence Livermore National Laboratory, UCID-20562 (Jan. 1986).

Koopman, R.P., T.G. McRae, H.C. Goldwire, Jr., D.L. Ermak, E.J. Kansa, "Results of Recent Large Scale NH_3 and N_2O_4 Dispersion Experiments", Symp. on Heavy Gases and Risk Assessment, Wissenschaftszentrum Bonn, West Germany (Nov. 2-13, 1984).

McQuaid, J., "Objectives and Design of the Phase I Heavy Gas Dispersion Trials", J. Haz. Matls., 11 (1985) 1-33.

Pfenning, D.B., and J.B. Cornwell, "Computerized Processing of Thorney Island Trial Data for Comparison with Model Predictions", J. Haz. Matls., 11 (1985) 347-368.

Puttock, J.S., "Comparison of Thorney Island Data with Predictions of HEGABOX/HEGADAS", presented at Health and Safety Executive Symposium on Thorney Island Trials, Sheffield, Great Britain, September, 1986.

Raj, P.K., "Atmospheric Dispersion of Chemical Agents: A Model Including Thermodynamic and Heavy Gas Effects", Report to Chemical Systems Laboratory, U.S. Army Aberdeen Proving Grounds, 1983.

Spicer, T.O., and J.A. Havens, "Modeling the Phase I Thorney Island Experiments", J. Haz. Matls., 11 (1985) 237-260.

Wheatley, C.J., P.W.M. Brighton, and A.J. Prince, "Comparison Between Data From the Heavy Gas Dispersion Experiments at Thorney Island and Predictions of Simple Models", presented at the Second Symposium on Heavy Gas Dispersion Trials at Thorney Island, held at the University of Sheffield, Great Britain, 23-25 September, 1986.

Wheatley, C.J., B. Crabol, R.J. Carpenter, S.F. Jagger, C. Nussey, R.P. Cleaver, R.D. Fitzpatrick, A.J. Prince, "Comparison and Test of Models for Atmospheric Dispersion of Continuous Releases of Chlorine", SRD Report R438, 1987.

APPENDIX B REFERENCE

Abramowitz, M. and I.A. Stegun, Handbook of Mathematical Functions, Dover Publications, Inc., NY, 1965.

APPENDIX A

CHEMICAL PROPERTY DATA BASE

A.1 INTRODUCTION

Numerous physical, thermodynamic, thermochemical, transport, toxicity, and other properties are needed to model the source and dispersion characteristics for each of the chemicals studied in this project. To meet these needs, a chemical property data base was created which provides a standard format for storing and accessing the necessary chemical property information. (The programs that access the data are included in the following discussion.) With this data base, only one set of data and equations is used to calculate a given property in all models, making the calculations consistent.

Several thermo-physical properties for over 1000 chemicals are available in computer files, as a part of the Coast Guard's Hazard Assessment Computer System (HACS). The HACS files for the six chemicals studied for this project were used as a basis for the needed data base. The HACS property data base, however, was not directly transferable to this project for several reasons, including: 1) the property retrieval and calculation programs had to be rewritten to interface with the source and dispersion modules and to run on microcomputers, 2) additional properties had to be added to the data base and the HACS format was not flexible enough to easily allow these changes, 3) some properties in the HACS data base needed to be updated and/or corrected, and 4) comment fields were needed in the data base to make it easier to use and to facilitate future enhancements.

Therefore, the chemical property data base was created taking advantage of the data in HACS, while addressing the four points above, making it useful for the source and dispersion models. The new data base consists of a set of six chemical property data files. These reside outside of the compiled program to permit parameters to be changed. A set of programs for retrieving and calculating the properties is also included in one FORTRAN library module, which is compiled as a part of the program. These features are described in more detail in the following sections.

A.2 DATA BASE FILE FORMAT

The chemical property parameters are stored outside of the thermodynamic, source, and dispersion programs in ASCII format data files. Each chemical has its own file, named according to its HACS three letter code (e.g., chlorine has the HACS code 'CLX' so its property file is CLXPROP.DAT). The file for each chemical was made by converting the data in the existing HACS data files into the new format. Then, several functions were

added, several others were changed, and missing or incorrect data were added or changed. New parameters were obtained from the literature.

The format of the new data base files is shown in Table A.2.1, which has the first 26 lines of the chlorine data file. (The complete data base files for all six chemicals are included as Tables A.6.1 to A.6.6.) The first three lines of each data file contain header information including the name of the file and what version of the data base retrieval and calculation programs is required to use the data. The four numbers in the first row are the property number (-1 denotes header information), the number of parameters for the property (0), the number of comment lines for the property (3) and what type of data the parameters are (0; 0=numeric, 1=character). The properties are organized in groups of rows following the three header lines. Each property has values for the four numbers described above followed by the name of the property. References and information are in the next row(s), and the parameter(s) is(are) in the next row(s) with a maximum of 5 parameters per row.

To enhance performance, the data are accessed on the disk only once. During program execution, the data in a given chemical's data base file are loaded into a RAM array the first time a property for that chemical is needed. If any other properties for the chemical are called for, the needed data are quickly accessed in the RAM array, speeding up the calculations. The ram array format is similar to the data base format, as Table A.2.2 shows. In the array shown, the number in the first column denotes what chemical the information in the row is for. The number is a pointer for a character array where the actual chemical names are stored. The number in the second column is the property number. The number of parameters for the property is in the third column and the parameter(s) follow in the next column(s).

The data base files described above require more disk storage space than the HACS files they are based on since they have additional properties and extensive comments. The HACS data base file for chlorine requires 1320 bytes of storage space, while the new data base file requires 4467 bytes for the same properties as are in HACS or 5349 bytes with the added properties. The new data base files take up much less space if the comments are removed. A program was written to remove the comments, since only a "master set" of the files needs to have this information. These condensed files require only half the space that the files with the comments require.

The improvements in the data base format shown in Table A.2.1 over the HACS format include: 1) each property can be changed without affecting other properties, 2) comments are included, 3) values of the parameters, descriptions of the properties, references for the information, and comments can be changed without making modifications to any other files, properties, or

TABLE A.2.1 Chlorine Property Data Base Disk File

```
 -1   0   3   0      CLXPROP.DAT
                     VERSION  2.11
-------------------------
  1   1   2   0      MOLECULAR WEIGHT (XMWT) kg/kgmole
     REF: HACS
   70.910
  2   1   2   0      CRITICAL POINT TEMPERATURE (TCRI) K
     REF: HACS
   417.00
  3   1   2   0      CRITICAL POINT PRESSURE (PCRI) N/m2
     REF: HACS
   .77040E+07
  4   1   2   0      NORMAL BOILING POINT (XNBP) K
     REF: HACS
   239.10
  5   1   2   0      NORMAL FREEZING POINT (XNFP) K
     REF: HACS
   172.00
  6   8   2   0      VAPOR HEAT CAPACITY (CPV) PARAMETERS J/kg K
     REF: Reid, Prausnitz, and Sherwood.
   379.80       .47720       -5.4560E-04    2.1820E-07    600.00
   172.00      0.0000         0.0000
  7   8   2   0      LIQ HEAT CAPACITY (CPL) PARAMETERS J/kg K
     REF: YAWS,C.L.,"PHYSICAL PROPERTIES",MCGRAW-HILL,NY,P.220.
  -553.49       19.762       -8.5285E-02    1.2117E-04    353.16
   172.16       946.22        239.10
    ...          ...           ...            ...           ...
    ...          ...           ...            ...           ...
    ...          ...           ...            ...           ...
```

TABLE A.2.2 Chlorine Property RAM Array

```
1.0   1.0   1.0   70.910      0.0        0.0           0.0          ...
1.0   2.0   1.0   417.00      0.0        0.0           0.0          ...
1.0   3.0   1.0   7.7040E+07  0.0        0.0           0.0          ...
1.0   4.0   1.0   239.10      0.0        0.0           0.0          ...
1.0   5.0   1.0   172.00      0.0        0.0           0.0          ...
1.0   6.0   8.0   379.80      0.47720   -5.4560E-04  2.1820E-07    ...
1.0   7.0   8.0  -553.49     19.762     -8.5285E-02  1.2117E-04    ...
 .     .     .      .           .          .            .           ...
 .     .     .      .           .          .            .           ...
 .     .     .      .           .          .            .           ...
```

programs, 4) error checking has been added, and 5) program performance is enhanced by loading the chemical property data into the RAM.

A.3 DATA BASE PROPERTY RETRIEVAL / CALCULATION PROGRAMS

The second part of the property data base is the set of programs in the data base library module which access the chemical property parameters stored in the RAM array. These programs retrieve or calculate the properties requested using the parameters in the array. The property programs are written as FORTRAN functions and subroutines, named according to the various chemical properties. A list of the property programs in the data base is shown in Table A.3.1.

The properties which are retrieved or calculated by functions can be used directly in FORTRAN codes, like any other FORTRAN function. For example, if the number of kgmoles of chlorine is known (xmolclx) and the mass of chlorine is desired (xmasclx), the molecular weight function (xmwt(chemical)) would be used as follows:

```
xmasclx = xmolclx * xmwt('clx')                    A.3.1
```

Similarly, the subroutines that retrieve properties which are character strings (such as chemical shipping state) are used as any other FORTRAN subroutines would be used; the chemical name is the input parameter, and the character string is the output parameter.

The properties are either dependent or independent of temperature (or, in one case, pressure). Table A.3.2 has a list of the equations used for those properties which have a temperature (or pressure) dependence. These properties are the functions in Table A.3.1 that have two arguments ('XXX' and either temperature or pressure). If the property is independent of temperature and pressure, its value is simply retrieved from the RAM array.

A.4 CHECKING DATA BASE FOR CORRECTNESS AND ACCURACY

The integrity and correctness of the data and programs in the data base were checked using a program that calculates all of the property values for a chemical at a specified temperature. An example output from this program, for chlorine at 239.1 K, is shown if Table A.4.1. The independent properties were quickly checked for accuracy. The values of properties that are functions of temperature or pressure were calculated at various temperatures in the range expected for the dispersion analysis and checked with data from the literature. Figure A.4.1 shows the comparison, using the same equation, of the HACS parameters and those in the new data base with measured liquid heat capacity data for chlorine. As the figure shows, the HACS data were

TABLE A.3.1 Property Retrieval Functions and Subroutines

FUNCTION NAME	PARAMETERS	DESCRIPTION	UNITS
ADFLT	('XXX')**	Adiabatic Flame Temperature	K
AFRT	('XXX')	Air/Fuel Ratio	-
BBEP	('XXX')	Black Body Emissive Power	kW/m2
BRAT	('XXX')	Burn Rate	m/s
CPV	('XXX',TEMP)	Specific Heat of Sat Vapor	J/kg K
CPL	('XXX',TEMP)	Specific Heat of Sat Liq	J/kg K
DHC	('XXX')	Enthalpy of Combustion	J/kg
DHDC	('XXX')	Enthalpy of Decomposition	J/kg
DHF	('XXX')	Enthalpy of Fusion	J/kg
DHPY	('XXX')	Enthalpy of Polymerization	J/kg
DHS	('XXX')	Enthalpy of Solution	J/kg
DHWR	('XXX')	Enthalpy of Reaction with H_2O	J/kg
FLTM	('XXX')	Flame Temperature	K
HLIQS	('XXX',TEMP)	Saturated Liquid Enthalpy	J/kg
HVAPS	('XXX',TEMP)	Saturated Vapor Enthalpy	J/kg
PCRI	('XXX')	Critical Pressure	N/m2
PSAT	('XXX',TEMP)	Saturated Vapor Pressure	N/m2
RGLQ	('XXX')	Liquid Regression Rate	m/s
RHOL	('XXX',TEMP)	Liquid Density	kg/m3
RHOV	('XXX',TEMP)	Vapor Density	kg/m3
SOL	('XXX',TEMP)	Solubility	kg/100 kg
STEN	('XXX',TEMP)	Surface Tension	N/m
TCRI	('XXX')	Critical Temperature	K
TOX1	('XXX')	Toxic Inhalation Limit TLV	ppm
TOX2	('XXX')	Toxic Short Term Inhal Limit	ppm
TOX3	('XXX')	Toxic Short Term Inhal Time	s
TOX4	('XXX')	Lower Toxicity Limit Ingest	kg/kg
TOX5	('XXX')	Upper ToxicITY Limit Ingest	kg/kg
TSAT	('XXX',PRESSURE)	Saturated Vapor Temperature	K
UPFLM	('XXX')	Upper Flammability Limit	%
XITEN	('XXX')	Interfacial Surface Tension	N/m
XKL	('XXX',TEMP)	Liquid Thermal Conductivity	W/m K
XKV	('XXX',TEMP)	Vapor Thermal Conductivity	W/m K
XLAMDA	('XXX',TEMP)	Enth of Vaporization	J/kg
XLOFLM	('XXX')	Lower Flammability Limit	%
XMFRC	('XXX')	Limiting Value Molec. Fn. Conc.	-
XMRAT	('XXX')	Molar Ratio of Reacts/Prods	-
XMUL	('XXX',TEMP)	Liquid Viscosity	Ns/m2
XMUV	('XXX',TEMP)	Vapor Viscosity	Ns/m2
XMWT	('XXX')	Molecular Weight	-
XNBP	('XXX')	Normal Boiling Point	K
XNFP	('XXX')	Normal Freezing Point	K

SUBROUTINE	(INPUT, OUTPUT)	DESCRIPTION	UNITS
SHIP	('XXX',SHIPPING STATE)	Shipping State	characters
TOX6	('XXX',LATE TOX LEVEL)	Late Toxicity Level	characters

** 'XXX' = HACS three letter chemical code

TABLE A.3.2 Equations Used in Functions Which Are Dependent on Temperature or Pressure

$CPL = A + B*T + C*T^2 + D*T^3$

$CPV = A + B*T + C*T^2 + D*T^3$

$HLIQS = HREF + A*(T-TREF) + B*(T^2-TREF^2)/2 + C*(T^3-TREF^3)/3 + D*(T^4-TREF^4)/4$

$HVAPS = HREF + A*(T-TREF) + B*(T^2-TREF^2)/2 + C*(T^3-TREF^3)/3 + D*(T^4-TREF4)/4$

$PSAT = 10.0(A - (B/(C + T)) + D*T + E*T^2)$

$RHOL = A + B*T + C*T^2$

$RHOV = (10.0(A - (B/(T+C)) + D*T + E*T^2) / (R * T)) *XMWT$

$SOL = A + B*T$

$STEN = STENA*(((TCRI-T)/(TCRI-TREF))^{XN})$

$TSAT$ = T such that $P = 10.0(A-B/(T+C)+D*T+E*T^2)$

$XKL = A + B*T + C*T^2$

$XKV = A + B*T + C*T^2 + D*T^3$

$XLAMDA = XLAMDAREF * (((TCRI-T)/(TCRI-TREF))^{XN})$

$XMUL = EXP(A + B/T + C*T + D*T^2)$

$XMUV = A + B*T + C*T^2$

TABLE A.4.1 Sample Output From Property Data Base Checking Program

CHEM= CLX TEMP= 239.10 DEG K

Properties With Temperature or Pressure Dependence

CPV IS	:	465.69	J/kg K
CPL IS	:	952.24	J/kg K
HLIQS IS	:	-32357.	J/kg K
HVAPS IS	:	0.25281E+06	J/kg K
RHOL IS	:	1548.5	kg/m3
RHOV IS	:	3.6195	kg/m3
XKL IS	:	0.16586	W/m K
XKV IS	:	0.75929E-02	W/m K
XMUL IS	:	0.49598E-03	N s/m2
XMUV IS	:	0.10936E-04	N s/m2
SOL IS	:	0.95604	kg/100 kg
XLAMDA IS	:	0.29139E+06	J/kg
STEN IS	:	0.24601E-01	N/m
PSAT IS	:	0.10147E+06	N/m2
TSAT AT	0.10147E+06 N/m2 IS	:	238.39 K

Temperature and Pressure Independent Properties

XMWT IS	:	70.910	
XNBP IS	:	239.10	K
XNFP IS	:	172.00	K
TCRI IS	:	417.00	K
PCRI IS	:	0.77040E+07	N/m2
DHF IS	:	90330.	J/kg
DHC IS	:	0.00000E+00	J/kg
DHDC IS	:	0.00000E+00	J/kg
DHS IS	:	0.00000E+00	J/kg
DHWR IS	:	0.00000E+00	J/kg
DHPY IS	:	0.00000E+00	J/kg
XITEN IS	:	0.00000E+00	N/m
XLOFLM IS	:	0.00000E+00	%
UPFLM IS	:	0.00000E+00	%
BRAT IS	:	0.00000E+00	m/s
TOX1 IS	:	1.0000	ppm
TOX2 IS	:	3.0000	ppm
TOX3 IS	:	300.00	s
TOX4 IS	:	0.00000E+00	kg/kg
TOX5 IS	:	0.00000E+00	kg/kg
TOX6 IS	:		
XMRAT IS	:	0.00000E+00	
AFRT IS	:	0.00000E+00	
ADFLT IS	:	0.00000E+00	DEG K
FLTM IS	:	0.00000E+00	DEG K
XMFRC IS	:	0.00000E+00	
SHIP IS	:	L	

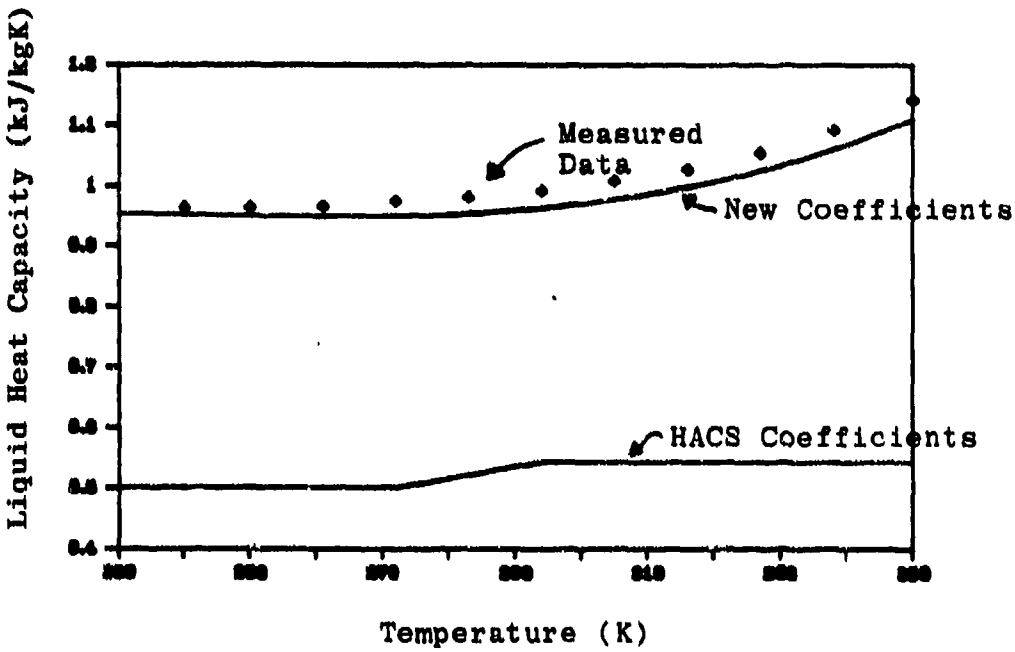

Figure A.4.1 Comparison of Measured Chlorine Liquid Heat Capacity Data with Modeled Values using the Original HACS Coefficients and the New Coefficients

erroneous. If no data were available, the computed values were checked for consistency and correct trends.

A.5 OTHER DATA BASE PROGRAMS

Besides the programs (described above) for: i) converting the data from the HACS format into the new data base format, ii) loading the data into the RAM, iii) condensing the data base files by removing comment lines, iv) retrieving or calculating the property values, and v) checking the data base for errors, other programs in the property FORTRAN library module include: vi) a program that resets the RAM array elements that hold the data to zero, and vii) a program that writes the RAM array data into a file for debugging purposes.

A.6 CHEMICAL DATA BASE FILES

The data base files for all of the six chemicals are included as Tables A.6.1 (Ammonia) to A.6.6 (Sulfur Dioxide). The majority of the data was obtained from the HACS data files, as the references show. Other data were obtained from the literature listed and from consultations with Dr. Bob Reid of MIT.

A.7 CONCLUSIONS

A chemical property data base has been developed which uses the vast amount of information available in the HACS data base but has an improved format that allows for easier parameter and property changes and in-file documentation. In addition, property retrieval and/or calculation programs that can interface with the microcomputer models have been created and property parameters and equations have been added, updated, changed, and/or corrected as required. The new chemical property data base provides a useful and versatile method for storing and using the chemical properties.

TABLE A.6.1 Ammonia Property Data Base File

```
 -1   0   3   0      AMAPROP.DAT
                     VERSION  2.11
-------------------------------------
  1   1   2   0      MOLECULAR WEIGHT (XMWT)
       REF: HACS
     17.030
  2   1   2   0      CRITICAL POINT TEMPERATURE (TCRI) K
       REF: HACS
     406.00
  3   1   2   0      CRITICAL POINT PRESSURE (PCRI) N/m2
       REF: HACS
     .11270E+08
  4   1   2   0      NORMAL BOILING POINT (XNBP) K
       REF: HACS
     239.80
  5   1   2   0      NORMAL FREEZING POINT (XNFP) K
       REF: HACS
     195.50
  6   8   2   0      VAPOR HEAT CAPACITY (CPV) PARAMETERS J/kg K
       REF: HACS
     1602.9           1.4014          1.0080E-03      6.8837E-07      600.0
     250.00           0.0000          0.0000
  7   8   2   0      LIQ HEAT CAPACITY (CPL) PARAMETERS J/kg K
       REF:YAWS,C.L.,"PHYSICAL PROPERTIES",MCGRAW-HILL,NY,P.221.
-8051.2           130.21          -.46432          5.7610E-04      373.16
 195.76           4396.1          239.73
  8   7   2   0      LIQUID DENSITY (RHOL) PARAMETERS kg/m3
       REF: HACS
    -5.8851           6.1299          -.13600E-01     253.16          195.1
     682.00           239.76
 10   7   2   0      VAPOR PRESSURE (PSAT) PARAMETERS N/m2
       REF: REID,PRAUSNITZ,SHERWOOD,"THE PROPERTIES...", P.633.
     9.4854           926.13          -32.980         0.0000          0.000
     300.00           179.00
 11   2   2   0      ENTHALPY OF SATURATED LIQUID (HLIQS) J/kg
       REF: BASIS
     .00000           273.16
 12   2   2   0      ENTHALPY OF SATURATED VAPOR (HVAPS) J/kg
       REF: BASIS + XLAMDA
     1.2574E+06       273.16
 13   6   2   0      ENTHALPY OF VAPORIZATION (XLAMDA) J/kg
       REF: HACS
     406.00           239.80          .13691E+07      .38000          406.0
     195.50
 14   6   2   0      SOLUBILITY (SOL) PARAMETERS kg/100 kg
       REF: HACS
     .00000           .00000          .00000          .00000          .0000
     .00000
 15   1   2   0      ENTHALPY OF FUSION (DHF) J/kg
       REF: PERRY, P. 3-111.
     3.3239E+05
```

TABLE A.6.1 (Cont.) Ammonia Property Data Base File

```
 16   1   2   0      ENTHALPY OF COMBUSTION (DHC) J/kg
       REF: HACS
    -.18589E+08
 17   1   2   0      ENTHALPY OF DECOMPOSITION (DHDC) J/kg
       REF: HACS
     .00000
 18   1   2   0      ENTHALPY OF SOLUTION (DHS) J/kg
       REF: HACS
    -.56500E+06
 19   1   2   0      ENTHALPY OF REACTION WITH WATER (DHWR) J/kg
       REF: HACS
     .00000
 20   1   2   0      ENTHALPY OF POLYMERIZATION (DHPY) J/kg
       REF: HACS
     .00000
101   7   2   0      LIQ THERMAL COND (XKL) PARAMETERS W/m K
       REF: YAWS, P.225.
     1.0675           -1.5758E-03      -1.2280E-06       1673.2          273.1
     2.6372E-02        298.16
102   8   2   0      VAP THERMAL COND (XKV) PARAMETERS W/m K
       REF: YAWS, P.208.
     3.8074E-04        5.3848E-05       1.2259E-07      -3.6317E-11      1673.
     279.16            2.6372E-02       298.16
103   8   2   0      LIQ VISCOSITY (XMUL) PARAMETERS N s/m2
       REF: YAWS, P.213.
    -26.690           2018.0           6.1732E-02      -8.3169E-05       405.5
     195.42           .13543E-03       298.16
104   7   2   0      VAP VISCOSITY (XMUV) PARAMETERS N s/m2
       REF: YAWS, P.211.
    -9.3720E-07       38.990E-09      -44.050E-13       1473.2          73.16
     1.0300E-05       298.16
105   8   2   0      SURFACE TENSION (STEN) N/m
       REF: YAWS, P.219.
     .03667           405.56           228.16           1.1548          405.5
     195.42           .00000           .00000
106   2   2   0      INTERFACIAL SURFACE TENSION (XITEN) N/m
       REF: HACS
     .00000            .00000
107   1   2   1      SHIPPING STATE CODE
       REF: HACS
L
201   1   2   0      LOWER FLAMMABILITY LIMIT (XLOFLM) %
       REF: HACS
     15.500
202   1   2   0      UPPER FLAMMABILITY LIMIT (UPFLM) %
       REF: HACS
     27.000
203   1   2   0      BURN RATE (BRAT) m/s
       REF: HACS
     .16667E-04
```

TABLE A.6.1 (Cont.) Ammonia Property Data Base File

```
204   1   2   0     ADIABATIC FLAME TEMPERATURE (ADFT) K
       REF: HACS
     .00000
205   1   2   0     MOLAR RATIO REACTANTS/PRODUCTS (MRAT)
       REF: HACS
     .87500
206   1   2   0     AIR FUEL RATIO (AFRT)
       REF: HACS
     6.0500
207   1   2   0     FLAME TEMPERATURE (FLTM) K
       REF: HACS
     .00000
301   1   2   0     TOXIC INHALATION LIMIT/TLV (TOX1) ppm
       REF: HACS
     25.000
302   1   2   0     SHORT TERM INHALATION LIMIT (TOX2) ppm
       REF: HACS
     50.000
303   1   2   0     SHORT TERM INHALATION TIME LIMIT (TOX3) s
       REF: HACS
     300.00
304   1   2   0     LOWER TOXICITY INGESTION LIMIT (TOX4) kg/kg
       REF: HACS
     .00000
305   1   2   0     UPPER TOXICITY INGESTION LIMIT (TOX5) kg/kg
       REF: HACS
     .00000
306   1   2   1     LATE TOXICITY LEVEL (TOX6)
       REF: HACS

701   1   2   0     LIMITING VALUE OF MOLECULAR FN CONC (XMFRC)
       REF: HACS
     .00000
```

TABLE A.6.2 Chlorine Property Data Base File

```
 -1   0   3   0      CLXPROP.DAT
                     VERSION  2.11
-------------------------------------
  1   1   2   0      MOLECULAR WEIGHT (XMWT)
       REF: HACS
     70.910
  2   1   2   0      CRITICAL POINT TEMPERATURE (TCRI) K
       REF: HACS
     417.00
  3   1   2   0      CRITICAL POINT PRESSURE (PCRI) N/m2
       REF: HACS
     .77040E+07
  4   1   2   0      NORMAL BOILING POINT (XNBP) K
       REF: HACS
     239.10
  5   1   2   0      NORMAL FREEZING POINT (XNFP) K
       REF: HACS
     172.00
  6   8   2   0      VAPOR HEAT CAPACITY (CPV) PARAMETERS J/kg K
       REF: REID
     379.80            .47720          -5.4560E-04      2.1820E-07      600.0
     172.00            0.0000           0.0000
  7   8   2   0      LIQ HEAT CAPACITY (CPL) PARAMETERS J/kg K
       REF: YAWS,C.L.,"PHYSICAL PROPERTIES",MCGRAW-HILL,NY,P.220.
    -553.49            19.762          -8.5285E-02      1.2117E-04      353.1
     172.16            946.22           239.10
  8   7   2   0      LIQUID DENSITY (RHOL) PARAMETERS kg/m3
       REF: HACS
     2170.2           -2.6000           .00000          293.16          233.1
     1424.0            288.16
 10   7   2   0      VAPOR PRESSURE (PSAT) PARAMETERS N/m2
       REF: REID
     13.041            1414.8           0.0000         -1.2060E-02      1.34E-
     317.00            172.00
 11   2   2   0      ENTHALPY OF SATURATED LIQUID (HLIQS) J/kg
       REF: BASIS
     .00000            273.16
 12   2   2   0      ENTHALPY OF SATURATED VAPOR (HVAPS) J/kg
       REF: HACS
     .26881E+06        273.16
 13   6   2   0      ENTHALPY OF VAPORIZATION (XLAMDA) J/kg
       REF: HACS
     417.16            239.01          .29145E+06       .38000          417.1
     172.16
 14   6   3   0      SOLUBILITY (SOL) PARAMETERS kg/100 kg
       REF: SCONCE,J.S.,"CHLORINE",KREIGER PUB.,HUNTINGTON,NY,1972.P.33.
       REF: FLDS 1-4          HACS FLDS 5,6
     5.3927           -.01569          323.16          282.77          .6500
     298.16
```

TABLE A.6.2 (Cont.) Chlorine Property Data Base File

```
 15   1   2   0      ENTHALPY OF FUSION (DHF) J/kg
       REF: SCONCE, P.23.
     .90330E+05
 16   1   2   0      ENTHALPY OF COMBUSTION (DHC) J/kg
       REF: HACS
     .00000
 17   1   2   0      ENTHALPY OF DECOMPOSITION (DHDC) J/kg
       REF: HACS
     .00000
 18   1   2   0      ENTHALPY OF SOLUTION (DHS) J/kg
       REF: HACS
     .00000
 19   1   2   0      ENTHALPY OF REACTION WITH WATER (DHWR) J/kg
       REF: HACS
     .00000
 20   1   2   0      ENTHALPY OF POLYMERIZATION (DHPY) J/kg
       REF: HACS
     .00000
101   7   2   0      LIQ THERMAL COND (XKL) PARAMETERS W/m K
       REF: YAWS, P.224.
     .25063           -2.0209E-04      -6.3764E-07      405.16          172.1
     .13682            293.16
102   8   2   0      VAP THERMAL COND (XKV) PARAMETERS W/m K
       REF: YAWS, P.208.
     1.3598E-03        2.4267E-05       8.7864E-09      -5.2300E-12     1673.
     193.16            9.2383E-03       298.16
103   8   2   0      LIQ VISCOSITY (XMUL) PARAMETERS N s/m2
       REF: YAWS, P.212.
    -8.6764           348.61           -1.8579E-03       9.3830E-07     417.1
     172.16            3.4000E-04       298.16
104   7   2   0      VAP VISCOSITY (XMUV) PARAMETERS N s/m2
       REF: YAWS, P.210.
     5.1750E-07        4.5690E-08      -8.8540E-12       1473.2          73.16
     1.3350E-05        298.16
105   8   2   0      SURFACE TENSION (STEN) N/m
       REF: YAWS, P.218.(PARS 1-6)          HACS(PARS 7,8)
     .01682            417.16           293.16            1.0508         417.1
     172.16            .26550E-01       237.86
106   2   2   0      INTERFACIAL SURFACE TENSION (XITEN) N/m
       REF: HACS
     .00000            .00000
107   1   2   1      SHIPPING STATE CODE
       REF: HACS
L
201   1   2   0      LOWER FLAMMABILITY LIMIT (XLOFLM) %
       REF: HACS
     .00000
202   1   2   0      UPPER FLAMMABILITY LIMIT (UPFLM) %
       REF: HACS
     .00000
```

TABLE A.6.2 (Cont.) Chlorine Property Data Base File

```
203   1   2   0     BURN RATE (BRAT) m/s
       REF: HACS
     .00000
204   1   2   0     ADIABATIC FLAME TEMPERATURE (ADFT) K
       REF: HACS
     .00000
205   1   2   0     MOLAR RATIO REACTANTS/PRODUCTS (MRAT)
       REF: HACS
     .00000
206   1   2   0     AIR FUEL RATIO (AFRT)
       REF: HACS
     .00000
207   1   2   0     FLAME TEMPERATURE (FLTM) K
       REF: HACS
     .00000
301   1   2   0     TOXIC INHALATION LIMIT/TLV (TOX1) ppm
       REF: HACS
     1.0000
302   1   2   0     SHORT TERM INHALATION LIMIT (TOX2) ppm
       REF: HACS
     3.0000
303   1   2   0     SHORT TERM INHALATION TIME LIMIT (TOX3) s
       REF: HACS
     300.00
304   1   2   0     LOWER TOXICITY INGESTION LIMIT (TOX4) kg/kg
       REF: HACS
     .00000
305   1   2   0     UPPER TOXICITY INGESTION LIMIT (TOX5) kg/kg
       REF: HACS
     .00000
306   1   2   1     LATE TOXICITY LEVEL (TOX6)
       REF: HACS

701   1   2   0     LIMITING VALUE OF MOLECULAR FN CONC (XMFRC)
       REF: HACS
     .00000
```

TABLE A.6.3 Hydrogen Sulfide Property Data Base File

```
 -1   0   3   0     HDSPROP.DAT
                    VERSION  2.11
-----------------------------------------
  1   1   2   0     MOLECULAR WEIGHT (XMWT)
       REF: HACS
     34.080
  2   1   2   0     CRITICAL POINT TEMPERATURE (TCRI) K
       REF: HACS
     373.60
  3   1   2   0     CRITICAL POINT PRESSURE (PCRI) N/m2
       REF: HACS
     .90100E+07
  4   1   2   0     NORMAL BOILING POINT (XNBP) K
       REF: HACS
     212.80
  5   1   2   0     NORMAL FREEZING POINT (XNFP) K
       REF: HACS
     190.40
  6   8   2   0     VAPOR HEAT CAPACITY (CPV) PARAMETERS J/kg K
       REF: HACS
     927.52           .14742          3.6854E-04      .00000          600.0
     250.00           0.0000          0.0000
  7   8   2   0     LIQ HEAT CAPACITY (CPL) PARAMETERS J/kg K
       REF: HACS
     1800.0           .00000          .00000          .00000          222.0
     202.00           1800.0          212.00
  8   7   2   0     LIQUID DENSITY (RHOL) PARAMETERS kg/m3
       REF: HACS
     1212.4           -1.4000         .00000          273.16          213.1
     916.00           213.16
 10   7   2   0     VAPOR PRESSURE (PSAT) PARAMETERS N/m2
       REF: HACS
     9.5589           970.00          .40039E-01      0.0000          0.000
     283.16           208.16
 11   2   2   0     ENTHALPY OF SATURATED LIQUID (HLIQS) J/kg
       REF: BASIS
     .00000           273.16
 12   2   2   0     ENTHALPY OF SATURATED VAPOR (HVAPS) J/kg
       REF: BASIS PLUS XLAMDA AT TEMP=273.16.
     .45515E+06       273.16
 13   6   2   0     ENTHALPY OF VAPORIZATION (XLAMDA) J/kg
       REF: HACS
     373.60           212.80          .54428E+06      .38000          373.6
     190.40
 14   6   2   0     SOLUBILITY (SOL) PARAMETERS kg/100 kg
       REF: HACS
     .00000           .00000          .00000          .00000          .0000
     .00000
 15   1   2   0     ENTHALPY OF FUSION (DHF) J/kg
       REF: HACS
     69919.
```

TABLE A.6.3 (Cont.) Hydrogen Sulfide Property Data Base File

```
 16   1   2   0     ENTHALPY OF COMBUSTION (DHC) J/kg
       REF: HACS
   -.15240E+08
 17   1   2   0     ENTHALPY OF DECOMPOSITION (DHDC) J/kg
       REF: HACS
      .00000
 18   1   2   0     ENTHALPY OF SOLUTION (DHS) J/kg
       REF: HACS
      .00000
 19   1   2   0     ENTHALPY OF REACTION WITH WATER (DHWR) J/kg
       REF: HACS
      .00000
 20   1   2   0     ENTHALPY OF POLYMERIZATION (DHPY) J/kg
       REF: HACS
      .00000
101   7   3   0     LIQ THERMAL COND (XKL) PARAMETERS W/m K
       REF: REID regression of data from Horvath, "Physical Properties of
            Inorganic Compounds", Edward Arnold Ltd., London, 1975.
      .59070          -2.0870E-03      1.8750E-06      300.00          190.0
      .14000           293.00
102   8   2   0     VAP THERMAL COND (XKV) PARAMETERS W/m K
       REF: Reid regression of data from Horvath, (see above).
   -4.8970E-03        6.5200E-05       .00000          .00000          450.0
      190.00           .02400          443.20
103   8   2   0     LIQ VISCOSITY (XMUL) PARAMETERS N s/m2
       REF: HACS (COEFFICIENT A IS JUST THE 5th PARAMETER REPEATED)
     -7.5811           .00000           .00000          .00000          .51E-
      193.16           .00000           .00000
104   7   2   0     VAP VISCOSITY (XMUV) PARAMETERS N s/m2
       REF: DATA FROM: PERRY, "CHEM. ENG. HANDBOOK",P3-211.
      1.7958E-06        3.5400E-08       .00000          373.16          173.1
      1.1500E-05        298.16
105   8   2   0     SURFACE TENSION (STEN) N/m
       REF: HACS (CORR PARS FROM EXAMPLE DATA, ALL GIVE .3E-01)
      .03000           373.60           212.80          0.0000          373.6
      212.80           .30000E-01       212.00
106   2   2   0     INTERFACIAL SURFACE TENSION (XITEN) N/m
       REF: HACS
      .00000           .00000
107   1   2   1     SHIPPING STATE CODE
       REF: HACS
L
201   1   2   0     LOWER FLAMMABILITY LIMIT (XLOFLM) %
       REF: HACS
      4.3000
202   1   2   0     UPPER FLAMMABILITY LIMIT (UPFLM) %
       REF: HACS
      45.000
203   1   2   0     BURN RATE (BRAT) m/s
       REF: HACS
      .38333E-04
```

TABLE A.6.3 (Cont.) Hydrogen Sulfide Property Data Base File

```
204   1   2   0      ADIABATIC FLAME TEMPERATURE (ADFT) K
       REF: HACS
     .00000
205   1   2   0      MOLAR RATIO REACTANTS/PRODUCTS (MRAT)
       REF: HACS
     1.2500
206   1   2   0      AIR FUEL RATIO (AFRT)
       REF: HACS
     6.0400
207   1   2   0      FLAME TEMPERATURE (FLTM) K
       REF: HACS
     .00000
301   1   2   0      TOXIC INHALATION LIMIT/TLV (TOX1) ppm
       REF: HACS
     10.000
302   1   2   0      SHORT TERM INHALATION LIMIT (TOX2) ppm
       REF: HACS
     .00000
303   1   2   0      SHORT TERM INHALATION TIME LIMIT (TOX3) s
       REF: HACS
     .00000
304   1   2   0      LOWER TOXICITY INGESTION LIMIT (TOX4) kg/kg
       REF: HACS
     .00000
305   1   2   0      UPPER TOXICITY INGESTION LIMIT (TOX5) kg/kg
       REF: HACS
     .00000
306   1   2   1      LATE TOXICITY LEVEL (TOX6)
       REF: HACS

701   1   2   0      LIMITING VALUE OF MOLECULAR FN CONC (XMFRC)
       REF: HACS
     .00000
```

TABLE A.6.4 Nitrogen Tetroxide Property Data Base File

```
-1   0   3   0      NOXPROP.DAT
                    VERSION  2.11
-------------------------------------
 1   1   2   0      MOLECULAR WEIGHT (XMWT)
       REF: CHRIS
     92.020
 2   1   2   0      CRITICAL POINT TEMPERATURE (TCRI) K
       REF: HACS
     431.40
 3   1   2   0      CRITICAL POINT PRESSURE (PCRI) N/m2
       REF: HACS
     .10100E+08
 4   1   2   0      NORMAL BOILING POINT (XNBP) K
       REF: HACS
     294.00
 5   1   2   0      NORMAL FREEZING POINT (XNFP) K
       REF: HACS
     262.00
 6   8   2   0      VAPOR HEAT CAPACITY (CPV) PARAMETERS J/kg K
     REF: YAWS,C.L.,"PHYSICAL PROPERTIES",MCGRAW-HILL,NY,P.198(NO2 DATA).
     251.61          .60058          -3.6217E-04     7.7803E-08      1500.
     298.16          400.39          298.00
 7   8   2   0      LIQ HEAT CAPACITY (CPL) PARAMETERS J/kg K
       REF: HACS
     1038.0          1.7000          .00000          .00000          295.0
     270.00          1536.0          293.00
 8   7   2   0      LIQUID DENSITY (RHOL) PARAMETERS kg/m3
       REF: HACS
     2182.9          -2.5000         .00000          313.16          273.1
     1450.0          293.16
10   7   2   0      VAPOR PRESSURE (PSAT) PARAMETERS N/m2
       REF: HACS
     11.042          1798.5          3.6399          0.0000          0.000
     373.16          234.16
11   2   2   0      ENTHALPY OF SATURATED LIQUID (HLIQS) J/kg
       REF:
     .00000          273.16
12   2   2   0      ENTHALPY OF SATURATED VAPOR (HVAPS) J/kg
       REF:
     .43788E+06      273.16
13   6   2   0      ENTHALPY OF VAPORIZATION (XLAMDA) J/kg
       REF: HACS
     431.40          294.00          .41500E+06      .38000          431.4
     262.00
14   6   2   0      SOLUBILITY (SOL) PARAMETERS kg/100 kg
       REF: HACS
     .00000          .00000          .00000          .00000          .0000
     .00000
15   1   2   0      ENTHALPY OF FUSION (DHF) J/kg
       REF: PERRY, "CHEM. ENG. HANDBOOK", 5th ed., P. 3-111.
     .25206E+06
```

TABLE A.6.4 (Cont.) Nitrogen Tetroxide Property Data Base File

```
 16   1   2   0     ENTHALPY OF COMBUSTION (DHC) J/kg
       REF: HACS
      .00000
 17   1   2   0     ENTHALPY OF DECOMPOSITION (DHDC) J/kg
       REF: HACS
      .00000
 18   1   2   0     ENTHALPY OF SOLUTION (DHS) J/kg
       REF: HACS
     -70000.
 19   1   2   0     ENTHALPY OF REACTION WITH WATER (DHWR) J/kg
       REF: HACS
      .00000
 20   1   2   0     ENTHALPY OF POLYMERIZATION (DHPY) J/kg
       REF: HACS
      .00000
101   7   2   0     LIQ THERMAL COND (XKL) PARAMETERS W/m K
       REF: YAWS, P.324 (NO2 DATA).
      .21746          2.6024E-05     -1.0765E-06      415.16          262.1
      .13263          293.16
102   8   2   0     VAP THERMAL COND (XKV) PARAMETERS W/m K
       REF: YAWS, P.207 (NO2 DATA).
     -1.4025E-02      1.1071E-04     -3.1589E-08      4.4811E-12      1673.
      298.16          1.6276E-02     298.16
103   8   2   0     LIQ VISCOSITY (XMUL) PARAMETERS N s/m2
       REF: YAWS, P.212 (NO2 DATA).
     -26.321          2147.4         6.3528E-02      -8.6439E-05     431.1
      261.96          3.9000E-04     298.16
104   7   2   0     VAP VISCOSITY (XMUV) PARAMETERS N s/m2
       REF: HACS
      .00000           .00000          .00000           .00000          .0000
      .00000           .00000
105   8   2   0     SURFACE TENSION (STEN) N/m
       REF: YAWS, P.218 (NO2 DATA).
      .02650          431.16         298.16           0.7627          431.1
      261.96           .00000          .00000
106   2   2   0     INTERFACIAL SURFACE TENSION (XITEN) N/m
       REF: HACS
      .00000           .00000
107   1   2   1     SHIPPING STATE CODE
       REF: HACS
L
201   1   2   0     LOWER FLAMMABILITY LIMIT (XLOFLM) %
       REF: HACS
      .00000
202   1   2   0     UPPER FLAMMABILITY LIMIT (UPFLM) %
       REF: HACS
      .00000
203   1   2   0     BURN RATE (BRAT) m/s
       REF: HACS
      .00000
```

TABLE A.6.4 (Cont.) Nitrogen Tetroxide Property Data Base File

```
204   1   2   0     ADIABATIC FLAME TEMPERATURE (ADFT) K
       REF: HACS
     .00000
205   1   2   0     MOLAR RATIO REACTANTS/PRODUCTS (MRAT)
       REF: HACS
     .00000
206   1   2   0     AIR FUEL RATIO (AFRT)
       REF: HACS
     .00000
207   1   2   0     FLAME TEMPERATURE (FLTM) K
       REF: HACS
     .00000
301   1   2   0     TOXIC INHALATION LIMIT/TLV (TOX1) ppm
       REF: HACS
     5.0000
302   1   2   0     SHORT TERM INHALATION LIMIT (TOX2) ppm
       REF: HACS
     25.000
303   1   2   0     SHORT TERM INHALATION TIME LIMIT (TOX3) s
       REF: HACS
     300.00
304   1   2   0     LOWER TOXICITY INGESTION LIMIT (TOX4) kg/kg
       REF: HACS
     .00000
305   1   2   0     UPPER TOXICITY INGESTION LIMIT (TOX5) kg/kg
       REF: HACS
     .00000
306   1   2   1     LATE TOXICITY LEVEL (TOX6)
       REF: HACS

701   1   2   0     LIMITING VALUE OF MOLECULAR FN CONC (XMFRC)
       REF: HACS
     .00000
```

TABLE A.6.5 Phosgene Property Data Base File

```
 -1   0   3   0      PHGPROP.DAT
                     VERSION  2.11
-------------------------------------
  1   1   2   0      MOLECULAR WEIGHT (XMWT)
       REF: HACS
     98.920
  2   1   2   0      CRITICAL POINT TEMPERATURE (TCRI) K
       REF: HACS
     455.00
  3   1   2   0      CRITICAL POINT PRESSURE (PCRI) N/m2
       REF: HACS
     .56700E+07
  4   1   2   0      NORMAL BOILING POINT (XNBP) K
       REF: HACS
     281.40
  5   1   2   0      NORMAL FREEZING POINT (XNFP) K
       REF: HACS
     147.00
  6   8   2   0      VAPOR HEAT CAPACITY (CPV) PARAMETERS J/kg K
       REF: HACS
     280.20            1.3142          -.99462E-04       .00000          600.0
     250.00            0.0000           0.0000
  7   8   2   0      LIQ HEAT CAPACITY (CPL) PARAMETERS J/kg K
       REF: HACS
     1046.7            .00000           .00000           .00000          323.1
     253.16            1046.7           293.16
  8   7   2   0      LIQUID DENSITY (RHOL) PARAMETERS kg/m3
       REF: HACS
     2112.9           -2.5000           .00000           333.16          273.1
     1380.0            293.16
 10   7   3   0      VAPOR PRESSURE (PSAT) PARAMETERS N/m2
       REF: REID,PRAUSNITZ,SHERWOOD,"THE PROPERTIES OF GASES AND LIQUIDS",
            MCGRAW-HILL,NY,1977. P.632.
     8.9679            941.25          -43.150           0.0000          0.000
     341.00            213.00
 11   2   2   0      ENTHALPY OF SATURATED LIQUID (HLIQS) J/kg
       REF: GIAGUE,JONES, J.AM.CHEM.SOC.,20,120-4(1948)
            PLUS REID,PRAUSNITZ,SHERWOOD
     .00000            273.00
 12   2   2   0      ENTHALPY OF SATURATED VAPOR (HVAPS) J/kg
       REF: GIAGUE, pp.120-4       REID,PRAUSNITZ,SHERWOOD APP.A.
     2.4894E+05        273.00
 13   6   2   0      ENTHALPY OF VAPORIZATION (XLAMDA) J/kg
       REF: HACS
     455.00            281.40          .24702E+06        .38000          455.0
     147.00
 14   6   2   0      SOLUBILITY (SOL) PARAMETERS kg/100 kg
       REF: HACS
     .00000            .00000           .00000           .00000          .0000
     .00000
```

TABLE A.6.5 (Cont.) Phosgene Property Data Base File

```
 15   1   2   0      ENTHALPY OF FUSION (DHF) J/kg
       REF: HACS
     58197.
 16   1   2   0      ENTHALPY OF COMBUSTION (DHC) J/kg
       REF: HACS
     .00000
 17   1   2   0      ENTHALPY OF DECOMPOSITION (DHDC) J/kg
       REF: HACS
     .00000
 18   1   2   0      ENTHALPY OF SOLUTION (DHS) J/kg
       REF: MANOGUE, W.H., R.L. PIGFORD,AIChE JOURNAL, SEPT. 1960, P.498.
     2.8762E+05
 19   1   2   0      ENTHALPY OF REACTION WITH WATER (DHWR) J/kg
       REF: HACS
    -.24606E+07
 20   1   2   0      ENTHALPY OF POLYMERIZATION (DHPY) J/kg
       REF: HACS
     .00000
101   7   2   0      LIQ THERMAL COND (XKL) PARAMETERS W/m K
       REF: HACS
     .00000           .00000          .00000          .00000          .0000
     .00000           .00000
102   8   2   0      VAP THERMAL COND (XKV) PARAMETERS W/m K
       REF:
     .00000           .00000          .00000          .00000          .0000
     .00000           .00000          .00000
103   8   2   0      LIQ VISCOSITY (XMUL) PARAMETERS N s/m2
       REF: HACS
     .00000           .00000          .00000          .00000          .0000
     .00000           .00000          .00000
104   7   2   0      VAP VISCOSITY (XMUV) PARAMETERS N s/m2
       REF: REID, PRAUSNITZ, SHERWOOD.
    -6.0000E-07       4.0000E-08      .00000          400.00          280.0
     1.2600E-05       330.00
105   8   3   0      SURFACE TENSION (STEN) N/m
       REF: KIRK & OTHMER, "ENCYCLOPEDIA OF CHEM. TECH.", P.675. FLDS 1-6
       REF: HACS.  FLDS 7,8.
     .02010           455.00          289.86          1.1700          319.2
     289.86           .22800E-01      273.16
106   2   2   0      INTERFACIAL SURFACE TENSION (XITEN) N/m
       REF: HACS
     .00000           .00000
107   1   2   1      SHIPPING STATE CODE
       REF: HACS
L
201   1   2   0      LOWER FLAMMABILITY LIMIT (XLOFLM) %
       REF: HACS
     .00000
202   1   2   0      UPPER FLAMMABILITY LIMIT (UPFLM) %
       REF: HACS
```

TABLE A.6.5 (Cont.) Phosgene Property Data Base File

```
203   1   2   0     BURN RATE (BRAT) m/s
       REF: HACS
     .00000
204   1   2   0     ADIABATIC FLAME TEMPERATURE (ADFT) K
       REF: HACS
     .00000
205   1   2   0     MOLAR RATIO REACTANTS/PRODUCTS (MRAT)
       REF: HACS
     .00000
206   1   2   0     AIR FUEL RATIO (AFRT)
       REF: HACS
     .00000
207   1   2   0     FLAME TEMPERATURE (FLTM) K
       REF: HACS
     .00000
301   1   2   0     TOXIC INHALATION LIMIT/TLV (TOX1) ppm
       REF: HACS
     .10000
302   1   2   0     SHORT TERM INHALATION LIMIT (TOX2) ppm
       REF: HACS
     1.0000
303   1   2   0     SHORT TERM INHALATION TIME LIMIT (TOX3) s
       REF: HACS
     300.00
304   1   2   0     LOWER TOXICITY INGESTION LIMIT (TOX4) kg/kg
       REF: HACS
     .00000
305   1   2   0     UPPER TOXICITY INGESTION LIMIT (TOX5) kg/kg
       REF: HACS
     .00000
306   1   2   1     LATE TOXICITY LEVEL (TOX6)
       REF: HACS

701   1   2   0     LIMITING VALUE OF MOLECULAR FN CONC (XMFRC)
       REF: HACS
     .00000
```

TABLE A.6.6 Sulfur Dioxide Property Data Base File

```
 -1   0   3   0      SFDPROP.DAT
                     VERSION  2.11
-------------------------------------
  1   1   2   0      MOLECULAR WEIGHT (XMWT)
       REF: HACS
     64.060
  2   1   2   0      CRITICAL POINT TEMPERATURE (TCRI) K
       REF: HACS
     430.00
  3   1   2   0      CRITICAL POINT PRESSURE (PCRI) N/m2
       REF: HACS
     .78700E+07
  4   1   2   0      NORMAL BOILING POINT (XNBP) K
       REF: HACS
     263.20
  5   1   2   0      NORMAL FREEZING POINT (XNFP) K
       REF: HACS
     197.70
  6   8   2   0      VAPOR HEAT CAPACITY (CPV) PARAMETERS J/kg K
       REF: HACS
     420.25            .77776          -3.2679E-04       .00000          600.0
     250.00            0.0000           0.0000
  7   8   2   0      LIQ HEAT CAPACITY (CPL) PARAMETERS J/kg K
       REF: YAWS,C.L.,"PHYSICAL PROPERTIES",MCGRAW-HILL,P.220.
    -2402.0            43.292          -.16864           2.2127E-04      423.1
     200.46            1339.8           263.16
  8   7   2   0      LIQUID DENSITY (RHOL) PARAMETERS kg/m3
       REF: HACS
     2085.6           -2.4000           .00000          303.16          223.1
     1450.0            263.16
 10   7   2   0      VAPOR PRESSURE (PSAT) PARAMETERS N/m2
       REF: HACS
     9.4072            999.90          -35.960           0.0000          0.000
     293.16            195.16
 11   2   2   0      ENTHALPY OF SATURATED LIQUID (HLIQS) J/kg
       REF: PERRY, "CHEM. ENG. HANDBOOK", 5th ed., P. 3-202.
     .00000            273.16
 12   2   2   0      ENTHALPY OF SATURATED VAPOR (HVAPS) J/kg
       REF: PERRY, P. 3-202.
     .38100E+06        273.16
 13   6   2   0      ENTHALPY OF VAPORIZATION (XLAMDA) J/kg
       REF:
     430.00            263.20          .39691E+06        .38000          430.0
     197.70
 14   6   2   0      SOLUBILITY (SOL) PARAMETERS kg/100 kg
       REF: HACS
     10.000            .00000          .00000            .00000          10.00
     293.16
 15   1   2   0      ENTHALPY OF FUSION (DHF) J/kg
       REF: PERRY, P. 3-112.
     .11554E+06
```

TABLE A.6.6 (Cont.) Sulfur Dioxide Property Data Base File

```
16   1   2   0     ENTHALPY OF COMBUSTION (DHC) J/kg
      REF: HACS
     .00000
 17   1   2   0     ENTHALPY OF DECOMPOSITION (DHDC) J/kg
      REF: HACS
     .00000
 18   1   2   0     ENTHALPY OF SOLUTION (DHS) J/kg
      REF: HACS
    -.21897E+06
 19   1   2   0     ENTHALPY OF REACTION WITH WATER (DHWR) J/kg
      REF: HACS
     .00000
 20   1   2   0     ENTHALPY OF POLYMERIZATION (DHPY) J/kg
      REF: HACS
     .00000
101   7   2   0     LIQ THERMAL COND (XKL) PARAMETERS W/m K
      REF: YAWS, P.224.
     .89571          -3.2797E-03       2.9886E-06       423.16          223.1
     .19163           293.16
102   8   2   0     VAP THERMAL COND (XKV) PARAMETERS W/m K
      REF: YAWS, P.208.
    -8.0793E-03       6.3388E-05      -1.3807E-08       2.3012E-12      1673.
     173.16           9.6525E-03       298.16
103   8   2   0     LIQ VISCOSITY (XMUL) PARAMETERS N s/m2
      REF: YAWS, P.212.
    -13.056           936.46           1.4140E-02      -2.8874E-05      430.7
     200.46           .26000E-03       298.16
104   7   2   0     VAP VISCOSITY (XMUV) PARAMETERS N s/m2
      REF: YAWS, P.210.
    -3.7930E-07       .46405E-07      -.72760E-11       1673.2          173.1
     .12820E-04       298.16
105   8   2   0     SURFACE TENSION (STEN) N/m
      REF: YAWS,C.L.,"PHYSICAL PROPERTIES",MCGRAW-HILL,NY,P.218.
     .02060           430.16           303.16           1.1768          430.7
     200.46           .02641           273.16
106   2   2   0     INTERFACIAL SURFACE TENSION (XITEN) N/m
      REF: HACS
     .00000           .00000
107   1   2   1     SHIPPING STATE CODE
      REF: HACS
L
201   1   2   0     LOWER FLAMMABILITY LIMIT (XLOFLM) %
      REF: HACS
     .00000
202   1   2   0     UPPER FLAMMABILITY LIMIT (UPFLM) %
      REF: HACS
     .00000
203   1   2   0     BURN RATE (BRAT) m/s
      REF: HACS
     .00000
```

TABLE A.6.6 (Cont.) Sulfur Dioxide Property Data Base File

```
204   1   2   0     ADIABATIC FLAME TEMPERATURE (ADFT) K
       REF: HACS
     .00000
205   1   2   0     MOLAR RATIO REACTANTS/PRODUCTS (MRAT)
       REF: HACS
     .00000
206   1   2   0     AIR FUEL RATIO (AFRT)
       REF: HACS
     .00000
207   1   2   0     FLAME TEMPERATURE (FLTM) K
       REF: HACS
     .00000
301   1   2   0     TOXIC INHALATION LIMIT/TLV (TOX1) ppm
       REF: HACS
     5.0000
302   1   2   0     SHORT TERM INHALATION LIMIT (TOX2) ppm
       REF: HACS
     20.000
303   1   2   0     SHORT TERM INHALATION TIME LIMIT (TOX3) s
       REF: HACS
     300.00
304   1   2   0     LOWER TOXICITY INGESTION LIMIT (TOX4) kg/kg
       REF: HACS
     .00000
305   .1  2   0     UPPER TOXICITY INGESTION LIMIT (TOX5) kg/kg
       REF: HACS
     .00000
306   1   2   1     LATE TOXICITY LEVEL (TOX6)
       REF: HACS

701   1   2   0     LIMITING VALUE OF MOLECULAR FN CONC (XMFRC)
       REF: HACS
     .00000
```

APPENDIX B

VOLUME SOURCE & AREA SOURCE GAUSSIAN DISPERSION MODELS

The passive dispersion of a chemical vapor in the post transition regime is modeled in this Appendix. Both instantaneously released puff type dispersion as well as continuously released plume type dispersion are analyses.

In the derivations given below the following ASSUMPTIONS are made:

1. The translational speed of the cloud is a constant and is equal to the wind speed at 10 m height.

2. The atmospheric stability during the dispersion duration is a constant.

3. The concentration at any point is equal to the sum of concentration contributions from infinitesimal sources of vapor. That is, the principle of superposition is valid.

B.1 DISPERSION FROM A CYLINDRICAL VAPOR PUFF

B.1.1 Derivation of the Equations

Consider a cylindrical vapor cloud indicated schematically in Figure B-1. This cylindrical puff of vapor is subject to a wind of mean speed U. It is desired to calculate the concentration at any point down wind at any given time.

Let R_T, H_T, X_T be, respectively, the radius, height and the down wind location of the center of the cylindrical cloud with respect to an origin located at (0,0,0). Let C_T be the uniform vapor concentration (in density units) within the cylindrical cloud.

At a given time t the concentration at a point P(x,y,z,t) due to an infinitesimal volume source of volume $dx_s\ dy_s\ dz_s$ located at xs, ys, zs, (relative to coordinate system located at ground level and the origin coinciding with the center of the cylinder) is given by,

$$dC(x,y,z,t) = C_T \frac{\exp\left[-\frac{(x-x_s-Ut)^2}{2\,\sigma_x^2(x-x_s)}\right]}{\sqrt{2\pi}\,\sigma_y(x-x_s)}\,dx_s \frac{\exp\left[-\frac{(y-y_s)^2}{2\,\sigma_y^2(x-x_s)}\right]}{\sqrt{2\pi}\,\sigma_y(x-x_s)}\,dy_s$$
$$* \frac{\left(\exp\left[-\frac{(z-z_s)^2}{2\,\sigma_z^2(x-x_s)}\right] + \exp\left[-\frac{(z+z_s)^2}{2\,\sigma_z^2(x-x_s)}\right]\right)}{\sqrt{2\pi}\,\sigma_z(x-x_s)}\,dz_s \qquad \text{(B.1)}$$

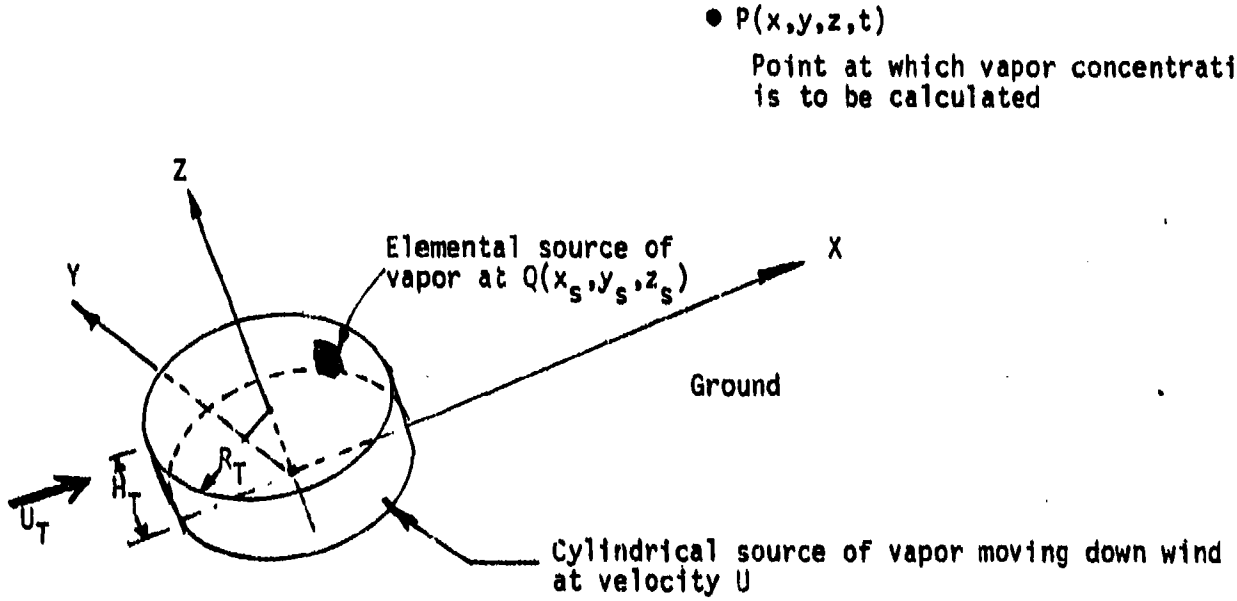

FIGURE B.1: Schematic Diagram Showing the Geometry and other Features of the Volume Source Dispersion Model ("Modified Gaussian")

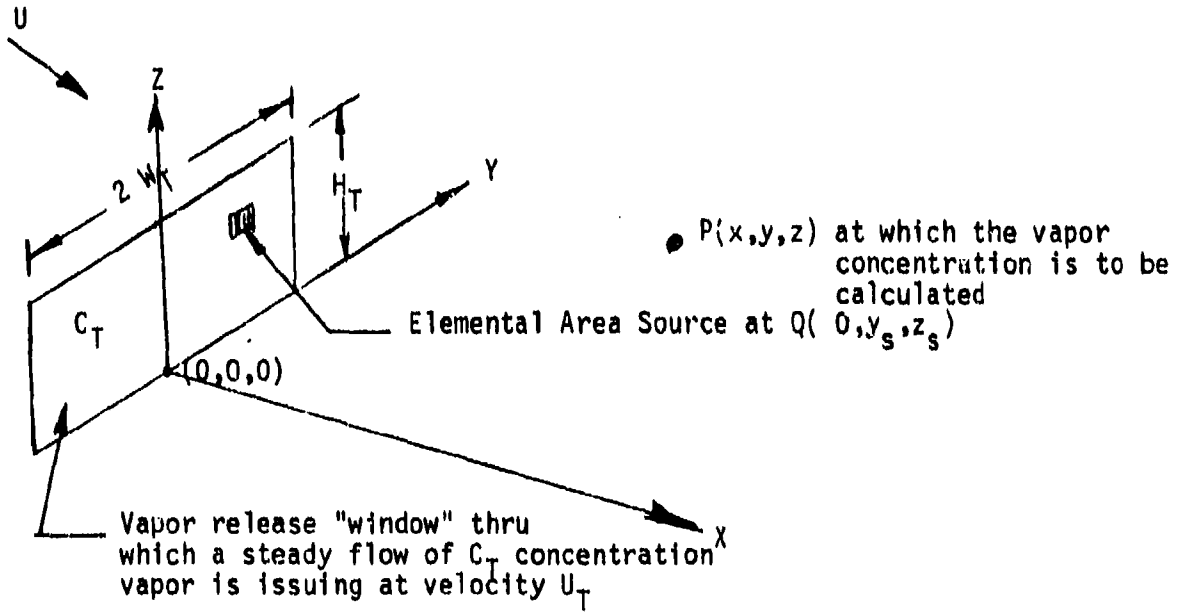

FIGURE B.2: Features of the Area Source Model ("Modified Gaussian")

The total contribution to the concentration value at P(x,y,z,t) can be calculated by integrating the RHS of equation B.1. The limits of integration are as follows:

$$\text{for } x_s; \qquad -R_T \le x_s \le R_T$$

$$\text{for } y_s; \qquad -\sqrt{R_T^2 - x_s^2} \le y_s \le \sqrt{R_T^2 - x_s^2}$$

$$\text{for } z_s; \qquad 0 \le z_s \le H_T$$

We further assume that $x >> x_s$ so that the dispersion coefficients, i.e., σ_y and σ_z, can be evaluated at the location of the center of the cloud, x_c, at any time. This cloud center has the coordinates (x_c, y_c, z_c) as follows.

$$x_c = x_T + U\,t \; ; \quad y_c = 0 \; ; \quad z_c = 0 \qquad \text{(B.2)}$$

Equation B.1 can be recast in terms of a cylindrical coordinate system as follows. Let,

$$x_s = r_s \cos\phi \; ; \quad x - x_c = r \cos\theta \qquad \text{(B.3a)}$$

$$y_s = r_s \sin\phi \; ; \quad y - y_c = r \sin\theta \qquad \text{(B.3b)}$$

Taking into account equations B.2 & B.3 the integral of equation B.1 can be written as follows:

$$C(r,\theta,z,t) = \frac{C_T}{(2\pi)^{3/2}\,\sigma_y^2\,\sigma_z} \int_{r_s=0}^{R_T} r_s dr_s \int_{\phi=0}^{2\pi} \exp\left[-\frac{(r^2 + r_s^2 - 2rr_s\cos\phi)}{2\,\sigma_y^2}\right] d\phi$$

$$\times \int_{z_s=0}^{H_T} \left[\exp\left(-\frac{(z-z_s)^2}{2\,\sigma_z^2}\right) + \exp\left(-\frac{(z+z_s)^2}{2\,\sigma_z^2}\right)\right] dz_s \qquad \text{(B.4)}$$

NON DIMENSIONAL PARAMETERS

We define the following non dimensional parameters.

$r_p = r/R_T$ = dimensionless radial coordinate of the observation point relative to the cloud center at time t.

$q_s = r_s/R_T$ = dimensionless radial position of the elemental source.

$\zeta = z/H_T$ = dimensionless vertical coordinate of the point at which concentration is to be calculated.

$\zeta_s = z_s/H_T$ = dimensionless vertical coordinate of the elemental source. (B.5)

$S_y = \sqrt{2}\ \sigma_y/R_T$ = dimensionless Y direction dispersion coefficient.

$S_z = \sqrt{2}\ \sigma_z/H_T$ = dimensionless Z direction dispersion coefficient.

Equation B.4 in now written in a simplified form as follows.

$$C(r_p, \theta, \zeta, t) = C_T \; B_Y \; B_Z \qquad (B.6)$$

where,

$$B_Y = \int_{q_s=0}^{1} \frac{2\ q_s}{s_y^2} \exp\left(- \frac{(r_p^2 + q_s^2)}{s_y^2} \right) I_0\left(\frac{2\ r_p}{s_y^2}\ q_s \right) dq_s \qquad (B.7)$$

and

$$B_Z = \frac{1}{2} \left[\operatorname{erf}\left(\frac{1 + \zeta}{s_z} \right) + \operatorname{erf}\left(\frac{1 - \zeta}{s_z} \right) \right] \qquad (B.8)$$

where I_0 is the modified Bessel function of first kind and zeroth order. This function is defined (see Abramowitz & Stegun, 1964, p376, equation 9.6.19) by the integral,

$$I_0(x) = \frac{1}{\pi} \int_{\phi=0}^{\pi} \exp(x \cos \phi)\ d\phi \qquad (B.9)$$

B.1.2 Behavior of Function B_Y

Case 1: when $S_y^2 >> 2\ r_p$

The above condition is satisfied when the value of the dispersion coefficient is very much larger than the radius of the "observation" point relative to the cloud conter.

It can than be shown that

$$I_0\left(\frac{2\ r_p}{s_y^2} \right) \longrightarrow 1 \qquad (B.10)$$

Hence, equation B.7 reduces to the following.

$$B_Y = \exp\left(-\frac{r_p^2}{S_Y^2}\right)\left[1 - \exp\left(-\frac{1}{S_Y^2}\right)\right] \qquad \text{(B.11)}$$

For large values of S_Y (i.e. for $S_Y > 3$) the above equation can be further reduced to

$$B_Y = \frac{\exp\left(-\frac{r_p^2}{S_Y^2}\right)}{S_Y^2} \qquad \text{(B.12)}$$

The above equation indicates the true Gaussian profile in the y direction.

Case 2: When $S_Y^2 << 2\ r_p$

This case arises when the point P at which the concentration is needed lies outside the standard deviation of the y - direction concentration profile. In this case the integral in equation B.7 has to be evaluated numerically.

Because of the presence of terms involving exp (- x^2) and the I_0 function in the integrand traditional numerical integration methods lead to round off errors resulting in completely erroneous estimation of the value of the integral. The integrand has to be re written in such a fashion that it becomes the product of functions whose behavior is well known under certain limiting conditions. We write one such resolution of the integrand.

Therefore, equation B.7 is written as

$$B_Y = \int_{q_s=0}^{1} \sqrt{\frac{q_s}{r_p}}\ f_1(q_s, r_p, S_Y)\ f_2(q_s, r_p, S_Y)\ dq_s \qquad \text{(B.13)}$$

where,

$$f_1(q_s, r_p, S_Y) = \frac{\exp\left[-(q_s - r_p)^2 / S_Y^2\right]}{\sqrt{\pi}\ S_Y} \qquad \text{(B.14)}$$

and

$$f_2(q_s, r_p, S_Y) = \sqrt{2\ \pi\ \left(\frac{2 r_p q_s}{S_Y^2}\right)}\ \exp\left(-\frac{2 r_p q_s}{S_Y^2}\right)\ I_0\left(\frac{2 r_p q_s}{S_Y^2}\right) \qquad \text{(B.15)}$$

In the limit of $S_Y \rightarrow 0$ it can be shown that the f_1 function tends to a delta function centered on r_p. The f_2 function in this limit tends to unity (See Abramowitz and Stegun, 1964). The integral represented by equation B.13 tends to unity if $r_p <= 1$ or tends to zero if $r_p > 1$.

B.1.3 Behavior of Function B_Z

Case 1: When z = 0. That is the ground level value

From equation B.8 it can be shown that

$$B_Z(z = 0) = B_Z^{max} = \text{erf}\ (1/S_Z) \qquad \text{(B.16)}$$

It can be shown, using the above equation that

$$\lim_{S_Z \to 0} B_Z^{max} = 1 \qquad \text{(B.17)}$$

Similarly from equation B.8 using the properties of error functions it can be shown that

$$\lim_{\zeta >> S_Z} B_Z(\zeta) = \frac{2}{\sqrt{\pi}\ S_Z} \exp\left(-\frac{\zeta^2}{S_Z^2}\right) \qquad \text{(B.18)}$$

The above equation also indicates that at far off vertical distance the concentration distribution profile is essentially a Gaussian.

B.2 DISPERSION FROM A FINITE CONCENTRATION CONTINUOUS SOURCE

Consider the release of a mixture of vapor and air continuously through a "window" as shown schematically in Figure B.2. The vapor issuing from this window is dispersed by atmospheric turbulence. The vapor air mixture is assumed to be of neutral density (relative to air). It is required to calculate the down wind concentration distribution within the vapor plume.

A model is discussed below to calculate the down wind concentrations. In developing the model we make the following ASSUMPTIONS.

1. There is no longitudinal dispersion.
2. The plume translational velocity is constant and is the same at all down wind locations.
3. The principle of concentration superpositions can be used.

B.2.1 Derivation of the Equations

Consider a Cartesian coordinate system whose origin is at the center of the source "window" on the ground level. The axes of coordinates are indicated in Figure B.2. With respect to these axes the coordinates of a point P at which the concentration value is desired is represented by $P(x_p, y_p, z_p)$.

We define the following parameters (see also Figure B.2).

C_T = Uniform concentration of vapor (in density units) at the source of vapor ("window").

W_T = Semi width of the "window" source.

H_T = Height of the "window" source.

U_T = Mean translational velocity of the plume

Consider an elemental source of vapor located at the "window" and whose coordinates are $Q(0,y_s,z_s)$. The concentration at the point P(xp,yp,zp) due to this elemental source can be written as,

$$dC(x_p,y_p,z_p) = \frac{d\dot{M}_s}{2\pi\, U_T\, \sigma_y(x_p)\, \sigma_z(x_p)} \exp\left(-\frac{(y_p - y_s)^2}{2\,\sigma_y^2}\right) * \exp\left(-\frac{(z_p - z_s)^2}{2\,\sigma_z^2}\right) \qquad (B.19)$$

where, $d\dot{M}_s$ is the vapor mass flux thru the elemental area at Q. This elemental mass flow rate is given by

$$dM_s = U_T\, C_T\, dx_s\, dy_s \qquad (B.20)$$

Integrating equation B.19 over the following ranges for y_s and z_s gives the concentration at the point P.

$$0 <= z_s <= H_T \quad \text{and} \quad -W_T <= y_s <= W_T \qquad (B.21)$$

To simplify the integration of equation B.19 we define below the following parameters.

$$\eta_s = y_s/W_T\,, \quad \eta = y_p/W_T = \text{Dimensionless Y coordinates}$$

$$\zeta_s = z_s/H_T\,, \quad \zeta = z_p/H_T = \text{Dimensionless Z coordinates} \qquad (B.22)$$

$$S_Y = 2\,\sigma_y(x_p)/W_T\,, \quad S_Z = 2\,\sigma_z(x_p)/H_T \quad \text{Dispersion coefficients.}$$

Using the above non dimensional parameters and integrating equation B.19 over the range indicated in equation B.21 we show that the concentration equation can be represented as

$$C(x_p, \eta, \zeta) = C_T\, B_Y\, B_Z \qquad (B.23)$$

where

$$B_Y = \frac{1}{2} \left[\text{erf} \left(\frac{1 + \eta}{S_Y} \right) + \text{erf} \left(\frac{1 - \eta}{S_Y} \right) \right] \quad \text{(B.24)}$$

$$B_Z = \frac{1}{2} \left[\text{erf} \left(\frac{1 + \zeta}{S_Z} \right) + \text{erf} \left(\frac{1 - \zeta}{S_Z} \right) \right] \quad \text{(B.25)}$$

It can be shown from the above equations that the maximum concentration in the plume at any down wind position is given by

$$C_{max}(X_p) = C_T \quad \text{erf}(1/S_Y) \quad \text{erf}(1/S_Z) \quad \text{(B.26)}$$

Further it can be shown that when $\eta >> S_Y$ and $\zeta >> S_Z$ the integral of equation B.19 becomes

$$C(x_p, \eta, \zeta) = C_{max}(x_p) \quad \exp(- \eta^2 / S_Y^2) \quad \exp(- \zeta^2 / S_Z^2) \quad \text{(B.27)}$$

The above equation clearly shows the Gaussian profiles for the distribution of concentration at lateral and vertical locations far off from the plume center.

APPENDIX C

COMPUTER IMPLEMENTATION OF THE MODELS

The scientific models developed in this project have been coded in FORTRAN into a number of subroutines and implemented on a computer-based dispersion analysis system. This system, titled ADAM ("Air Force Dispersion Assessment Model") consists of all of the models described in the report, the chemical property data files and other library subroutines. The overall architecture of the model is described in Section C.1. Volume II of the report (under separate cover) contains a detailed User's Manual for the computer codes.

C.1 PROGRAM ORGANIZATION

The overall program flow is shown in Figure C.1.1. The individual modules libraries are discussed in Sections C.1.1 through C.1.3. The models described in Chapters 2 through 6 and Appendix A are contained in the scientific subroutine modules libraries. These are shown in the figure as the libraries enclosed by the dashed line. The other programs are Input and Output (I/O) support programs and the overall executive program. The models were implemented on the Air Force's Zenith (IBM PC/AT compatible) microcomputers using the FORTRAN language for all functions except graphical output which is implemented using the HALO* graphics software.

C.1.1 Overall Executive Program

The dispersion model is run on the computer by entering the name of the overall executive batch program (ADAM.BAT) shown in Figure C.1.2. The program execution is described in Volume II, "The User Manual for ADAM". Upon completion of all calculations, temporary files are erased and the control of the computer is returned back to the operating system (DOS).

C.1.2 Input and Output (I/O) Programs

The input programs are called by the overall executive program. They read data from a user input file and other data files. The output module contains subroutines which output the results graphically on the terminal screen and in a tabular form in data files. After the output is complete, the overall executive program ends the simulation. The contents and formats of the various I/O files are discussed in more detail in Volume II.

---

* HALO is a registered trademark of Media Cybernetics, Inc.

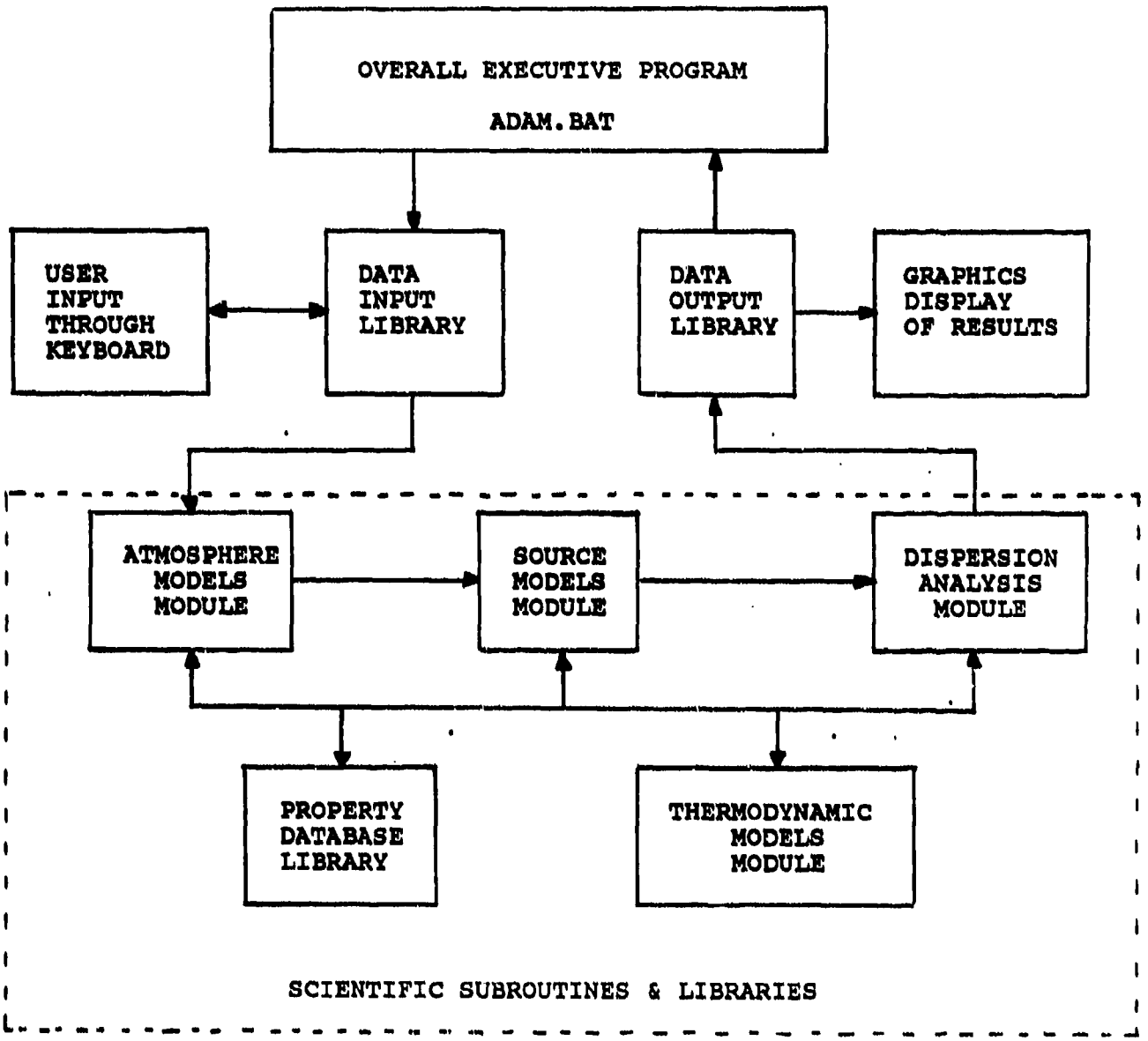

FIGURE C.1.1 Air Force Dispersion Assessment Model (ADAM) System Architecture

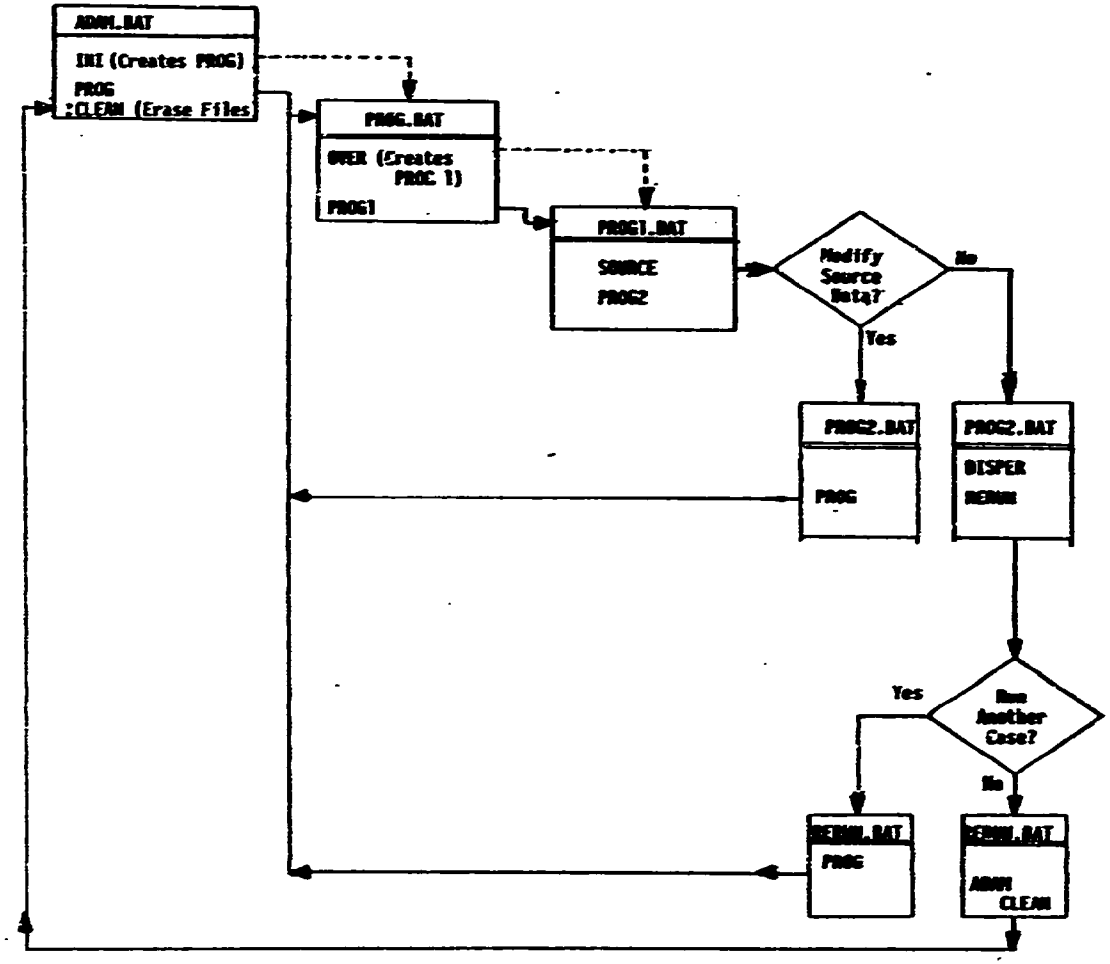

FIGURE C.1.2: Program Control Flow Diagram for Executing ADAM

C.1.3 Scientific Subroutines and Functions

There are five scientific subroutine modules libraries, as shown in Figure C.1.1. Each module or library contains FORTRAN subroutines and functions for the models developed, grouped by function and purpose.

The five scientific model modules and libraries are:

Atmosphere Models Module

The atmosphere module contains the programs needed to calculate the Pasquill stability category of the atmosphere based on the input weather conditions (discussed in Chapter 4). Other output data from this module are the wind velocity at 10 meters and wind friction velocity.

Source Models Module

Once the atmospheric calculations are complete, the source module is called. It contains programs for calculating the source strength, dimension, and composition (discussed in Chapter 2) based on the user input data and atmospheric conditions.

Dispersion Analysis Module

The source, atmosphere, and user input data are then passed to the programs in the dispersion analysis module. It uses these data to model the dispersion of the chemicals in the air (discussed in Chapter 5). Once the results are calculated, they are passed to the output programs for graphical and tabular output.

Thermodynamic Models Module

The thermodynamic module contains the programs for calculating the thermodynamic equilibrium conditions for the "box" (discussed in Chapter 3). This module is not called in a set sequence, as the above three libraries are, but is called by them as thermodynamic calculations are required.

Property Database Library

The last scientific subroutine library, the property database library, contains the subroutines that calculate various properties of the chemicals based on the data contained in the property database data files and input information on temperature or pressure, if needed. It is also not called in a set sequence, but as needed by the programs in the other four scientific modules. This library is discussed in detail in Appendix A.